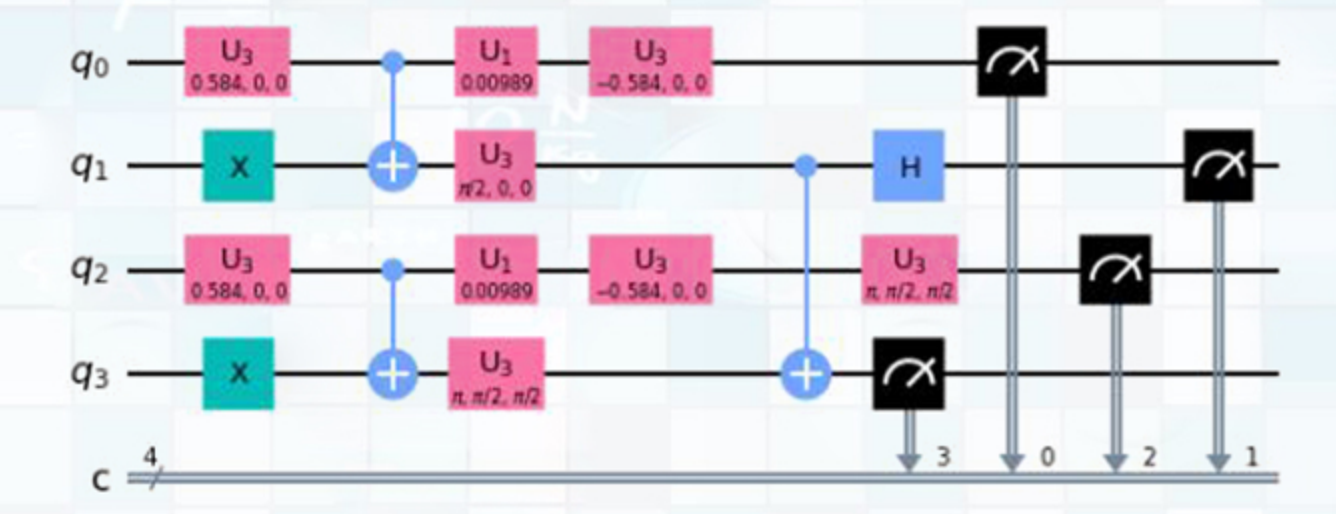
Quantum Aspects

Oscillatory leutrinos

BY ABHISHEK KUMAR JHA





SCHOOL OF PHYSICS
UNIVERSITY OF HYDERABAD
APRIL 2022

Quantum Aspects of Oscillatory Neutrinos

A thesis submitted for the award of

DOCTOR OF PHILOSOPHY

by

Abhishek Kumar Jha

(Reg. No : 17PHPH34)





Under the supervision of

Prof. BINDU A. BAMBAH

School of Physics
University of Hyderabad
Central University PO, Prof. C. R. Rao road,
Gachibowli, Hyderabad-500046, Telangana, India.

April-2022

Dedicated to ...

My parents and my teachers

DECLARATION

I here by declare that the work reported in this thesis entitled "Quantum Aspects of Oscillatory Neutrinos" has been carried out by me independently in the School of Physics, University of Hyderabad, under the supervision of Prof. Bindu A. Bambah. I also declare that this is my own work and effort, and it has not been submitted at any other University or Institution for any degree. Wherever contributions of others are involved, every effort is made to indicate that clearly with due reference to literature, and acknowledgement of collaborative research and discussions. I hereby agree that my thesis can be deposited in Shodganga/INFLIBNET.

A report on plagiarism statistics from the University Librarian is enclosed.

(Abhishek Kumar Jha)

Place: Hyderabad

Date: 18/04/2022



CERTIFICATE

(For Ph. D. Dissertation)

This is to certify that the thesis entitled "Quantum Aspects of Oscillatory Neutrinos" has been carried out by Abhishek Kumar Jha (Reg.No.17PHPH34), under my supervision for the full period prescribed under Ph.D. ordinance of the University of Hyderabad. It has been screened by the Turnitin software at the library of the University of Hyderabad. The software shows 29% similarity index out of which, 24% came from the candidate's research articles related to this thesis. 10% came from his publication in journal Modern Physics Letters A, 4% and 3% (link.springer.com) are from The European Physical Journal Special Topics, 3% (export.arxiv.org) and 3%(arxiv.org) are from his article in arxiv(2004.14853, 2010.06458) and 2%(indico.fnal.gov) has come from his poster and oral contributions to the many National/International conferences which are now available online. The remaining may be from use of some scientific terms and equations, which have not been detected by the software. Therefore, this thesis is free from plagiarism and has not been submitted previously in part or in full to this or any other University or Institution for award of any degree or diploma.

Further, the studies has the following publications before submission of the thesis for adjudication and has produced evidence for the same in the form of acceptance letter or the reprint in the relevant area of his research:

Published Papers

- Abhishek Kumar Jha, Supratik Mukherjee and Bindu A. Bambah, "Tri-Partite entanglement in Neutrino Oscillations," Mod. Phys. Lett. A 36 no.09, 2150056 (2021). doi:10.1142/S0217732321500565, [arXiv:2004.14853 [hep-ph]]. https://doi.org/10.1142/S0217732321500565
- 2. **Abhishek Kumar Jha** and Akshay Chatla, "Quantum studies of neutrinos on IBMQ processors," Eur. Phys. J. Spec. Top. **231**, 141–149 (2022), https://doi.org/10.1140/epjs/s11734-021-00358-9 [arXiv:2010.06458 [hep-ph]].
- 3. Abhishek Kumar Jha, Akshay Chatla and Bindu A. Bambah, "Neutrinos as Qubits and Qutrits," [arXiv:2203.13485 [hep-ph]]. https://doi.org/10.48550/arXiv.2203.13485 (under review)

Conference Proceedings

1. Abhishek Kumar Jha (2021, April 12) "Quantum Studies of Neutrinos," The proceedings of the XIX International Workshop on Neutrino Telescopes (Neutel 21), Padova (Italy) have been published on the Zenodo Platform online. https://doi.org/10.5281/zenodo.4680524

He has participated in Schools and Conferences and his contributed talks/posters are:

- Completed SERB preparatory school in Theoretical High Energy Physics at University of Hyderabad during 20^{th} August -15^{th} September, 2018.
- Contributed a poster on "Quantum entanglement and Neutrino oscillations" in The National conference on Frontiers in Particle Physics and Cosmology (FIPPC-2019) at University of Hyderabad, Hyderabad, India, held during $23^{rd} 25^{th}$ January 2019.
- Completed SERB XXXIII Main school in Theoretical High Energy Physics at SGTB Khalsa College, University of Delhi, during $7^{th} 26^{th}$ December, 2019.
- Contributed a poster on "Two and Three- Particle Entanglement In Neutrino oscillations" in National Symposium on Theoretical High Energy Physics, December 20, 2019, SGTB Khalsa College, University of Delhi, India.
- Contributed a poster on "Tri-Partite Entanglement In Neutrino Oscillations" (Poster ID-337), at The XXIX International Conference on Neutrino Physics and Astrophysics (Neutrino-2020) held online during June 22nd-July 2nd 2020, Fermilab, USA.
- Contributed a poster on "Quantum Entanglement In Neutrino Oscillations" (Poster ID-44), in 53rd Annual Users Meeting, Fermi National Accelerator Laboratory, held during 10th 13th August, 2020.
- Contributed an oral talk on "Quantum simulation of oscillating neutrinos" in the 5th International Conference on Particle Physics and Astrophysics at Moscow, Russia held online during $5^{th} 9^{th}$ October, 2020.
- Contributed a poster on "Quantum simulation of oscillating neutrinos" in the Young Quantum 2020 (YouQu-2020) meeting at HRI, Allahabad, India, during $12^{th} 15^{th}$ October, 2020.
- Contributed a poster on "Quantum simulation of entangled oscillating neutrinos" in DAE-BRNS High Energy Physics Symposium 2020 at NISER, India held online during $14^{th} 18^{th}$ December, 2020.
- Contributed an oral talk on "Quantum studies of neutrinos" in XIX International Workshop on Neutrino Telescopes (Neutel 21) at Padova (Italy) held online during $18^{th} 26^{th}$ February, 2021.

- Contributed a poster on "Quantum simulation of entangled oscillating neutrinos on IBMQ processors" in Quantum Computing Hard- and Software Summer School (QCHS-2021)- held online during $15^{th} - 18^{th}$ June 2021, organized by ETH, Zurich and EPFL, Lausanne, Switzerland.
- Completed a mini-project on "Coherence in Neutrino Oscillations" in International Neutrino Summer School (INSS-2021), CERN-held online during $2^{nd} - 13^{th}$ August 2021.
- Contributed an oral talk on "Entangled states of neutrinos as qutrits" in New Perspectives conference held online during $16^{th} - 19^{th}$ August, 2021, Fermilab, USA.

Further, the student has passed the following courses towards fulfillment of course work requirement for his Ph.D.

S.No.	Subject code	Name	Credits	Pass/Fail
1.	PY801	Research Methodology	4	Pass
2.	PY802	Advanced Quantum Mechanics	4	Pass
3.	PY803	Advanced Experimental Techniques	4	Pass

Bindu A Bambal Aul (Prof. Bindu A. Bambah)

Thesis Supervisor pah School of Physics

University of Hyders badad Or Hydersity Of Hyder (T.S.) INDI-Hyderabad-500 046. (T.S.)INDIA

(Dr. Soma Sanyal)

Co-Supervisor,

School of Physics

University of New density of Profession of Physics Asst. Profession of Physics and School of Hyderabases of School of Hyd University of Hyderabad Hyderabad-500 046.

(Prof. K. C. James Raju)

Dean,

School of Physics, University of Hyderabad.

संकाय अध्यक्ष / Dean भौतिकी संकाय / School of Physics हैदरावाद विश्वविद्यालय UNIVERSITY OF HYDERABAD हैदराबाद / HYDERABAD-500 046. भारत / INDIA

Acknowledgements

First and foremost, I offer my deep and sincere gratitude to my supervisor **Prof. Bindu A. Bambah** for all the encouragement and motivation she has provided me with throughout the thesis. I am grateful to her for suggesting me few problems of physics which are current interesting areas of research and have a great future. I sincerely thank her for believing in my capabilities as a researcher.

I would like to acknowledge the use of IBM Quantum Experience for this thesis work. The views are expressed by me and do not reflect the official policy or position of IBM or the IBMQ team.

I would like to thank **Prof. C. Mukku** (IIIT-Hyderabad) for his insightful inputs in my research papers and **Prof. S. Umasankar** (IIT- Mumbai) for his valuable suggestions to putting forward of my research work. I am thankful to my collaborators **Mr. Akshay Chatla** and **Mr. Supratik Mukherjee** for their fruitful discussions. I am extremely thankful to **Prof. Rukmani Mohanta**, **Prof. E. Harikumar**, **Dr. Soma Sanyal** (Co-Supervisor), and **Prof. V. Subrahmanyam** for their valuable suggestions during my Doctoral Committee meetings.

I am extremely grateful to Vice-Chancellors: **Prof. Apparao Podule** and **Prof. B. J. Rao**, and the Deans, School of Physics: **Prof. Bindu A. Bambah**, **Prof. V. Sheshubai**, **Prof. Ashok Chatterjee** and **Prof. K. C. James Raju** for providing excellent facilities, good conferences and a nice atmosphere for during my Ph.D. work.

I thank Mrs. Deepika, Mrs. Shailaja and Mr. Sudarshan for their help in administrative matters and Mr. Shekar, Mr. Prasad, Mr. Mahesh, and all non-teaching staff for their help in school office.

I would like to thank all of my teachers and friends during my Ph.D., M.Sc, B.Sc, Intermediate and School and all of my well wishers for their love, affection and constant encouragement. I thank my friend Mr. Abhishek Nandan and Ms. Devaparna Bhattacharya, and my senior Dr. Naveen Kumar Mogurampally for their help in many occasions.

I thank all my family members for their unfailing cooperation and support during my Ph.D. study. I especially thank my elder brother, Mr. Jitendra Narayan Jha for his

unlimited support through out my educational career.

Finally, I would like to thank everyone whosoever is involved in this effort.

Regards, Abhishek Kumar Jha.

Abstract

This thesis focuses on the interconnection between two rapidly advancing fields, neutrino oscillations in high energy physics and quantum information theory. Quantum entanglement and coherence are two properties emerging from the rule of quantum superposition. Since neutrinos are weakly interacting particles in superposition states, they should be entangled. We map the neutrino states to bipartite and tripartite states utilized in quantum optics. We use the entanglement measures of concurrence, tangle, linear entropy, negativity, threetangle, and three- π to characterize the time evolved flavour superposition neutrino states. We find that the correlations exhibited by neutrino oscillations in the tripartite system resemble the W-states, making them tangible assets for quantum information tasks. In the quantum computing language, superposition states are like qubits, which are fundamental building blocks of quantum computers. We map two flavour neutrino eigenstates to qubits. We prepare a quantum computer circuit to simulate bipartite flavour mode entanglement in the two neutrino systems on the IBM quantum processor. Furthermore, we construct the Poincaré sphere representation for two and three-flavour neutrino states using Pauli and Gell-Mann matrices. We generalize the concept of tripartite mode flavour entanglement in the three-neutrino system by considering them as qutrits. These quantum studies enable us to model neutrinos on quantum computers. The potential viability of neutrinos as quantum information resources is discussed.

Contents

D	ECL.	ARAT	ION	iii
C.	ERT:	IFICA	${f TE}$	iv
\mathbf{A}	ckno	wledge	ements	vii
\mathbf{A}	bstra	ıct		ix
\mathbf{C}	onter	nts		x
Li	st of	Figur	es	xiii
Li	st of	Table	S	xvii
1	Intr	oducti	ion to neutrino oscillations	1
	1.1	Introd	uction	. 1
	1.2	Plane-	wave approximation	. 4
		1.2.1	Two-flavour neutrino oscillations	. 8
		1.2.2	Three-flavour neutrino oscillations	. 9
		1.2.3	Neutrino oscillations in constant matter background	. 10
		1.2.4	Same energy and same momentum approach in neutrino oscillations.	. 12
	1.3	The w	rave-packet description of neutrino oscillations	. 14

C	ONTI	ENTS	xi
	1.4	Outline of thesis	17
2	$Th\epsilon$	eory of distributed entanglement	20
	2.1	The Qubit	21
	2.2	Density operator	22
	2.3	Bi-partite entanglement	23
		2.3.1 Peres-Horodecki Criterion	26
		2.3.2 Negativity	27
		2.3.3 Entanglement of formation	27
		2.3.4 Concurrence and Tangle	28
		2.3.5 Linear entropy	29
	2.4	Tri-partite entanglement	30
		2.4.1 Three-tangle	33
		2.4.2 Three- π	34
3	Tri-	-partite entanglement in neutrino oscillations	37
	3.1	Bi-partite entanglement in two-flavour neutrino oscillations	39
	3.2	Tri-partite entanglement in three-flavour neutrino oscillations	44
4	Qua	antum Computing	56
	4.1	Geometrical representation of Qubit	57
	4.2	Quantum gate	59
		4.2.1 Universal gate	59
		4.2.2 Pauli gates	60
		4.2.3 Hadamard gate	60
		4.2.4 Controlled NOT gate	61
		4.2.5 Controlled-U3 gate	62
	4.3	Quantum circuit	63
	4.4	IBM quantum cloud computer	65
	4.5	Concurrence circuit	67

CC	ONTE	ENTS	xii
5	Qua	antum studies of neutrinos on IMBQ processors	72
	5.1	Quantifying concurrence and l_1 -norm of coherence in the two neutrino system	73
	5.2	Quantum circuit of two flavour neutrino states	75
	5.3	Quantum simulation of bi-partite entanglement in the two neutrino system .	78
		5.3.1 Quantum circuit in vacuum	79
		5.3.2 Quantum circuit in the uniform matter background	82
6	Neu	trinos as Qubits and Qutrits	86
	6.1	SU(2) Poincaré sphere for two-flavour neutrinos	88
	6.2	Bloch matrix construction of two qubit neutrino states	91
	6.3	SU(3) Poincaré sphere for three-flavour neutrinos	96
	6.4	Two qutrits flavour neutrino states and generalized concurrence	104
7	Con	aclusion and Future work	109
	7.1	Experimental consideration	109
	7.2	Conclusion	111
	7.3	Future work	113
Bi	bliog	graphy	116

List of Figures

3.1	(Color online) Measures of bipartite quantum correlations Tangle $(\tau_{e\mu})$ = linear entropy $(S_{e\mu})$ (dotted line), Negativity $(N_{e\mu})$ (full line) vs scaled time $T \equiv (\frac{\Delta m^2 t}{2E})$ for an initial electron neutrino state. The dependence on oscillation probabilities, the transition probabilities P_s (dashed line) and P_d (dotted dash line) are also plotted. The mixing angle θ is fixed at the experimental value $\sin^2 \theta = 0.310$ [54]	43
3.2	Different possible ways of visualizing three-mode state entanglement [136]	45
3.3	(Color online) Entanglement of formation (E_f) vs $\frac{L}{E}\frac{Km}{GeV}$ graph between e,μ , and τ satisfying: $E_f(\tau_{e\mu}) + E_f(\tau_{e\tau}) > E_f(\tau_{e(\mu\tau)})$ where $E_f(\tau_{e\mu})$ (Red line), $E_f(\tau_{e\tau})$ (Blue line), the sum $E_f(\tau_{e\mu}) + E_f(\tau_{e\tau})$ (Green line) and $E_f(\tau_{e(\mu\tau)})$ (Black line). Here A, B and C are three qubit e, μ and τ flavour mode neutrino states, respectively.	49
3.4	(Color online) Negativity $(N_{e\mu}^2 + N_{e\tau}^2)$ (Red line) and $N_{e(\mu\tau)}^2$ (Black line) vs $\frac{L}{E}(\frac{Km}{GeV})$ graph between flavour modes electron, muon, and tau neutrinos satisfying: $N_{e\mu}^2 + N_{e\tau}^2 < N_{e(\mu\tau)}^2$. Parameters θ_{ij} and Δm_{ij}^2 are fixed at the experimental values [54]	51
3.5	(Color online) Residual entanglement π_e (Black line), π_{μ} (Green line), π_{τ} (Red line) vs $\frac{L}{E}(\frac{Km}{GeV})$ graph between flavour modes of electron, muon and tau neutrinos satisfying: $\pi_e \neq \pi_{\mu} \neq \pi_{\tau}$. Parameters θ_{ij} and Δm_{ij}^2 are fixed at the experimental values [54]	52
3.6	(Color online) Residual entanglement $\pi_{e\mu\tau}$ (Black line) vs $\frac{L}{E}(\frac{Km}{GeV})$ graph between the flavour modes electron, muon and tau neutrinos. Parameters θ_{ij} and Δm_{ij}^2 are fixed at the experimental values [54]. The transition probabilities $P_{\nu_{e\to e}}$ (Red line), $P_{\nu_{e\to \mu}}$ (Blue line) and $P_{\nu_{e\to \tau}}$ (Green line) are reported as well for comparison	53

LIST OF FIGURES xiv

3.7	(Color online) Residual entanglement $\pi_{\mu e \tau}$ (Black line) vs $\frac{L}{E}(\frac{Km}{GeV})$ graph between the flavour modes electron, muon and tau neutrinos. Parameters θ_{ij} and Δm_{ij}^2 are fixed at the experimental values [54]. The transition probabilities $P_{\nu_{\mu \to e}}$ (Red line), $P_{\nu_{\mu \to \mu}}$ (Blue line) and $P_{\nu_{\mu \to \tau}}$ (Green line) are reported	
	as well for comparison	54
4.1	This figure represent the Bloch sphere where $ 0\rangle$ and $ 1\rangle$ are north and south poles, respectively and which are opposite points of mutual orthogonal states. The x, y-axes have an eigenstates σ_x and σ_y , respectively	58
4.2	The Symbol of CNOT gate with two input qubits where a is control qubit and b is target qubit	62
4.3	The symbol of two qubit Controlled-U3 gate	62
4.4	The figure represent the quantum circuit of two qubit Bell's state	64
4.5	The figure represent quantum circuit of three-qubit GHZ state	64
4.6	The figure represent the quantum circuit of three-qubit prototype W-state $ W_3\rangle$.	64
4.7	The quantum circuit symbol for measurement	65
4.8	Image of IBM quantum computer [44]	66
4.9	The quantum circuit and its simulations is shown for the two qubit Bell's state on IBMQ computer. The lower part of Fig.(a), Fig.(b), Fig.(c) and Fig.(d) show the generation of four Bell's state $ \xi_{00}\rangle$, $ \xi_{01}\rangle$, $ \xi_{10}\rangle$ and $ \xi_{11}\rangle$, respectively on IBMQ simulator.	66
4.10	The quantum circuit and its simulations is shown for the GHZ state $ GHZ\rangle$ and prototype W-state $ W_3\rangle$ in Fig.(4.9(a)), Fig.(4.9(b)), respectively on IBMQ simulator	67
4.11	The figure represent concurrence quantum circuit of two-qubit pure state	68
4.12	In Fig.(a) and Fig.(b), top and bottom figure represent the quantum circuit of concurrence and histogram plot for Bell's state $ \xi_{00}\rangle$ and $ \xi_{01}\rangle$, respectively on IBMQ simulator.	69
4.13	In Fig.(a) and Fig.(b), top and bottom figure represent the quantum circuit of concurrence and histogram plot for Bell's state $ \xi_{10}\rangle$ and $ \xi_{11}\rangle$, respectively on IBMQ simulator.	69
4.14	In Fig.(a) Concurrence circuit for the two-qubit Bell state $ \xi_{01}\rangle = \frac{1}{\sqrt{2}}(01\rangle + 10\rangle)$ is shown where q_0, q_1, q_2, q_3 are initialize to $ 0\rangle$ state. In Fig.(b) concurrence information is encoded in four qubit computational basis on IBMQ	70
	simulator and on a real quantum hardware	70

LIST OF FIGURES xv

5.1	(a) The ν_e survival probability (Black, dashed line) is shown in the blue band the concurrence (Red, solid line) is within the orange band [197]. (b) The ν_e disappearance probability (Black, dash dotted line) is in the green band the concurrence (Red, solid line) is shown as red band [197]	75
5.2	Quantum computer circuit representation of two-flavor neutrino states in two-qubit systems: (a) $ \nu_e\rangle = \tilde{U}_{ee} 10\rangle_1 + \tilde{U}_{e\mu} 01\rangle_2$, (b) $ \nu_e(t)\rangle = \tilde{U}_{ee}(t) 10\rangle_e + \tilde{U}_{e\mu}(t) 01\rangle_{\mu}$, (c) $ \nu_{\mu}\rangle = \tilde{U}_{\mu e} 10\rangle_1 + \tilde{U}_{\mu\mu} 01\rangle_2$, (d) $ \nu_{\mu}(t)\rangle = \tilde{U}_{\mu e}(t) 10\rangle_e + \tilde{U}_{\mu\mu}(t) 01\rangle_{\mu}$. Here, two input qubits 1 and 2 are initiated to $ 0\rangle$	77
5.3	The circuit represent the concurrence measurement of ν_e disappearance in two-flavour neutrino oscillations	79
5.4	Concurrence circuit for the two qubit ν_e disappearance bipartite state on the IBMQ platform [44, 197]	80
5.5	The concurrence varies with time at the IBMQ computer for an initial electron neutrino flavour state. The concurrence information is shown Histogram (probabilities in percentage) plot on quantum simulator and IBM quantum hardware [44,197]	80
5.6	(a) The time evolution of the concurrence (Red line) compared to the disappearance P_d (Green line) and survival P_s (Black Dashed line) probabilities of $ \nu_{\mu}(t)\rangle$ in the vacuum A=0 [197]. (b) The time evolution of the concurrence (Red line) compared to the disappearance P_d (Green line) and survival P_s (Black Dashed line) probabilities of $ \nu_{\mu}(t)\rangle$ in the constant effective matter potential $A \neq 0$ [197]	82
5.7	Implementation of concurrence circuit for $ \nu_{\mu}(t)\rangle$ on IBMQ processor [44, 197].	83
5.8	The concurrence varies with time at the IBMQ computer for an initial muon neutrino flavour state in vaccum (A=0). The concurrence information is shown through Histogram (probabilities in percentage) plot on quantum simulator and IBM quantum hardware [44,197]	83
5.9	The concurrence varies with time at the IBMQ computer for an initial muon neutrino flavour state in the uniform matter background ($A\neq 0$) is shown on quantum simulator and IBM quantum hardware [44, 197]	84
6.1	In Fig.(a) the equi-mixing curves of $E(\rho_d^e)$ in the n_3 and n_8 plane is shown using the current experimental bounds of the 3σ range of neutrino parameters [197]. Fig.(b) shows the equi-mixing curves of $E(\rho_d^e)$ in the n_3 and n_8 plane inside the qutrit triangle	102
6.2	The equi-mixing curves of $E(\rho_d^e)$ is shown in the n_3 and n_8 plane when θ and η are vary from 0 to $\pi/2$	102

LIST OF FIGURES xvi

6.3	The violet band shows the ν_e concurrence $C(\rho^e(t))$ (Red, solid line) in the	
	bi-partite qubit system and the pink band shows the generalized concurrence	
	$C_3(\rho_{f_{9\times 9}}^e)$ (Blue, dash dotted line) in the bi-partite qutrit system. Both en-	
	tanglement measures are compared with the green band which shows the ν_e	
	probability $P_{e\to e}$ (Black, dash dotted line) and with the orange band which	
	shows the $P_{e\to\mu}$ probability (Green, dashed line), using the current experi-	
	mental bounds of the 3σ range of neutrino parameters [197]	107
7.1	The blue band shows the short range ν_e disappearance probability (Black,	
	dashed line) and the orange band shows concurrence (Red, solid line) in two	
	flavour neutrino oscillations, using the Daya Bay experimental data [197, 211].	110
7.2	The blue band represents the long-range survival probability $\nu_{\mu} \rightarrow \nu_{\mu}$ (Black,	
	dashed line) and it compared with orange band which gives concurrence (Red,	
	solid line) in two flavour neutrino oscillations, using the Minos experimental	
	data [197, 212]	110
7.3	The Coherence length L^{Coh} (Km) vs Energy (MeV) graph is shown using the	
1.5	wave packet sizes σ_x from ref [197, 222]	114
	$\gamma \gamma \omega \gamma \phi \rho \omega \phi \alpha \phi \phi$	

List of Tables

1.1	The neutrino mixing parameters in normal ordering $(m_1 < m_2 < m_3)$ from the NuFIT data [54]	10
4.1	The truth table of two qubit Bell states	63
6.1	The three constraints coming from star product condition $\hat{n} \star \hat{n} = \hat{n}$ (see Eq.(6.43)) and their corresponding orthonormal unit vectors	100

Chapter 1

Introduction to neutrino oscillations

1.1 Introduction

Despite being the most abundant fermion in the universe, the existence of the neutrino was postulated by Pauli in 1930 [1]. The investigation of the β -decay process was the first compelling evidence for the neutrino. The β -decay process is of two types: β^- and β^+ -decay, in β^- -decay¹ neutron (n) gets converted into a proton (p), and in that process, an electron (e^{-}) emitted from the fixed energy of a nucleus, i.e., $n \to p + e^{-}$. Before 1930, this theory troubled physicists for two main reasons: first, the energy spectrum of the emitted electrons is continuous in comparison to the spectrum of α , and γ radiation [2–7]. Second, because both parent and daughter nuclei have either integral spin or half-integer spin, a single $e^$ of spin $\frac{1}{2}$ is inconsistent with angular momentum conservation in β --decay. In 1930, Pauli made a hypothesis that solved these difficulties [8]. He proposed that an electrically neutral particle of spin $-\frac{1}{2}$ with negligible mass is created and emitted at the same time as the electron in β^- -decay. Thus, the actual decay process of β^- is $n \to p + e^- + \bar{\nu}_e$ [8]. It means that only a fraction of maximum kinetic energy is taken by e^- and the rest of the kinetic energy is used by antineutrino $(\bar{\nu}_e)$ in the decay process. Since the neutron was found in 1932 by J.Chadwick [6], Fermi used the name "neutrino" (little neutron) and later proposed the Fermi hypothesis of beta decay [9]. The finding of an electron type antineutrino was done by Reines and Cowan in 1956 [10].

In 1957, the first quantum mechanical description of neutrino oscillations was by B. Pon-

¹Note that an isolated neutron is unstable, and so it decays easily, unlike an isolated proton. A proton transforms to a neutron within a nucleus via the β^+ -decay process.

tecorvo [11,12] in which he used an analogy of Kaon oscillations suggested by M.Gell-Mann and A.Pais [13]. In 1959, Pontecorvo proposed the muon neutrino [14] and later, in 1962, the discovery of muon neutrinos were made in the Brookhaven experiment [15]. Neutrinos are produced from a charged lepton or together with a charged antilepton in charged current weak interaction processes. The leptonic charge current generates a superposition of massive neutrinos termed as "flavour state". Oscillations between different flavour states are possible if neutrinos are massive. In 1962, a model describing the mixing of different massive neutrinos in a flavour state was proposed [16]. Pontecorvo in 1967 predicted the Solar Neutrino Problem as a consequence of $\nu_e \to \nu_\mu$ or $\nu_e \to \nu_\tau$ transitions [18] before Homestake experiment [17]. Later, in 1969 Gribov and Pontecorvo discussed solar neutrino oscillations due to neutrino mixing [19]. In the year 2000, tau neutrino ν_{τ} was discovered in DONUT experiment [20]. Finally, the Super-Kamiokande Observatory [21–24] and the Sudbury Neutrino Observatory [25, 26] discovered neutrino oscillations and neutrino mass leading to the 2015 Nobel Prize for Physics. Today, we know neutrinos come in three flavours in the lepton family, electron neutrinos (ν_e) , muon neutrinos (ν_μ) and tau neutrinos (ν_τ) . One strange aspect of neutrinos is that they do not pick just one flavour and stick to it. They oscillate between all three. With time, the probability of finding a given neutrino flavour in another flavour state can be seen experimentally in many ongoing running observatories like CERN, Fermilab and Japan, in particular NOvA and T2K.

In most theories, neutrino oscillation probabilities are derived based on the plane wave approximation, which is strictly valid when the neutrino mass eigenstates composing a given flavour eigenstate either have the same momentum or the same energy [27]. A significant degree of coherence at great lengths is necessary to sustain the oscillations. Given the spatial localisation of neutrinos, a more general wave-packet description should be more appropriate for a complete understanding of neutrino oscillations². Although the plane-wave treatment is a good approximation for neutrino flavour transitions, the wave-packet decoherence and dispersion effects could still be minor corrections to oscillation parameters. In 1981, Kayser discussed quantum mechanical aspects of neutrino oscillations and emphasised the wave packet treatment [28]. However, detailed calculations and experiments (Daya Bay) have shown that the plane wave description fits closely with observations [29, 30]. The fact that neutrino oscillations are coherent over large space-time scales warrants a study of the entanglement properties of neutrinos. Thus, it is intellectually appealing to evaluate how entangled a neutrino system is quantitative. The entanglement of neutrinos, its relation to the mixing probabilities and the somewhat futuristic notion of "Neutrino Quantum Computers"

²The theory of neutrino oscillations using the quantum field theoretical approach is not discussed in this thesis [31–34].

are the impetus for this study. The philosophy is that once we understand our actual limits, we can be free to investigate our imagination.

There are still some unsolved issues, like whether there exist different quantifiers of entanglement to measure quantum entanglement. How do we measure them in the phenomenon of neutrino oscillations? Can we simulate such entanglement measures on a quantum computer? Is there any possibility to investigate neutrino oscillations beyond the qubit dimension? Answers to these questions will play an essential role in exploiting neutrinos as a resource in quantum information processing. In this thesis, we examine these questions by investigating the quantum nature of neutrinos to study the entanglement of the mass eigenstates, simulating entangled oscillating neutrinos on the IBM quantum computer, and mapping three flavour neutrinos to qutrit systems.

In general, we study entanglement with quantum objects called qubits, and a particular superposition of two-qubit is an example of an entangled state. In quantum optics, the Bell's state of two-qubit and the three-qubit GHZ (Greenberger-Horn-Zeilinger) state and W-state are bi-partite and tri-partite entangled states, respectively [35]. These entangled states have several applications in quantum information processing [36–41].

The linear superposition state of two flavours of neutrinos is a two-qubit system. Blasone et al. [42] initiated the study of three-qubit entanglement in three flavour neutrino systems. Alok et al. [43] quantified entanglement measures such as Bell's inequalities in oscillation probabilities. This thesis investigates and quantifies bi-partite and tri-partite entanglement measures of two and three flavour neutrino oscillations. The bi-partite entanglement resembles the entanglement swapping of a beam splitter in quantum optics. The various entanglement measures that we calculate are the concurrence, negativity, and three-tangle for the three neutrino systems. Expressing the monogamy inequality in terms of negativity leads to a residual entanglement, a signature of genuine tripartite entanglement in the three neutrino systems. The three neutrino state is similar to a generalised W-state class in quantum optics. The critical point is that quantification of entanglement measures in terms of neutrino oscillations probabilities simplifies the use of neutrinos for quantum information tasks.

In 2016, the IBMQ team designed cloud-based quantum computers, which are made freely accessible to researchers and scientists online for novel investigations concerning quantum processing [44]. Qubits are the central building blocks on which quantum computers run [45]. The superconducting-qubit-based quantum processors in quantum computers tackle exceptionally significant complex problems which are difficult to address using classical super-

computers. The quantum computing innovations guarantee reform estimations in numerous physics, chemistry, and data science spaces. Considering the ongoing advancement in developing quantum computing facilities dependent on optical and cold-atom techniques, the algorithm for quantum simulations in the particle physics framework is quickly advancing. The principle undertaking of the quantum algorithm is to decompose a quantum operator within the language of quantum gates and circuits acting on qubits. Argüelles and Jones pioneered the simulation of neutrino oscillations on IBMQ processors [46]. In this thesis, we discuss the implementation of bi-partite entanglement in the two-neutrino systems in the vacuum and a uniform matter background on the IBM quantum processor [44]. The novelty of our work is that we found a way to encode the concurrence measure of entangled oscillating neutrinos on a quantum computer. The studies show that quantum computers can simulate the bi-partite entanglement in two flavour neutrinos oscillations.

The application of bipartite entanglement is limited, but entangled states involving more than two qubits (multipartite entanglement) can establish new protocols for quantum communication. This thesis maps the neutrino states to the qutrit states [47], which generalises tripartite entanglement in the three-neutrino system.

1.2 Plane-wave approximation

The theory of neutrino oscillations usually use the plane-wave approximation [48–51]. The three neutrino flavour eigenstates are not neutrino mass eigenstates but a linear superposition of them given by

$$|\nu_{\alpha}\rangle = \sum_{j} U_{\alpha j}^{*} |\nu_{j}\rangle, \qquad (1.1)$$

where, $|\nu_{\alpha}\rangle$ ($\alpha = e, \mu, \tau$) are the flavor eigenstates, $|\nu_{j}\rangle$ (j = 1, 2, 3) are the mass eigenstates and the asterisk (*) denotes the complex conjugation of $U_{\alpha j}$, where $U_{\alpha j}$ are the elements of a leptonic mixing matrix called the PMNS (Pontecorvo-Maki-Nakagawa-Sakita) matrix, characterized by three mixing angles (θ_{12} , θ_{13} , θ_{23}) and a charge conjugation and parity (CP) violating phase δ_{CP} [52,53].

$$\mathbf{U}(\theta_{\mathbf{i}\mathbf{j}}, \delta) = \begin{pmatrix} c_{12}c_{13} & s_{12}c_{13} & s_{13}e^{-i\delta_{CP}} \\ -s_{12}c_{23} - c_{12}s_{13}s_{23}e^{i\delta_{CP}} & c_{12}c_{23} - s_{12}s_{13}s_{23}e^{i\delta_{CP}} & c_{13}s_{23} \\ s_{12}s_{23} - c_{12}s_{13}c_{23}e^{i\delta_{CP}} & -c_{12}s_{23} - s_{12}s_{13}c_{23}e^{i\delta_{CP}} & c_{13}c_{23} \end{pmatrix} \equiv \begin{pmatrix} U_{e1} & U_{e2} & U_{e3} \\ U_{\mu 1} & U_{\mu 2} & U_{\mu 3} \\ U_{\tau 1} & U_{\tau 2} & U_{\tau 3} \end{pmatrix},$$

$$(1.2)$$

where, $c_{ij} = \cos \theta_{ij}$ and $s_{ij} = \sin \theta_{ij}$ (i, j = 1, 2, 3). Further, orthonormal mass eigenstates are chosen such that

$$\langle \nu_j | \nu_k \rangle = \delta_{jk}. \tag{1.3}$$

Thus, $|\nu_j\rangle$ are eigenstates of the Hamiltonian (H) with energy eigenvalues E_j

$$E_j = \sqrt{\vec{p}^2 + m_j^2},\tag{1.4}$$

such that

$$H|\nu_j\rangle = E_j|\nu_j\rangle. \tag{1.5}$$

The Schrodinger equation

$$i\frac{d}{dt}|\nu_j(t)\rangle = H|\nu_j(t)\rangle,$$
 (1.6)

implies that the mass eigenstates states evolve as plane waves with time

$$|\nu_j(t)\rangle = e^{-iE_j t} |\nu_j\rangle. \tag{1.7}$$

Using the unitary transformation relation

$$U^{\dagger}U = \mathbf{1} \leftrightarrow \delta_{\alpha\beta} = \sum_{\alpha} U_{\alpha j}^* U_{\alpha k} = \delta_{jk}, \tag{1.8}$$

the massive neutrino states can be expressed in flavour states as

$$|\nu_j\rangle = \sum_{\alpha} U_{\alpha j} |\nu_{\alpha}\rangle. \tag{1.9}$$

In the plane wave picture, from Eq.(1.1) and Eq.(1.7) the time evolved flavour neutrino state is

$$|\nu_{\alpha}(t)\rangle = \sum_{j} U_{\alpha j}^{*} e^{-iE_{j}t} |\nu_{j}\rangle, \qquad (1.10)$$

in which $|\nu_{\alpha}(t)\rangle$ refers to the state of the neutrino that started out in flavour ν_{α} at t=0. Thus, using Eq.(1.9) in Eq.(1.10), the evolved neutrino flavour state in a coherent superposition of flavour basis can be written as,

$$|\nu_{\alpha}(t)\rangle = \sum_{\beta=e,\mu,\tau} \left(\sum_{j} U_{\alpha j}^{*} e^{-iE_{j}t} U_{\beta j}\right) |\nu_{\beta}\rangle \tag{1.11}$$

where the coefficient of $|\nu_{\beta}\rangle$, $\tilde{U}_{\alpha\beta}(t) \equiv \sum_{j} U_{\alpha j}^{*} e^{-iE_{j}t} U_{\beta j}$ is the amplitude of transition from $|\nu_{\alpha}\rangle$ to $|\nu_{\beta}\rangle$. Consequently, the transition probability $|<\nu_{\beta}|\nu_{\alpha}(t)>|^{2}$ is then $|\tilde{U}_{\alpha\beta}(t)|^{2}$ which is

$$P_{\alpha\beta}(t) = \sum_{jk} U_{\alpha j}^* U_{\beta j} U_{\alpha k} U_{\beta k}^* e^{-i(E_j - E_k)t}.$$
 (1.12)

Taking the universal constant $c = 1, \hbar = 1$, for ultra-relativistic neutrinos, the dispersion relation in Eq.(1.4) can be approximated by

$$E_j \simeq E + \frac{\Delta m_j^2}{2E}.\tag{1.13}$$

In this case,

$$E_j - E_k \simeq \frac{\Delta m_{jk}^2}{2E},\tag{1.14}$$

where $\Delta m_{jk}^2 \equiv m_j^2 - m_k^2$ and $E = |\vec{P}|$ is the energy, neglecting the mass contribution. In experiments, the propagation time t is not measured. The known parameter is the distance L. Since velocity of neutrinos is nearly of light speed, we approximate t = L. The probability of finding flavour neutrino $\beta = (e, \mu, \tau)$ from an initial α neutrino is

$$P_{\alpha\beta}(L,E) = \sum_{j,k} U_{\alpha j}^* U_{\beta j} U_{\alpha k} U_{\beta k}^* e^{(-i\frac{\Delta m_{jk}^2 L}{2E})}.$$
 (1.15)

This expression shows that the source-detector distance L, the mass square difference Δm_{jk}^2 and the neutrino energy E (which varies based on experiments) are the quantities that determine the phases of neutrino oscillations

$$\Phi_{jk} = -\frac{\Delta m_{jk}^2 L}{2E}.\tag{1.16}$$

It is clear that oscillations between different flavours are possible for L>0 because the unitary relation

$$UU^{\dagger} = \mathbf{1} \Leftrightarrow \sum_{i} U_{\alpha j} U_{\beta j}^{*} = \delta_{\alpha \beta}, \tag{1.17}$$

implies that

$$P_{\alpha\beta}(L=0,E) = \delta_{\alpha\beta}.\tag{1.18}$$

Sometimes it is convenient to write the transition probability in Eq.(1.15) as

$$P_{\alpha\beta}(L,E) = \sum_{j} |U_{\alpha j}|^2 |U_{\beta j}|^2 + 2Re \sum_{j>k} U_{\alpha j}^* U_{\beta j} U_{\alpha k} U_{\beta k}^* e^{(-2\pi i \frac{L_{\alpha jc}}{U_{jk}})}, \tag{1.19}$$

in which we have separated a constant term from the oscillating term and we have defined the oscillation lengths

$$L_{jk}^{osc} = \frac{4\pi E}{\Delta m_{jk}^2}. ag{1.20}$$

The oscillation length L_{jk}^{osc} is the length at which the phase generated by Δm_{jk}^2 becomes 2π . Another useful way to write the transition probability in Eq.(1.15) is to separate the real and the imaginary parts of $U_{\beta j}U_{\alpha j}^*U_{\beta k}^*U_{\alpha k}$. From the square of the unitary relation in Eq.(1.17), we obtain

$$\sum_{j} |U_{\alpha j}|^2 |U_{\beta j}|^2 = \delta_{\alpha \beta} - 2 \sum_{j>k} Re[U_{\alpha j}^* U_{\beta j} U_{\alpha k} U_{\beta k}^*], \tag{1.21}$$

which allows one to write the transition probability as

$$P_{\alpha\beta}(L,E) = \delta_{\alpha\beta} - 4\sum_{j>k} Re(U_{\alpha j}^* U_{\beta j} U_{\alpha k} U_{\beta k}^*) \sin^2\left(\Delta m_{jk}^2 \frac{L}{4E}\right)$$
$$+2\sum_{j>k} Im(U_{\alpha j}^* U_{\beta j} U_{\alpha k} U_{\beta k}^*) \sin\left(\Delta m_{jk}^2 \frac{L}{2E}\right). \tag{1.22}$$

In the neutrino oscillation experiments, the transition probability of the channel with $\alpha \neq \beta$ is the usual disappearance probability (P_d) , whereas the transition probability of the channels with $\alpha = \beta$ is the survival probability (P_s) . The survival probability is

$$P_{\alpha\alpha}(L,E) = |\tilde{U}_{\alpha\alpha}(t)|^2 = 1 - 4\sum_{i>k} |U_{\alpha_i}|^2 |U_{\alpha_k}|^2 \sin^2(\frac{\Delta m_{jk}^2 L}{4E}). \tag{1.23}$$

In order to analyze the experimental data of neutrino oscillations, we write the oscillatory term as

$$\sin^2(\frac{\Delta m_{jk}^2 L}{4E}) = \sin^2(1.27 \frac{\Delta m_{jk}^2 (eV^2) L(km)}{4E(GeV)}). \tag{1.24}$$

The factor of 1.27 stems from the conversion between the different units. Eq.(1.22) and Eq.(1.23) is still the general case that applies for any number of generations. The following subsection derives flavour oscillation probabilities in a vacuum for two and three generations

of neutrinos.

1.2.1 Two-flavour neutrino oscillations

We consider the oscillation between two flavour neutrinos for e.g., (ν_e, ν_μ) in which ν_1 and ν_2 are mass eigenstates of neutrinos. In this case the PMNS matrix in Eq.(1.2) is a 2x2 unitary rotation mixing matrix

$$U(\theta) = \begin{pmatrix} \cos\theta & \sin\theta \\ -\sin\theta & \cos\theta \end{pmatrix}. \tag{1.25}$$

Thus, using Eq.(1.1), the unitary matrix U connect flavour state to mass eigenstate as

$$\begin{pmatrix} \nu_e \\ \nu_\mu \end{pmatrix} = U^*(\theta) \begin{pmatrix} \nu_1 \\ \nu_2 \end{pmatrix} \tag{1.26}$$

Using Eq.(1.9), the neutrino mass eigenstates in linear superposition of flavour basis can be written as

$$|\nu_1\rangle = \cos\theta |\nu_e\rangle + \sin\theta |\nu_\mu\rangle$$
 (1.27)

$$|\nu_2\rangle = -\sin\theta |\nu_e\rangle + \cos\theta |\nu_\mu\rangle \tag{1.28}$$

Using Eq.(1.10), the time evolved neutrino flavour state in a linear superposition of mass basis can be written as

$$|\nu_e(t)\rangle = \cos\theta e^{-iE_1 t} |\nu_1\rangle - \sin\theta e^{-E_2 t} |\nu_2\rangle$$
 (1.29)

$$|\nu_{\mu}(t)\rangle = \sin\theta e^{-iE_1 t} |\nu_1\rangle + \cos\theta e^{-E_2 t} |\nu_2\rangle \tag{1.30}$$

Substituting Eq.(1.27) in the Eq.(1.29), the time evolved electron neutrino flavour state in flavour basis is

$$|\nu_{e}(t)\rangle = \cos\theta e^{-iE_{1}t}(\cos\theta |\nu_{e}\rangle + \sin\theta |\nu_{\mu}\rangle) + -\sin\theta e^{-E_{2}t}(-\sin\theta |\nu_{e}\rangle + \cos\theta |\nu_{\mu}\rangle,$$

$$= (\cos^{2}\theta e^{-iE_{1}t} + \sin^{2}\theta e^{-iE_{2}t}) |\nu_{e}\rangle + \sin\theta \cos\theta (e^{-iE_{1}t} - e^{-iE_{2}t}) |\nu_{\mu}\rangle. \quad (1.31)$$

Since neutrinos are ultra-relativistic particles ($t \simeq L$), therefore the standard transition probabilities are

$$P_d = \langle \nu_{\mu} | \nu_e(L) |^2 = \sin^2(2\theta) \sin^2(1.27 \frac{\Delta m_{21}^2 (eV^2) L(km)}{4E(GeV)}), \quad (\alpha \neq \beta),$$
 (1.32)

and

$$P_s = \langle \nu_e | \nu_e(L) |^2 = 1 - P_d, \quad (\alpha = \beta).$$
 (1.33)

We can observe from Eq.(1.32) and Eq.(1.33) that the probability of the presence of neutrino in the state $|\nu_{\mu}\rangle$ and $|\nu_{e}\rangle$ is maximal and minimal, respectively, at the distance $\frac{L_{osc}}{2} = \frac{1}{1.27}(\frac{2\pi E}{\Delta m_{21}^2})$, where $\Delta m_{21}^2 = m_2^2 - m_1^2$. The amplitude of the oscillation is determined by the mixing angle θ , where $\theta = \frac{\pi}{4}$ corresponds to maximal oscillations. Note that Eq.(1.32) and Eq.(1.33) does not depend on L and E independently, but only on the ratio $\frac{L}{E}$. Using Eq.(1.6), the evolution equation of the mass eigenstates ν_1 and ν_2 are

$$i\frac{d}{dt} \begin{pmatrix} \nu_1(t) \\ \nu_2(t) \end{pmatrix} = H \begin{pmatrix} \nu_1(t) \\ \nu_2(t) \end{pmatrix}. \tag{1.34}$$

Using the approximated expression Eq.(1.13), the Hamiltonian H in diagonal matrix form can be written as

$$H = \begin{pmatrix} E_1 & 0 \\ 0 & E_2 \end{pmatrix} \simeq E + \begin{pmatrix} m_1^2/2E & 0 \\ 0 & m_2^2/2E \end{pmatrix}. \tag{1.35}$$

Recalling Eq.(1.26), we can rewrite Eq.(1.34) as

$$i\frac{d}{dt} \begin{pmatrix} \nu_e \\ \nu_\mu \end{pmatrix} = H_{vac} \begin{pmatrix} \nu_e \\ \nu_\mu \end{pmatrix}, \tag{1.36}$$

where

$$H_{vac} = UHU^{\dagger} = E + \frac{m_1^2 + m_2^2}{4E} + \frac{\Delta m^2}{4E} \begin{pmatrix} -\cos 2\theta & \sin 2\theta \\ \sin 2\theta & \cos 2\theta \end{pmatrix}, \tag{1.37}$$

It is a Hamiltonian of flavour eigenstate on a mass basis in a vacuum. In the later section (see Subsec.(1.2.3)), we use this Hamiltonian to generalise the neutrino oscillation in the matter.

1.2.2 Three-flavour neutrino oscillations

For simple calculation, we assume the CP conserving case, when the PMNS matrix U is real i.e., $\delta_{CP} = 0$. Thus, Eq.(1.2) become

$$\mathbf{U}(\theta_{ij}) = \begin{pmatrix} c_{12}c_{13} & s_{12}c_{13} & s_{13} \\ -s_{12}c_{23} - c_{12}s_{13}s_{23} & c_{12}c_{23} - s_{12}s_{13}s_{23} & c_{13}s_{23} \\ s_{12}s_{23} - c_{12}s_{13}c_{23} & -c_{12}s_{23} - s_{12}s_{13}c_{23} & c_{13}c_{23} \end{pmatrix}.$$
(1.38)

In this case the transition probability in Eq.(1.22) i.e, $P_{\alpha\beta}$ is dependent on the three mixing angles and two independent squared-mass differences which is written as Δm_{21}^2 and Δm_{31}^2 , then $\Delta m_{32}^2 = \Delta m_{31}^2 - \Delta m_{21}^2$. We consider a case where the mass squared differences are minimal, such that

$$\frac{\Delta m_{21}^2 L}{2E} << 1. (1.39)$$

Neglecting mass square difference, we get $\Delta m_{31}^2 = \Delta m_{32}^2$. Thus, using Eq.(1.38) in Eq.(1.11) and following Eq.(1.23), the survival probability of the three flavour neutrino oscillations is reduced to

$$P_s = 1 - \sin^2(2\theta_{13})\sin^2(1.27 \frac{\Delta m_{32}^2(eV^2)L(km)}{4E(GeV)}). \tag{1.40}$$

This equation is similar to the two flavour survival probability with terms θ_{21} and Δm_{21}^2 in Eq.(1.33) is replaced by θ_{13} and Δm_{32}^2 , respectively. We observe from Eq.(1.22) and Eq.(1.23) that the transition probabilities depend on seven independent parameters ³ i.e., three mixing angles, two mass-squared differences, distance, and energy. The allowed ranges of these parameters are obtained by global fit to the accelerator, reactor, atmospheric and solar neutrino data. Under these neutrino oscillation experiments, for $m_1 < m_2 < m_3$ (normal hierarchy), the 3σ range best-fit values are listed in Table.(1.1). In the later chapter of this thesis, we will use the data of Table.(1.1) to plot graphs.

Parameters	Best fit $\pm 1\sigma$	3σ range
$\frac{\Delta m_{21}^2}{10^{-5} eV^2}$	$7.42^{+0.21}_{-0.20}$	$6.82 \to 8.04$
$ \begin{array}{c} 10^{-5} eV^{2} \\ \Delta m_{31}^{2} \\ 10^{-3} eV^{2} \end{array} $	$2.514^{+0.028}_{-0.0.027}$	$2.431 \to 2.598$
$\theta_{12}(\deg)$	$33.44^{+0.78}_{-0.75}$	$31.27 \to 35.86$
$\theta_{23}(\deg)$	$49.0^{+1.1}_{-1.4}$	$39.6 \rightarrow 51.8$
$\theta_{13}(\deg)$	$8.57^{+0.13}_{-0.12}$	$8.20 \to 8.97$

Table 1.1: The neutrino mixing parameters in normal ordering $(m_1 < m_2 < m_3)$ from the NuFIT data [54].

1.2.3 Neutrino oscillations in constant matter background

In 1978, L. Wolfenstein [55] and other authors in the early 1980s [56] studied neutrino propagation in a medium with constant matter density. The effective Hamiltonian which governs

³Is neutrino a Dirac fermion or a Majorana fermion? Apart from one CP-violation phases in PMNS matrix of Dirac neutrinos (see Eq.(1.2)), there exist two Majorana phases if we consider neutrinos as Majorana fermion. However, neutrino transition probabilities are independent of Majorana phases.

the propagation of neutrino flavour state in matter is

$$H_{eff} = H_{Vac} + H_{mat}, (1.41)$$

$$H_{vac} = \frac{1}{2E} U \begin{pmatrix} m_1^2 & 0 & 0\\ 0 & m_2^2 & 0\\ 0 & 0 & m_3^2 \end{pmatrix} U^{\dagger}; \quad H_{mat} = \sqrt{2} G_F N_e \begin{pmatrix} 1 & 0 & 0\\ 0 & 0 & 0\\ 0 & 0 & 0 \end{pmatrix}, \tag{1.42}$$

where U is given in Eq.(1.2), N_e is the electron number density and G_F is the Fermi constant. For the two-flavour neutrino evolution equation in flavour basis, (for e.g., ν_e and ν_μ), the effective Hamiltonian is

$$H_{eff} = \frac{1}{2E} \left[U \begin{pmatrix} m_1^2 & 0 \\ 0 & m_2^2 \end{pmatrix} U^{\dagger} + \begin{pmatrix} \frac{A}{2} & 0 \\ 0 & -\frac{A}{2} \end{pmatrix} \right], \tag{1.43}$$

$$=H_{vac}+H_{mat}, (1.44)$$

such that

$$i\frac{d}{dt} \begin{pmatrix} \nu_e \\ \nu_\mu \end{pmatrix} = H_{eff} \begin{pmatrix} \nu_e \\ \nu_\mu \end{pmatrix}, \tag{1.45}$$

where, $A = 2\sqrt{2}EG_FN_e$ is the constant effective matter potential induced by ordinary charge-current (contribution from W Boson exchange) weak interactions with electrons; $U = \begin{pmatrix} \cos\theta & \sin\theta \\ -\sin\theta & \cos\theta \end{pmatrix}$ is a two-flavour mixing matrix in vacuum. By using the approximated value H_{vac} of Eq.(1.37) (by neglecting the terms proportional to the unit matrix) in Eq.(1.43), the effective Hamiltonian in symmetric form can be obtained as [57]

$$H_{eff} = \frac{1}{4E} \begin{pmatrix} -\Delta m^2 cos 2\theta + \frac{A}{2} & \Delta m^2 sin 2\theta \\ \Delta m^2 sin 2\theta & \Delta m^2 cos 2\theta - \frac{A}{2} \end{pmatrix}, \tag{1.46}$$

where $\Delta m^2 = m_2^2 - m_1^2$ and θ is the mixing angle parameters in vacuum. This H_{eff} matrix is diagonalized by the unitary transformation,

$$U_M^T H_{eff} U_M = H_M, (1.47)$$

where, $H_M=\frac{1}{4E}\begin{pmatrix} -\Delta m_M^2 & 0 \\ 0 & \Delta m_M^2 \end{pmatrix}$ is the effective matrix in the mass basis in matter. The unitary matrix

$$U_M = \begin{pmatrix} \cos\theta_M & \sin\theta_M \\ -\sin\theta_M & \cos\theta_M \end{pmatrix}, \tag{1.48}$$

is the effective mixing matrix in matter. Thus, using Eq.(1.45) and following Eq.(1.23), the two flavour neutrino survival probability in matter can be obtained from as

$$P_s = 1 - \sin^2(2\theta_M)\sin^2(1.27 \frac{\Delta m_M^2 (eV^2)L(km)}{4E(GeV)}), \tag{1.49}$$

where θ_M and Δm_M^2 are the effective neutrino oscillations in matter. The relation between the vacuum neutrino oscillations parameters and effective neutrino oscillations parameters are

$$\Delta m_M^2 = \sqrt{[\Delta m^2 cos(2\theta) - A]^2 + [\Delta m^2 sin(2\theta)]^2},$$
(1.50)

$$sin^2 2\theta_M = \frac{(\Delta m^2 sin 2\theta)^2}{(\Delta m^2 cos 2\theta - A)^2 + (\Delta m^2 Sin 2\theta)^2}.$$
 (1.51)

By comparing Eq.(1.49) with Eq.(1.33), we can say that the two flavour neutrino oscillations in vacuum is modified due to constant matter effect. At the resonance,

$$A^R = \Delta m^2 Cos2\theta, \tag{1.52}$$

the electron number density is given by

$$N_e^R = \frac{\Delta m^2 Cos2\theta}{2\sqrt{2}EG_F}. (1.53)$$

Although θ is small, at $\theta_M = \frac{\pi}{4}$ the transition from ν_e and ν_μ mix maximally. This is called resonance condition. The possibility of resonant flavour transitions of neutrinos travelling in a medium with varying matter potential was discovered in 1985 [58, 59]. The MSW (Mikheeev-Smirnov-Wolfenstein) mechanism specifies the region along the neutrino path in which the maximum mixing angle is $\frac{\pi}{4}$ and this could explain the flavour transition of solar neutrinos during their propagation out of the Sun, even in the case of small θ [60]. The developments and concepts behind the MSW effect in 1978-85 are described recently by A. Yu. Smirnov [61].

1.2.4 Same energy and same momentum approach in neutrino oscillations

In Sec.(1.2), in the plane wave picture, when neutrinos propagate in time, the mass eigenstates ν_j gets associate with the phase factor $e^{i\phi_j}$. In general, this phase factor depends on

both space and time and is defined as

$$\phi_i = E_j t - \vec{p_j} \cdot \vec{x}. \tag{1.54}$$

In order to calculate the disappearance $P_{\alpha\beta}$ (see Eq.(1.22)) or survival $P_{\alpha\beta}$ (see Eq.(1.23)) probabilities, we need to calculate the phase differences between different mass eigenstates i.e., (the oscillation phases) $\Delta\phi_{jk}$:

$$\Delta \phi = \Delta E.t - \Delta \vec{p}.\vec{x}. \tag{1.55}$$

Here, the subscripts jk are omitted from $\Delta\phi$, ΔE and $\Delta\vec{p}$ in order to simplify the notation. Different neutrino mass eigenstates composing a given flavour state cannot simultaneously have the same energy and momentum, as otherwise, they would have the same mass. Therefore in many studies, two simplified approaches were adopted:

• Same momentum approach: Assuming the momentum of all the mass eiegenstate are same, i.e, $\Delta \vec{p} = 0$. Then, Eq.(1.55) gives $\Delta \phi = \Delta E.t$ and transition probabilities Eq.(1.22) depends only on the evolution time t. Since for ultra-relativistic neutrinos $E_j = \sqrt{\vec{p}^2 + m_j^2} \simeq p + \frac{m_j^2}{2p}$, for the oscillation phase one finds

$$\Delta \phi = \Delta E.t \simeq \frac{\Delta m^2}{2p}t,\tag{1.56}$$

with the approximation⁴ of $t \simeq L$, Eq.(1.56) yields the usual oscillation phase which leads to the standard transition probability Eq.(1.22).

• Same energy approach: Assuming the energy of all mass eigennstates same, $\Delta E = 0$, then Eq.(1.55) gives $\Delta \phi = -\Delta \vec{p}.\vec{x}$. When L is large, we can assume that \vec{x} is parallel to momentum \vec{p} ($\vec{x}||\vec{p}$). For ultra-relativistic neutrinos, $p_j = \sqrt{E^2 - m_j^2} \simeq E - \frac{m_j^2}{2E}$, and the oscillation phase Eq.(1.55) become

$$\Delta \phi = -\Delta p.L \simeq \frac{\Delta m^2}{2E} L. \tag{1.57}$$

The resulting transition probability is again the same Eq.(1.22).

⁴Note that for supernova and solar neutrinos, the approximation $t \simeq L$ is no longer justified [28, 64].

It is to be noted that by assuming the mass eigenstates to have the same momentum or same energy, the neutrino transition probabilities $P_{\alpha\beta}$ (Eq.(1.22) or $P_{\alpha\alpha}$ (Eq.(1.23)) in-plane wave picture does not change. This assumption shows that this model is inconsistent because plane waves are completely delocalised in space. These assumptions contradict energy-momentum conservation. In ref. [62], R. G. Winter considered neutrino emission in orbital electron capture by nuclei, a process with a 2-body final state and simple kinematics. Another process with a 2-body final form -charged pion decay- was discussed by Giunti and Kim [63]. Let us follow their argument, for a $\pi \to \mu\nu$ decay at rest, E_j and p_j of the produced neutrino mass eigenstates ν_j with mass m_j is obtained from the 4-momentum conservation law as

$$E_j^2 = \frac{m_\pi^2}{4} \left(1 - \frac{m_\mu^2}{m_\pi^2}\right)^2 + \frac{m_j^2}{2} \left(1 - \frac{m_\mu^2}{m_\pi^2}\right) + \frac{m_j^4}{4m_\pi^2},\tag{1.58}$$

$$p_j^2 = \frac{m_\pi^2}{4} (1 - \frac{m_\mu^2}{m_\pi^2})^2 - \frac{m_j^2}{2} (1 + \frac{m_\mu^2}{m_\pi^2}) + \frac{m_j^4}{4m_\pi^2},\tag{1.59}$$

Neglecting terms of order m_i^4 , one finds

$$E_j \simeq E + \xi \frac{m_j^2}{2E}, \quad p_j \simeq E - (1 - \xi) \frac{m_j^2}{2E},$$
 (1.60)

where

$$E \equiv \frac{m_{\pi}}{2} (1 - \frac{m_{\mu}^2}{m_{\pi}^2}) \simeq 30 Mev, \quad \xi \equiv \frac{1}{2} (1 - \frac{m_{\mu}^2}{m_{\pi}^2}) \simeq 0.2.$$
 (1.61)

As seen from Eq.(1.61), the same energy and momentum assumptions correspond to $\xi = 0$ and $\xi = 1$, respectively; in reality, however, ξ is neither 0 nor 1 but somewhere between 0 to 1, i.e., 0.2. Thus, an explanation of neutrino oscillations using the wave packet approach is needed.

1.3 The wave-packet description of neutrino oscillations

In 1976, Nussinov used the wave-packet approach of oscillating neutrinos and showed a coherence length [64]. He suggested that the wave packets corresponding to different mass eigenstates propagate at varying velocities, so they do not overlap anymore after a while. Thus, beyond the coherence length, one would not see the interference of different massive

neutrinos as they would lose coherence [65]. In 1981, Kayser discussed the issues of neutrino oscillations in quantum mechanics and the need for the wave-packet approach [28]. In 1998, Carlo and Kim used the Gaussian wave packets to calculate the flavour changing probability by incorporating the temporal and spatial coherence widths of the detection process [66]. In 2003, Carlo Giunti used the density matrix formalism to describe wave-packet of neutrino oscillations in stationary beam and disproved the requirement of equal energy or equal momentum of different massive neutrinos [67]. The analysis in this paper is as follows:

Let us rewrite Eq.(1.1) by associating the mass eigenstates ν_j with wave function $\psi_j(x,t)$ such that

$$|\nu_{\alpha}(x,t)\rangle = \sum U_{\alpha j}^* \psi_j(x,t) |\nu_j\rangle. \tag{1.62}$$

Using the Fourier transformation, we can relate this wave function $\psi_j(x,t)$ with a Gaussian wave $\psi_j(p)$ for the momentum distribution of the massive neutrino ν_j with mass m_j as

$$\psi_j(x,t) = \frac{1}{\sqrt{2\pi}} \int dp \psi_j(p) e^{i(px - E_j(p)t)}, \qquad (1.63)$$

where

$$\psi_j(p) = \frac{1}{(2\pi\sigma_p^{P^2})^{\frac{1}{4}}} e^{-\frac{(p-p_j)^2}{4\sigma_p^{P^2}}}.$$
(1.64)

Here, the momentum uncertainty σ_p^P is obtained from the production process with p_j and $E_j(p) = \sqrt{p^2 + m_j^2}$ as average momentum and energy, respectively.

In order to get the solution of Eq.(1.63) analytically, the Gaussian momentum distribution is taken, Eq.(1.64), which shows sharp peak around the average momentum p_j , satisfying the condition $\sigma_p^P \ll E_j^2(p_j)/m_j$. Thus, approximated energy is

$$E_j(p) \simeq E_j + v_j(p - p_j), \tag{1.65}$$

where average energy is $E_j = \sqrt{p_j^2 + m_j^2}$ and group velocity of wave packet of massive neutrinos ν_j is $v_j = \frac{\partial E_j(p)}{\partial p}|_{P=P_j} = \frac{p_j}{E_j}$. By solving the integration over p of Eq.(1.63) using the above approximation, we find that the solution is Gaussian as

$$\psi_j(x,t) = \frac{1}{(2\pi\sigma_x^{P^2})^{\frac{1}{4}}} e^{-iE_j t + ip_j x - \frac{(x - v_j t)^2}{4\sigma_x^{P^2}}},$$
(1.66)

where $\sigma_x^P = \frac{1}{2\sigma_p^P}$ is the wave packet width in space. We observe that Eq.(1.62) is a pure

state, therefore we construct the density matrix operator

$$\rho_{\alpha}(x,t) = |\nu_{\alpha}(x,t)\rangle \langle \nu_{\alpha}(x,t)|. \tag{1.67}$$

On substituting Eq.(1.66) in Eq.(1.62) and then using it in Eq.(1.67), the density operator which depends on both space and time is

$$\rho_{\alpha}(x,t) = \frac{1}{\sqrt{2\pi\sigma_{x}^{P^{2}}}} \sum_{jk} U_{\alpha j}^{*} U_{\alpha k} e^{[-i(E_{j}-E_{k})t+i(p_{j}-p_{k})x-(x-v_{j}t)^{2}/4\sigma_{x}^{P^{2}}-(x-v_{k}t)/4\sigma_{x}^{P^{2}}]} |\nu_{j}\rangle \langle \nu_{k}|.$$
(1.68)

By applying the Gaussian time integration we get $\rho_{\alpha}(x)$ (relevant density operator) as

$$\rho_{\alpha}(x) = \sum_{j,k} U_{\alpha j}^* U_{\alpha k} e^{\left\{-i\left[\frac{v_j + v_k}{v_j^2 + v_k^2} (E_j - E_k) - (p_j - p_k)\right]x - \frac{(v_j - v_k)^2 x^2}{4(v_j^2 + v_k^2)\sigma_x^{P^2}} - \frac{(E_j - E_k)^2}{4(v_j^2 + v_k^2)\sigma_p^{P^2}}\right\}} |\nu_j\rangle \langle \nu_k|.$$
 (1.69)

Thus, in Eq.(1.69) the density matrix of a stationary beam in neutrino oscillations is independent of time. To find the flavour transition probability, we use the ultra-relativistic neutrinos which approximates $E_j \simeq E + \xi_P \frac{m_j^2}{2E}$, where massless neutrino energy is E, the dimensionless quantity dependent on the features of the production process is ξ_p , $p_j \simeq E - (1 - \xi_P) \frac{m_j^2}{2E}$ and $v_j \simeq 1 - \frac{m_j^2}{2E_i^2}$. Considering these approximations, $\rho_{\alpha}(x)$ becomes

$$\rho_{\alpha}(x) = \sum_{j,k} U_{\alpha j}^* U_{\alpha k} e^{\left[-i\frac{\Delta m_{jk}^2 x}{2E} - \left(\frac{\Delta m_{jk}^2 x}{4\sqrt{2}E^2\sigma_x^P}\right)^2 - \left(\xi_P \frac{\Delta m_{jk}^2}{4\sqrt{2}E\sigma_p^P}\right)^2\right]} |\nu_j\rangle \langle \nu_k|, \tag{1.70}$$

where $\Delta m_{jk}^2 = m_j^2 - m_k^2$. To detect β flavour neutrino at distance L, we define an operator $\mathcal{O}(x-L)$ of flavour β in an analogy with the production process such that

$$\mathcal{O}_{\beta}(x-L) = \sum_{j,k} U_{\beta j}^* U_{\beta k} e^{\left[-i\frac{\Delta m_{jk}^2(x-L)}{2E} - (\frac{\Delta m_{jk}^2(x-L)}{4\sqrt{2}E^2\sigma_x^D})^2 - (\xi_D \frac{\Delta m_{jk}^2}{4\sqrt{2}E\sigma_p^D})^2\right]} |\nu_j > < \nu_k|. \tag{1.71}$$

The probability of transitions from ν_{α} to ν_{β} is

$$P_{\nu_{\alpha}\to\nu_{\beta}}(L) = Tr(\rho_{\alpha(x)}\mathcal{O}_{\beta}(x-L)) = \int dx \sum_{j} \langle \nu_{j} | \rho_{\alpha}(x)\mathcal{O}_{\beta}(x-L) | \nu_{j} \rangle, \qquad (1.72)$$

$$= \sum_{jk} U_{\alpha j}^* U_{\alpha k} U_{\beta j}^* U_{\beta k} e^{\left[-2\pi i \frac{L}{L_{jk}^{osc}} - \left(\frac{L}{L_{jk}^{coh}}\right)^2 - 2\pi^2 (1-\xi)^2 \left(\frac{\sigma_x}{L_{jk}^{osc}}\right)^2\right]}, \tag{1.73}$$

where L_{jk}^{osc} is the oscillation length and the $L_{jk}^{coh} = \frac{4\sqrt{2}E^2}{|\Delta m_{jk}^2|}\sigma_x$ is the coherence length, defined by

$$L_{jk}^{osc} = \frac{4\pi E}{\Delta m_{jk}^2}, \quad L_{jk}^{coh} = \frac{4\sqrt{2}E^2}{|\Delta m_{jk}^2|}\sigma_x,$$
 (1.74)

with $\sigma_x^2 = \sigma_x^{P^2} + \sigma_x^{D^2}$ and $\xi^2 \sigma_x^2 = \xi_P^2 \sigma_x^{P^2} + \xi_D^2 \sigma_x^{D^2}$, where $\sigma_x^D = \frac{1}{2\sigma_p^D}$ is the detection process uncertainty and ξ_D (dimensionless quantity) dependent on the features of the detection process. The three exponential factors in the Eq.(1.73) are the phase factor $(e^{-2\pi i \frac{L}{L_{osc}^{osc}}})$, the coherence term $(e^{-(\frac{L}{L_{osc}^{coh}})})$, and the localisation term $(e^{-2\pi^2(1-\xi)^2(\frac{\sigma_x}{L_{osc}^{osc}})^2})$. The localisation term suppresses the oscillation if $\sigma_x >> L_{jk}^{osc}$. We can ignore this term because in usual experiments this condition is very well satisfied. Therefore, we use the effective probability

$$P_{\nu_{\alpha} \to \nu_{\beta}} = \sum_{jk} U_{\alpha j}^* U_{\alpha k} U_{\beta j}^* U_{\beta k} e^{\left[-2\pi i \frac{L}{L_{jk}^{osc}} - \left(\frac{L}{L_{jk}^{coh}}\right)^2\right]}.$$
 (1.75)

We notice that the wave packet approach affirms the standard plane-wave approximated oscillation length L_{jk}^{osc} . Beyond the coherence length, L_{jk}^{coh} the interference between the massive neutrinos is impossible. The reason is that the wave packet cannot be absorbed coherently because of its significant separation during its arrival at the detector. If $L \ll L_{jk}^{coh}$, the coherence condition is satisfied, and the effective probability Eq.(1.75) reduces to the standard transition probability Eq.(1.19) (or Eq.(1.22)) in the plane-wave picture. We present a chapter-wise description of the thesis in the next section at this juncture.

1.4 Outline of thesis

Chapter 2 of the thesis explores the meaning of two and three-qubit entangled quantum systems in detail. A density matrix formalism review helped us characterise the bi-partite and tri-partite entanglement for two and three-qubit quantum systems. Considering two-qubit Bell's state, we investigate bi-partite entanglement measures like the Positive Partial Transpose (PPT) criterion, negativity, the entanglement of formation, concurrence, tangle, and linear entropy [68–71]. Further, considering prototype three-qubit GHZ and W-state, we evaluate two different tri-partite entanglement measures: three-tangle [72] and three- π [35].

In three flavour neutrino oscillations, the neutrino state is $|\nu(t)\rangle = a |100\rangle + b |010\rangle + c |001\rangle$,

which is the "generic form" of the W-class of states in quantum information theory. In Chapter 3, we have asserted this by examining entanglement measures discussed in chapter 2. Our investigations show that the three-neutrino state has, for sure, genuine tripartite entanglement more similar to the W-state than the GHZ-state.

Presently, analogues of a quantum system can be encoded coherently in a quantum computer. The first step in this direction is to express the building blocks of a known physical system in terms of the language of quantum gates and circuits. Chapter 4 is devoted to the formalism of quantum computing [44]. We have geometrically explained the qubit structure and defined a few quantum gates of single-qubit and two-qubits. We analyse the universal quantum gates U3 and other unitary quantum gates, enabling us to create the prototype GHZ and W-state quantum circuits in Bell's state. We also explored the simulation of these circuits on an IBMQ cloud computer. Further, we propose a quantum circuit to simulate the entanglement measure-concurrence of a two-qubit arbitrary pure state on the IBM quantum cloud computer.

Chapter 5 quantifies two entanglement measures such as concurrence [70] and l_1 norm of coherence [73] in the two neutrino systems and finds their relation. The construction of the SU(2) rotation matrix from the Universal quantum gate U3 is encoded on the IBMQ platform. Using the unitary quantum gates and circuits of chapter 4, we find a way to simulate the bi-partite entanglement of two neutrino systems in the vacuum and the constant matter background on the IBM quantum computer.

In Chapter 6, we started our calculation from the SU(2) Pauli matrices and SU(3) Gell-Mann matrices to develop Poincaré sphere representation for two and three-flavour neutrino states that describes entanglement of neutrino and also map the neutrino states to the qutrit states of quantum information theory. This enables us to generalise the concept of tripartite entanglement in the three-neutrino system. We extend our discussion to construct the Bloch matrix and Generalised matrix for the two-qubit and two-qutrit neutrino states. Finally, we quantify and compare the measures of bi-partite qubit entanglement with bi-partite qutrit entanglement in the two neutrino systems.

Chapter 7 starts with some experimental evidence of neutrino entanglement and presents the conclusion of the thesis. This chapter also discusses the future perspective of quantum aspects of oscillatory neutrinos using the wave-packet approach. In addition to entanglement, coherence is an essential topic globally. Besides the local level, coherence in neutrinos also occurs at an astronomical level like Supernova. A global-scale neutrino usually maintains coherence, meaning that the wave-packet size is small and neutrinos do not decohere over

large distances. We present some preliminary work in this direction with the intention of future exploration.

Chapter 2

Theory of distributed entanglement

In 1935, the EPR (Einstein, Podolsky, and Rosen) paradox of quantum mechanics was developed in which they have addressed the issue that the principle of locality and reality can't be violated in quantum regimes [74]. To explain this, a hybrid quantum system of particles A and B is taken with the system's total spin as zero. Suppose particles A and B are separated on a certain axis in millions of light-years, and they are in a superposition state. If the spin of the first particle A is measured up spin on that axis, then the measured spin of B will be off down spin on the same axis. Thus, measurement done on the first particle A depends on the outcome of the second particle B. Einstein, and others disagreed with this result because the event at one point can't have immediate effect at other points as some field should mediate the action otherwise the information would travel faster than the light speed. In fact, in their paradox, they argued that any property measurement on a particle changes the original quantum state and, therefore, certain quantum effects contradicts the theory of relativity. They called it "spooky action at a distance" and suggested that the acknowledged definition of quantum mechanics is incomplete. They said there must be some hidden variable in the quantum mechanical description that may be responsible for such effect and proposed Hidden Variable Theory. Later, Schrödinger published a paper expressing the idea of "entanglement" [75].

In 1964, John Stewart Bell proposed that no hidden variable theory can produce predictions in quantum mechanics [76]. He introduced inequalities assuming local realism. By many quantum systems, Bell's inequalities were violated experimentally [77]. The EPR paradox is now the basis for defining entanglement, which show the correlation between non-classical particles. Bell's work introduced correlations as a resource of quantum information.

In recent times the study of entanglement is now turned into a fundamental asset in quantum information science, which is the investigation of cutting edge computation and communication dependent on the laws of quantum mechanics [45, 78, 79]. Accordingly, its quantification has attracted much consideration in the twenty recent years [80]. To accomplish such quantification, one has to define legitimate measures of entanglement.

The current notable bi-partite measures of two-qubit entanglement are the concurrence and the tangle derived analytically by Wooters et al. [70,72]. The entanglement of formation is a function of the concurrence and tangle that is monotonical [81,82]. One more valuable entanglement measure is Negativity [83], viewed as a quantitative adaptation of Peres' criterion for separability. Moreover, the linear entropy can also quantify bi-partite entanglement, which is a lower approximation of the von Neumann entropy [84]. The study of all these bi-partite entanglement measures is necessary because they are entanglement monotones. Therefore they can enter into the fundamental monogamy inequalities for distributed entanglement in the multi-partite setting [85]. Multi-partite entanglement is an essential aspect in large scale quantum-information processing [86]. Presently, the widely used basis for characterizing and quantifying tri-partite entanglement in a three-qubit system are the three-tangle [72], and three-pi [35].

The chapter's organization is: In Sec.(2.1), we briefly discuss the one qubit system, and in Sec.(2.2), density operator formalism is given. Considering two-qubit Bell's state, we investigated bi-partite entanglement and explored its various entanglement measures in Sec.(2.3). Further in Sec.(2.4), we evaluate tri-partite entanglement measures in the three-qubit system.

2.1 The Qubit

Classical communication theory is based on bits that are described by 0 or 1. In quantum mechanics, the corresponding quantity is called a qubit. The quantum mechanical laws permit a qubit to truly exist in any linear combinations of the states $|0\rangle$ and $|1\rangle$, and mathematically it is given by

$$|\psi\rangle = c_1 |0\rangle + c_2 |1\rangle, \qquad (2.1)$$

where c_1 and c_2 are complex numbers such that $|c_1|^2 + |c_2|^2 = 1$. A qubit lies in a 2-dimensional complex Hilbert space where a possible orthonormal basis of this qubit are two orthonormal vectors $|0\rangle = \begin{pmatrix} 1 \\ 0 \end{pmatrix}$ and $|1\rangle = \begin{pmatrix} 0 \\ 1 \end{pmatrix}$. Qubits are used in atoms and photons, superconducting circuits and semiconductor quantum dots, and super-fast computing appli-

cations or fundamentally secure communication. A detailed explanation of qubits is given in chapter 4.

2.2 Density operator

In finite-dimensional systems, the density matrix ρ is a mathematical representation of the state of a quantum system which is $n \times n$ matrix constrained by the hermiticity, positivity and trace conditions. Mathematically, a pure state of a quantum system can be represented by a state vector $|\psi\rangle$ which is a unit vector in a Hilbert space \mathcal{H} . Moreover, when there is not enough information to specify the normalized state $|\psi\rangle$, we have a probabilistic mixture of pure states called mixed quantum states. In this case, if the probabilities of determining the system in the normalized state $|\psi_n\rangle$ are p_n , then the expectation value of an operator A is

$$\langle A \rangle = \sum_{n} p_n \langle \psi_n | A | \psi_n \rangle. \tag{2.2}$$

Due to partial information about the system, we use density matrix formalism to describe the mixed state quantum system. Its general form can be written as

$$\rho = \sum_{n} p_n |\psi_n\rangle \langle \psi_n|. \tag{2.3}$$

Here, ρ is a hermitian density operator which represent a statistical mixture of states. For a pure state, the density operator becomes

$$\rho = |\psi_i\rangle \langle \psi_i| \quad and \quad \rho^2 = \rho. \tag{2.4}$$

Given that for a pure state, $tr(\rho) = 1$, it follows that $tr(\rho^2) = 1$. However, for mixed states $tr(\rho^2) = \sum_n p_n^2 < 1$. When density operators are positive, any state $|\phi\rangle$ can be represented by

$$\langle \phi | \rho | \phi \rangle = \sum_{n} p_n | \langle \phi | \psi_n \rangle |^2 \ge 0.$$
 (2.5)

Further, in order to define the unitary time evolution of density operator i.e, $\rho(t)$, we assumed that the initial state of the system is $|\psi_n(0)\rangle$ with probability p_n . Thereby, the initial density

operator can be written in the diagonalized form as

$$\rho(0) = \sum_{n} p_n |\psi_n(0)\rangle \langle \psi_n(0)|, \qquad (2.6)$$

The time evolution of the state $|\psi_n(0)\rangle$ is

$$|\psi_n(t)\rangle = U(t) |\psi_n(0)\rangle \tag{2.7}$$

We obtained the above equation by solving the Schrodinger equation: $i\hbar \frac{d}{dt} |\psi_n\rangle \psi = H |\psi_n\rangle$, where $U(t) = e^{-i\frac{Ht}{\hbar}}$ is a unitary time evolution operator generated by the Hamiltonian H of the quantum system. Then, the evolved density matrix under unitary condition $U^{\dagger}U = UU^{\dagger} = I$ is given by

$$\rho(t) = \sum_{n} p_n U(t) |\psi_n(0)\rangle \langle \psi_n(0)| U^{\dagger}(t) = U(t)\rho(0)U^{\dagger}(t).$$
(2.8)

A density operator is an essential tool for studying sub-systems of a composite quantum system given by the reduced density operator and partial positive transposition of the density operator.

2.3 Bi-partite entanglement

A bi-partite system is composed of two non-interactive sub-systems A and B, and whose state, pure or mixed, lies in a Hilbert space $\mathcal{H}_{\mathcal{AB}} = \mathcal{H}_{\mathcal{A}} \otimes \mathcal{H}_{\mathcal{B}}$ that is the tensor product of Hilbert spaces of two sub-systems. Entanglement is a feature of bi-partite systems. A bi-partite pure state $|\Psi\rangle \in \mathcal{H}_{\mathcal{AB}}$ of dimension $d_A \otimes d_B$ is called a separable or product state if and only if it can be written as tensor product of states $|\chi\rangle_A \in \mathcal{H}_B$ of dimension d_A and $|\phi\rangle_B \in \mathcal{H}_{\mathcal{B}}$ of dimension d_B

$$|\Psi\rangle = |\chi\rangle_A \otimes |\phi\rangle_B, \qquad (2.9)$$

otherwise, $|\Psi\rangle$ is called an entangled state. For example, Bell states that the EPR states or EPR pairs are pure bi-partite entangled states. There are four maximally bi-partite entangled two-qubit Bell states in a composite quantum system seen in different experiments. These

Bell's states are generally written as follows

$$|\Psi^{+}\rangle = \frac{1}{\sqrt{2}}(|0\rangle_{A} \otimes |1\rangle_{B} + |1\rangle_{A} \otimes |0\rangle_{B}), \tag{2.10}$$

$$|\Psi^{-}\rangle = \frac{1}{\sqrt{2}}(|0\rangle_{A} \otimes |1\rangle_{B} - |1\rangle_{A} \otimes |0\rangle_{B}), \tag{2.11}$$

$$|\Phi^{+}\rangle = \frac{1}{\sqrt{2}}(|0\rangle_{A} \otimes |0\rangle_{B} + |1\rangle_{A} \otimes |1\rangle_{B}), \tag{2.12}$$

$$|\Phi^{-}\rangle = \frac{1}{\sqrt{2}}(|0\rangle_{A} \otimes |0\rangle_{B} - |1\rangle_{A} \otimes |1\rangle_{B}), \tag{2.13}$$

where $\{|0\rangle \otimes |0\rangle = |00\rangle, |0\rangle \otimes |1\rangle = |01\rangle, |1\rangle \otimes |0\rangle = |10\rangle, |1\rangle \otimes |1\rangle = |11\rangle\} \in \mathcal{H}_{AB}$ are the basis of two qubit Bell's state. In vector forms, we have

$$|00\rangle = \begin{pmatrix} 1\\0 \end{pmatrix} \otimes \begin{pmatrix} 1\\0 \end{pmatrix} = \begin{pmatrix} 1\\0\\0\\0 \end{pmatrix}; |01\rangle = \begin{pmatrix} 1\\0 \end{pmatrix} \otimes \begin{pmatrix} 0\\1 \end{pmatrix} = \begin{pmatrix} 0\\1\\0\\0 \end{pmatrix}$$
$$|10\rangle = \begin{pmatrix} 0\\1\\0 \end{pmatrix} \otimes \begin{pmatrix} 1\\0 \end{pmatrix} = \begin{pmatrix} 0\\0\\1\\0 \end{pmatrix}; |11\rangle = \begin{pmatrix} 0\\1\\0 \end{pmatrix} \otimes \begin{pmatrix} 0\\1 \end{pmatrix} = \begin{pmatrix} 0\\0\\0\\1 \end{pmatrix}$$

These basis are called two qubit mode or occupation number basis. Let $|\phi_1\rangle = p|0\rangle + q|1\rangle$ and $|\phi_2\rangle = r|0\rangle + s|1\rangle$ be a normalized states from Hilbert space \mathcal{H}_2 of dimension 2, which are single qubit state, where $p, q, r, s \in \mathbb{C}$. Here $|0\rangle$ and $|1\rangle$ are known as computational basis states and form an orthonormal basis for the states $|\phi_1\rangle$ and $|\phi_2\rangle$. Then, from Eq.(2.9) and Eq.(2.10), the state of composite system $|\psi^+\rangle \in \mathcal{H}_2 \otimes \mathcal{H}_2$ is separable if it can be written as

$$|\Psi^{+}\rangle = |\phi_{1}\rangle \otimes |\phi_{2}\rangle = (p|0\rangle + q|1\rangle) \otimes (r|0\rangle + s|1\rangle).$$
 (2.14)

Therefore,

$$\frac{1}{\sqrt{2}}(|01\rangle + |10\rangle) = pr\,|00\rangle + ps\,|01\rangle + qr\,|10\rangle + qs\,|11\rangle. \tag{2.15}$$

However, there are no individual values of p, q, r, s but they have relations such that $ps = qr = \frac{1}{\sqrt{2}}$ and pr = qs = 0, thus we obtain

$$|\Psi^{+}\rangle \neq |\phi_{1}\rangle \otimes |\phi_{2}\rangle$$
, (2.16)

so the state $|\Psi^{+}\rangle$ is entangled. Moreover, If $\rho^{AB} \in \mathcal{H}_{AB}$ is the density operator, then entanglement of quantum state ρ^{AB} is characterized by the von Neumann entropy¹ and defined as [87]

$$S(\rho^{AB}) \equiv -Tr(\rho^{AB}log_2\rho^{AB}). \tag{2.17}$$

If g_i are the eigenvalues of ρ^{AB} then the above formula can be re-written as:

$$S(\rho^{AB}) = -\sum_{i} g_i log_2(g_i). \tag{2.18}$$

For example, a qubit contains maximum entropy of 1. In 1930, the idea of a reduced density matrix was introduced by Paul Dirac. In general, the reduced density operator is defined as

$$\rho^A = Tr_B(\rho^{AB}) \tag{2.19}$$

where Tr_B is known as the partial trace over sub-system B defined by

$$Tr_B(|a_1\rangle\langle a_2|\otimes|b_1\rangle\langle b_2|) = |a_1\rangle\langle a_2| tr(|b_1\rangle\langle b_2|) = |a_1\rangle\langle a_2| < b_2|b_1 >$$
 (2.20)

where $|a_1\rangle$, $|a_2\rangle$ are any two basis $\in \mathcal{H}_A$, and $|b_1\rangle$, $|b_2\rangle \in \mathcal{H}_B$. Using Eq.(2.10) in Eq.(2.4), the density operator of the state $|\Psi^+\rangle$ is

$$\rho^{AB} = |\Psi^{+}\rangle \langle \Psi^{+}| = \frac{1}{2}(|01\rangle \langle 01| + |01\rangle \langle 10| + |10\rangle \langle 01| + |10\rangle |10\rangle) = \frac{1}{2} \begin{pmatrix} 0 & 0 & 0 & 0 \\ 0 & 1 & 1 & 0 \\ 0 & 1 & 1 & 0 \\ 0 & 0 & 0 & 0 \end{pmatrix}, (2.21)$$

where $Tr[(\rho^{AB})^2] = 1$. The reduced density operator read now as follows: $\rho^A = Tr_B(\rho^{AB})$

$$= \frac{1}{2} (|0\rangle \langle 0| < 1|1 > + |0\rangle \langle 1| < 1|0 > |1\rangle \langle 0| < 0|1 > + |1\rangle \langle 1| < 0|0 >) = \frac{1}{2} \begin{pmatrix} 1 & 0 \\ 0 & 1 \end{pmatrix}, \tag{2.22}$$

and equally

$$\rho^B = Tr_A(\rho^{AB}) = \frac{1}{2} \begin{pmatrix} 1 & 0 \\ 0 & 1 \end{pmatrix}. \tag{2.23}$$

¹The expected information of a system in information theory is measured by Shannon entropy [88]. Its quantum counterpart is the von Neumann entropy.

Even though the total system is pure, it is surprising that the reduced density operator ρ^A and ρ^B correspond to a mixed state. It means that when one state is entangled with another, specifying the exact state of a single qubit is not possible. Thus, $Tr[(\rho^A)^2] < 1$ or $Tr[(\rho^B)^2] < 1$ for a subsystem of a bi-partite pure state is an example of entanglement.

Bennett et al. have shown that it is sensible to characterize the entanglement as the von Neumann entropy of both sub-systems (A and B) when considered separately. Thus, the entanglement of a state with density operator ρ^{AB} is

$$E(\rho^{AB}) = -Tr(\rho^A log_2 \rho^A) = -Tr(\rho^B log_2 \rho^B). \tag{2.24}$$

 $E(\rho^{AB})$ is termed as the entropy of entanglement, which is an entanglement measures for pure bipartite states. It varies from 0 for product states to 1 for the maximally entangled state. Thus, for the state $|\Psi^{+}\rangle$, we get $E(\rho^{AB}) = 1$.

Unlike pure states, all correlated mixed states are not entangled. A non-correlated mixed state of two systems A and B is taken which is defined as $\mathcal{H}_{AB} = \mathcal{H}_{A} \otimes \mathcal{H}_{B}$:

$$\rho = \rho^A \otimes \rho^B. \tag{2.25}$$

An unentangled correlated state developed from mixture of states will not give any direct quantum correlations linked with entanglement. It is called separable state:

$$\rho = \sum_{i} p_i \rho_i^A \otimes \rho_i^B. \tag{2.26}$$

Any mixed state that does not follow the above equation is called entangled state [79]. To develop a universal method, we have discussed some operational criteria to measure the entanglement in the bi-partite system.

2.3.1 Peres-Horodecki Criterion

The Peres-Horodocki criterion (or positive partial transpose (PPT) criterion) is a separability criterion for density matrices [68] and a condition for find out entanglement in the bi-partite system [89]. It states that if the partial transposition $\rho_{pq,rs}^{T_A}(t) = \rho_{rq,ps}^{AB}(t)$ or $\rho_{pq,rs}^{T_B}(t) = \rho_{ps,rq}^{AB}(t)$ of a density matrix $\rho_{pq,rs}^{AB} = \langle p | \langle q | \rho^{AB}(t) | r \rangle | s \rangle$ (where p,q,r,s are matrix elements) is a positive operator with all positive eigenvalues then the system is unentangled. If the system

has even one negative eigenvalues then it is entangled. For example, the positive partial transpose ρ^{T_B} of the density operator ρ^{AB} for the state $|\Psi^+\rangle$ can be obtained from Eq.(2.21) as

$$\rho^{T_B}(\Psi^+) = \frac{1}{2} \begin{pmatrix} 0 & 0 & 0 & 0 \\ 0 & 1 & 0 & 0 \\ 0 & 0 & 1 & 0 \\ 1 & 0 & 0 & 0 \end{pmatrix}. \tag{2.27}$$

The eigenvalues of the density operator ρ^{T_B} are $-\frac{1}{2}, \frac{1}{2}, \frac{1}{2}$ in which one eigenvalue is smaller than 0, the state $|\Psi^+\rangle$ becomes a bi-partite entangled state.

2.3.2 Negativity

The negativity is the violation of the PPT criterion and it is defined as [83]

$$N(\rho^{AB}) = ||\rho^{T_B}|| - 1, \tag{2.28}$$

where the trace norm

$$||\rho^{T_B}|| = Tr \sqrt{\rho^{T_B} \rho^{T_B \dagger}(t)} = 1 + 2|\sum_i \lambda_i|,$$
 (2.29)

and $\lambda_i < 0$ are the negative eigenvalues of partial transposition ρ^{T_B} . Thus, in other words negativity measures by how much ρ^{T_B} fails to be positive definite [90, 91]. $N(\rho^{AB}) > 0$ is the necessary and sufficient condition of the bi-partite entanglement [69]. For example, one of the eigenvalue of ρ^{T_B} for the state $|\Psi^+\rangle$ is negative, i.e, $\lambda_1 = -\frac{1}{2}$. Consequently, $||\rho^{T_B}|| = 2$ implies $N(\rho^{AB}) = 1$, which mean that the Bell's state $|\Psi^+\rangle$ is a maximally bi-partite entangled state.

2.3.3 Entanglement of formation

The density operator of bi-partite mixed state ρ (see Eq.(2.3)) can be decomposed into pure state as

$$\rho = \sum_{n} p_n \rho_n, \tag{2.30}$$

where $\rho_n = |\psi_n\rangle \langle \psi_n|$ is a pure state density operator and p_n are non-negative numbers satisfying $\sum_n p_n = 1$. The quantification of the entropy of entanglement $(E(\rho_n))$ for pure

state to mixed state is given by the entanglement of formation $E_f(\rho)$ which is the minimum entanglement that can be obtained from all such decomposition defined as [70,81]

$$E_f(\rho) = \min \sum_n p_n E(\rho_n)$$
 (2.31)

where, $E(\rho_n)$ is given by Eq.(2.24). A state with $E_f = 0$ is separable and when $E_f = 1$, the state is maximally entangled.

2.3.4 Concurrence and Tangle

Concurrence is the quantification of bi-partite quantum correlations which is based on reduced density matrix mathematics. For the two-qubit pure state it is defined as [70]

$$C(|\Psi\rangle) = \sqrt{2[1 - Tr\{(\rho^A)^2\}]} = 2\sqrt{\det \rho^A},$$
 (2.32)

where $\rho^A = Tr_B(\rho^{AB})$ the reduced state of ψ . More general formula of concurrence for pure or mixed two-qubit states is defined as

$$C(\rho^{AB}) = [max(\mu_1 - \mu_2 - \mu_3 - \mu_4, 0)], \tag{2.33}$$

where the μ_i s are the square roots of the eigenvalues of the non-Hermitian matrix $\rho^{AB}\rho^{\tilde{A}B}$ in decreasing order and each μ_i is a non-negative real number. Here, $\tilde{\rho}^{AB}$ is defined as spin-flipped density operator

$$\tilde{\rho}^{AB} = (\sigma_y \otimes \sigma_y) \rho^{*AB} (\sigma_y \otimes \sigma_y), \tag{2.34}$$

where ρ^{*AB} denotes the complex conjugation in the computational basis $\{|00\rangle, |01\rangle, |10\rangle, |11\rangle\}$ and $\sigma_y = \begin{pmatrix} 0 & -i \\ i & 0 \end{pmatrix}$ is Pauli matrix. Accordingly, if we consider a general 2-qubit pure state as $|\Psi\rangle = p_{00} |00\rangle + p_{01} |01\rangle + p_{10} |10\rangle + p_{11} |11\rangle$ the concurrence is given by $C(\rho) = 2|p_{00}p_{11} - p_{01}p_{10}|$. Moreover, for two qubits $E_f(\rho^{AB})$ (see Eq.(2.31) can be expressed in terms of the Concurrence $(C(\rho^{AB}))$ as [81,82]

$$E_f(\rho^{AB}) = h(\frac{1 + \sqrt{1 - C^2(\rho^{AB})}}{2}); \ h(z) = -zlog_2(z) - (1 - z)log_2(1 - z)$$
 (2.35)

where, h(z) is the binary entropy function. h is a monotonically increasing function of its argument and ranges from 0 corresponding to $C(\rho^{AB}) = 0$ and to 1 for $C(\rho^{AB}) = 1$. The quantity $C^2(\rho^{AB})$ in Eq.(2.35) is termed as Tangle (τ) and it is defined as [72]:

$$\tau(\rho^{AB}) = C^2(\rho^{AB}) = [\max(\mu_1 - \mu_2 - \mu_3 - \mu_4, 0)]^2.$$
(2.36)

Thus, $E_f(\rho^{AB})$ is a monotonically increasing convex function of concurrence and concave function of tangle. For bi-partite pure state the matrix $\rho^{AB}\tilde{\rho}^{AB}$ has only one non-zero eigenvalue, so the above Eq.(2.36) of tangle is reduced to

$$\tau(|\Psi\rangle) = C^2(|\Psi\rangle) = 4det\rho^A. \tag{2.37}$$

Thus, for $|\Psi^+\rangle$, using Eq.(2.22) in Eq.(2.32) and Eq.(2.37), we get $C(|\Psi^+\rangle) = \tau(|\Psi^+\rangle) = 1$.

2.3.5 Linear entropy

The linear entropy (S_L) is the first order approximation of von Neumann entropy. Its physical significance is that it is straightforwardly connected to the purity of the mixed states. It is easy to compute because there is no need of diagonalizing the density matrix. The expression of linear entropy can be obtained by using the Newton-Mercator series², where we can approximate the term $log_2\rho^{AB}$ of Eq.(2.17) with first order term $(\rho^{AB} - 1)$ such as

$$-Tr(\rho^{AB}log_2\rho^{AB}) \to -Tr(\rho^{AB}(\rho^{AB}-1)) = Tr(\rho^{AB}-[\rho^{AB}]^2)$$
 (2.38)

Since, $Tr(\rho^{AB}) = 1$ (unit trace property of the density matrix). Thus,

$$S_L(\rho^{AB}) = 1 - Tr[(\rho^{AB})^2].$$
 (2.39)

It is also defined with a different normalization as [84]

$$S_L(\rho^{AB}) = \frac{d}{d-1} (1 - Tr[(\rho^{AB})^2])$$
 (2.40)

$$log(1+q) = q - \frac{q^2}{2} + \frac{q^3}{3} - \frac{q^4}{4} + \dots$$

²Newton-Mercator series is the Taylor series for the natural logarithm (-1 < q < 1):

where d is the dimension of the density matrix ρ^{AB} . The linear entropy ranges from zero which is a completely pure state to $1 - \frac{1}{d}$ which describes a completely mixed state. For $|\psi^{+}\rangle$, using Eq.(2.21) in Eq.(2.40), we get $S_{L}(\rho^{AB}) = 0$. Thus, $|\psi^{+}\rangle$ is a bi-partite pure state. The linear entropy associated to reduced density operator ρ^{A} and ρ^{B} can be written as

$$S_L(\rho^A) = \frac{d}{d-1}(1 - Tr[(\rho^A)^2]) \; ; \; S_L(\rho^B) = \frac{d}{d-1}(1 - Tr[(\rho^B)^2])$$
 (2.41)

For $|\psi^{+}\rangle$, using the reduced density matrix Eq.(2.22) and Eq.(2.23) in Eq.(2.41), where the dimension of ρ^{A} and ρ^{B} is d=2, we get $S_{L}(\rho^{A})=S_{L}(\rho^{B})=\frac{1}{2}$.

2.4 Tri-partite entanglement

A tri-partite system in three-qubit mode states comprises of A, B and C whose state (pure or mixed) lies in a Hilbert space represented by tensor product $\mathcal{H}_{ABC} = \mathcal{H}_A \otimes \mathcal{H}_B \otimes \mathcal{H}_C$ with dimension $d_A \otimes d_B \otimes d_C$. There are two different types of separable states that exist for pure three-qubit states: the entirely separable states can be composed as:

$$|\Psi^{fs}\rangle_{A|B|C} = |\chi\rangle_A \otimes |\phi\rangle_B \otimes |\eta\rangle_c \tag{2.42}$$

and the bi-separable states are formed when two of the three qubits are assembled to one sub-system or in other words it is the product state in the bi-partite system. There are three prospects of combining 2 qubits together, thereby forming 3 classes of biseparable states represented as

$$\begin{split} |\Psi^{bs}\rangle_{A|BC} &= |\chi\rangle_A \otimes |\zeta\rangle_{BC}\,,\\ |\Psi^{bs}\rangle_{B|AC} &= |\chi\rangle_B \otimes |\zeta\rangle_{AC}\,,\\ |\Psi^{bs}\rangle_{C|AB} &= |\chi\rangle_C \otimes |\zeta\rangle_{AB}\,. \end{split}$$

Here, $|\zeta\rangle_{BC}$, $|\zeta\rangle_{AC}$, and $|\zeta\rangle_{AB}$ are bi-partite states that might be entangled. A state $|\Psi^{bs}\rangle=\frac{1}{2}(|001\rangle+|010\rangle+|101\rangle+|110\rangle)$ can be tensor product of a single qubit state and a Bell-state

$$|\Psi^{bs}\rangle_{A|BC} = \frac{1}{\sqrt{2}}(|0\rangle + |1\rangle)_A \otimes \frac{1}{\sqrt{2}}(|01\rangle + |10\rangle)_{BC}$$
(2.43)

which is an example of biseparable state. A pure three-qubit state is called genuine tripartite entangled if it is neither fully separable nor biseparable.

The genuine entangled three-qubit states are divided into two inequivalent classes. If two three-qubit states $|\Psi\rangle$ and $|\Phi\rangle$ are given, then the transformation of a single copy of $|\Psi\rangle$ into $|\Phi\rangle$ without local operations and classical communication is accurate. These operations are called stochastic local operations and classical communication (SLOCC). Surprisingly, in ref. [92] it is shown that two different equivalent classes of genuine tripartite entangled states exist, i.e., Greenberger Horne Zeilinger (GHZ) class and W class, which could not be transformed into another by SLOCC. The GHZ-state can be written as [93,94]

$$|GHZ\rangle = \frac{1}{\sqrt{2}}(|000\rangle + |111\rangle). \tag{2.44}$$

In a tri-partite system there are 8 three-qubit mode computational basis $\{|000\rangle, |001\rangle, |010\rangle, |011\rangle, |100\rangle, |101\rangle, |110\rangle, |111\rangle\}$. Then the density operator of the GHZ state is

The reduced density operator ρ^{AB} is a mixed state calculated by tracing over the qubit C such that

By taking its partial positive transposition ρ^{T_A} (or ρ^{T_B}), we find no negative eigenvalues of the resulting matrix. Thus, according to the PPT criterion, ρ^{AB} is a remaining mixed state which is unentangled. Similarly, tracing the other two qubits will give the same result. Thus, if one qubit is lost in the GHZ state, the state becomes separable. Furthermore, tracing over

either of the remaining qubits give

$$\rho^A = \rho^B = \rho^C = \frac{1}{2} \begin{pmatrix} 1 & 0 \\ 0 & 1 \end{pmatrix}. \tag{2.47}$$

with $Tr[(\rho^A)^2] = Tr[(\rho^B)^2] = Tr[(\rho^C)^2] < 1$. This is the same reduced density operator which we have obtained in the previous Sec.(2.3) (see Eq.(2.22) and Eq.(2.23)) for the bipartite two-qubit pure state example, i.e., $|\Psi^+\rangle$. These mixed states indicate that the three-qubit GHZ state is fully entangled and generalizes the two-qubit Bell states.

Another example of a three-qubit pure state in a tri-partite system is the W-state [92]. A prototype W-state is

$$|W_1\rangle = \frac{1}{\sqrt{3}}(|001\rangle + |010\rangle + |100\rangle),$$
 (2.48)

which gives

$$\rho^{ABC}(W_1) = |W_1\rangle\langle W_1| = \frac{1}{3} \begin{pmatrix}
0 & 0 & 0 & 0 & 0 & 0 & 0 & 0 \\
0 & 1 & 1 & 0 & 1 & 0 & 0 & 0 \\
0 & 1 & 1 & 0 & 1 & 0 & 0 & 0 \\
0 & 0 & 0 & 0 & 0 & 0 & 0 & 0 \\
0 & 1 & 1 & 0 & 1 & 0 & 0 & 0 \\
0 & 1 & 1 & 0 & 1 & 0 & 0 & 0 \\
0 & 0 & 0 & 0 & 0 & 0 & 0 & 0 \\
0 & 0 & 0 & 0 & 0 & 0 & 0 & 0 \\
0 & 0 & 0 & 0 & 0 & 0 & 0 & 0
\end{pmatrix}$$
(2.49)

and

$$\rho^{AB} = \rho^{AC} = \rho^{BC} = \frac{1}{3} \begin{pmatrix} 1 & 0 & 0 & 0 \\ 0 & 1 & 1 & 0 \\ 0 & 1 & 1 & 0 \\ 0 & 1 & 1 & 0 \\ 0 & 0 & 0 & 0 \end{pmatrix}, \tag{2.50}$$

and

$$\rho^A = \rho^B = \rho^C = \frac{1}{3} \begin{pmatrix} 2 & 0 \\ 0 & 1 \end{pmatrix}. \tag{2.51}$$

Taking the partial positive transposition, ρ^{T_A} (or ρ^{T_B}) of the remaining two-qubit mixed state density operator ρ^{AB} given in Eq.(2.50), we find that all eigenvalues are not positive or zero. Therefore, according to the PPT criterion, ρ^{AB} is entangled. This result shows that, unlike the GHZ state, the entanglement of the W state is more robust against qubit losses. In general, if one qubit is lost in the W-state, the remaining state retains some entanglement.

Now we define the classification of mixed three-qubit state in tri-partite system [95,96]. If p_n are the probabilities to find a fully separable states $|\Psi_n^{fs}\rangle$, then the general form of mixed

states density operator as fully separable ρ^{fs} is

$$\rho^{fs} = \sum_{n} p_n |\Psi_n^{fs}\rangle \langle \Psi_n^{fs}|. \qquad (2.52)$$

Similarly, the density operator for the bi-separable mixed state is

$$\rho^{bs} = \sum_{n} p_n |\Psi_n^{bs}\rangle \langle \Psi_n^{bs}| \qquad (2.53)$$

and there are 3 classes of biseparable mixed states that are biseparable with respect to fixed partition. Finally, in a combination of W-type pure state, a fully entangled mixed state belongs to the W class defined as

$$\rho^{W} = \sum_{n} p_{n} |\Psi_{n}^{W}\rangle \langle \Psi_{n}^{W}|, \qquad (2.54)$$

otherwise it belongs to the GHZ class. Now, we explore two type of entanglement measures in tri-partite system.

2.4.1 Three-tangle

Considering three bits A, B and C, in classical theory if A and B are correlated, then there is no correlation with C. However, in quantum theory, if A, B, C are three qubits, then all are correlated with each other. For pure 3-qubit states the trade-off is described by Coffman-Kundu-Wooters (CKW) inequality which is a monogamy inequality in terms of tangle and it is a criterion for determining tri-partite entanglement [72]. Mathematically, the relation between A, B and C is

$$\tau_{AB} + \tau_{AC} \le \tau_{A(BC)}.\tag{2.55}$$

where

$$\tau_{AB} \le Tr(\rho^{AB}\tilde{\rho}^{AB}); \text{ and } \tau_{AC} \le Tr(\rho^{AC}\tilde{\rho}^{AC});$$
(2.56)

are the tangle of the mixed states $\rho^{AB} = Tr_C(\rho^{ABC})$ and $\rho^{AC} = Tr_B(\rho^{ABC})$, respectively and $\tau_{A(BC)} = 4det(\rho^A)$. Here, $\tilde{\rho}^{AB}$ and $\tilde{\rho}^{AC}$ are spin-flipped density operator defined by Eq.(2.34). It is to be noted that the definition of τ_{AB} and τ_{AC} in Eq.(2.56) is true when the product $\rho^{AB}\tilde{\rho}^{AB}$ having at most two non-zero eigenvalues. The CKW monogamy inequality

can be also defined in terms of concurrence. Since tangle is square of concurrence, therefore the expression in Eq.(2.55) looks like $C_{AB}^2 + C_{AC}^2 \leq C_{A(BC)}^2$. Accordingly to Eq.(2.56) the three-tangle τ_{ABC} can be defined as

$$\tau_{ABC} = \tau_{A(BC)} - \tau_{AB} - \tau_{AC}. \tag{2.57}$$

which is used to characterize three-way entanglement of the state [92]. For example, quantified by three-tangle the state $|GHZ\rangle$ has only three-way entanglement since $\tau_{ABC}(GHZ) \geq 0$, while the state $|W_1\rangle$ has only-two way entanglement because $\tau_{ABC}(W_1) = 0$.

For a general mixed 3-qubit state of ρ^{ABC} , the three-tangle should be

$$\tau_{ABC} = min[\tau_{A(BC)}] - \tau_{AB} - \tau_{AC}, \qquad (2.58)$$

where $\tau_{A(BC)}$ has to be minimized for all possible decomposition of ρ^{ABC} . Later, the generalized CKW inequality for n-qubit states was also proved [97].

2.4.2 Three- π

Interestingly the monogamy of tangle implies monogamy of negativity [35]. For a pure 3-qubit states of tri-partite system the CKW inequality in terms of negativity is defined as

$$N_{AB}^2 + N_{AC}^2 \le N_{A(BC)}^2 \tag{2.59}$$

where N_{AB}^2 and N_{AC}^2 are the negativities of the mixed states $\rho^{AB} = Tr_C(\rho^{ABC})$ and $\rho^{AC} = Tr_B(\rho^{ABC})$, respectively and $N_{A(BC)}^2 = \tau_{A(BC)} = 4det\rho^A$. In the similar way, if one takes the different subscript of qubits B and C, the monogamy inequalities become

$$N_{BA}^2 + N_{BC}^2 \le N_{B(AC)}^2, \tag{2.60}$$

and

$$N_{CA}^2 + N_{CB}^2 \le N_{C(AB)}^2. (2.61)$$

If the relation given in Eq.(2.59) is strict for any pure state of three-qubits i.e,

$$N_{AB}^2 + N_{AC}^2 < N_{A(BC)}^2 (2.62)$$

then the difference between the two sides of above equation can be interpreted as the residual entanglement

$$\pi_A = N_{A(BC)}^2 - N_{AB}^2 - N_{AB}^2. (2.63)$$

Similarly, Eq.(2.60) and Eq.(2.61) forms residual entanglement as

$$\pi_B = N_{B(AC)}^2 - N_{BA}^2 - N_{BC}^2. (2.64)$$

and

$$\pi_C = N_{C(AB)}^2 - N_{CA}^2 - N_{CB}^2. (2.65)$$

respectively. The subscript A, B, and C in π_A , π_B and π_C mean that qubit A, qubit B, and qubit C are taken into consideration respectively. Unlike the three-tangle, in general $\pi_A \neq \pi_B \neq \pi_c$ for the class of W-state. This indicates that under permutations of the qubits the residual entanglement corresponding to the different subscript varies. We take three- π (π_{ABC}) as the average of π_A , π_B and π_C , i.e.,

$$\pi_{ABC} = \frac{1}{3}(\pi_A + \pi_B + \pi_C), \tag{2.66}$$

which thus becomes invariant under permutations of the qubits, since, for example, permutation of qubit A and qubit B leads to exchanging π_A , π_B with each other in π_{ABC} . Three- π is a natural entanglement measure, which satisfies three necessary conditions:

- it should be local unitary (LU) invariant;
- it has zero value for pure product states; and
- it has a value greater than zero for genuine tripartite entanglement [35].

In general, for a pure 3-qubit state of ABC belongs to the W-class

$$|\Phi\rangle = \kappa |100\rangle + \zeta |010\rangle + \eta |001\rangle$$
 (2.67)

where $|\kappa|^2 + |\zeta|^2 + |\eta|^2 = 1$ and $\kappa \neq 0$, $\zeta \neq 0$, and $\eta \neq 0$, substituting $N_{AB}^2 = 4|\kappa|^2|\zeta|^2 + 2|\eta|^4 - 2|\eta|^2 \sqrt{|\eta|^4 + 4|\kappa|^2|\zeta|^2}$, $N_{AC}^2 = 4|\kappa|^2|\zeta|^2 + 2|\zeta|^4 - 2|\zeta|^2 \sqrt{|\zeta|^4 + 4|\kappa|^2|\eta|^2}$ and $N_{A(BC)}^2 = 4|\kappa|^2(|\zeta|^2 + |\eta|^2)$ into Eq.(2.63), Eq.(2.64) and Eq.(2.65) and using its result in Eq.(2.66), an

entanglement measure three- π we gate as

$$\pi_{ABC}(\Phi) = \frac{4}{3} (|\kappa|^2 \sqrt{|\kappa|^4 + 4|\kappa|^2 |\eta|^2} + |\zeta|^2 \sqrt{|\zeta|^4 + 4|\kappa|^2 |\zeta|^2} + |\eta|^2 \sqrt{|\eta|^4 + 4|\kappa|^2 |\zeta|^2} - |\kappa|^4 - |\zeta|^4 - |\eta|^4), \tag{2.68}$$

but substituting $\tau_{AB} = 4|\kappa|^2|\zeta|^2$, $\tau_{AC} = 4|\kappa|^2|\eta|^2$, and $\tau_{A(BC)} = 4|\kappa|^2(|\zeta|^2 + |\eta|^2)$ in Eq.(2.57), the three-tangle vanish i.e.,

$$\tau_{ABC}(\Phi) = 0. \tag{2.69}$$

When $\kappa = \zeta = \eta = \frac{1}{\sqrt{3}}$, the state $|\Phi\rangle$ become a prototype W-state $|W_1\rangle$ (see Eq.(2.48) and for this state we get $\pi_{ABC}(W_1) = \frac{4}{9}(\sqrt{5}-1) = 0.549363$ and $\tau_{ABC}(W_1) = 0$. Thus, under the different classes of SLOCC, to quantify tri-partite entanglement of W class we have the property that

$$\pi_{ABC}(W) > \tau_{ABC}(W) = 0.$$
 (2.70)

For the GHZ class,

$$\pi_{ABC}(GHZ) \ge \tau_{ABC}(GHZ) > 0,$$
(2.71)

while

$$\pi_{ABC}(\phi) = \tau_{ABC}(\phi) = 0 \tag{2.72}$$

for the states $|\phi\rangle_{ABC}$ belonging to the classes excluding the W and GHZ classes. Note that for the mixed state density operator ρ^{ABC} of 3-qubit states of ABC, the monogamy inequality Eq.(2.59) turns out to be

$$N_{AB}^2 + N_{AC}^2 \le \min[N_{A(BC)}^2], \tag{2.73}$$

which has to be minimized for all possible decomposition of ρ^{ABC} . In this case, $N_{AB}^2 \leq \tau_{AB}$ and $N_{AC}^2 \leq \tau_{AC}$. The other inequalities in Eq.(2.60) and Eq.(2.61) need the same manipulation [98]. The next chapter investigates and quantifies such bi-partite and tripartite entanglement measures for two and three-flavour neutrino oscillations, respectively.

Chapter 3

Tri-partite entanglement in neutrino oscillations

The quantum phenomenon of neutrino oscillations in which a neutrino in a given flavour state can be found in a different flavour state as it progresses in time is a topic of current, and theoretical activity [51,99–103]. Oscillations arise because the neutrino flavour state is a linear superposition of non-degenerate mass eigenstates of neutrinos. Quantum entanglement and coherence [104] are two fundamental features arising from the principle of quantum superposition. Therefore, it is natural to examine quantum entanglement in neutrino systems [79,105]. For two flavours, the linear superposition state of a neutrino can be mapped to a two-qubit system [42]. Blasone et al., initially mapped the three flavour system as a 3-qubit system [106–109]. In this chapter, we investigates the entanglement properties of the three-particle superposition flavour-neutrino state. We show that the three neutrino state has a specific three-way entanglement akin to the W-state in quantum optics.

Neutrino oscillations take place because there is a misalignment of mass and flavour states of the neutrinos [43]. Oscillations are observed over large distances. Therefore there must be quantum coherence of the mass states [43]. It turns out that the quantum mechanical approximation of neutrinos has been so successful that they have been used to perform fundamental tests of quantum mechanics [27,110,111]. At the Daya Bay experiment, they have searched for the fingerprints of the wave packet nature of neutrinos that could affect its probability of oscillation within a 95% confidence level and found no significant effect of wave packet over the plane wave treatment [29,30]. Thus the standard plane wave approximation of neutrinos with significant distance coherently function well and decoherence due to the

wave packet nature is very small because of the small neutrino masses. This means, albeit theoretically, that neutrinos are candidates for quantum computation [46, 112]. This also makes a study of their quantum properties fascinating. Neutrino entanglement has been studied in both modes, flavour mode as well as in mass mode [42, 43, 106–109]. The three-flavour mode entangled states are analyzed using information-theoretic tools [113]. Besides mode entanglement, which is the primary subject of this chapter, some astrophysical studies show the possible effects of neutrino many-body entanglement on flavor oscillations [114–120]. For an all-encompassing perspective on quantum entanglement in neutrino oscillations such studies are informative.

The entanglement measures that have been studied for two flavour neutrino systems are Bell's inequality and Bell-CHSH (Clauser-Horn-Shimoy-Holt) inequality violations, teleportation fidelity, and geometric discord. They have been related to the neutrino oscillation probabilities [43]. Along with this, the other entanglement measures like "the nonlocal advantage of quantum coherence" (NAQC), the Bell nonlocality and the entropic uncertainty have been investigated in the three neutrino systems by comparing their results using the data obtained from different types of neutrino oscillations experiments [121–123]. Bell's inequality derives correlations of measurements on separated systems based on space. In analogy to that, Leggett and Garg investigated time-based correlations, which they extended to apply on a macroscopic system [124]. Recent work [125–128] shows that this analogue is sensitive to the neutrino mass-hierarchy in three neutrino system.

In this chapter, we show that the temporal behaviour of the two-mode entangled neutrino state resembles entanglement swapping (the procedure of entangling photons without direct interaction) between two-photon states emerging from a Beam Splitter (BS) [129, 130]. We extend the study to three-flavour neutrino oscillations by considering distributed entanglement measures for three-mode states [72]. There are two types of non-separable classes in the 3-qubit system, W and GHZ states. For the W-state there is a property that if one of the 3 qubits is lost, the remaining 2-qubit state is still entangled. This robustness of W-type entanglement contrasts sharply with the GHZ-state, which is entirely separable after losing 1 qubit.

In three flavour neutrino oscillations, the neutrino state can always be written in the form $|\nu(t)\rangle = a\,|100\rangle + b\,|010\rangle + c\,|001\rangle$, which is the "generic form" of the W-class of states in quantum optics. We will later reaffirm this by analysis of various entanglement measures. We do so by examining a measure of distributed entanglement, a monogamy inequality known as Coffman-Kundu-Wooters (CKW) inequality, which characterizes genuine tri-partite entanglement and enables us to distinguish between different tri-partite states [35, 72]. Our

studies show that the three neutrino state has robust tripartite state entanglement more akin to the W-state than the GHZ-state. Laboratory production of a 3-qubit entangled W-state can be done using spontaneous parametric down-conversion (SPDC) and two BS [131] (similarly GHZ-state can also be created via experiments [132]). The analogy between W-states (which can be produced in the lab) and the three neutrino states can lead to a further understanding of the nature of entanglement in neutrino oscillations. In quantum optical experiments, one can physically manipulate the system by identifying neutrino states as quantum optical states; one may be able to get information about the quantum properties of the neutrino system and demonstrate factors contributing to the decoherence and even many-body entanglement relevant to astrophysical settings.

The chapter's organization is: In Sec.(3.1), we investigate and quantify various measures of bi-partite entanglement such as tangle, concurrence, the entanglement of formation, negativity and linear entropy in the two-neutrino system. In Sec.(3.2), we examine tri-partite entanglement measures such as three-tangle and three- π in the three-neutrino system.

3.1 Bi-partite entanglement in two-flavour neutrino oscillations

In the plane wave picture, we expand Eq.(1.11) of Chapter 1 to re-write an equation for the time evolution of the flavour neutrino state in a coherent superposition of flavour basis as,

$$|\nu_{\alpha}(t)\rangle = \tilde{U}_{\alpha e}(t) |\nu_{e}\rangle + \tilde{U}_{\alpha \mu}(t) |\nu_{\mu}\rangle + \tilde{U}_{\alpha \tau}(t) |\nu_{\tau}\rangle, \qquad (3.1)$$

where, $|\tilde{U}_{\alpha e}(t)|^2 + |\tilde{U}_{\alpha \mu}(t)|^2 + |\tilde{U}_{\alpha \tau}(t)|^2 = 1$ and $\tilde{U}_{\alpha \beta}(t) \equiv \sum_j U_{\alpha j}^* e^{-iE_j t/\hbar} U_{\beta j}$; E_j is the energy associated with the mass eigenstate $|\nu_j\rangle$.

First, we characterize 2 qubit entanglement for two-flavour mixing which are relevant, as a first approximation, to three cases of neutrino experiments. $\nu_{\mu} \leftrightarrow \nu_{\tau}$ transitions are relevant for atmospheric neutrinos, $\nu_{e} \leftrightarrow \nu_{\mu}$ at reactor experiments and $\nu_{\mu} \leftrightarrow \nu_{e}$ at accelerator experiments [100, 101, 103, 133]. 2 qubit states are identified with the electron and muon neutrino with the flavour state at time t=0 by using the occupation number states as [42]

$$|\nu_e\rangle = |1\rangle_e \otimes |0\rangle_\mu \equiv |10\rangle_e,$$

and $|\nu_\mu\rangle = |0\rangle_e \otimes |1\rangle_\mu \equiv |01\rangle_\mu.$

For two neutrino mixing the SU(2) rotation matrix

$$R(\theta) = \begin{pmatrix} \cos \theta & \sin \theta \\ -\sin \theta & \cos \theta \end{pmatrix}, \tag{3.2}$$

can be identified with the mixing matrix $U(\theta)$.

The time evolution of an initial electron-flavour neutrino state in two mode (flavour) system can be written as,

$$|\nu_e(t)\rangle = \tilde{U}_{ee}(t) |10\rangle_e + \tilde{U}_{e\mu}(t) |01\rangle_\mu, \qquad (3.3)$$

where $\tilde{U}_{ee}(t) = (\cos^2\theta e^{-iE_1t} + \sin^2\theta e^{-iE_2t})$; $\tilde{U}_{e\mu}(t) = \sin\theta\cos\theta(e^{-iE_1t} - e^{-iE_2t})$ and $|\tilde{U}_{ee}(t)|^2 + |\tilde{U}_{e\mu}(t)|^2 = 1$ (also see Sec.(1.2.1)). The probability of generating and detecting electron-neutrino flavour state as a survival probability $P_s = |\tilde{U}_{ee}(t)|^2$ and, the probability of generating electron-neutrino flavour state and detecting muon-neutrino flavour state as a disappearance probability $P_d = 1 - |\tilde{U}_{ee}(t)|^2$ are,

$$P_s = \cos^4 \theta + \sin^4 \theta + 2\sin^2 \theta \cos^2 \theta \cos \left(\frac{\Delta m^2 t}{2E}\right)$$
 (3.4)

and
$$P_d = 4\sin^2\theta\cos^2\theta\sin^2\left(\frac{\Delta m^2t}{4E}\right)$$
. (3.5)

where θ is a generic two flavour mixing angle and $\Delta m^2 = m_2^2 - m_1^2$ is the corresponding mass-square difference. The corresponding density matrix $\rho^e(t)$ is given by $\rho^e(t) = |\nu_e(t)\rangle \langle \nu_e(t)|$ such that,

$$\rho^{e}(t) = \begin{pmatrix} 0 & 0 & 0 & 0 \\ 0 & |\tilde{U}_{ee}(t)|^{2} & \tilde{U}_{ee}(t)\tilde{U}_{e\mu}^{*}(t) & 0 \\ 0 & \tilde{U}_{e\mu}(t)\tilde{U}_{ee}^{*}(t) & |\tilde{U}_{e\mu}(t)|^{2} & 0 \\ 0 & 0 & 0 & 0 \end{pmatrix}.$$
(3.6)

An excellent optical analogy to the phenomenon of neutrino oscillation is the following situation. In quantum optics, the action of a quantum mechanical BS (Beam splitter) interferometer is given by the SU(2) matrix $R(\theta)$, which performs precisely the same transformation on photons as the neutrino mixing matrix does. Thus, the entanglement in a two flavour neutrino mixing is akin to entanglement via mode swapping due to a BS [130].

Let $\rho^e(t)$ be a density operator of an initial electron-neutrino flavour state $|\nu_e(t)\rangle$ (see Eq.(3.3)) which contains electron flavour mode (e) and muon flavour mode (μ) in 2-qubit mode (flavor) bases (i.e, $|10\rangle_e$ and $|01\rangle_{\mu}$). $\rho^e_{pq,rs}(t) = \langle p|\langle q|\rho^e(t)|r\rangle|s\rangle$. The partial transpositions of operator $\rho^e(t)$ in flavour modes e and μ are defined as $\rho^{T_e}_{pq,rs}(t) = \rho^e_{rq,ps}(t)$ and

 $\rho_{pq,rs}^{T_{\mu}}(t) = \rho_{ps,rq}^{e}(t)$. In Sec.(2.3.1) of Chapter 2, we defined the Peres-Horodecki criterion, which is a sufficient condition for separability in bi-partite quantum system. The composite state $\rho^{e}(t)$ is separable if and only if $\rho^{T_{e}}(t)$ or $\rho^{T_{\mu}}(t)$ is a positive operator, with all positive eigenvalues, otherwise the composite state $\rho^{e}(t)$ is an entangled state [89]. The partial transpose in muon-flavour mode from Eq.(3.6) is

$$\rho^{T_{\mu}}(t) = \begin{pmatrix} 0 & 0 & 0 & \tilde{U}_{ee}(t)\tilde{U}_{e\mu}^{*}(t) \\ 0 & |\tilde{U}_{ee}(t)|^{2} & 0 & 0 \\ 0 & 0 & |\tilde{U}_{e\mu}(t)|^{2} & 0 \\ \tilde{U}_{e\mu}(t)\tilde{U}_{ee}^{*}(t) & 0 & 0 & 0 \end{pmatrix}.$$
(3.7)

In terms of probabilities, the eigenvalues λ_i of $\rho^{T_\mu}(t)$ are $\lambda_1 = P_s$, $\lambda_2 = P_d$, $\lambda_3 = \sqrt{P_s P_d}$, $\lambda_4 = -\sqrt{P_s P_d}$. Thus, λ_4 is not positive which means $\rho^{T_\mu}(t)$ is not a positive operator and therefore the neutrino state $|\nu_e(t)\rangle$ is entangled.

In Sec.(2.3.2) of chapter 2, we have also defined that Negativity (N) is a quantity which measures by how much $\rho^{T_{\mu}}(t)$ fails to be positive definite [83,90]. The condition Negativity $N_{e\mu} > 0$ is the necessary and sufficient inseparable condition for the bi-partite quantum system to be entangled and for $e\mu$ system it is defined as

$$N_{e\mu} = N(\rho^e(t)) = ||\rho^{T_{\mu}}(t)|| - 1, \tag{3.8}$$

where the trace norm

$$||\rho^{T_{\mu}}(t)|| = Tr\sqrt{\rho^{T_{\mu}}(t)\rho^{T_{\mu}\dagger}(t)} = 1 + 2|\sum_{i} \lambda_{i}|,$$
 (3.9)

and $\lambda_i < 0$ are the negative eigenvalues of partial transposition $\rho^{T_{\mu}}(t)$ [91]. For the two flavour neutrino oscillations,

$$||\rho^{T_{\mu}}(t)|| = 1 + 2\sqrt{P_s P_d}. (3.10)$$

Thus, the negativity is $N_{e\mu} = 2\sqrt{P_s P_d}$ which is always greater than 0, so e- μ neutrino system is entangled [35].

Concurrence and tangle are strong measures of quantum correlations [72]. A general bipartite state ψ of a 2 qubit system AB can be written as $|\psi\rangle = a|10\rangle + b|01\rangle$, where $|a|^2 + |b|^2 = 1$. A and B are the e and μ flavour modes respectively. In that case, Eq.(2.34) of chapter 2 become the "spin-flipped" operator $\tilde{\rho}^e(t)$ of the state $|\nu_e(t)\rangle$ as $\tilde{\rho}^e(t) = (\sigma_y \otimes \sigma_y)\rho^{*e}(t)(\sigma_y \otimes \sigma_y)$, where $\rho^{*e}(t)$ denotes the complex conjugation in the standard basis $(|00\rangle, |01\rangle, |10\rangle, |11\rangle)$ and

 $\sigma_y = \begin{pmatrix} 0 & -i \\ i & 0 \end{pmatrix}$ is Pauli matrix. Thus,

$$\tilde{\rho}^{e}(t) = \begin{pmatrix} 0 & 0 & 0 & 0 \\ 0 & |\tilde{U}_{e\mu}(t)|^{2} & \tilde{U}_{ee}^{*}(t)\tilde{U}_{e\mu}(t) & 0 \\ 0 & \tilde{U}_{e\mu}^{*}(t)\tilde{U}_{ee}(t) & |\tilde{U}_{ee}(t)|^{2} & 0 \\ 0 & 0 & 0 & 0 \end{pmatrix}.$$
(3.11)

As both $\rho^e(t)$ and $\tilde{\rho}^e(t)$ are positive operators, it follows that the product

though non-hermitian also has only real and non-negative eigenvalues. Denoting the square roots of these eigenvalues in decreasing order by μ_1 , μ_2 , μ_3 and μ_4 , the tangle of the density matrix $\rho^e(t)$ is :

$$\tau_{e\mu} = [max(\mu_1 - \mu_2 - \mu_3 - \mu_4, 0)]^2. \tag{3.13}$$

Since, the product $\rho^e(t)\tilde{\rho}^e(t)$ has only one non-zero eigenvalue i.e., $\mu_4 = 2\sqrt{|\tilde{U}_{e\mu}(t)|^2|\tilde{U}_{ee}(t)|^2}$, using Eq.(3.6) one can show that the tangle is $\tau_{e\mu} = 4det[\rho_{2\times2}^e(t)] = 2[1-Tr(\rho_{2\times2}^e(t))^2]$, where $\rho_{2\times2}^e(t)$ is the density matrix associated to the reduced state after tracing over muon flavor mode i.e, $\rho_{2\times2}^e(t) = Tr_{\mu}(\rho^e(t)) = \begin{pmatrix} |\tilde{U}_{ee}(t)|^2 & 0 \\ 0 & |\tilde{U}_{e\mu}(t)|^2 \end{pmatrix}$. Therefore, the tangle $(\tau_{e\mu})$ for two flavour neutrino oscillations is:

$$\tau_{e\mu} = 4|\tilde{U}_{ee}(t)|^2|1 - \tilde{U}_{ee}(t)|^2 = 4P_sP_d. \tag{3.14}$$

Similarly, concurrence¹ [70,134] is a measure of entanglement defined in Eq.(2.33) of chapter 2 which for the electron-neutrino flavour system is [43]: $C_{e\mu} = 2\sqrt{P_s P_d}$. The tangle is the square of concurrence [72], thus $\tau_{e\mu} = C_{e\mu}^2$.

In the ultra-relativistic approximation, Fig.(3.1) shows all measures of bi-partite quantum correlations, $\tau_{e\mu}$ (dotted line) and $N_{e\mu}$ (full line), with transition probabilities P_s (dashed line) and P_d (dotted dash line), of an initial electron-neutrino flavour state as a function of scaled time $T \equiv \frac{\Delta m^2 t}{2E}$. The mixing angle θ and the squared mass differences (Δm^2) are fixed at the most recent experimental values reported in ref. [54] (see Table.(1.1)). At T=0,

¹In Chapter 5, we execute quantum circuit to simulate concurrence in the two neutrino system on the IBM quantum computer.

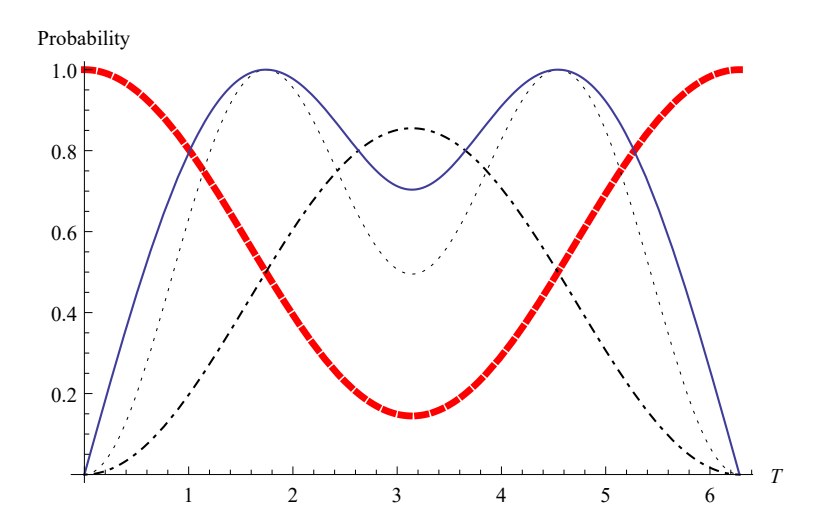


Figure 3.1: (Color online) Measures of bipartite quantum correlations Tangle $(\tau_{e\mu})$ = linear entropy $(S_{e\mu})$ (dotted line), Negativity $(N_{e\mu})$ (full line) vs scaled time $T \equiv (\frac{\Delta m^2 t}{2E})$ for an initial electron neutrino state. The dependence on oscillation probabilities, the transition probabilities P_s (dashed line) and P_d (dotted dash line) are also plotted. The mixing angle θ is fixed at the experimental value $\sin^2 \theta = 0.310$ [54]

all measures of entanglement are zero, i.e, $N_{e\mu}$ and $\tau_{e\mu}$ corresponds to an unentangled state and the two flavour modes are not mixed. For T>0, initial electron-neutrino flavour state exhibits oscillatory behavior. When transition probabilities is maximum $P_s=P_d=0.5$, all measure of entanglement tends to 1 i.e, $N_{e\mu}=\tau_{e\mu}$, which corresponds to maximally entangled state. In two flavour neutrino oscillation, among entanglement monotones, linear entropy (S) $(S=\frac{d}{d-1}[1-Tr(\rho_{2\times 2}^e(t))^2]$, see Sec.(2.3.5) of Chapter 2), where d is the dimension of the reduced density matrix $\rho_{2\times 2}^e(t)$ is linked to the variances associated with the average neutrino number [42]. The linear entropy for electron-neutrino flavour state, $S_{e\mu}=4P_sP_d=\tau_{e\mu}$.

All entanglement measures in the bipartite system- the negativity, and tangle is directly proportional to the product of survival and disappearance probabilities and coincide with linear entropy such that

$$N_{e\mu}^2 = \tau_{e\mu} = S_{e\mu} = 4P_s P_d. \tag{3.15}$$

The electron-neutrino flavour state is a pure state and these quantum correlations have a direct experimental connection with physical quantities in neutrino oscillations [134]. In the case of bipartite systems, the tangle is the square of negativity. Therefore, it is a redundant measure for bi-partite entanglement for a pure system. For the mixed state density matrix ρ , the square of the negativity can be less than tangle (concurrence also) [98].

At this juncture, we are in a position to compare our single-particle neutrino state with a single photon system, where the quantum uncertainty on "which path" of the photon at the output of an unbalanced Beam Splitter (BS) is replaced by the uncertainty on "which flavour" of the produced neutrino is measured [42]. The coefficients $\tilde{U}_{\alpha e}(t)$ and $\tilde{U}_{\alpha \mu}(t)$ play the role of transmissivity (T) and the reflectivity (R) of the BS, respectively and $BS = R(\theta) \equiv U(\theta)$ (i.e, here BS is identified as a beam splitter transformation matrix $U(\theta)$), in two-flavour neutrino oscillations. Let us consider the simplest case, Eq.(3.3), when time-evolved electron neutrino flavour state $|\nu_e(t)\rangle$ enters from port 1, and no neutrino enters from port two into the BS. The single-particle neutrino state take two paths - it either gets transmitted $T \equiv \tilde{U}_{ee}(t)$ or is reflected $T \equiv \tilde{U}_{e\mu}(t)$. Thus, the state produced by the $|\nu_e(t)\rangle$ has the form of two-mode entangled state $T \equiv T_{ee}(t)$ more precisely it is a flavour-entangled state like the Bell's state/two-qubit state in quantum optics.

3.2 Tri-partite entanglement in three-flavour neutrino oscillations

In the three generation framework of neutrino oscillation system we identify neutrino modes in the occupation number basis at time t=0 as:

$$|\nu_{e}\rangle = |1\rangle_{e} \otimes |0\rangle_{\mu} \otimes |0\rangle_{\tau} \equiv |100\rangle_{e},$$

$$|\nu_{\mu}\rangle = |0\rangle_{e} \otimes |1\rangle_{\mu} \otimes |0\rangle_{\tau} \equiv |010\rangle_{\mu},$$

$$|\nu_{\tau}\rangle = |0\rangle_{e} \otimes |0\rangle_{\mu} \otimes |1\rangle_{\tau} \equiv |001\rangle_{\tau}.$$
(3.16)

Even though it is discussed in Sec.(2.4) of Chapter 2, for the purpose of specifying entanglement, we are again debating here in brief that there are five possible partitions of three systems (A—B—C, A—BC, B—AC, C—AB, ABC)(see, e.g., Fig.(3.2)), where A, B and C are denoted by e, μ , and τ flavour modes, respectively. There exist separable (i.e., 2-separable) states of the following kind: 1-qubit separable states, which are separable for A—BC but not for B—AC nor C—AB; 2-qubit separable states, which are separable for A—BC and B—AC but not for C—AB; and 3-qubit tri-separable states are separable to any bipartition but not fully separable. Together with the fully inseparable states and the fully separable ones, the above classes constitute a complete classification of mixed three-qubit state systems; modulo permutations [135].

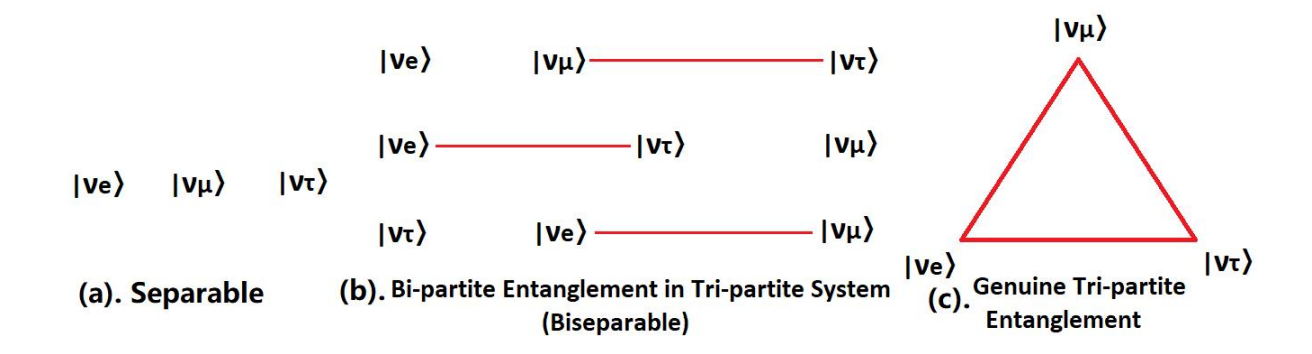


Figure 3.2: Different possible ways of visualizing three-mode state entanglement [136].

In this section, the tri-partite quantum system is studied with two measures of entanglement. First, the pairwise entanglement, which treats one flavour mode as one object (e.g. e) and the other two as a single object (e.g. $\mu\tau$), and the other two permutations of this system (see Fig.(3.2(b))). This type of bi-partite entanglement (separable) in a three-flavour (tri-partite) system can be quantified by bi-partite measures like the tangle and negativity defined earlier. Later, we will consider genuine tri-partite entanglement (see Fig.(3.2(c))), for which a measure called residual entanglement in terms of tangle and negativity is constructed separately. The genuine tri-partite entanglement measure helps us distinguish between two types of tri-partite states in quantum optics, the W-state or the GHZ-state. While the generalized W-state has a residual entanglement called three- π (which will defined later), the GHZ-state has a zero residual three- π . For the three neutrino system, the existence of a non-zero residual entanglement three- π puts neutrino states in the same class as W-states.

In reactor type neutrino experiment where an electron neutrino produced at the source can oscillate into other flavours, using Eq.(3.16) in Eq.(3.1), the time evolution of electron

flavour neutrino state in the occupation number basis can be written as [108]

$$|\nu_e(t)\rangle = \tilde{U}_{ee}(t) |100\rangle_e + \tilde{U}_{e\mu}(t) |010\rangle_\mu + \tilde{U}_{e\tau}(t) |001\rangle_\tau$$
 (3.17)

with normalization condition $|\tilde{U}_{ee}(t)|^2 + |\tilde{U}_{e\mu}(t)|^2 + |\tilde{U}_{e\tau}(t)|^2 = 1$, where e, μ and τ are a three modes (flavour) neutrino state $|100\rangle_e$, $|010\rangle_{\mu}$, and $|001\rangle_{\tau}$ respectively, in 3-qubit system. The corresponding density matrix in the standard basis $|ijk\rangle$, where each index takes the values 0 and 1 is given by

In pairwise entangled tri-partite quantum system, the probability of the three flavour state to be an e neutrino mode is $P_s = |\tilde{U}_{ee}(t)|^2$ and to be in the $\mu\tau$ mode (treating as a single quantum object) is $P_d = 1 - |\tilde{U}_{ee}(t)|^2$. The partial transposition operator on the density matrix $\rho^e(t)$ acts to the matrix elements change under the rule $|ijk\rangle \langle i'j'k'| \longrightarrow |i'jk\rangle \langle ij'k'|$. Thus,

The eigenvalues of $\rho^{T_e}(t)$ are,

$$\lambda_1 = \lambda_2 = \lambda_3 = \lambda_4 = 0,$$

 $\lambda_5 = P_s, \lambda_6 = P_d, \lambda_7 = \sqrt{P_s P_d}, \lambda_8 = -\sqrt{P_s P_d}.$
(3.20)

Thus λ_8 is not positive which means $\rho^{T_e}(t)$ is not positive operator and therefore $\rho^e(t)$ is entangled with reference to the PPT criterion. Consequently, finding $||\rho^{T_e}(t)|| = 1 + 2\sqrt{P_sP_d}$, the negativity is given $N_{e(\mu\tau)} = 2\sqrt{P_sP_d}$ and is positive, fulfilling the criterion of entanglement.

The reduced density matrix $\rho_{2\times 2}^e(t)$ after tracing one mode (flavor) is

$$\rho_{2\times2}^{e}(t) = Tr_{\mu\tau}(\rho^{e\mu\tau}(t)) = \begin{pmatrix} |\tilde{U}_{ee}(t)|^2 & 0\\ 0 & |\tilde{U}_{e\mu}(t)|^2 + |\tilde{U}_{e\tau}(t)|^2 \end{pmatrix}.$$
(3.21)

The tangle, $\tau_{e(\mu\tau)}=2[1-Tr(\rho_{2\times 2}^e(t))^2]=4P_sP_d$. When neutrino oscillates in between different modes (flavour), the linear entropy of the reduced state is $S_{e(\mu\tau)}=4P_sP_d$. Hence all measures of quantum correlations of bi-partite states of 3-qubit mode (flavour) entangled single particle neutrino state $|\nu_e(t)\rangle$ are satisfied. They are related by

$$N_{e(\mu\tau)}^2 = \tau_{e(\mu\tau)} = S_{e(\mu\tau)} = 4P_s P_d. \tag{3.22}$$

Similar calculations for the other two permutations of this system i.e., between flavour modes μ and single object $e\tau$, and between flavour modes τ and single object $e\mu$ (see Fig.(3.2(b))) correspond to $N_{\mu(e\tau)}^2 = \tau_{\mu(e\tau)} = S_{\mu(e\tau)} = 4|\tilde{U}_{e\mu}(t)|^2(|\tilde{U}_{ee}(t)|^2 + |\tilde{U}_{e\tau}(t)|^2)$ and $N_{\tau(e\mu)}^2 = \tau_{\tau(e\mu)} = 4|\tilde{U}_{e\tau}(t)|^2(|\tilde{U}_{ee}(t)|^2 + |\tilde{U}_{e\mu}(t)|^2)$, respectively. This analysis shows that the entanglement quantified by the tangle and negativity between flavour modes e and single object $\mu\tau$, between μ and single object $e\tau$, and between τ and single object $e\mu$ for the time evolved electron-neutrino flavour state (see Eq.(3.17)) has pairwise bipartite entanglement.

However, to understand a genuine tripartite entanglement, the neutrino state should be neither entirely separable nor biseparable (see Fig.(3.2(c))). The criteria genuine tri-partite entanglement:

• The quantum correlations in electron-neutrino flavour state Eq.(3.17) have to satisfy the CKW inequality, which is a monogamy inequality for tangles:

$$\tau_{e\mu} + \tau_{e\tau} \leq \tau_{e(\mu\tau)}$$
.

• The monogamy inequality for negativity $N_{e\mu}^2 + N_{e\tau}^2 \leq N_{e(\mu\tau)}^2.$

We can also define two quantities that quantify three particle entanglement called the residue of tangle and negativity $\tau_{e\mu\tau}$ and $\pi_{e\mu\tau}$, respectively by

$$\tau_{e\mu\tau} = \tau_{e(\mu\tau)} - \tau_{e\mu} - \tau_{e\tau},
\pi_{e\mu\tau} = \frac{1}{3} \left(N_{e(\mu\tau)}^2 + N_{\mu(e\tau)}^2 + N_{\tau(e\mu)}^2 - 2N_{e\mu}^2 - 2N_{e\tau}^2 - 2N_{\mu\tau}^2 \right).$$
(3.23)

These quantities represent a collective property of three flavour modes of an electron-neutrino flavour state in a three-qubit system that is unchanged by permutations, similar terms for μ and τ neutrinos can also be defined [35].

The tangle between e and μ flavour modes $\tau_{e\mu}$ and between e and τ flavour modes $\tau_{e\tau}$ is found by calculating reduced density matrix

$$\rho^{e\mu}(t) = Tr_{\tau}(\rho^{e}(t)) = \begin{pmatrix} 0 & 0 & 0 & 0\\ 0 & |\tilde{U}_{ee}(t)|^{2} & \tilde{U}_{ee}(t)\tilde{U}_{e\mu}^{*}(t) & 0\\ 0 & \tilde{U}_{e\mu}(t)\tilde{U}_{ee}^{*}(t) & |\tilde{U}_{e\mu}(t)|^{2} & 0\\ 0 & 0 & 0 & |\tilde{U}_{e\tau}(t)|^{2} \end{pmatrix}$$
(3.24)

and

$$\rho^{e\tau}(t) = Tr_{\mu}(\rho^{e}(t)) = \begin{pmatrix} 0 & 0 & 0 & 0\\ 0 & |\tilde{U}_{ee}(t)|^{2} & \tilde{U}_{ee}(t)\tilde{U}_{e\tau}^{*}(t) & 0\\ 0 & \tilde{U}_{e\tau}(t)\tilde{U}_{ee}^{*}(t) & |\tilde{U}_{e\tau}(t)|^{2} & 0\\ 0 & 0 & 0 & |\tilde{U}_{e\mu}(t)|^{2} \end{pmatrix},$$
(3.25)

respectively. For $e\tau$ flavour modes, the eigen values of the product

$$\rho^{e\tau}(t)\tilde{\rho}^{e\tau}(t) = \begin{pmatrix} 0 & 0 & 0 & 0\\ 0 & 2|\tilde{U}_{ee}(t)|^2|\tilde{U}_{e\tau}(t)|^2 & 2|\tilde{U}_{ee}(t)|^2\tilde{U}_{ee}(t)\tilde{U}_{e\tau}^*(t) & 0\\ 0 & 2|\tilde{U}_{e\tau}(t)|^2\tilde{U}_{e\tau}(t)\tilde{U}_{ee}^*(t) & 2|\tilde{U}_{ee}(t)|^2|\tilde{U}_{e\tau}(t)|^2 & 0\\ 0 & 0 & 0 & 0 \end{pmatrix}$$
(3.26)

are $\mu_1 = \mu_2 = \mu_3 = 0$ and $\mu_4 = 4|\tilde{U}_{ee}(t)|^2|\tilde{U}_{e\tau}(t)|^2$, where $\tilde{\rho}^{e\tau}(t)$ is a "spin-flipped "density matrix $\tilde{\rho}^{e\tau}(t) = (\sigma_y \otimes \sigma_y)\rho^{*e\tau}(t)(\sigma_y \otimes \sigma_y)$. This leads to the tangle for $e\tau$ and similarly, for $e\mu$ flavour modes given by ,

$$\tau_{e\tau} = Tr(\rho^{e\tau}(t)\tilde{\rho}^{e\tau}(t)) = 4|\tilde{U}_{ee}(t)|^2|\tilde{U}_{e\tau}(t)|^2,$$

$$\tau_{e\mu} = Tr(\rho^{e\mu}(t)\tilde{\rho}^{e\mu}(t)) = 4|\tilde{U}_{ee}(t)|^2|\tilde{U}_{e\mu}(t)|^2.$$
(3.27)

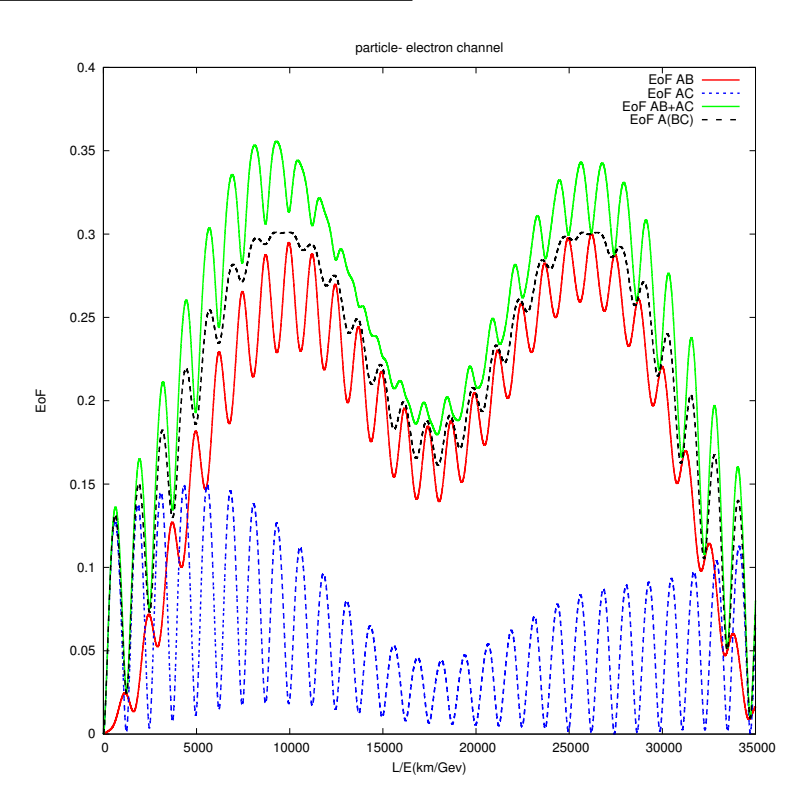


Figure 3.3: (Color online) Entanglement of formation (E_f) vs $\frac{L}{E}\frac{Km}{GeV}$ graph between e,μ , and τ satisfying: $E_f(\tau_{e\mu}) + E_f(\tau_{e\tau}) > E_f(\tau_{e(\mu\tau)})$ where $E_f(\tau_{e\mu})$ (Red line), $E_f(\tau_{e\tau})$ (Blue line), the sum $E_f(\tau_{e\mu}) + E_f(\tau_{e\tau})$ (Green line) and $E_f(\tau_{e(\mu\tau)})$ (Black line). Here A, B and C are three qubit e, μ and τ flavour mode neutrino states, respectively.

The CKW inequality in terms of tangle is: $\tau_{e\mu} + \tau_{e\tau} = \tau_{e(\mu\tau)}$ and is unchanged by permutation (i.e, $\tau_{\mu e} + \tau_{\mu\tau} = \tau_{\mu(e\tau)}$, $\tau_{\tau e} + \tau_{\tau\mu} = \tau_{\tau(e\mu)}$). Thus, the residual tangle between flavour mode e, μ and τ is zero i.e, $\tau_{e\mu\tau} = 0$. The result shows that for any values of the tangle satisfying equality $\tau_{e\mu} + \tau_{e\tau} = \tau_{e(\mu\tau)}$, there is a quantum state that is consistent with those values. The CKW inequality is valid when the density matrix of the product $\rho^{AC}\tilde{\rho}^{AC}$ should have \leq two non-zero eigenvalues [72]. Since we get a one non-zero eigenvalue $\mu_4 = 4|\tilde{U}_{ee}(t)|^2|\tilde{U}_{e\tau}(t)|^2$ of the product $\rho^{e\tau}\tilde{\rho}^{e\tau}$ which satisfied the condition. In particular, the CKW inequality becomes equality for this case, and the three-tangle $(\tau_{e\mu\tau})$ vanishes as it does for the W-state [35]. Thus the tri-partite neutrino system in the case of three qubits in a pure state satisfies the CKW inequality. The GHZ state, on the other hand, obeys the CKW inequality (not-equality); therefore, the three-tangle is greater than zero.

Unlike tangle, the entanglement of formation ² (EOF or $E_f(\tau)$) [72] defined in Eq.(2.35) of chapter 2 do not satisfy fully the additive property for the tri-partite three neutrino system.

²The solution of an important unsolved problem of whether the EOF is additive in nature is still not found [71].

For the time evolved electron flavour neutrino state, the relation follows

$$E_f(\tau_{e\mu}) + E_f(\tau_{e\tau}) > E_f(\tau_{e(\mu\tau)}).$$
 (3.28)

This result is shown in Fig.(3.3).

 $N_{e\mu}$ and $N_{e\tau}$ are the negativities of the mixed states $\rho^{e\mu}(t) = Tr_{\tau}(\rho^{e\mu\tau}(t))$ and $\rho^{e\tau}(t) = Tr_{\mu}(\rho^{e\mu\tau}(t))$, respectively [35]. We find that the entanglement negativity of the e μ flavour modes is

$$N_{e\mu}^2 = 4|\tilde{U}_{ee}(t)|^2|\tilde{U}_{e\mu}(t)|^2 + 2|\tilde{U}_{e\tau}(t)|^4 - 2|\tilde{U}_{e\tau}(t)|^2\sqrt{|\tilde{U}_{e\tau}(t)|^4 + 4|\tilde{U}_{ee}(t)|^2|\tilde{U}_{e\mu}(t)|^2}.$$
 (3.29)

For $e \tau$ flavour modes the negativity is

$$N_{e\tau}^2 = 4|\tilde{U}_{ee}(t)|^2|\tilde{U}_{e\tau}(t)|^2 + 2|\tilde{U}_{e\mu}(t)|^4 - 2|\tilde{U}_{e\mu}(t)|^2\sqrt{|\tilde{U}_{e\mu}(t)|^4 + 4|\tilde{U}_{ee}(t)|^2|\tilde{U}_{e\tau}(t)|^2}, \quad (3.30)$$

and also, for the e and $(\mu\tau)$ system we have $N_{e(\mu\tau)}^2=4|\tilde{U}_{ee}(t)|^2(|\tilde{U}_{e\mu}(t)|^2+|\tilde{U}_{e\tau}(t)|^2)$. The resulting CKW inequality: $N_{e\mu}^2+N_{e\tau}^2\leq N_{e(\mu\tau)}^2$ implies:

$$|\tilde{U}_{e\mu}(t)|^{4} + |\tilde{U}_{e\tau}(t)|^{4} < |\tilde{U}_{e\tau}(t)|^{2} \sqrt{|\tilde{U}_{e\tau}(t)|^{4} + 4|\tilde{U}_{ee}(t)|^{2}|\tilde{U}_{e\mu}(t)|^{2}} + |\tilde{U}_{e\mu}(t)|^{2} \sqrt{|\tilde{U}_{e\mu}(t)|^{4} + 4|\tilde{U}_{ee}(t)|^{2}|\tilde{U}_{e\tau}(t)|^{2}}.$$
(3.31)

Fig.(3.4) shows that in the ultra-relativistic approximation, the time evolution of the sum of the entanglement negativity between flavour mode e and μ and between e and τ is less than entanglement negativity between flavour mode e and $\mu\tau$ i.e, $N_{e\mu}^2 + N_{e\tau}^2 < N_{e(\mu\tau)}^2$. With this result, we can say that the CKW inequality in terms of negativity is strict (because $U_{ee}(t) \neq 0$, $U_{e\mu}(t) \neq 0$, $U_{e\tau}(t) \neq 0$) and that, the inequality in terms of a tangle between different flavour modes of neutrino is characteristic of a general class of W-states. To understand the tightness of the monogamy inequality in terms of negativity (see Sec.(2.4.2) of chapter 2), the three- π is analogous to three tangles ($\tau_{e\mu\tau}$) is studied in the context of three flavour neutrino oscillations.

For electron-neutrino flavour (and analogously for a muon or tau neutrino system), it can be defined as [35]: $\pi_{e\mu\tau} = \frac{\pi_e + \pi_\mu + \pi_\tau}{3}$, where $\pi_e = N_{e(\mu\tau)}^2 - N_{e\mu}^2 - N_{e\tau}^2$, $\pi_\mu = N_{\mu(e\tau)}^2 - N_{\mu e}^2 - N_{\mu e}^2$, and $\pi_\tau = N_{\tau(e\mu)}^2 - N_{\tau e}^2 - N_{\tau \mu}^2$ are the residual entanglement in terms of negativity and the subscript e, μ and τ in π_e , π_μ , π_τ mean the flavour mode e, flavour mode μ , and flavour mode

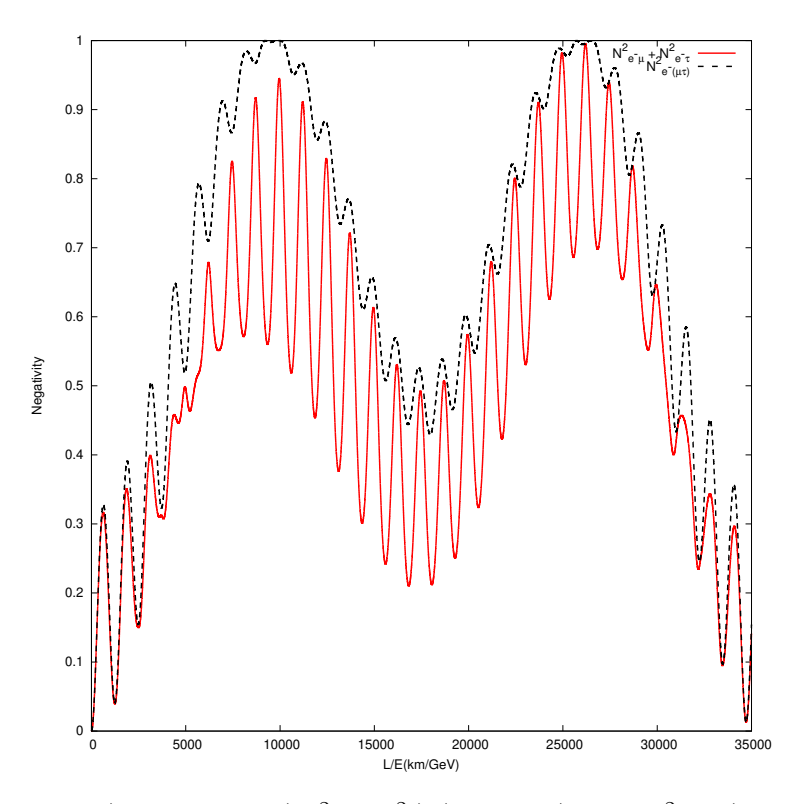


Figure 3.4: (Color online) Negativity $(N_{e\mu}^2 + N_{e\tau}^2)$ (Red line) and $N_{e(\mu\tau)}^2$ (Black line) vs $\frac{L}{E}(\frac{Km}{GeV})$ graph between flavour modes electron, muon, and tau neutrinos satisfying: $N_{e\mu}^2 + N_{e\tau}^2 < N_{e(\mu\tau)}^2$. Parameters θ_{ij} and Δm_{ij}^2 are fixed at the experimental values [54].

au are taken as the focus respectively. Using the negativity values calculated earlier to get π_e , π_μ , and π_τ we find $\pi_e \neq \pi_\mu \neq \pi_\tau$. We can see from Fig.(3.5) that unlike tangle, the residual entanglement have the different maxima $(\pi_e, \pi_\mu \text{ and } \pi_\tau)$ at scale of distance per energy unit $\frac{L}{E} > 0$, and $\pi_e \neq \pi_\mu \neq \pi_\tau$. This gives clear indication that the residual entanglement π_e , π_μ and π_τ are quantified but it can not be the measure of genuine tri-partite entanglement as the measures are not invariant under permutations. As the measure of genuine tri-partite entanglement in three flavour neutrino oscillations, we define $\pi_{e\mu\tau}$ as the average of π_e , π_μ , and π_τ , such that $\pi_{e\mu\tau} = \frac{1}{3}(N_{e(\mu\tau)}^2 + N_{\mu(e\tau)}^2 + N_{\tau(e\mu)}^2 - 2N_{e\mu}^2 - 2N_{e\tau}^2 - 2N_{\mu\tau}^2)$ (see Eq.(3.23)). $\pi_{e\mu\tau}$ is now invariant under permutations of flavour mode in an electron- neutrino flavour state. Thus,

$$\pi_{e\mu\tau} = \frac{4}{3} [|\tilde{U}_{ee}(t)|^2 \sqrt{|\tilde{U}_{ee}(t)|^4 + 4|\tilde{U}_{e\mu}(t)|^2 |\tilde{U}_{e\tau}(t)|^2}$$

$$+ |\tilde{U}_{e\mu}(t)|^2 \sqrt{|\tilde{U}_{e\mu}(t)|^4 + 4|\tilde{U}_{ee}(t)|^2 |\tilde{U}_{e\tau}(t)|^2}$$

$$+ |\tilde{U}_{e\tau}(t)|^2 \sqrt{|\tilde{U}_{e\tau}(t)|^4 + 4|\tilde{U}_{ee}(t)|^2 |\tilde{U}_{e\mu}(t)|^2}$$

$$- |\tilde{U}_{ee}(t)|^4 - |\tilde{U}_{e\mu}(t)|^4 - |\tilde{U}_{e\tau}(t)|^4].$$
(3.32)

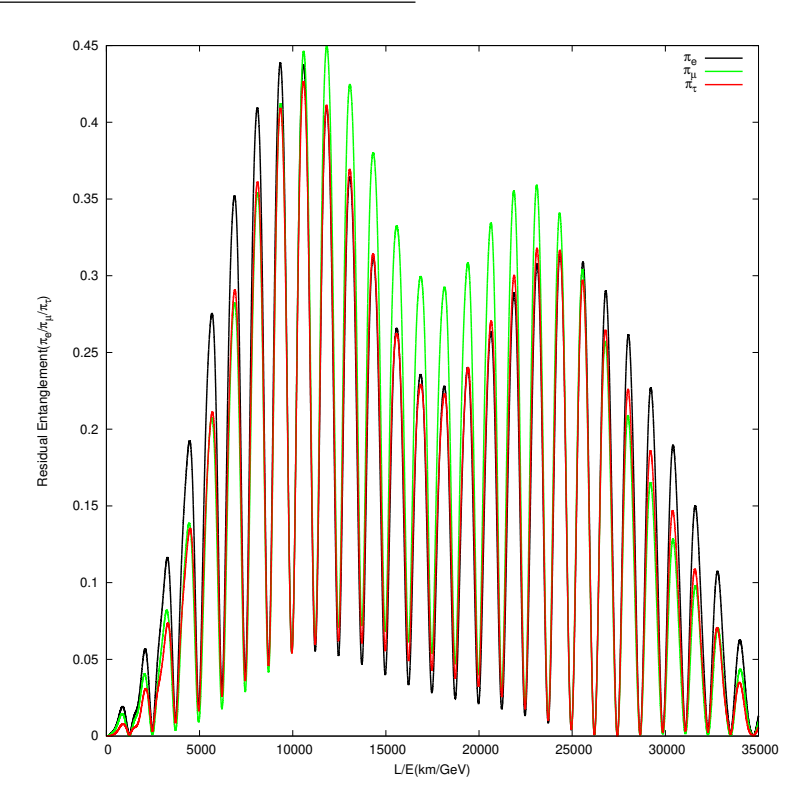


Figure 3.5: (Color online) Residual entanglement π_e (Black line), π_{μ} (Green line), π_{τ} (Red line) vs $\frac{L}{E}(\frac{Km}{GeV})$ graph between flavour modes of electron, muon and tau neutrinos satisfying: $\pi_e \neq \pi_{\mu} \neq \pi_{\tau}$. Parameters θ_{ij} and Δm_{ij}^2 are fixed at the experimental values [54].

From Fig.(3.6), we note that for $\frac{L}{E} > 0$, entanglement among three-flavour modes occurs i.e, $\pi_{e\mu\tau} > 0$, and exhibits a typical oscillatory behavior. At largest mixing i.e, when transition probabilities are $P_{\nu_{e\to e}} = 0.39602$, $P_{\nu_{e\to \mu}} = 0.435899$, and $P_{\nu_{e\to \tau}} = 0.168081$, we find that $\pi_{e\mu\tau}$ reaches the maximum value 0.436629.

So far, we have considered the time evolution of entanglement characteristics of an electron neutrino state, which are relevant for reactor experiments. For completeness, we give the appropriate entanglement measures for a muon neutrino state relevant to accelerator experiments.

$$|\nu_{\mu}(t)\rangle = \tilde{U}_{\mu e}(t) |100\rangle_{e} + \tilde{U}_{\mu\mu}(t) |010\rangle_{\mu} + \tilde{U}_{\mu\tau} |001\rangle_{\tau}$$
 (3.33)

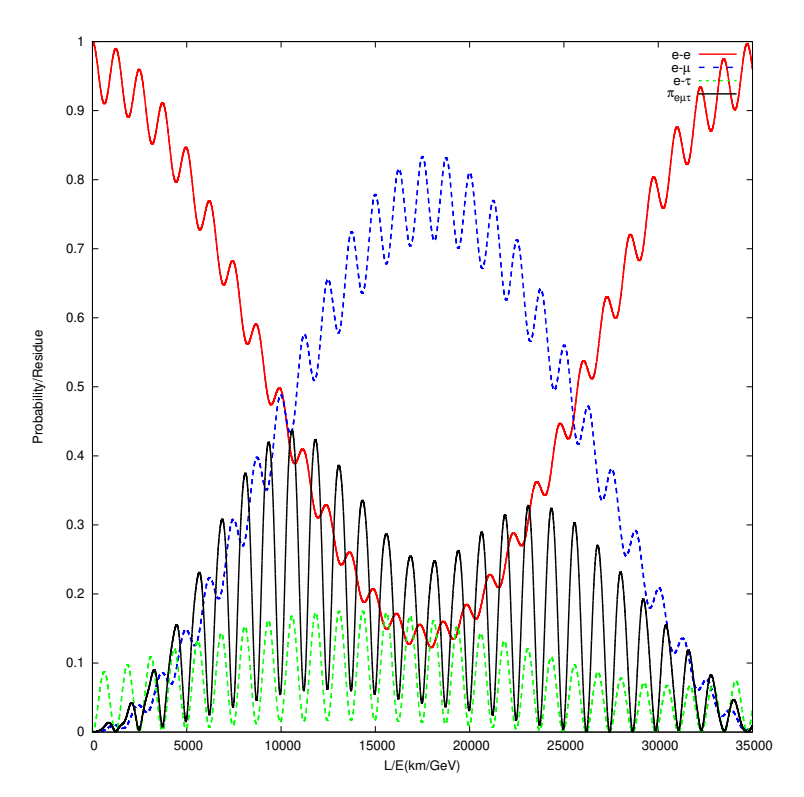


Figure 3.6: (Color online) Residual entanglement $\pi_{e\mu\tau}$ (Black line) vs $\frac{L}{E}(\frac{Km}{GeV})$ graph between the flavour modes electron, muon and tau neutrinos. Parameters θ_{ij} and Δm_{ij}^2 are fixed at the experimental values [54]. The transition probabilities $P_{\nu_{e\to e}}$ (Red line), $P_{\nu_{e\to \mu}}$ (Blue line) and $P_{\nu_{e\to \tau}}$ (Green line) are reported as well for comparison.

where, $|\tilde{U}_{\mu e}(t)|^2 + |\tilde{U}_{\mu \mu}(t)|^2 + |\tilde{U}_{\mu \tau}(t)|^2 = 1$. The relevant density matrix is

For the initial muon-flavour neutrino state the CKW inequality in terms of tangle becomes equal, consequently the residual tangle vanishes, i.e $\tau_{\mu e \tau} = 0$. Whereas, the CKW inequality in terms of negativity is strict i.e, $N_{\mu e}^2 + N_{\mu \tau}^2 < N_{\mu (e \tau)}^2$.

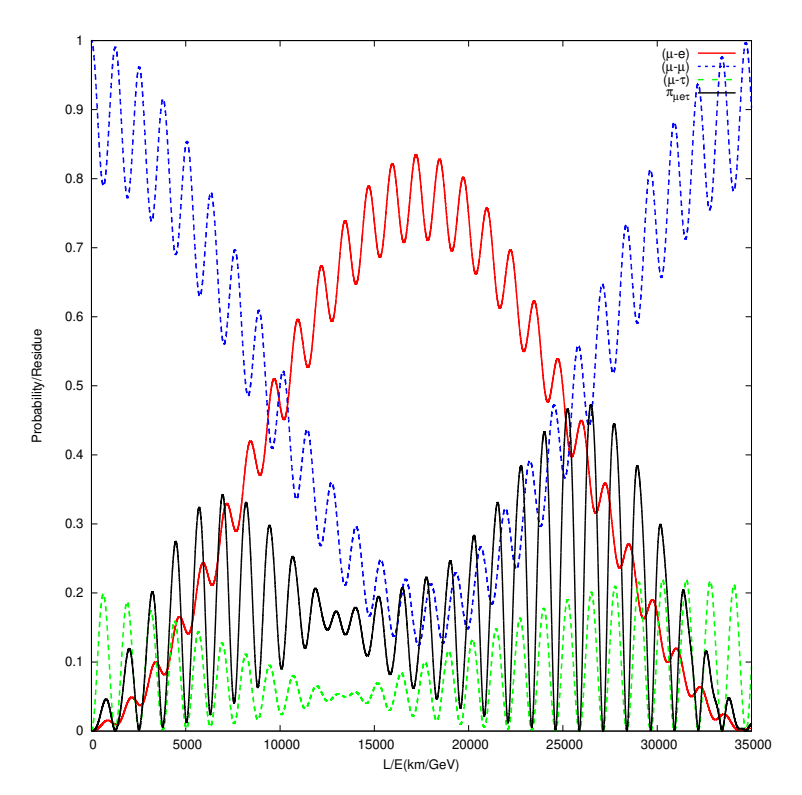


Figure 3.7: (Color online) Residual entanglement $\pi_{\mu e \tau}$ (Black line) vs $\frac{L}{E}(\frac{Km}{GeV})$ graph between the flavour modes electron, muon and tau neutrinos. Parameters θ_{ij} and Δm_{ij}^2 are fixed at the experimental values [54]. The transition probabilities $P_{\nu_{\mu \to e}}$ (Red line), $P_{\nu_{\mu \to \mu}}$ (Blue line) and $P_{\nu_{\mu \to \tau}}$ (Green line) are reported as well for comparison.

The measure of tri-partite entanglement is

$$\pi_{\mu e \tau} = \frac{4}{3} [|\tilde{U}_{\mu e}(t)|^2 \sqrt{|\tilde{U}_{\mu e}(t)|^4 + 4|\tilde{U}_{\mu \mu}(t)|^2 |\tilde{U}_{\mu \tau}(t)|^2}$$

$$+ |\tilde{U}_{\mu \mu}(t)|^2 \sqrt{|\tilde{U}_{\mu \mu}(t)|^4 + 4|\tilde{U}_{\mu e}(t)|^2 |\tilde{U}_{\mu \tau}(t)|^2}$$

$$+ |\tilde{U}_{\mu \tau}(t)|^2 \sqrt{|\tilde{U}_{\mu \tau}(t)|^4 + 4|\tilde{U}_{\mu e}(t)|^2 |\tilde{U}_{\mu \mu}(t)|^2}$$

$$- |\tilde{U}_{\mu e}(t)|^4 - |\tilde{U}_{\mu \mu}(t)|^4 - |\tilde{U}_{\mu \tau}(t)|^4].$$
(3.35)

From Fig.(3.7), we observe that at $\frac{L}{E} = 0$, $\pi_{\mu e \tau} = 0$, which mean the initial muon-neutrino flavour state is separable. At $\frac{L}{E} > 0$, entanglement among three-flavour modes occur and $\pi_{\mu e \tau} > 0$ oscillates. For maximum mixing, $\pi_{\mu e \tau}$ reaches a value 0.472629 showing tri-partite entanglement.

The three neutrino state exhibits tri-partite entanglement akin to the W-state. The threetangle and the residual entanglement measures of genuine tri-partite entanglement. The three-tangle is maximal for the GHZ state but vanishes for the W-state. This means that the three-tangle is not suitable as a measure of genuine tri-partite entanglement. The three-tangle reveals the existence of two inequivalent kinds of tripartite entanglement for pure three-qubit states. This is very briefly explained in the reference [92]. Compared to the residual entanglement three- π , the three-tangle generally underestimates the entanglement [35]. For the three-neutrino case, Eq.(3.32) (and Eq.(3.35)) of non-zero $\pi_{e\mu\tau}$ (and $\pi_{\mu e\tau}$) gives a reliable measures of tri-partite entanglement. In quantum optics, there are also measures of entanglement for qutrits, which may be relevant to tri-partite entanglement [47].

We compare the value of $\pi_{e\mu\tau}$ and $\pi_{\mu e\tau}$ with the three- π value of prototype W-state i.e., $\pi_{ABC}(W_1) = 0.549363$ [35] (see Sec.(2.4.2) of chapter 2), we get

$$\pi_{e\mu\tau}(\nu_e) < \pi_{\mu e\tau}(\nu_\mu) < \pi_{ABC}(W_1).$$
(3.36)

Hence, satisfying CKW inequality and with all properties of W-state (see Eq.(2.70))

$$\pi_{e\mu\tau} > 0; \tau_{e\mu\tau} = 0$$
or, $\pi_{\mu e\tau} > 0; \tau_{\mu e\tau} = 0,$
(3.37)

implies that the form of mode (flavour) entangled neutrino state Eq.(3.1) has the general properties of tri-partite entangled W-state.

Chapter 4

Quantum Computing

The theory of quantum computing depends on quantum mechanics to perform quantum calculations [45]. The method of assembling quantum computers was pioneered by Paul Benioff in 1980 where he proposed Turing machine which is a quantum mechanical model [137]. Later Richard Feynman introduced an idea that quantum computer could efficiently simulate quantum systems which a classical computer couldn't possibly [138, 139]. In 1985, Deutsch's model of a quantum computer showed us that quantum computers have computational power more than classical computers [140, 141]. Since then the improved version of Deutsch's model was experimentally proved by many scientist like Richard Jozsa [142], Ethan Bernstein and Umesh Vazirani [143], Daniel R. Simon [144], Peter W. Shor [145], Lov K. Grover [146] etc., to tackle specific computational issues a lot quicker than classically.

Today, the idea of investigating quantum simulation on quantum computer has reached out to a wide topics of science like entanglement in many-body systems [147–149], quantum phase transitions [150], molecular physics [151–153], quantum field theoretic problem [154–157], biology [158], neural networks [159], pharmacology [160], quantum gravity [161], quantum chaos [162], quantum chromodynamics [163] etc. Likewise, experimental realization of quantum simulation have effectively been made in frameworks like NMR [164–166], iontrap [167, 168], atomic [150, 169] and photonic quantum computers [153, 170]. The current status of this field can be determined from these recent papers [171–177].

The quantum gates and circuit model is the most broadly used model to study quantum computing in light of the quantum bit, or "qubit" (a property known as superposition). In general, IBM quantum provides a superconducting-qubit based quantum computer that is accessible online to a wide class of researchers [44]. The tasks which can be executed

effectively on IBMQ platform are very well explained in references [178–187].

Chapter 2 of the thesis shows that the superposed Bell's state of 2 qubit, the GHZ and W states of 3 qubit are maximally entangled. In this chapter, we construct quantum gates and circuits to simulate these entangled states on IBM quantum cloud computer [44].

The chapter's organization is: In Sec.(4.1), we have geometrically explained the structure of the qubit. Sec.(4.2) defined a few quantum gates of single-qubit and two-qubits. In Sec.(4.3), the quantum circuits of Bell's states, the GHZ state, and prototype W-state are constructed, and Sec.(4.4) shows the simulation of these quantum circuits on the IBM quantum cloud computer. Sec.(4.5) extends our study further and proposes a quantum circuit to simulate the entanglement measure-concurrence of 2-qubit arbitrary pure state on the IBM quantum cloud computer.

4.1 Geometrical representation of Qubit

An actual execution of a qubit can be given on a basic level by any quantum framework with two states ($|0\rangle$ and $|1\rangle$), for example, the orientation of spin-half particle or 2 orthogonal polarization states of photon. Another convenient representation of a state of single-qubit $|\psi\rangle = c_1 |0\rangle + c_2 |1\rangle$ (see Eq.(2.1) of chapter 2) is

$$|\psi\rangle = \cos(\frac{\theta}{2})|0\rangle + e^{i\phi}\sin(\frac{\theta}{2})|1\rangle.$$
 (4.1)

where $0 \le \phi \le 2\pi$ and $0 \le \theta \le \pi$. In order to check whether the qubit state $|\psi\rangle$ is pure or mixed, it is possible to express a density matrix ρ of a qubit using the Bloch sphere in which the points on the surface of sphere are qubit states shown in Fig.(4.1). A general equation with a positive semi-definite Hermitian matrix of trace 1 which is ρ , is given as

$$\rho = \frac{1}{2}(I + u_x\sigma_x + u_y\sigma_y + u_z\sigma_z) \tag{4.2}$$

where $I=\begin{pmatrix} 1 & 0 \\ 0 & 1 \end{pmatrix}$, $\sigma_x=\begin{pmatrix} 0 & 1 \\ 1 & 0 \end{pmatrix}$, $\sigma_y=\begin{pmatrix} 0 & -i \\ i & 0 \end{pmatrix}$ and $\sigma_z=\begin{pmatrix} 1 & 0 \\ 0 & -1 \end{pmatrix}$ are Pauli matrices and u_x , u_y and u_z are real coefficients. This permits us to associate u_x , u_y and u_z with the x, y and z components of the Bloch vector i.e, $\vec{u}=u_x\hat{x}+u_y\hat{y}+u_z\hat{z}$ and the eigenvectors $|\lambda\rangle$ and $|\phi\rangle$ of ρ are also eigenvectors of $u_x\sigma_x+u_y\sigma_y+u_z\sigma_z$ corresponding to the eigenvalues

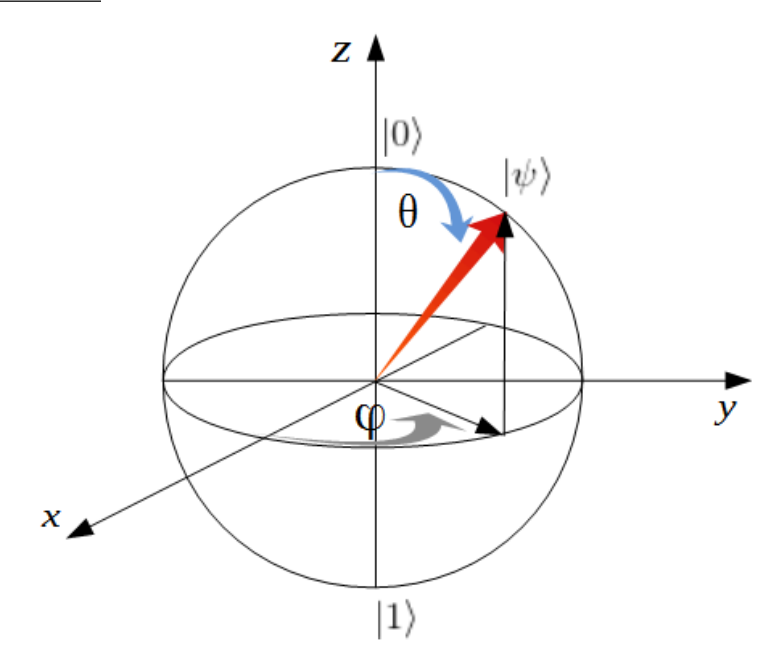


Figure 4.1: This figure represent the Bloch sphere where $|0\rangle$ and $|1\rangle$ are north and south poles, respectively and which are opposite points of mutual orthogonal states. The x, y-axes have an eigenstates σ_x and σ_y , respectively.

 $\pm\sqrt{u_x^2+u_y^2+u_z^2}$. Therefore, the diagonalized density operator ρ is

$$\rho = \frac{1}{2} (1 + \sqrt{u_x^2 + u_y^2 + u_z^2}) |\lambda\rangle \langle \lambda| + \frac{1}{2} (1 - \sqrt{u_x^2 + u_y^2 + u_z^2}) |\phi\rangle \langle \phi|.$$
 (4.3)

The states which lie on the surface of the Bloch sphere reduces to pure state $|\lambda\rangle\langle\lambda|$ satisfying condition $u_x^2 + u_y^2 + u_z^2 = 1$, while the condition $u_x^2 + u_y^2 + u_z^2 < 1$ represent mixed states where the Bloch vector is a point within the sphere. In general, the components of the Bloch vector can be determined by (i = x, y, z)

$$\langle \sigma_i \rangle = Tr(\rho \sigma_i) = u_i.$$
 (4.4)

For the state $|\psi\rangle$ in Eq.(4.1),

$$\rho = |\psi\rangle\langle\psi| = \begin{pmatrix} \cos^2(\frac{\theta}{2}) & e^{-i\phi}\frac{\sin(\theta)}{2} \\ e^{i\phi}\frac{\sin(\theta)}{2} & \sin^2(\frac{\theta}{2}) \end{pmatrix},\tag{4.5}$$

with $Tr(\rho) = 1$. Using Eq.(4.5) in Eq.(4.4), the components of the Bloch vector are obtained as $u_x = sin\theta cos\phi$, $u_y = sin\theta sin\phi$ and $u_z = cos\theta$. Thus, the Bloch vector correspond to unit

length i.e, $|\vec{u}|^2 = 1$ implying the state $|\psi\rangle$ as a single qubit pure state lying on the Bloch-sphere surface.

4.2 Quantum gate

To put the qubit in different states of the Bloch-sphere, we require the idea of a quantum gate. Quantum computers control qubits utilizing quantum gates. A quantum gate of single qubit is a 2×2 unitary matrix where the unitary matrix is chosen such that the quantum gate is reversible and probability amplitudes are preserved. Therefore, a quantum state can be evolved using quantum gate where an underlying state $|\psi\rangle$ changes into the new state as

$$|\psi'\rangle = U |\psi\rangle, \tag{4.6}$$

where U addresses the unitary quantum gate with $U^{\dagger}U=1$, which is matrix-vector multiplication. In the following sub-sections, we explore a few unitary quantum gates of one and two qubits, which would be useful to construct a quantum circuit of a state of a quantum system.

4.2.1 Universal gate

The most general form of a single-qubit unitary quantum gate is the U3 universal gate implemented on IBM quantum machine. It is defined in matrix form as

$$U3(\theta,\phi,\lambda) = \begin{pmatrix} \cos\frac{\theta}{2} & -\sin\frac{\theta}{2}e^{i\lambda} \\ \sin\frac{\theta}{2}e^{i\phi} & \cos\frac{\theta}{2}e^{i(\lambda+\phi)} \end{pmatrix}. \tag{4.7}$$

The unitary operators on single qubits can be pictured in the Bloch sphere. One way of visualizing this picture is by writing the U3 gate as an arrangement of rotation operators with respect to x, y, z axes. Setting $\lambda = \frac{\pi}{2}$ and $\phi = -\frac{\pi}{2}$ define the x-axis rotation gate, $R_x(\theta)$:

$$R_x(\theta) = \begin{pmatrix} \cos\frac{\theta}{2} & -i\sin\frac{\theta}{2} \\ -i\sin\frac{\theta}{2} & \cos\frac{\theta}{2} \end{pmatrix} = U3(\theta, -\frac{\pi}{2}, \frac{\pi}{2}). \tag{4.8}$$

Similarly, the y-axis rotation gate can be obtained by setting $\lambda = 0$ and $\phi = 0$

$$R_y(\theta) = \begin{pmatrix} \cos\frac{\theta}{2} & -\sin\frac{\theta}{2} \\ \sin\frac{\theta}{2} & \cos\frac{\theta}{2} \end{pmatrix} = U3(\theta, 0, 0). \tag{4.9}$$

Further, setting $\theta = 0$ and $\lambda = 0$ and multiplying by a global-phase $e^{-i\frac{\phi}{2}}$, we get the z-axis rotation gate as

$$R_z(\phi) = \begin{pmatrix} e^{-i\frac{\phi}{2}} & 0\\ 0 & e^{i\frac{\phi}{2}} \end{pmatrix} = e^{-i\frac{\phi}{2}}U3(0,\phi,0). \tag{4.10}$$

These gates are themselves unitary and so is

$$U \equiv R_z(\phi)R_y(\theta)R_z(\theta) = U3(\theta,\phi,\lambda). \tag{4.11}$$

Thus, we have the unitary operator quantum gates to rotate the state anywhere in the Bloch sphere.

4.2.2 Pauli gates

The least complex single qubit gate is a bit-flip gate known as NOT gate denoted by X. Its matrix representation is obtained from $U3(\theta, \phi, \lambda)$ by

$$X \equiv \begin{pmatrix} 0 & 1 \\ 1 & 0 \end{pmatrix} = U3(\pi, 0, \pi). \tag{4.12}$$

The above matrix is similar to Pauli σ_x matrix. The action of Pauli-X gate is to flip the state $|0\rangle$ to $|1\rangle$ and vice-versa. A qubit can also flip its superposition state if $X(c_1|0\rangle + c_2|1\rangle) = c_2|0\rangle + c_1|1\rangle$.

Similarly, Pauli-Y and Z gate are called phase flip gate and its matrix representation obtained from U3 gate can be written as $Y = \begin{pmatrix} 0 & -i \\ i & 0 \end{pmatrix} = U3(\pi, \pi/2, \pi/2)$ and $Z = \begin{pmatrix} 1 & 0 \\ 0 & -1 \end{pmatrix} = U3(0,0,\pi)$.

4.2.3 Hadamard gate

In quantum computing the Hadamard gate is an essential quantum gate because if the qubit starts in a definite $|0\rangle$ or $|1\rangle$ state, the Hadamard gate places each into a superposition of

 $|0\rangle$ and $|1\rangle$ states. Mathematically, this gate has following matrix representation

$$H = \frac{1}{\sqrt{2}} \begin{pmatrix} 1 & 1\\ 1 & -1 \end{pmatrix} = U3(\frac{\pi}{2}, 0, \pi). \tag{4.13}$$

Using matrix multiplication, this gate acts on initial states $|0\rangle$ and $|1\rangle$ such as:

$$H|0\rangle = \frac{1}{\sqrt{2}}(|0\rangle + |1\rangle); \quad H|1\rangle = \frac{1}{\sqrt{2}}(|0\rangle - |1\rangle). \tag{4.14}$$

To recover qubit to its definite state we need to apply Hadamard gate two times on $|0\rangle$ or $|1\rangle$ state i.e., $HH|0\rangle = |0\rangle$ and $HH|1\rangle = |1\rangle$.

4.2.4 Controlled NOT gate

In all the previous sub-sections, we studied the Universal gate, NOT gate, and Hadamard (H) gate, a single qubit quantum gate. Now we look at the two-qubit quantum gate. The Controlled-NOT gate (CNOT), also known as the controlled-X (CX) gate, is used for entangling the 2 qubits together and is essential in quantum computing or algorithm. This gate has two input qubits, the control qubit and the target qubit, respectively. On the computational basis, this gate flips the target qubit if the control qubit is in the $|1\rangle$ state. In equations:

$$|00\rangle \rightarrow |00\rangle; |01\rangle \rightarrow |01\rangle; |10\rangle \rightarrow |11\rangle; |11\rangle \rightarrow |10\rangle.$$
 (4.15)

In this sense, the CNOT gate is a generalization of the classical XOR gate, and the action of the gate may be summarized as

$$|a,b\rangle \to |a,b\oplus a\rangle$$
 (4.16)

where a is a control qubit and b is the target qubit, and \oplus is addition modulo two, which is exactly what the XOR gate does. The control qubit and the target qubit are XORed and stored in the target qubit. The matrix representation of the CNOT gate is given by

$$CNOT = \begin{pmatrix} 1 & 0 & 0 & 0 \\ 0 & 1 & 0 & 0 \\ 0 & 0 & 0 & 1 \\ 0 & 0 & 1 & 0 \end{pmatrix} \tag{4.17}$$

with unitary condition $(CNOT)^{\dagger}(CNOT) = I$. The schematic symbol notation for the CNOT gate is given in Fig.(4.2). Even though the CNOT gate is not derived directly from the Universal gate, both CNOT and single-qubit gates are essential gates in quantum computing because any multiple qubit logic gates can be composed of them.

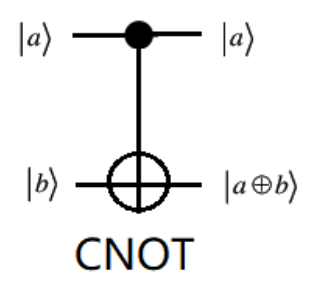


Figure 4.2: The Symbol of CNOT gate with two input qubits where a is control qubit and b is target qubit.

4.2.5 Controlled-U3 gate

A controlled version of the Universal (U3) gate (generic single qubit rotation), also called Controlled-U3 (CU3) gate includes a global phase $e^{i\gamma}$ of the U3 gate along with four parameter two-qubit gate. The matrix representation of CU3-gate is

$$CU3(\theta, \phi, \lambda, \gamma) = \begin{pmatrix} 1 & 0 & 0 & 0\\ 0 & e^{i\gamma}cos(\frac{\theta}{2}) & 0 & -e^{i(\gamma+\lambda)}sin(\frac{\theta}{2})\\ 0 & 0 & 1 & 0\\ 0 & e^{i(\gamma+\phi)}sin(\frac{\theta}{2}) & 0 & e^{i(\gamma+\phi+\lambda)}cos(\frac{\theta}{2}) \end{pmatrix}$$
(4.18)

The circuit symbol of CU3-gate is shown in Fig.(4.3). In the next section, we introduce some primary quantum circuits using the combination of U3, $R_y(\theta)$, X, H, CNOT, and CU3 gates.

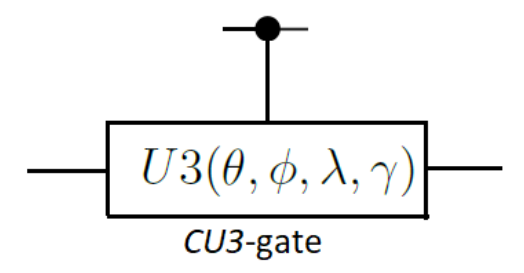


Figure 4.3: The symbol of two qubit Controlled-U3 gate.

Input	Output (Bell states)
$(ab\rangle)$	
$ 00\rangle$	$(00\rangle + 11\rangle)/\sqrt{2} \equiv \xi_{00}\rangle$
$ 01\rangle$	$(01\rangle + 10\rangle)/\sqrt{2} \equiv \xi_{01}\rangle$
$ 10\rangle$	$(00\rangle - 11\rangle)/\sqrt{2} \equiv \xi_{10}\rangle$
$ 11\rangle$	$(01\rangle - 10\rangle)/\sqrt{2} \equiv \xi_{11}\rangle$

Table 4.1: The truth table of two qubit Bell states.

4.3 Quantum circuit

Changes to a quantum state are well explained with quantum computing tools. To study quantum data, a quantum computer consists of quantum circuits of wires and elementary quantum gates unlike classical computer that uses electrical circuits and logic gates. With the arrangement of quantum gates and coherent quantum operations on qubits (quantum data), a quantum circuit also uses data from classical computation. In this segment, we construct the quantum circuit of quantum states such as Bell states, the GHZ state, and prototype W-state. The properties of these states are already discussed in Chapter 2.

We construct two-qubit Bell states by applying the Hadamard gate on an initial qubit and adding a CNOT gate. This is a transformation operation of the four computational basis states given in the Truth Table.(4.1). For example, to create an output state $|\xi_{00}\rangle$, the input of the Hadamard gate is taken as $|00\rangle$ to $\{\frac{\langle |00\rangle+|11\rangle\rangle}{\sqrt{2}}\otimes |0\rangle\}$, and later the operation of the CNOT gate will give the output state $\frac{\langle |00\rangle+|11\rangle\rangle}{\sqrt{2}}\equiv |\xi_{00}\rangle$. Fig.(4.4) shows the Bell states quantum circuit in which the Hadamard transformation puts the upper qubit in superposition, acting as a control input to the CNOT while the inversion of target qubit is possible only when the control is 1. The mnemonic notation of two-qubit Bell states ξ_{00} , ξ_{01} , ξ_{10} , and ξ_{11} may be understood via the following equation:

$$|\xi_{ab}\rangle \equiv \frac{|0,b\rangle + (-1)^a |1,\bar{b}\rangle}{\sqrt{2}},\tag{4.19}$$

where \bar{b} is the negation of b.

The GHZ state is a three-qubit generalization of Bell's state. The quantum circuit of the prototype GHZ state $|GHZ\rangle = \frac{|000\rangle + |111\rangle}{\sqrt{2}}$ can be seen in Fig.(4.5). The quantum circuit of the GHZ state comprises of one Hadamard gate and two CNOT gates. Similarly, Fig.(4.6) shows the prototype W-state quantum circuit. Using $R_y(\theta)$ at $\theta \approx 1.91$ degree, $CU3(\frac{\pi}{2}, \frac{\pi}{2}, \frac{\pi}{2}, \frac{\pi}{2})$,

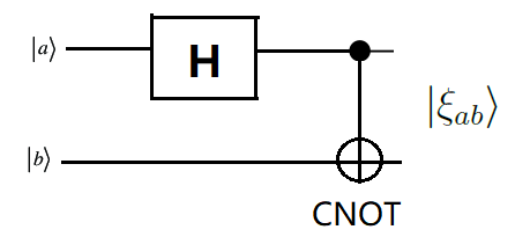


Figure 4.4: The figure represent the quantum circuit of two qubit Bell's state

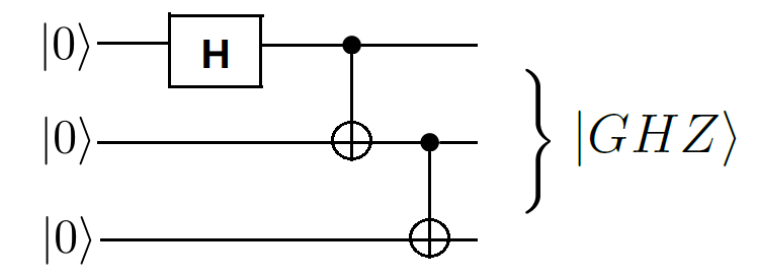


Figure 4.5: The figure represent quantum circuit of three-qubit GHZ state.

two CNOT and one X quantum gates, we construct the prototype W-state quantum circuit i.e., $|W_3\rangle = \frac{1}{\sqrt{3}}(|001\rangle + |010\rangle + |100\rangle)$.

To generate such quantum states, we need a measurement circuit on the standard basis, also known as the z basis or computational basis, which when combined with gates can execute any measurement. The quantum circuit symbol for measurement is represented by a "meter" symbol shown in Fig.(4.7). Being a non-unitary quantum gate, it does non-reversible operations. The measurement circuit destroys the superposition, thereby losing quantum information, and so only one classical state can be observed. This is the reason why copying of qubit's state is not allowed. This is also called the "no-cloning theorem" of quantum computing. For example, the measurement operation transforms a single qubit

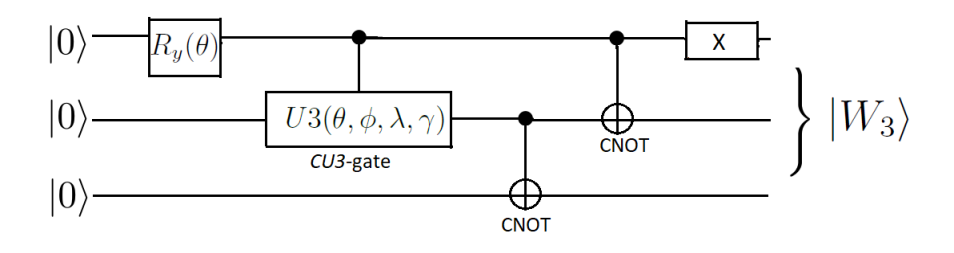


Figure 4.6: The figure represent the quantum circuit of three-qubit prototype W-state $|W_3\rangle$.

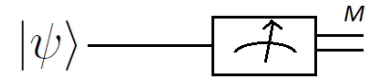


Figure 4.7: The quantum circuit symbol for measurement.

state $|\psi\rangle = c_1 |0\rangle + c_2 |1\rangle$ into a probabilistic classical state M of either 0 value with probability $|c_1|^2$, or 1 with probability $|c_2|^2$ as shown in Fig.(4.7).

In the next section, we measure and simulate the Bell's state, the GHZ-state and the prototype W-state quantum circuits on the IBM quantum computer, a cloud-based quantum computer that was recently launched online in 2016.

4.4 IBM quantum cloud computer

We associate a quantum computer in IBM Quantum (see Fig. (4.8)) [44], which uses a physical qubit called a superconducting transmon qubit (acts as an artificial atom), constructed using superconducting materials like niobium and aluminum designed on a silicon substrate. These are artificial qubits formed by considering two non-interacting energy levels out of many. Advanced ages of IBM quantum processors show the capability of superconducting transmon qubits to be the reason for an electrically controlled solid-state quantum computer. With the development of architecture of chips and improvisation of error correction and mitigation, new age IBM quantum creates system with higher quantum volume to have advantage in various applications. In the virtual platform of quantum cloud administrations, IBM quantum devices can be freely accessible by users through Qiskit (IBM quantum composer), which is a graphical quantum programming device that allows us to drag and drop operations to construct quantum circuits and run them on real hardware or simulator. A useful general-purpose simulator for recreating quantum circuits both ideally and subject to noise modeling is the QASM (Quantum assembly language) simulator (ibmq_gasm_simulator). The simulation technique is consequently chosen dependent on the input circuits and parameters.

In Fig.(4.9), Fig.(4.10(a)) and Fig.(4.10(b)), we construct and test the quantum circuit of the Bell's state (see Fig.(4.4)), a prototype of the GHZ-state (see Fig.(4.5) and the W-state (see Fig.(4.6)), respectively, on simulator of IBM quantum computer and shows measurement Histograms generated by running these circuits. According to the bottom figures of Fig.(4.9),

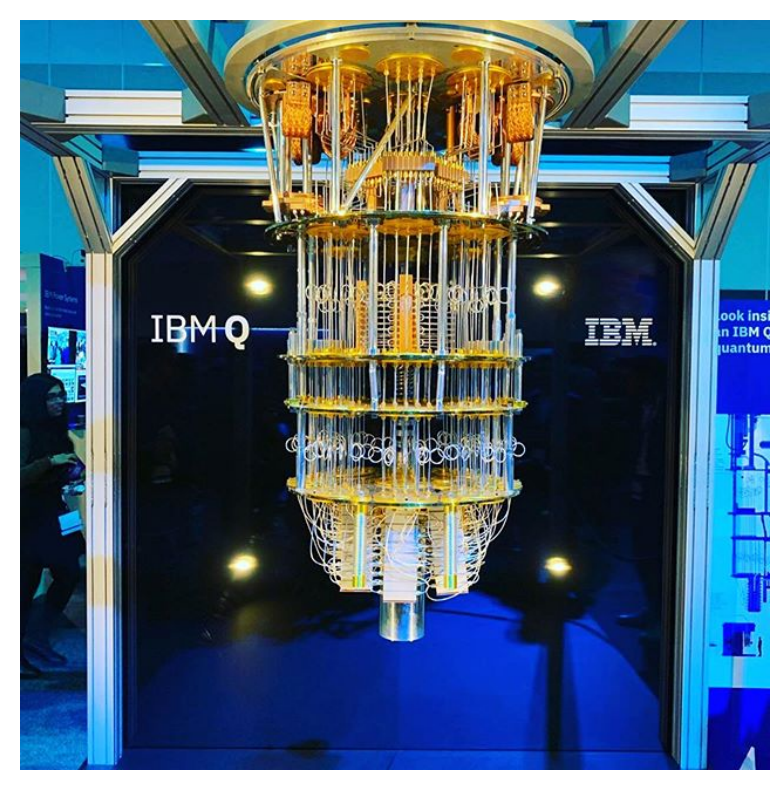


Figure 4.8: Image of IBM quantum computer [44].

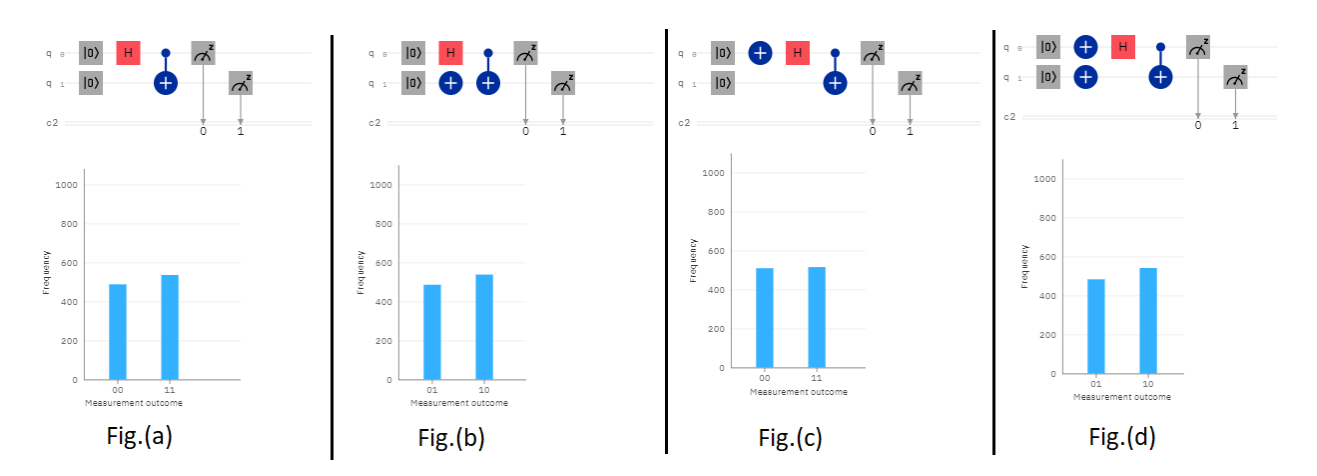


Figure 4.9: The quantum circuit and its simulations is shown for the two qubit Bell's state on IBMQ computer. The lower part of Fig.(a), Fig.(b), Fig.(c) and Fig.(d) show the generation of four Bell's state $|\xi_{00}\rangle$, $|\xi_{01}\rangle$, $|\xi_{10}\rangle$ and $|\xi_{11}\rangle$, respectively on IBMQ simulator.

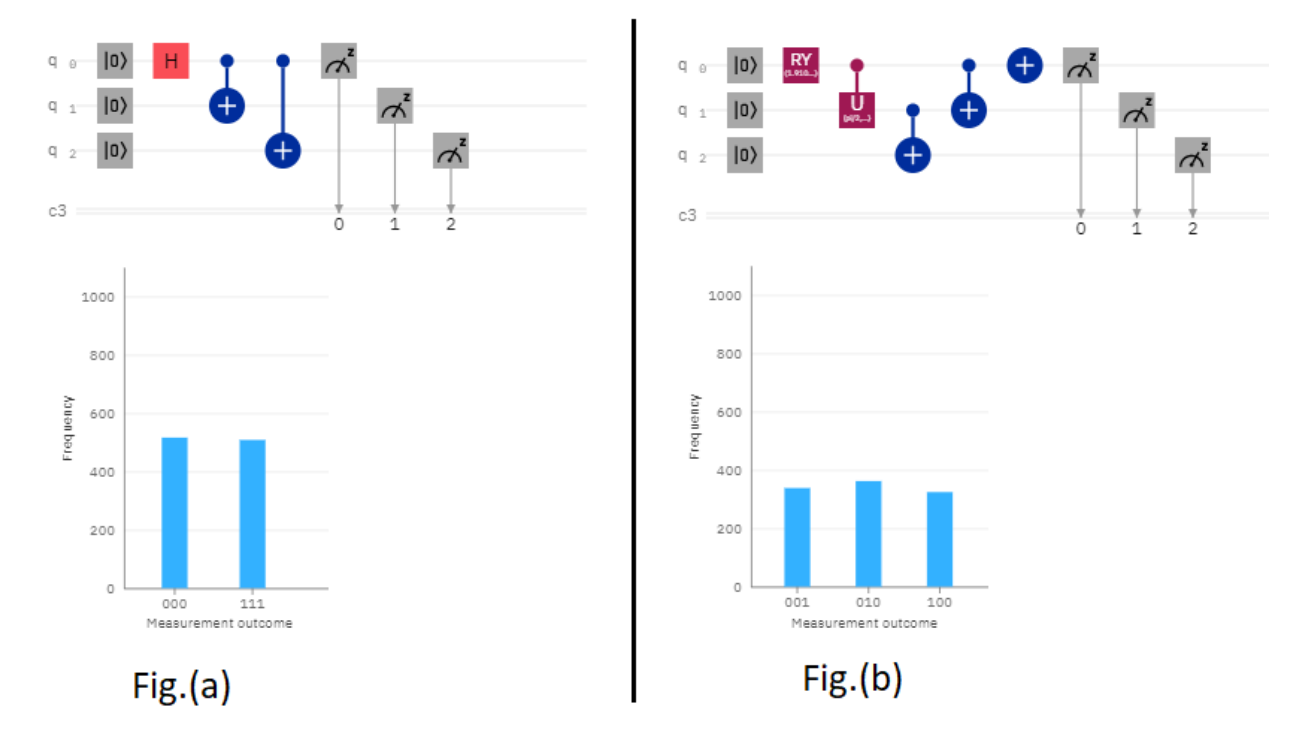


Figure 4.10: The quantum circuit and its simulations is shown for the GHZ state $|GHZ\rangle$ and prototype W-state $|W_3\rangle$ in Fig.(4.9(a)), Fig.(4.9(b)), respectively on IBMQ simulator.

Fig.(4.10(a)) and Fig.(4.10(b)), each bin in the histograms show almost equal frequency (or probability) of measurement of the Bell's state $(|\xi_{ab}\rangle)$ in the basis $(|00\rangle, |01\rangle, |10\rangle, |11\rangle)$, the GHZ state $(|GHZ\rangle)$ in the basis $(|000\rangle, |111\rangle)$ and the W-state $(|W_3\rangle)$ in the basis $(|001\rangle, |010\rangle, |100\rangle)$, respectively. The output from each circuit measurement in histogram exhibits that the quantum state such as Bell's state, the prototype GHZ, and W-state are maximally entangled.

4.5 Concurrence circuit

Here, we come up with a quantum circuit to compute concurrence of a 2-qubit pure state on IBM Quantum simulator and on real quantum hardware. The Concurrence defined in Eq.(2.33) of chapter 2 can be reduced to simple expression for a pure state as [188,189]

$$C(|\Psi\rangle) = |\langle \Psi | \sigma_y \otimes \sigma_y | \Psi^* \rangle |. \tag{4.20}$$

The quantum measurement circuit of concurrence for an arbitrary 2-qubit pure state is

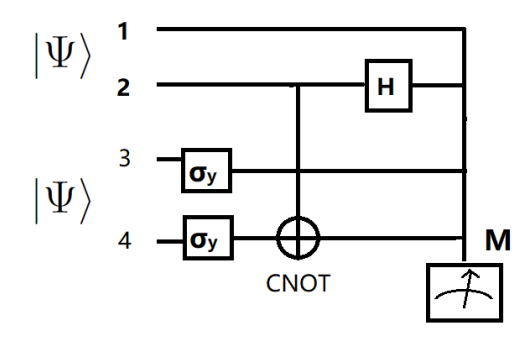


Figure 4.11: The figure represent concurrence quantum circuit of two-qubit pure state.

shown in Fig.(4.11). It is constructed with one CNOT gate, two Pauli σ_y gates and one Hadamard gate followed by a measurement gate. The proposed quantum circuit depends upon the accessibility of two copies of the bi-partite state and the quick estimation of the occupation probability of the total state of the two copies. The central thought of this proposition is the transition of the separable form of two copies into a concurrence informative state which simulate in terms of frequency/probability on four qubits computational basis. Let us assume that we want to measure the concurrence of the general 2-qubit pure state

$$|\Psi\rangle = \alpha_0 |00\rangle + \alpha_1 |01\rangle + \alpha_2 |10\rangle + \alpha_3 |11\rangle,$$
 (4.21)

and we are provided with two decoupled copies of it $|\Psi\rangle\otimes|\Psi\rangle$. It can be shown from Eq.(4.21) that the concurrence state of $|\Psi\rangle$ in terms of coefficients α_i is given by

$$C(|\Psi\rangle) = 2|\alpha_1\alpha_2 - \alpha_0\alpha_3|. \tag{4.22}$$

Following the proposed quantum circuit of Fig.(4.11), we apply local operations on the second copy such that global state is depicted by

$$|\Phi\rangle = |\Psi\rangle \otimes (\sigma_y \otimes \sigma_y |\Psi\rangle).$$
 (4.23)

This state can be written as superposition of states having four qubit computational basis as

$$\begin{split} |\Phi\rangle &= -\alpha_0 \alpha_3 \, |0000\rangle + \alpha_2 \alpha_0 \, |0001\rangle + \alpha_0 \alpha_1 \, |0010\rangle - \alpha_1 \alpha_3 \, |0100\rangle - \alpha_2 \alpha_3 \, |1000\rangle - \alpha_0^2 \, |0011\rangle \\ &- \alpha_3^2 \, |1100\rangle + \alpha_1 \alpha_2 \, |0101\rangle + \alpha_1^2 \, |0110\rangle + \alpha_2^2 \, |1001\rangle + \alpha_2 \alpha_1 \, |1010\rangle - \alpha_1 \alpha_0 \, |0111\rangle \\ &- \alpha_2 \alpha_0 \, |1011\rangle + \alpha_3 \alpha_2 \, |1101\rangle + \alpha_3 \alpha_1 \, |1110\rangle - \alpha_3 \alpha_0 \, |1111\rangle \, . \quad (4.24) \end{split}$$

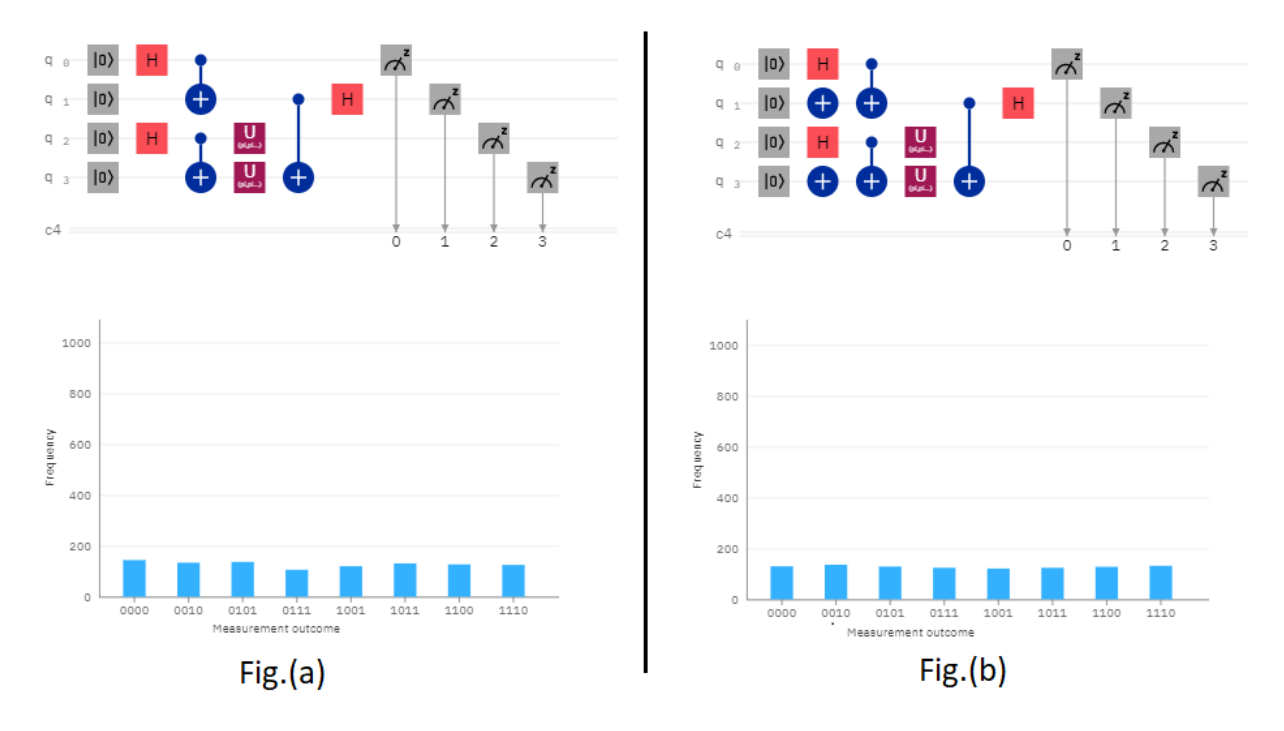


Figure 4.12: In Fig.(a) and Fig.(b), top and bottom figure represent the quantum circuit of concurrence and histogram plot for Bell's state $|\xi_{00}\rangle$ and $|\xi_{01}\rangle$, respectively on IBMQ simulator.

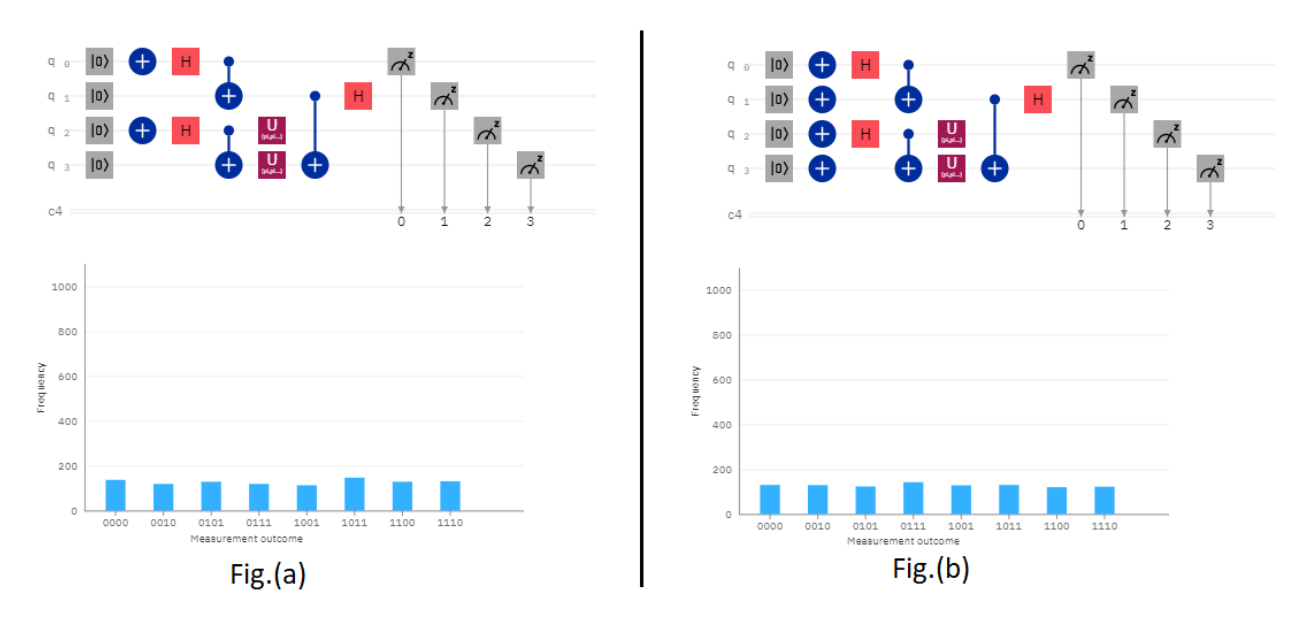


Figure 4.13: In Fig.(a) and Fig.(b), top and bottom figure represent the quantum circuit of concurrence and histogram plot for Bell's state $|\xi_{10}\rangle$ and $|\xi_{11}\rangle$, respectively on IBMQ simulator.

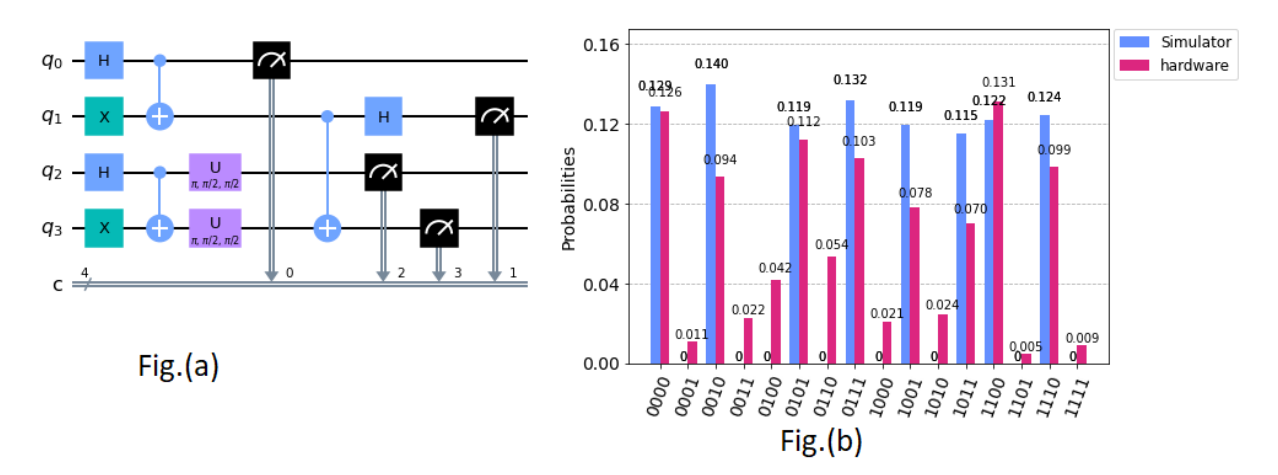


Figure 4.14: In Fig.(a) Concurrence circuit for the two-qubit Bell state $|\xi_{01}\rangle = \frac{1}{\sqrt{2}}(|01\rangle + |10\rangle)$ is shown where q_0, q_1, q_2, q_3 are initialize to $|0\rangle$ state. In Fig.(b) concurrence information is encoded in four qubit computational basis on IBMQ simulator and on a real quantum hardware.

Now we apply a CNOT gate operation between the second qubit acting as the control and the fourth acting as the target, followed by a Hadamard rotation on the second qubit. The state of the overall systems become

$$|\Phi_{1}\rangle = \frac{1}{\sqrt{2}} \{A_{-}|0000\rangle + A_{+}|0100\rangle + B_{-}|0001\rangle - B_{+}|0101\rangle + 2\alpha_{2}\alpha_{3}|1100\rangle - 2\alpha_{0}\alpha_{1}|0110\rangle$$

$$C_{10}^{-}|0011\rangle + C_{10}^{+}|0111\rangle + C_{23}^{-}|1001\rangle - C_{23}^{+}|1101\rangle + A_{-}|1010\rangle - A_{+}|1110\rangle$$

$$+B_{+}|1111\rangle - B_{-}|1011\rangle\}, \tag{4.25}$$

where $A_{\pm} = \alpha_1 \alpha_2 \pm \alpha_0 \alpha_3$, $B_{\pm} = \alpha_0 \alpha_2 \pm \alpha_1 \alpha_3$, and $C_{ij}^{\pm} = \alpha_i^2 \pm \alpha_j^2$. Thus, in Eq.(4.25) the concurrence information of the state $|\Psi\rangle$ is present in the coefficient of four qubit computational basis.

For example, in Fig.(4.12) and Fig.(4.13), by considering the two copies of two-qubit Bell's state quantum circuit, we do concurrence simulation on IBMQ simulator. The histogram plot shows an approximately equal distribution of frequency/probability on four qubits computational basis, which verify that the two-qubit Bell's state is a bi-partite maximally entangled pure state. Here, an approximately equal distribution of frequency/probability means that the quantum computer may have some hardware errors.

It is to be noted that in this chapter, all quantum circuits run only on the IBM quantum simulator, which tests circuits with no noise. However, in Fig.(4.14), we do python pro-

gramming on Qiskit 0.23.0 to create the quantum circuit of concurrence for the Bell state $|\xi_{01}\rangle = \frac{1}{\sqrt{2}}(|01\rangle + |10\rangle)$ and run the circuit for 1024 shots for a given time to generate the histogram of probability on IBMQ simulator (ibmq_qasm_simulator) and also on real quantum hardware (the 5-qubit machine (ibm_santiago)). The difference between the simulated case and the code run on the actual quantum hardware is that the simulator simulates a perfect quantum device. In the meantime, the real quantum hardware is susceptible to small quantum errors. These quantum errors are improving every day as the result of the technology is improving. So, we expect to see the results obtained from real quantum hardware getting lower and lower and getting closer to the ideal simulations. However, as we see in Fig.(4.14), the hardware is not perfect, resulting in a difference in the Histogram plots with the ideal quantum computer simulator.

In the next chapter, we extend such field of study in particle physics domain and use idea of quantum simulation to study entanglement in neutrino oscillations on quantum computer.

Chapter 5

Quantum studies of neutrinos on IMBQ processors

This chapter studies implementation of entangled neutrinos on an IBM quantum computer. Since neutrinos are weakly interacting, a neutrino beam retains coherence for a significant distance. Such long-distance coherence can have implications in quantum information theory. Entanglement of neutrino flavour states means that the coherent evolution of neutrino beams can be studied using quantum information techniques. The tools of quantum resource theory quantify quantum coherence using the data from neutrino oscillations experiments [190, 191]. This is the first demonstration of the "quantumness" of quantum particles (neutrinos) other than photons over a significant macroscopic distance. In this chapter, we examine the concurrence and coherence of the bi-partite two neutrino system and find an algorithm to encode our result on the IBM quantum cloud computer within the language of quantum gates and circuits [44].

In a recent paper, Argüelles and Jones have outlined quantum circuits to simulate neutrino oscillations on IBMQ processors [46]. Before this, neutrino oscillations were analyzed using quantum walks [112]. In other similarly significant wonders like in neutral kaon oscillations, the computation of oscillation probabilities has been done utilizing quantum computing [192]. Apart from this, the study of collective neutrino oscillations on a quantum computer is also informative [194–196].

5.1 Quantifying concurrence and l_1 -norm of coherence in the two neutrino system

In the two flavour $(\nu_{\alpha} \to \nu_{\beta})$ neutrino mixing, the SU(2) rotation matrix $\mathbf{U}(\theta) = \mathbf{R}(\theta) = \begin{pmatrix} \cos\theta & -\sin\theta \\ \sin\theta & \cos\theta \end{pmatrix}$ resolved the atmospheric and solar neutrino problem. Following from the discussion of Sec.(1.2) of Chapter 1, and using Eq.(1.9), the mass eigenstates (ν_1, ν_2) can be obtained as a linear superposition of flavor basis (ν_e, ν_{μ}) explicitly in matrix form as¹

$$\begin{pmatrix} |\nu_1\rangle \\ |\nu_2\rangle \end{pmatrix} = \begin{pmatrix} \cos\theta & -\sin\theta \\ \sin\theta & \cos\theta \end{pmatrix} \begin{pmatrix} |\nu_e\rangle \\ |\nu_\mu\rangle \end{pmatrix}. \tag{5.1}$$

Using Eq.(1.11), the time evolved flavour eigenstates of neutrinos in flavour basis are

$$\begin{pmatrix} |\nu_{e}(t)\rangle \\ |\nu_{\mu}(t)\rangle \end{pmatrix} = \begin{pmatrix} \cos\theta & \sin\theta \\ -\sin\theta & \cos\theta \end{pmatrix} \begin{pmatrix} 1 & 0 \\ 0 & e^{i\psi} \end{pmatrix} \begin{pmatrix} \cos\theta & -\sin\theta \\ \sin\theta & \cos\theta \end{pmatrix} \begin{pmatrix} \nu_{e}(0) \\ \nu_{\mu}(0) \end{pmatrix} \equiv \begin{pmatrix} \tilde{U}_{ee}(t) & \tilde{U}_{e\mu}(t) \\ \tilde{U}_{\mu e}(t) & \tilde{U}_{\mu\mu}(t) \end{pmatrix} \begin{pmatrix} \nu_{e}(0) \\ \nu_{\mu}(0) \end{pmatrix}, \tag{5.2}$$

where $\psi = \frac{\Delta m^2 t}{2E}$, $\Delta m^2 \equiv m_2^2 - m_1^2$. Subsequently, in the ultra-relativistic limit, the survival $(P_{ee} = |\tilde{U}_{ee}(t)|^2)$ and disappearance $(P_{e\mu} = |\tilde{U}_{e\mu}(t)|^2)$ probabilities of the state $|\nu_e(t)\rangle$ are

$$P_s = P_{e \to e} = 1 - 4\sin^2\theta\cos^2\theta\sin^2\frac{\psi}{2},\tag{5.3}$$

and
$$P_d = P_{e \to \mu} = 1 - P_{ee}$$
. (5.4)

The two neutrino state space \mathcal{H}_{ν} is a two-qubit Hilbert space $\mathcal{H}_1 \otimes \mathcal{H}_2$ spanned by $\{|1\rangle_1 \otimes |0\rangle_2, |0\rangle_1 \otimes |1\rangle_2\}$. The matrix $\{|0\rangle = \begin{pmatrix} 1 \\ 0 \end{pmatrix}; |1\rangle = \begin{pmatrix} 0 \\ 1 \end{pmatrix}\}$ is defined by means of the unitary equivalence defined on the mass basis $|\nu_1\rangle = |1\rangle_1 \otimes |0\rangle_2$ and $|\nu_2\rangle = |0\rangle_1 \otimes |1\rangle_2$. There is a bi-partition of the space of quantum states and a neutrino state which is entangled as a two qubit state is said to be mode entangled. The normalized time evolved electron and muon neutrino flavour state are two qubit bipartite flavour mode states and yield the Bell like superposition (see Sec.(3.1) of Chapter 3),

$$|\nu_e(t)\rangle = \tilde{U}_{ee}(t) |10\rangle_e + \tilde{U}_{e\mu}(t) |01\rangle_{\mu},$$
 (5.5)

¹We are using $\mathbf{U}(\theta) = \mathbf{R}(\theta) = \begin{pmatrix} \cos\theta & -\sin\theta \\ \sin\theta & \cos\theta \end{pmatrix}$. On the IBMQ platform this corresponds to the universal quantum gate U3 (see Eq.(4.7)). The neutrino transition probabilities will not change because U is a unitary transformation.

$$|\nu_{\mu}(t)\rangle = \tilde{U}_{\mu e}(t) |10\rangle_{e} + \tilde{U}_{\mu\mu}(t) |01\rangle_{\mu},$$
 (5.6)

where, $|\nu_e(0)\rangle = |1\rangle_e \otimes |0\rangle_\mu = |10\rangle_e$ and $|\nu_\mu(0)\rangle = |0\rangle_e \otimes |1\rangle_\mu = |01\rangle_\mu$ are two flavour mode basis at time t=0. Using Eq.(5.5) and Eq.(5.6), the density matrix for $|\nu_e(t)\rangle$ and $|\nu_\mu(t)\rangle$ are

$$\rho^{e}(t) = |\nu_{e}(t)\rangle\langle\nu_{e}(t)| = \begin{pmatrix} 0 & 0 & 0 & 0\\ 0 & |\tilde{U}_{ee}(t)|^{2} & \tilde{U}_{ee}(t)\tilde{U}_{e\mu}^{*}(t) & 0\\ 0 & \tilde{U}_{e\mu}(t)\tilde{U}_{ee}^{*}(t) & |\tilde{U}_{e\mu}(t)|^{2} & 0\\ 0 & 0 & 0 & 0 \end{pmatrix}$$
(5.7)

and
$$\rho^{\mu}(t) = |\nu_{\mu}(t)\rangle \langle \nu_{\mu}(t)| = \begin{pmatrix} 0 & 0 & 0 & 0 \\ 0 & |\tilde{U}_{\mu e}(t)|^2 & \tilde{U}_{\mu e}(t)\tilde{U}_{\mu \mu}^*(t) & 0 \\ 0 & \tilde{U}_{\mu \mu}(t)\tilde{U}_{\mu e}^*(t) & |\tilde{U}_{\mu \mu}(t)|^2 & 0 \\ 0 & 0 & 0 & 0 \end{pmatrix},$$
 (5.8)

respectively. In Sec.(3.1) of Chapter 3, we have discussed various bi-partite entanglement measures in the two neutrino system. The concurrence is the study of non-locality of a bi-partite quantum system (see Eq.(2.33) of chapter 2 for concurrence definition). Using the "spin-flipped" density matrix $\tilde{\rho}^e(t) = (\sigma_y \otimes \sigma_y) \rho^{*e}(t) (\sigma_y \otimes \sigma_y)$, we find only one square root of eigenvalue of matrix $\rho^e(t)\tilde{\rho}^{e\mu}(t)$ is non zero i.e., $\mu_4 = 2\sqrt{|\tilde{U}_{e\mu}(t)|^2|\tilde{U}_{ee}(t)|^2}$, thus the concurrence is quantified for the time evolved electron flavour neutrino states in terms of survival and disappearance probabilities as

$$C(\rho^e(t)) = 2\sqrt{P_s P_d}. (5.9)$$

Note that $P_s < 1$, immediately implies $P_d > 0$. Hence, entanglement is non-zero if the transition probabilities are non-zero. When $P_s = P_d = 0.5$, concurrence tends to 1 i.e, $C(\rho^e(t)) = 1$, which corresponds to maximally entangled state. Thus, in a pure bipartite 2-qubit framework, concurrence is associated with physical parameters in neutrinos oscillations.

Researching quantum measures in neutrino oscillations can be fascinating because it is a minimal quantum effect. Quantities such as quantum coherence can be studied over an enormous distance, as much as a few hundred kilometres away. Using the tools of quantum resource theory, the entanglement measure l_1 - norm of coherence $(C_{l_1}(\rho))$ is the summation over the absolute values of all the off-diagonal elements ρ_{ij} of a density matrix ρ [190]. This has been investigated in the context of three-flavour neutrino oscillations in ref. [73, 191].

$$C_{l_1}(\rho) = \sum_{i \neq j} |\rho_{ij}| \ge 0.$$
 (5.10)

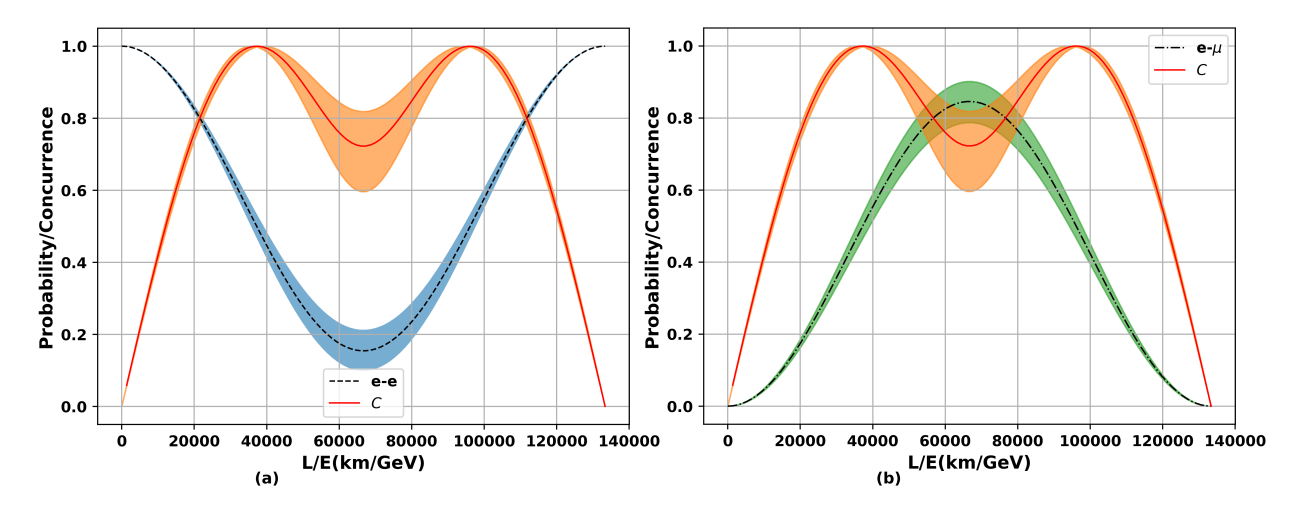


Figure 5.1: (a) The ν_e survival probability (Black, dashed line) is shown in the blue band the concurrence (Red, solid line) is within the orange band [197]. (b) The ν_e disappearance probability (Black, dash dotted line) is in the green band the concurrence (Red, solid line) is shown as red band [197].

We find that for a given density matrix $\rho^e(t)$ (see Eq.(5.7)), the l_1 - norm of coherence $C_{l_1}(\rho^e(t))$ and concurrence $C(\rho^e(t))$ coincide in the bi-partite two neutrino systems i.e.,

$$C(\rho^e(t)) = C_{l_1}(\rho^e(t)) = 2\sqrt{P_s P_d}.$$
 (5.11)

This result shows the similarity of the origin of flavor mode entanglement in neutrino oscillations with quantum coherence in the bi-partite two neutrino system. Thus, one can treat entanglement and coherence on equal footing. The concurrence for an initial electron flavour neutrino ν_e is quantified in terms of the survival P_{ee} and disappearance $P_{e\mu}$ probabilities. The dependence of this on L/E(Km/GeV) is plotted in the Fig.(5.1(a)) and Fig.(5.1(b)). We find that when the survival probability P_{ee} is minimum and the disappearance $P_{e\mu}$ probability is maximum, the concurrence is minimum which implies disentanglement. The next section prepares a quantum computer circuit of two-flavour neutrino states in the bipartite system.

5.2 Quantum circuit of two flavour neutrino states

In Sec.(4.2) of Chapter 4 various types of single qubit and two-qubit quantum gates have been defined. The SU(2) rotation matrix $R(\theta)$ can be encoded in the IBM quantum computer

by using universal U3 gate

$$U3(\Phi, \psi, \lambda) = \begin{pmatrix} \cos\frac{\Phi}{2} & -\sin\frac{\Phi}{2}e^{i\lambda} \\ \sin\frac{\Phi}{2}e^{i\psi} & \cos\frac{\Phi}{2}e^{i(\lambda+\psi)} \end{pmatrix}.$$
 (5.12)

The universal gate U3 is dependent on the three-parameter² Φ , ψ and λ . In the two flavour neutrino oscillation, the parameters ψ and λ can be removed by rephasing the charged muon field via $|\nu_{\mu}\rangle \rightarrow e^{-i\psi} |\nu_{\mu}\rangle$ and the $|\nu_{2}\rangle$ field as $|\nu_{2}\rangle \rightarrow e^{i\lambda} |\nu_{2}\rangle$, respectively. We set the parameter value $\psi = 0$ and $\lambda = 0$ and therefore we can construct a 2x2 unitary quantum gate via the definition

$$R(\theta) = U3(2\theta, 0, 0) = \begin{pmatrix} \cos\theta & -\sin\theta \\ \sin\theta & \cos\theta \end{pmatrix} \equiv \begin{pmatrix} \tilde{U}_{ee} & \tilde{U}_{e\mu} \\ \tilde{U}_{\mu e} & \tilde{U}_{\mu\mu} \end{pmatrix}.$$
 (5.13)

Two flavour neutrino oscillations are equivalent to a beam splitter transformation. In two-qubit Bell's state, the beam splitter transformation is called the Hadamard transformation $H = \frac{1}{\sqrt{2}} \begin{pmatrix} 1 & 1 \\ 1 & -1 \end{pmatrix}$ which is a unitary transformation. In two flavour neutrino mixing, SU(2) rotation matrix $R(\theta)$ is also a unitary transformation. Therefore similar to the Bell state quantum circuit, we construct the Bell-like superposition quantum circuit of two flavour neutrino oscillations (see Eq.(5.5) and Eq.(5.6)). In the two-qubit system, we first prepare a quantum circuit of the pure electron neutrino state in the linear superposition of mass mode basis (see Fig.(5.2(a))). This can be achieved by operating the $U3(-2\theta,0,0)$ gate on first qubit (1) (by rotating the mixing angle θ of $U3(2\theta,0,0)$ gate from 2θ to -2θ), followed by the $CNOT_{12}$ quantum gate operation between first (1) and second (2) qubit, where the action of Controlled Not gate (CNOT) gate can be represented by the matrix form as

$$CNOT = \begin{pmatrix}
1 & 0 & 0 & 0 \\
0 & 1 & 0 & 0 \\
0 & 0 & 0 & 1 \\
0 & 0 & 1 & 0
\end{pmatrix}.$$
The defined gate arrangement of electron flavour neutrino state in

the two-qubit mass mode basis is

$$|\nu_e(0)\rangle = CNOT_{12}[U3(-2\theta, 0, 0) |0\rangle_1 \otimes X |0\rangle_2],$$
 (5.14)

where the input qubits in a quantum computation conventionally initialize to the $|0\rangle$, and the $|1\rangle$ state can be prepared by application of the Pauli-X gate, $|1\rangle = X |0\rangle$. The $CNOT_{12}$ gate is defined as if the control qubit (first (1) qubit) is in the state $|0\rangle$ the target qubit

²In Sec.(4.2.1) of Chapter 4, U3 gate is defined as a function of three different parameters θ , ϕ , λ . However, for the convenience of this chapter we defined U3 gate with parameters Φ , ψ and λ .

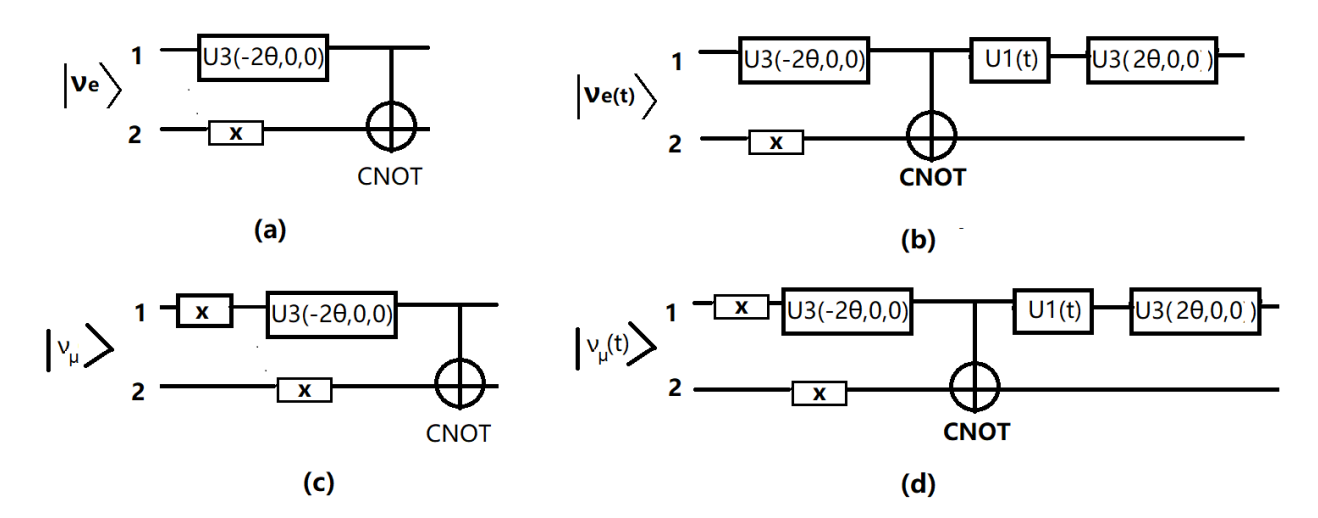


Figure 5.2: Quantum computer circuit representation of two-flavor neutrino states in two-qubit systems: (a) $|\nu_e\rangle = \tilde{U}_{ee} |10\rangle_1 + \tilde{U}_{e\mu} |01\rangle_2$, (b) $|\nu_e(t)\rangle = \tilde{U}_{ee}(t) |10\rangle_e + \tilde{U}_{e\mu}(t) |01\rangle_{\mu}$, (c) $|\nu_{\mu}\rangle = \tilde{U}_{\mu e} |10\rangle_1 + \tilde{U}_{\mu\mu} |01\rangle_2$, (d) $|\nu_{\mu}(t)\rangle = \tilde{U}_{\mu e}(t) |10\rangle_e + \tilde{U}_{\mu\mu}(t) |01\rangle_{\mu}$. Here, two input qubits 1 and 2 are initiated to $|0\rangle$.

(second (2) qubit) is not affected, conversely if the control qubit in the state $|1\rangle$, the target is flipped. $U_3(-2\theta,0,0)$ gate transforms the first (1) qubit $|0\rangle_1$ in a superposition state, therefore:

$$U3(-2\theta,0,0)|0\rangle_1 \otimes X|0\rangle_2 \to (\tilde{U}_{ee}|1\rangle_1 + \tilde{U}_{e\mu}|0\rangle_1) \otimes |1\rangle_2, \tag{5.15}$$

where $U3(-2\theta, 0, 0)$ can transfer each bit into qubit as

$$U3(-2\theta, 0, 0) |0\rangle = \tilde{U}_{ee} |1\rangle + \tilde{U}_{e\mu} |0\rangle,$$

$$U3(-2\theta, 0, 0) |1\rangle = \tilde{U}_{ee} |0\rangle + \tilde{U}_{e\mu} |1\rangle.$$
(5.16)

Further operating $CNOT_{12}$ gate between first (1) and second (2) qubit will produce an output state in a linear combination of mass mode basis as (from Eq.(5.14))

$$|\nu_e(0)\rangle = \tilde{U}_{ee} |10\rangle_1 + \tilde{U}_{e\mu} |01\rangle_2.$$
 (5.17)

The time-evolution operator is identified as S-gate on IBMQ processor

$$S(\psi) = \begin{pmatrix} 1 & 0 \\ 0 & e^{i\psi} \end{pmatrix} = U1(t) \tag{5.18}$$

where, $\psi = \frac{\Delta m^2 t}{2E}$. Only the relative phase between the mass eigenstates are relevant for oscillations. Finally by applying $U3(2\theta, 0, 0)$ gate on the first (1) qubit, the overall gate arrangement of a time evolved electron flavour neutrino state Eq.(5.5) can be obtained as (see Fig.(5.2(b)))

$$|\nu_e(t)\rangle = CNOT_{12}[U3(2\theta, 0, 0)U1(t)U3(-2\theta, 0, 0) |0\rangle_1 \otimes X |0\rangle_2]$$

$$\longrightarrow \tilde{U}_{ee}(t) |10\rangle_e + \tilde{U}_{e\mu}(t) |01\rangle_\mu.$$
(5.19)

Similarly, we can prepare $|\nu_{\mu}\rangle$ in a linear superposition of mass mode basis (see Fig.(5.2(c))) via

$$|\nu_{\mu}(0)\rangle = CNOT_{12}[U3(-2\theta, 0, 0)X |0\rangle_{1} \otimes X |0\rangle_{2}]$$

$$\longrightarrow \tilde{U}_{\mu e} |10\rangle_{1} + \tilde{U}_{\mu\mu} |01\rangle_{2}.$$
(5.20)

The gate arrangement of the time evolved muon flavour neutrino state in a flavoured basis Eq.(5.6) can be prepared as (see Fig.(5.2(d)))

$$|\nu_{\mu}(t)\rangle = CNOT_{12}[U3(2\theta, 0, 0)U1(t)U3(-2\theta, 0, 0)X |0\rangle_{1} \otimes X |0\rangle_{2}]$$

$$\longrightarrow \tilde{U}_{\mu e}(t) |10\rangle_{e} + \tilde{U}_{\mu\mu}(t) |01\rangle_{\mu}.$$

$$(5.21)$$

5.3 Quantum simulation of bi-partite entanglement in the two neutrino system

In this section, we propose a quantum computing technique to measure the concurrence on IBMQ platform [44, 188, 189]. In the previous section, we constructed a quantum circuit for the time evolved flavour neutrino state $|\nu_{\alpha}(t)\rangle$ in a two-qubit bi-partite mode (flavour) system. For the concurrence, we perform a spin-flip operation on the density matrix. To construct a quantum circuit to enable spin-flipping, we have to prepare two copies of bi-partite neutrino state $|\nu_{\alpha}(t)\rangle\otimes|\nu_{\alpha}(t)\rangle$ in the two flavour system (where $\alpha=e,\mu$), and apply a "spin-flipped" operation $\sigma_y\otimes\sigma_y$ on one of the two copies. We can extract the concurrence value of the time evolved flavour neutrino oscillation from this global state.

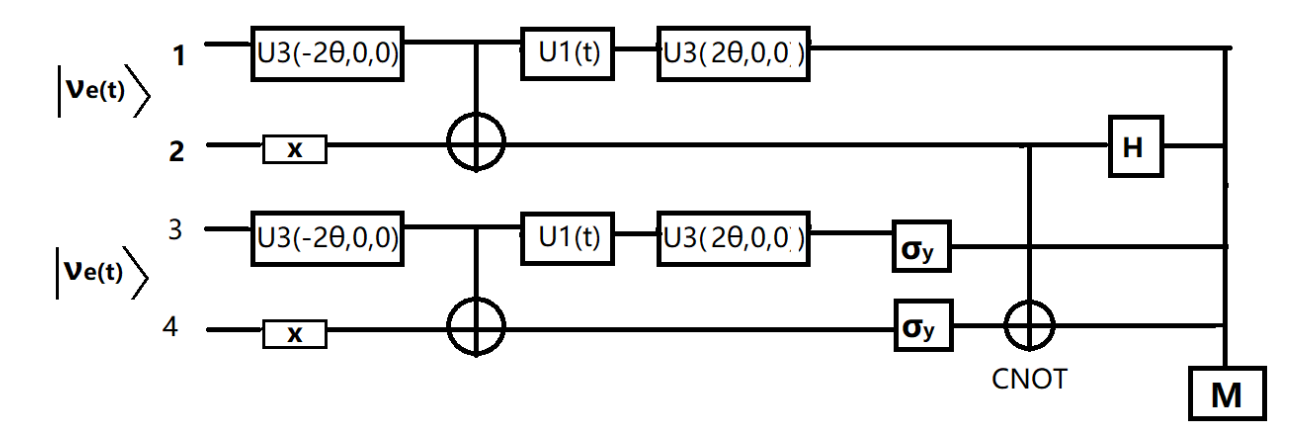


Figure 5.3: The circuit represent the concurrence measurement of ν_e disappearance in two-flavour neutrino oscillations.

5.3.1 Quantum circuit in vacuum

Now, in order to measure concurrence $C(\rho^e(t))$ on the IBMQ processors, let us prepare a concurrence circuit for the time evolved electron flavour neutrino state $|\nu_e(t)\rangle$ in the two qubit system in vacuum (see Fig.(5.3)). The required operations to create concurrence circuit are $\sigma_y \otimes \sigma_y$ spin-flip gate, CNOT gate, as well as local rotations Hadamard (H) gate, followed by a global measurement (M) of all four qubits. In the circuit diagram Fig.(5.3), the first two channels (1 and 2) stand for the entangled state $|\nu_e(t)\rangle$ that we want to measure. The third and fourth channel (3 and 4) denote the copy of $|\nu_e(t)\rangle$. Take two copies of the bi-partite state $|\nu_e(t)\rangle \otimes |\nu_e(t)\rangle$, and apply spin-flipped operation $\sigma_y \otimes \sigma_y$ on the second copy such that the global state is described by

$$|\Phi(t)\rangle = |\nu_e(t)\rangle \otimes (\sigma_y \otimes \sigma_y |\nu_e(t)\rangle).$$
 (5.22)

By using Eq.(5.19) in Eq.(5.22), four qubit global state we get as

$$|\Phi(t)\rangle = (\tilde{U}_{ee}(t) |10\rangle + \tilde{U}_{e\mu}(t) |01\rangle) \otimes (\tilde{U}_{ee}(t) |01\rangle + \tilde{U}_{e\mu}(t) |10\rangle)$$

$$= (\tilde{U}_{ee}(t))^{2} |1001\rangle + \tilde{U}_{ee}(t) \tilde{U}_{e\mu}(t) |1010\rangle$$

$$+ \tilde{U}_{e\mu}(t) \tilde{U}_{ee}(t) |0101\rangle + (\tilde{U}_{e\mu}(t))^{2} |0110\rangle.$$
(5.23)

Now apply $CNOT_{24}$ operation between second (2) and fourth (4) qubit, and the target qubit (4) is inverted only when the control qubit (2) is $|1\rangle$ i.e, $|0101\rangle \rightarrow |0100\rangle$ and $|0110\rangle \rightarrow |0111\rangle$,

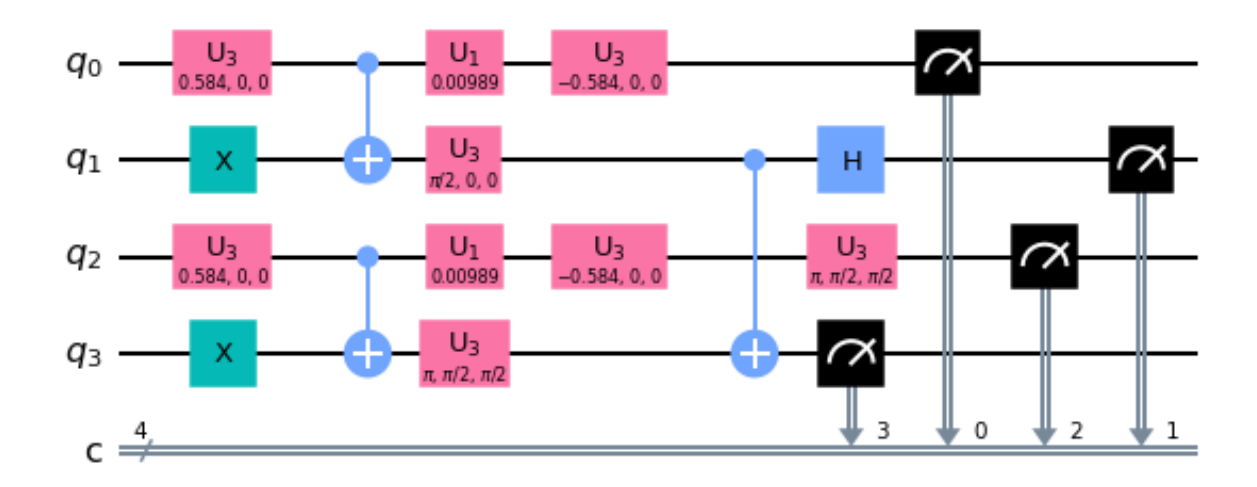


Figure 5.4: Concurrence circuit for the two qubit ν_e disappearance bipartite state on the IBMQ platform [44, 197].

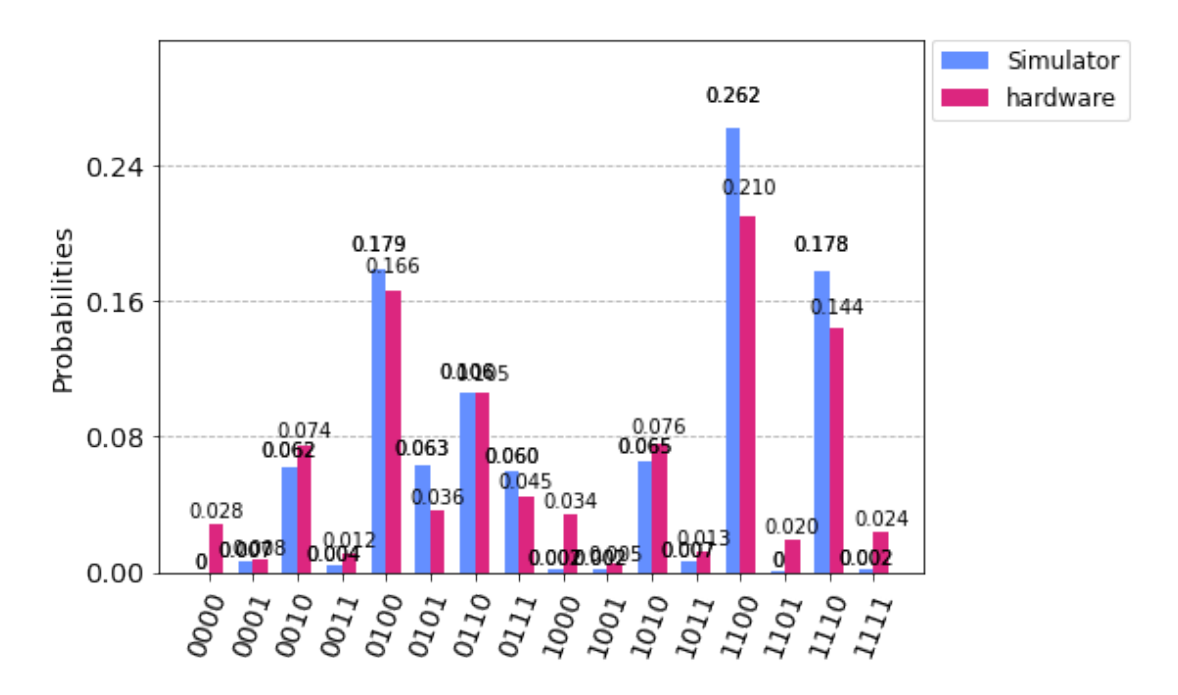


Figure 5.5: The concurrence varies with time at the IBMQ computer for an initial electron neutrino flavour state. The concurrence information is shown Histogram (probabilities in percentage) plot on quantum simulator and IBM quantum hardware [44,197].

such that we get

$$|\Phi_{1}(t)\rangle = (\tilde{U}_{ee}(t))^{2} |1001\rangle + \tilde{U}_{ee}(t)\tilde{U}_{e\mu}(t) |1010\rangle + \tilde{U}_{e\mu}(t)\tilde{U}_{ee}(t) |0100\rangle + (\tilde{U}_{e\mu}(t))^{2} |0111\rangle.$$
(5.24)

Finally, we perform a rotation operator H which act like the Hadamard transformation, $H = \frac{1}{\sqrt{2}} \begin{pmatrix} 1 & 1 \\ 1 & -1 \end{pmatrix}$ on the second (2) qubit. The H operation can transfer each qubit as:

$$H|0\rangle = \frac{1}{\sqrt{2}}(|0\rangle + |1\rangle); H|1\rangle = \frac{1}{\sqrt{2}}(|0\rangle - |1\rangle).$$
 (5.25)

The state of the overall system is

$$|\Phi_{2}(t)\rangle = \frac{1}{\sqrt{2}} [(\tilde{U}_{ee}(t))^{2} |1001\rangle - (\tilde{U}_{ee}(t))^{2} |1101\rangle + \tilde{U}_{ee}(t)\tilde{U}_{e\mu}(t) |1010\rangle - \tilde{U}_{ee}(t)\tilde{U}_{e\mu}(t) |1110\rangle + \tilde{U}_{e\mu}(t)\tilde{U}_{ee}(t) |0100\rangle + \tilde{U}_{e\mu}(t)\tilde{U}_{ee}(t) |0000\rangle + (\tilde{U}_{e\mu}(t))^{2} |0111\rangle + (\tilde{U}_{e\mu}(t))^{2} |0011\rangle].$$
 (5.26)

Thus, we observe from Eq.(5.26) that the concurrence information of the electron neutrino flavour state $|\nu_e(t)\rangle$ is then the coefficient $\tilde{U}_{ee}(t)\tilde{U}_{e\mu}(t)$ and

$$C(|\nu_e(t)\rangle) = 2\sqrt{2P_{0000}} = 2\sqrt{P_s P_d},$$
 (5.27)

where $P_{0000} = \frac{|\tilde{U}_{ee}(t)|^2 |\tilde{U}_{e\mu}(t)|^2}{2} = \frac{P_s P_d}{2}$. The quantum computer circuit to simulate concurrence for the time evolved electron flavour neutrino state is shown in Fig.(5.4) on the IBM quantum platform [44]. In this circuit $U3(\pi, \frac{\pi}{2}, \frac{\pi}{2})$ quantum gate is identified as Pauli σ_y gate. We used Python code to program our quantum circuits on the cloud based IBM quantum computer with the package Qiskit 0.23.0. We run the circuit for 1024 shots for a given time on an ideal quantum simulator and real quantum hardware of IBM. The quantum simulator that we used is ibmq_qasm_simulator and quantum hardware is the five-qubit machine $ibm_santiago$. The simulation results obtained from simulator and hardware are shown in Fig.(5.5) in the form of Histogram. The contrast between the outcomes in these two cases can be attributed to the noises of the quantum devices. If we make envelop of these histogram plots, we can see the simulation of quantum oscillatory behavior of neutrinos. So far, we have simulated the concurrence for the time evolved electron flavour neutrino state $|\nu_e(t)\rangle$ in a vacuum. For

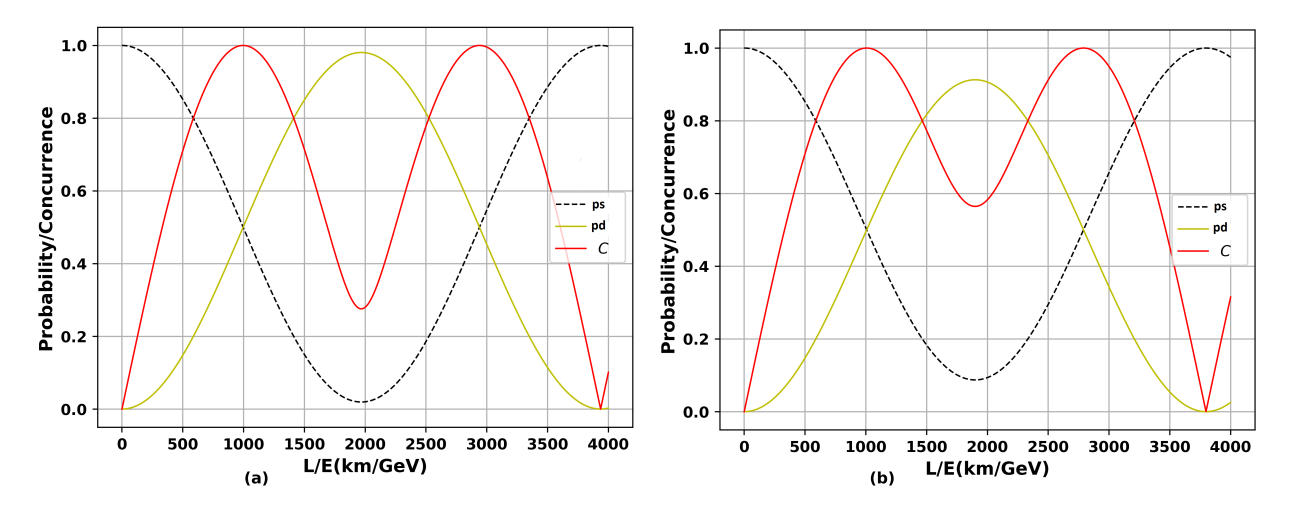


Figure 5.6: (a) The time evolution of the concurrence (Red line) compared to the disappearance P_d (Green line) and survival P_s (Black Dashed line) probabilities of $|\nu_{\mu}(t)\rangle$ in the vacuum A=0 [197]. (b) The time evolution of the concurrence (Red line) compared to the disappearance P_d (Green line) and survival P_s (Black Dashed line) probabilities of $|\nu_{\mu}(t)\rangle$ in the constant effective matter potential $A \neq 0$ [197].

completeness, in the next section, we encode concurrence for the time evolved muon flavour neutrino state $|\nu_{\mu}(t)\rangle$ in the constant matter potential on the IBMQ platform.

5.3.2 Quantum circuit in the uniform matter background

In Sec.(1.2.3) of Chapter 1, we have discussed neutrino oscillations in the constant matter background. In neutrino experiments, when neutrinos are traveling through the earth, they have a minimal weak interaction with the matter of the earth, which can be quantified as the effective Hamiltonian H_{eff} given in Eq.(1.46). The investigation is how much background matter affects entanglement, i.e., whether neutrinos decohere by traveling through the earth? According to Eq.(1.49), the survival (P_s) and disappearance (P_d) probabilities for $|\nu_{\mu}(t)\rangle$ (see Eq.(5.6)) in matter can be modify as:

$$P_{s} = P_{\mu \to \mu} = 1 - 4\sin^{2}\theta_{M}\cos^{2}\theta_{M}\sin^{2}(\frac{\psi_{M}}{2}),$$

$$P_{d} = P_{\mu \to e} = 4\sin^{2}\theta_{M}\cos^{2}\theta_{M}\sin^{2}(\frac{\psi_{M}}{2}),$$
(5.28)

where $\psi_M = \frac{\Delta m_M^2 t}{2E}$, θ_M and Δm_M^2 are the effective neutrino oscillations parameters in matter. These effective neutrino oscillation parameters are related to the vacuum neutrino

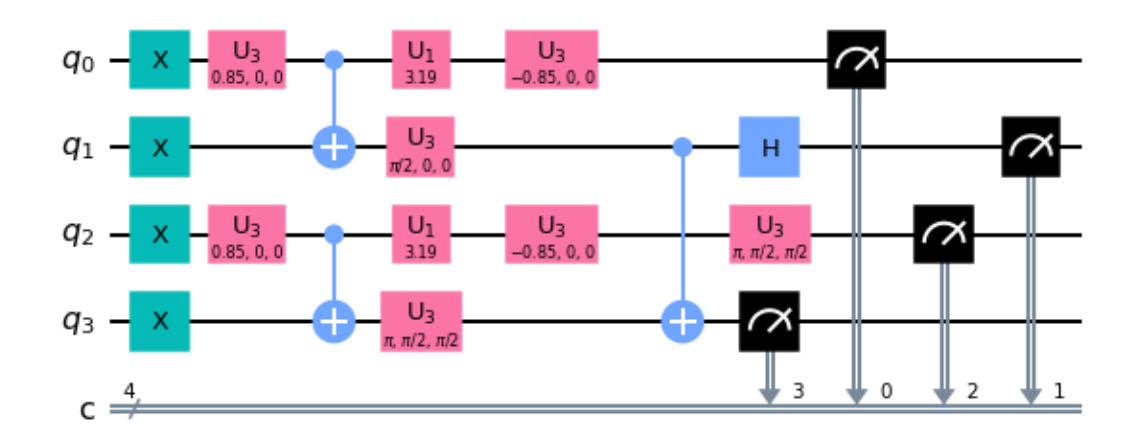


Figure 5.7: Implementation of concurrence circuit for $|\nu_{\mu}(t)\rangle$ on IBMQ processor [44, 197].

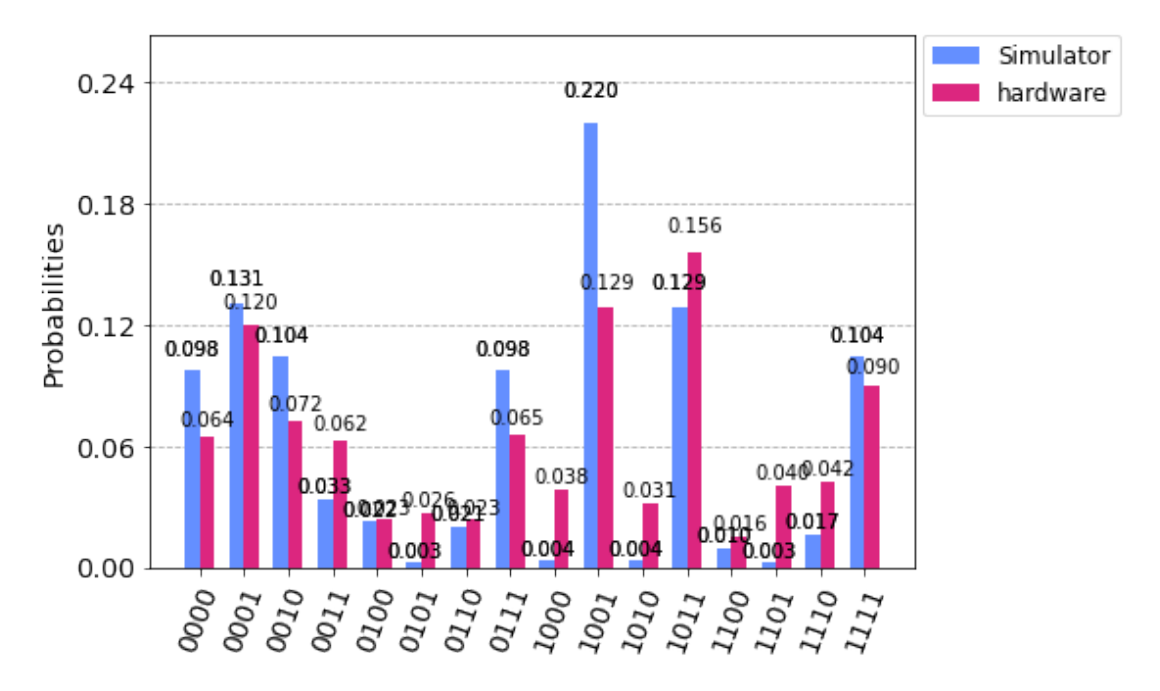


Figure 5.8: The concurrence varies with time at the IBMQ computer for an initial muon neutrino flavour state in vaccum (A=0). The concurrence information is shown through Histogram (probabilities in percentage) plot on quantum simulator and IBM quantum hardware [44, 197].

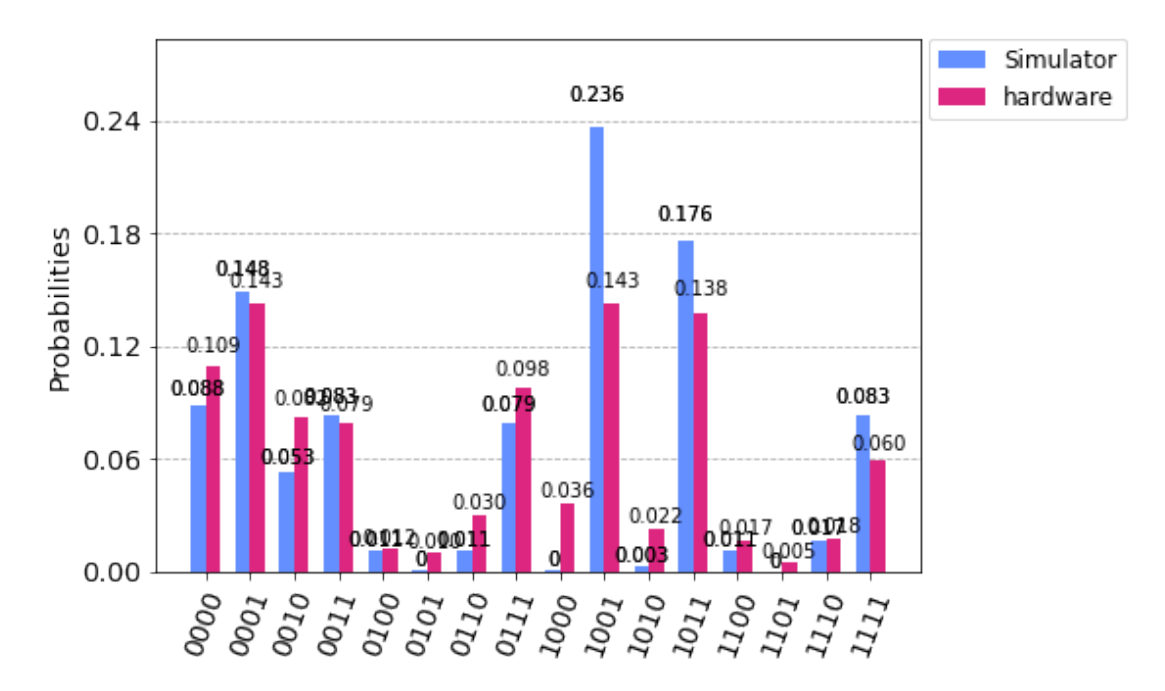


Figure 5.9: The concurrence varies with time at the IBMQ computer for an initial muon neutrino flavour state in the uniform matter background ($A\neq 0$) is shown on quantum simulator and IBM quantum hardware [44,197].

oscillation parameters Δm^2 and θ are given by

$$\Delta m_M^2 = \sqrt{[\Delta m^2 Cos(2\theta) - A]^2 + [\Delta m^2 Sin(2\theta)]^2},$$
(5.29)

$$Sin\theta_M = \frac{1}{\sqrt{2}} \left[1 - \frac{\Delta m^2 Cos2\theta - A}{\sqrt{(\Delta m^2 Cos2\theta - A)^2 + (\Delta m^2 Sin2\theta)^2}}\right],\tag{5.30}$$

where A is the effective matter potential. In Fig.(5.6(a)) and Fig.(5.6(b)), we show the time evolution of the concurrence plot vs $\frac{L}{E}(\frac{Km}{Gev})$ for $|\nu_{\mu}(t)\rangle$ in vacuum and matter, respectively. In the uniform matter background disappearance and survival probabilities get modified slightly due to the effective neutrino oscillations parameters Δm_M^2 and θ_M . Infact, due to the effect of the uniform matter background, the concurrence is less (see Fig.(5.6(b))), which is a sign of decoherence. Moreover, to simulate this results on IBMQ processor [44], in Fig.(5.7) first we prepare quantum computer circuit to measure concurrence for $|\nu_{\mu}(t)\rangle$ on the IBMQ platform. We do not have to construct a new quantum circuit for the inclusion of matter effects; we can replace the eigenvalue and the vacuum mixing angle for the expression given in Eq.(5.29) and (Eq.5.30). The result of the time-varying concurrence in a vacuum as well as in matter for $|\nu_{\mu}(t)\rangle$ is in the histogram plot (probabilities in percentage) on an ideal quantum simulator and quantum hardware of IBM in Fig.(5.8) and Fig.(5.9), respectively. We find that the

behaviour of the histogram plot of the evolved concurrence slightly changes when we induce a uniform matter effect to the neutrino system. Thus, in brief, we implemented a way of finding concurrence information of entangled oscillating neutrinos on a quantum computer, and we have shown that matter effects do not decohere the neutrinos much.

Chapter 6

Neutrinos as Qubits and Qutrits

Quantum entanglement results from the non-classical correlations between separated quantum systems [45]. Correlations between subsystems of a more extensive system that are not expressable in terms of correlation between local classical properties of the subsystem characterize quantum entanglement [47]. A superposition of two orthogonal states is called a qubit, and most quantum entanglement measures are realized between pairs of the qubit in a 2-dimensional Hilbert space \mathcal{H}^2 . Such measures include the partial transpose condition to determine entangled two qubits, and other bi-partite entanglement measures like concurrence and the entanglement of formation [70,72,198]. Bi-partite entanglement is limited in its applicability. Studying multipartite entanglement opens up new possibilities in developing quantum theory and new quantum communication protocols. Tri-partite entanglement is the simplest example of multipartite entanglement in the three-qubit system. The W state and the GHZ state of quantum optics are examples of tri-partite entangled states. Genuine tri-partite measures of entanglement such as the three-tangle and the three- π have been used to characterize these states [35] and discussed in Chapter 2.

Along with this type of tri-partite entanglement, there has been an interest in generalizing the concept of a qubit to a qutrit. A qutrit is the superposition of three orthogonal states rather than the two which characterize a qubit. An operator representation of the qutrit density matrix has been developed, and qutrit entanglement has been studied in ref. [47]. Physically implementing a qutrit quantum computer in the context of trapped ions has been studied [199] and quantum computer simulation packages for qutrits have been implemented [200]. Furthermore, the generalized concurrence formula as a measure of two qutrits entanglement has also been studied [201].

Most of the systems in which quantum entanglement is studied are photonic or atomic systems. In chapter 3, the ideas of quantum entanglement have been extended to the realm of particle physics by the study of two and three flavour neutrino systems. We have placed three-mode entanglement in neutrino oscillations on the same footing as mode entanglement in optical systems by mapping the neutrinos to the three mode W-state. We have studied tri-partite measures such as the three-tangle and the three- π for three flavour neutrino entanglement. In addition to this, in chapter 4, quantum states such as Bell's states, W state and GHZ state are realized by quantum computer and in chapter 5, the simulation of bi-partite entanglement in the two flavour neutrino oscillation has also been shown on IBMQ processors.

This chapter illustrates tri-partite entanglement in neutrinos by considering them as "qutrits". A qutrit is a linear superposition of three orthonormal basis states, $|1\rangle$, $|2\rangle$ and $|3\rangle$: $|\psi\rangle = \alpha |1\rangle + \beta |2\rangle + \gamma |3\rangle$, where $|\alpha|^2 + |\beta|^2 + |\gamma|^2 = 1$ and $\alpha, \beta, \gamma \in \mathbb{C}$. Since neutrino flavour states are a superposition of three states, it is only natural to try and characterize them as qutrits. We do this by mapping the density matrix for neutrinos to a generalized Poincaré sphere [47, 202]. In the two-flavour neutrino oscillation, geometric and topological phases such as the Berry's and Panchratnam's phase in terms of oscillation probabilities have been calculated using the Poincaré sphere and are directly observable [203, 204]. The Poincaré sphere has its origin in optics and is a way of visualizing different types of polarized light using the mapping from SU(2) to S^3 . A qubit represents a point on the Poincaré sphere of SU(2) defined as, complex projective line $\mathcal{H}^2 = \mathcal{C}P^1 = SU(2)/U(1)$. A generalization of the Poincaré sphere to SU(3) can be constructed [205–207]. This construction has been the basis for characterizing qutrits that live in a 3-dimensional Hilbert space \mathcal{H}^3 . A qutrit is taken as a point on the complex projective plane $\mathcal{H}^3 = \mathcal{C}P^2 = SU(3)/U(2)$ [208]. This work describes the entanglement of neutrinos by constructing Poincaré sphere representation for two and three-flavour neutrino states using SU(2) Pauli matrices and SU(3) Gell-Mann matrices, respectively, to map the neutrino states to the qutrits states of quantum information theory.

The chapter's organization is: In Sec.(6.1), we represent a single qubit density matrix of two flavour neutrino states in the basis of SU(2) Pauli matrices. In Sec.(6.2), we use the tensor product of Pauli matrices as a basis to represent a two-qubit density matrix that led to Bloch matrix construction in the two-qubit neutrino system. We also show bi-partite entanglement measure concurrence quantification in the two neutrino system. In Sec.(6.3), we describe a qutrit density matrix of three flavour neutrino states in the basis of SU(3) Gell-Mann matrices. Under a particular set of constraints, the measure for entanglement

characterized by the entropy of mixing for a three flavour neutrino system is found. In Sec.(6.4), we represent a two qutrit density matrix in the basis of SU(3) Gell-Mann matrices tensor products which describe the generalized matrix construction for two qutrits neutrino states. Furthermore, we compute generalized concurrence as a measure of bi-partite qutrits entanglement in the two neutrino system and compared it with the concurrence of the bi-partite qubit neutrino system.

6.1 SU(2) Poincaré sphere for two-flavour neutrinos

In chapter 3, the two flavour neutrino system has been mapped onto a qubit system in quantum optics, with the two flavours mixing matrix playing the role of the beam splitter in a two-level quantum optical system. It is well known that a two-level system can be mapped to the Poincaré sphere of two level quantum systems [205]. For a two-dimensional complex Hilbert space \mathcal{H}^2 , a quantum state $|\psi\rangle$ can be written as a superposition

$$|\psi\rangle = c_1 |0\rangle + c_2 |1\rangle, \tag{6.1}$$

where, $|c_1|^2 + |c_2|^2 = 1$ and $c_1, c_2 \in \mathbb{C}$

$$|0\rangle = \begin{pmatrix} 1\\0 \end{pmatrix}; |1\rangle = \begin{pmatrix} 0\\1 \end{pmatrix}. \tag{6.2}$$

Using the polar representation $c_1 = r_1 e^{i\varphi_0}$ and $c_2 = r_2 e^{\varphi_1}$ and the fact that, in the case of quantum bits, a quantum state $|\psi\rangle$ does not change if multiplied by an overall phase $e^{-\varphi_0}$ the equivalent quantum state is

$$e^{-i\varphi_0} |\psi\rangle = r_1 |0\rangle + r_2 e^{i\varphi_1 - i\varphi_0} |1\rangle.$$
(6.3)

Using the angular representation of complex variables and the fact that $r_1^2 + r_2^2 = 1$ and $\phi = \varphi_1 - \varphi_0$ we get a representation of the equivalent representation of $|\psi\rangle$ as

$$|\psi\rangle = cos(\theta) |0\rangle + sin(\theta)e^{i\varphi} |1\rangle.$$
 (6.4)

For a two dimensional complex Hilbert space \mathcal{H}^2 , the density matrix correspond to a pure state $|\psi\rangle$ is given by $\rho = |\psi\rangle\langle\psi|$. Its expansion in terms of Pauli matrices σ_j leads to the

Poincaré sphere construction

$$\rho = |\psi\rangle\langle\psi| = \frac{1}{2}(1 + \hat{n}.\vec{\sigma}),\tag{6.5}$$

where $\rho^{\dagger} = \rho^2 = \rho \geq 0$, $Tr\rho = 1 \Longrightarrow \hat{n}^* = \hat{n}$, $\hat{n}.\hat{n} = 1 \Longleftrightarrow \hat{n} \in S^2$ is the unit vector on the sphere. Thus there is a one to one correspondence between pure qubit states and points on the unit sphere S^2 embedded in \mathcal{R}^3 , which is known as the Poincaré sphere construction (of which the Bloch sphere is a particular case). If $|\psi'\rangle$ and $|\psi\rangle$ are two pure states then

$$Tr(\rho'\rho) = |\langle \psi'|\psi\rangle\rangle|^2 = \frac{1}{2}(1+\hat{n}'.\hat{n}),$$
 (6.6)

where \hat{n}' is the unit vector on the sphere corresponding to $|\psi'\rangle$. For orthogonal states $|\langle \psi'|\psi\rangle\rangle|^2 = 0$, so that $1 + \hat{n}'.\hat{n} = 0$ and thus correspond to the diametrically opposite point on S^2 correspond to mutually orthogonal Hilbert space vectors where, $\langle \psi'|\psi\rangle$ is the inner product in \mathcal{H}^2 . Applying an SU(2) transformation to $|\psi\rangle\in\mathcal{H}^2$ the representative point in SU(2) $\hat{n}\in S^2$ (circle) undergoes a rotation belonging to SO(3)

$$|\psi'\rangle = u |\psi\rangle, u \in SU(2) \Longrightarrow n'_j = R_{jk}(u)n_k; R_{jk}(u) = \frac{1}{2}Tr(\sigma_j u \sigma_k u^{\dagger}),$$
 (6.7)

 $R(u) \in SO(3)$. Thus all elements $R \in SO(3)$ are realized in this way, and we have the coset space identifications (since multiplication by a phase leads to equivalent representations) $S^2 = SU(2)/U(1) = SO(3)/SO(2)$.

Two-flavour neutrino oscillations involve a Hilbert space of two dimension \mathcal{H}^2 , and the mixing matrix is given by the SU(2) matrix [209]. The expression for the time evolved flavour neutrino states ($|\nu_e(t)\rangle$ and $|\nu_{\mu}(t)\rangle$) in linear superposition of two mass eigenstate basis ($|\nu_1\rangle$, $|\nu_2\rangle$) are given in Eq.(1.29) and Eq.(1.30).

 $|\nu_e(t)\rangle$ can be parametrized by two angles θ and ϕ as

$$|\nu_{e}(\theta,\phi)\rangle = e^{-iE_{1}t/\hbar}(\cos\theta |\nu_{1}\rangle - \sin\theta e^{-i(E_{2}-E_{1})t/\hbar} |\nu_{2}\rangle),$$

$$= e^{-iE_{1}t/\hbar}(\cos\theta |\nu_{1}\rangle - \sin\theta e^{-i\phi} |\nu_{2}\rangle),$$
(6.8)

where $E_1 = (p^2 + m_1^2)^{1/2}$ and $E_2 = (p^2 + m_2^2)^{1/2}$ and in the ultra-relativistic limit $\phi = \frac{(E_2 - E_1)t}{\hbar} = \frac{\Delta m^2 t}{2E\hbar}$. The overall phase is redundant and leads to an equivalent representation such that the coefficient of $|\nu_1\rangle$ is real. Thus, the normalized time evolved electron neutrino

and muon neutrino flavour state are,

$$|\nu_{e}(\theta,\phi)\rangle = \cos\theta |\nu_{1}\rangle - \sin\theta e^{-i\phi} |\nu_{2}\rangle,$$

$$|\nu_{\mu}(\theta,\phi)\rangle = \sin\theta |\nu_{1}\rangle + \cos\theta e^{-i\phi} |\nu_{2}\rangle,$$
(6.9)

respectively. Now we can easily identify the mass eigenstates of a flavour neutrino state to the qubit states

$$|0\rangle = |\nu_1\rangle = \begin{pmatrix} 1\\0 \end{pmatrix}; |1\rangle = |\nu_2\rangle = \begin{pmatrix} 0\\1 \end{pmatrix}.$$
 (6.10)

Identifying the states $|\psi\rangle$ and $|\psi'\rangle$ with time evolved flavour neutrino states $|\nu_e(\theta,\phi)\rangle = \begin{pmatrix} \cos\theta \\ -e^{-i\phi}\sin\theta \end{pmatrix}$ and, $|\nu_{\mu}(\theta,\phi)\rangle = \begin{pmatrix} \sin\theta \\ e^{-i\phi}\cos\theta \end{pmatrix}$, thus $|\nu_e(\theta,\phi)\rangle$ is an eigenstate with eignvalue +1.

$$\hat{O} = \hat{n}(\theta, \phi).\vec{\sigma} = \begin{pmatrix} \cos 2\theta & -\sin 2\theta e^{i\phi} \\ -\sin 2\theta e^{-i\phi} & -\cos 2\theta \end{pmatrix} \in SU(2). \tag{6.11}$$

Here $\vec{\sigma} = (\sigma_1, \sigma_2, \sigma_3)$ and $\hat{n}(\theta, \phi) = -\sin 2\theta \cos \phi \hat{e}_1 + \sin 2\theta \sin \phi \hat{e}_2 + \cos 2\theta \hat{e}_3$ is a real unit vector called the Poincaré unit vector. Therefore,

$$\hat{O} |\nu_e(\theta, \phi)\rangle = |\nu_e(\theta, \phi)\rangle. \tag{6.12}$$

Thus a state $|\nu_e(\theta,\phi)\rangle \in \mathcal{H}^2$ is expressed in terms of a unit vector $\hat{n}(\theta,\phi)$ on the surface of the Poincaré sphere. This correspondence is one-to-one if the ranges of θ and ϕ are restricted to $0 \le \theta \le \pi$ and $0 \le \phi < 2\pi$. The 2×2 density matrix is given by

$$\rho_{2\times 2}^{e} = \begin{pmatrix} \cos^{2}\theta & -e^{i\phi}\sin\theta\cos\theta \\ -e^{-i\phi}\sin\theta\cos\theta & \sin^{2}\theta \end{pmatrix} = \frac{1}{2}(I + \hat{n}.\vec{\sigma}), \tag{6.13}$$

which is the same as Eq.(6.5). The eigenvalues of $\rho_{2\times 2}^e$ are 1 and 0, therefore $\rho_{2\times 2}^e$ is a rank 1 density matrix. This maps the neutrino state $|\nu_e(t)\rangle$ to the the surface of the unit sphere in the three dimensional vector space. A similar mapping can be done for the neutrino state $|\nu_{\mu}(t)\rangle$. The density matrix correspond to $|\nu_{\mu}(\theta,\phi)\rangle$ is

$$\rho_{2\times 2}^{\mu} = \begin{pmatrix} \sin^2\theta & e^{i\phi}\sin\theta\cos\theta \\ e^{-i\phi}\sin\theta\cos\theta & \cos^2\theta \end{pmatrix} = \frac{1}{2}(I + \hat{n}'.\vec{\sigma}), \tag{6.14}$$

where $\hat{n}'(\theta, \phi) = \sin 2\theta \cos \phi \hat{e}_1 - \sin 2\theta \sin \phi \hat{e}_2 - \cos 2\theta \hat{e}_3$. When $\theta \to \frac{\theta}{2}$ then the Poincaré sphere becomes the Bloch sphere used in quantum optics. In the next section, we use Eq.(6.13) and Eq.(6.14) to describe the Bloch vector and its generalized representation in the two-qubit neutrino systems.

6.2 Bloch matrix construction of two qubit neutrino states

A 4×4 density matrix $\rho_{4\times4} \in \mathcal{H}^2 \otimes \mathcal{H}^2$ represent either a single four-level system, or a pair of coupled two-level systems [202]: two qubits. The study of the Bloch matrix using the density matrix $\rho_{4\times4}$ will give useful symmetries in the Bloch-vector space. This section studies two-qubit density matrices of two flavour neutrino states in the Dirac-basis to construct the Bloch-matrix. We extend this idea to study the entanglement nature of two-qubit neutrino systems.

In general, any 2×2 density matrix $\rho_{2\times 2}$ of a single qubit state in terms of the Pauli basis is written as

$$\rho_{2\times 2} = \frac{1}{2}(1 + \vec{u}.\sigma_{\mu}) = \frac{1}{2}r_{\mu}\sigma_{\mu}, \tag{6.15}$$

where the scalar coefficients $r_{\mu} = Tr(\rho_{2\times 2}\sigma_{\mu})$ ($\mu = 0, 1, 2, 3$) in which r_0 is always unity to ensure $Tr\rho_{2\times 2} = 1$, and r_1 , r_2 , r_4 are the components of the Bloch vector \vec{u} , and σ_{μ} are the Pauli matrices. Similarly, using Eq.(6.15), the density matrix $\rho_{4\times 4}$ of any two qubit states can be constructed using the Dirac matrices, denoted $D_{\mu\nu} = \sigma_{\mu} \otimes \sigma_{\nu}$ as its basis such that

$$\rho_{4\times 4} = \frac{1}{4} r_{\mu\nu} D_{\mu\nu}. \tag{6.16}$$

where $\mu, \nu = 0, 1, 2, 3$. The characterization of the Pauli matrices and Dirac matrices are shown in ref. [202]. The scalar coefficients $r_{\mu\nu}$ is defined as

$$r_{\mu\nu} = Tr(\rho_{4\times 4}D_{\mu\nu}) = \langle \sigma_{\mu} \otimes \sigma_{\nu} \rangle \tag{6.17}$$

constitute 16 components of the Bloch matrix M which is split into four major components:

a scalar of unity, two three-dimensional vectors, and a 3×3 matrix written as [202]

$$\mathbf{M} = \begin{bmatrix} \frac{1}{r_{01}} & r_{02} & r_{03} \\ \hline r_{10} & r_{11} & r_{12} & r_{13} \\ r_{20} & r_{21} & r_{22} & r_{23} \\ r_{30} & r_{31} & r_{32} & r_{33} \end{bmatrix},$$
(6.18)

where $u_i = r_{i0}$ and $v_j = r_{0j}$ (i, j = 1, 2, 3) are the components of two local Bloch vectors \vec{u} and \vec{v} , respectively. $R_{ij} = r_{ij}$ is the matrix elements of correlation matrix R, and $r_{00} = 1$ implies $\rho_{4\times4}$ be a Hermitian matrix, of unit trace, and positive semidefinite.

Using Eq.(6.13) and Eq.(6.14), we construct the density matrix of two qubit neutrino states $|\nu_{e\mu}(\theta,\phi)\rangle = |\nu_e(\theta,\phi)\rangle \otimes |\nu_{\mu}(\theta,\phi)\rangle$ in the standard basis $(|0\rangle \otimes |0\rangle \equiv |00\rangle, |0\rangle \otimes |1\rangle \equiv |01\rangle, |1\rangle \otimes |0\rangle \equiv |10\rangle, |1\rangle \otimes |1\rangle \equiv |11\rangle)$ as

$$\rho_{4\times4}^{e\mu} = \rho_{2\times2}^{e} \otimes \rho_{2\times2}^{\mu} = |\nu_{e\mu}(\theta,\phi)\rangle \langle \nu_{e\mu}(\theta,\phi)|$$

$$= \begin{pmatrix} \cos^{2}\theta \sin^{2}\theta & e^{i\phi}\cos^{3}\theta \sin\theta & -e^{i\phi}\cos\theta \sin^{3}\theta & -e^{2i\phi}\cos^{2}\theta \sin^{2}\theta \\ e^{-i\phi}\cos^{3}\theta \sin\theta & \cos^{4}\theta & -\cos^{2}\theta \sin^{2}\theta & -e^{i\phi}\cos^{3}\theta \sin\theta \\ -e^{-i\phi}\cos\theta \sin^{3}\theta & -\sin^{2}\theta\cos^{2}\theta & \sin^{4}\theta & e^{i\phi}\cos\theta \sin^{3}\theta \\ -e^{-2i\phi}\sin^{2}\theta\cos^{2}\theta & -e^{-i\phi}\sin\theta\cos^{3}\theta & e^{-i\phi}\cos\theta\sin^{3}\theta & \sin^{2}\theta\cos^{2}\theta \end{pmatrix} . \quad (6.19)$$

We can expand the above two qubit density matrix $\rho_{4\times4}^{e\mu}$ uniquely as

$$\rho_{4\times4}^{e\mu} = \rho_{2\times2}^{e} \otimes \rho_{2\times2}^{\mu} = \frac{1}{4} [(I + \hat{n}.\vec{\sigma}^{e}) \otimes (I + \hat{n}'.\vec{\sigma}^{\mu})]$$

$$= \frac{1}{4} [I \otimes I + \vec{\sigma}^{e}.\hat{n} \otimes I + I \otimes \vec{\sigma}^{\mu}.\hat{n}' + \sum_{i,j=1}^{3} r_{ij}\sigma_{i}^{e} \otimes \sigma_{j}^{\mu}], \qquad (6.20)$$

the expansion coefficients are

$$n_{i} = tr(\rho^{e\mu}\sigma_{i} \otimes I),$$

$$n'_{j} = tr(\rho^{e\mu}I \otimes \sigma_{j}),$$

$$r_{ij} = tr(\rho^{e\mu}\sigma_{i} \otimes \sigma_{j}),$$
(6.21)

where i, j = 1, 2, 3. In Eq.(6.21), n_i and n'_j are the elements of Poincaré unit vector \hat{n} and \hat{n}' , respectively and the coefficients r_{ij} of the basis $\sigma_i \otimes \sigma_j$ is defined as a correlation matrix

R between the two sub-system ρ^e and ρ^{μ} as

$$R = \begin{pmatrix} r_{11} & r_{12} & r_{13} \\ r_{21} & r_{22} & r_{23} \\ r_{31} & r_{32} & r_{33} \end{pmatrix}. \tag{6.22}$$

Using Eq.(6.21), the elements of r_{ij} can be obtained as: $r_{11} = -4cos^2\theta sin^2\theta cos^2\phi$, $r_{12} = r_{21} = 2cos^2\theta sin^2\theta sin^2\phi$, $r_{13} = r_{31} = \frac{1}{2}sin^4\theta cos^2\phi$, $r_{22} = -sin^22\theta sin^2\phi$, $r_{23} = r_{32} = -\frac{1}{2}sin^4\theta sin^2\phi$, $r_{33} = -cos^22\theta$. Alternative representation of Eq.(6.20) is Eq.(6.16). So, we can incorporate this correlation matrix R (see Eq.(6.22)) into the Bloch-matrix M shown in Eq.(6.18).

Following Eq.(6.16) and using Eq.(6.19) in Eq.(6.17), the Bloch matrix for $\rho_{4\times4}^{e\mu}$ can be constructed as

$$\mathbf{M}_{e\mu} = \begin{bmatrix} 1 & cos\phi sin2\theta & -sin2\theta sin\phi & -cos2\theta \\ -cos\phi sin2\theta & -4cos^2\theta cos^2\phi sin^2\theta & 2cos^2\theta sin^2\theta sin2\phi & \frac{1}{2}cos\phi sin4\theta \\ sin2\theta sin\phi & 2cos^2\theta sin^2\theta sin2\phi & -sin^22\theta sin^2\phi & -\frac{1}{2}sin4\theta sin\phi \\ cos2\theta & \frac{1}{2}cos\phi sin4\theta & -\frac{1}{2}sin4\theta sin\phi & -cos^22\theta \end{bmatrix}. \quad (6.23)$$

By comparing the matrix elements of $\mathbf{M}_{e\mu}$ (see Eq.(6.23)) with \mathbf{M} (see Eq.(6.18)), we find that r_{i0} and r_{0j} are the components of local unit Bloch vectors \hat{n} and \hat{n}' , respectively (i,j=1,2,3). The matrix elements r_{ij} are the elements of the correlation matrix R which is exactly equal to Eq.(6.22). Thus, we have incorporated the correlation matrix R inside the Bloch matrix $\mathbf{M}_{e\mu}$. Since, we can decompose the Bloch matrix $\mathbf{M}_{e\mu}$ in terms of Bloch-vectors components of two sub-systems ($\rho_{2\times 2}^e$ and $\rho_{2\times 2}^\mu$), therefore, the two-qubit density matrix $\rho_{4\times 4}^{e\mu} = \rho_{2\times 2}^e \otimes \rho_{2\times 2}^\mu$ is a separable state (or product state). In fact, such interpretations of the Bloch matrix \mathbf{M} is also valid for the other product states $\rho_{4\times 4}^{ee} = \rho_{2\times 2}^e \otimes \rho_{2\times 2}^e$, $\rho_{4\times 4}^{\mu\mu} = \rho_{2\times 2}^\mu \otimes \rho_{2\times 2}^\mu$, and $\rho_{4\times 4}^{\mu e} = \rho_{2\times 2}^\mu \otimes \rho_{2\times 2}^e$.

Furthermore, the concurrence is the measure of entanglement in the two qubit system and it is defined in Eq.(2.33). Using Eq.(6.19) in Eq.(2.34), we construct the spin-flipped density matrix $\tilde{\rho}_{4\times4}^{e\mu} = (\sigma_y \otimes \sigma_y) \rho_{4\times4}^{e\mu} (\sigma_y \otimes \sigma_y)$ and find that for the state $\rho_{4\times4}^{e\mu} = \rho_{2\times2}^e \otimes \rho_{2\times2}^\mu$ (see Eq.(6.19)), all eigenvalues of $\rho_{4\times4}^{e\mu} \tilde{\rho}_{4\times4}^{e\mu}$ are zero i.e., $\lambda_1 = \lambda_2 = \lambda_3 = \lambda_4 = 0$, which mean according to Eq.(2.33) the concurrence $C(\rho_{4\times4}^{e\mu})$ is 0. Similarly, for all other possible states: $\rho_{4\times4}^{ee} = \rho_{2\times2}^e \otimes \rho_{2\times2}^e$, $\rho_{4\times4}^{\mu\mu} = \rho_{2\times2}^\mu \otimes \rho_{2\times2}^\mu$, and $\rho_{4\times4}^{\mu e} = \rho_{2\times2}^\mu \otimes \rho_{2\times2}^e$, the concurrence is

$$C(\rho_{4\times 4}^{e\mu}) = C(\rho_{4\times 4}^{ee}) = C(\rho_{4\times 4}^{\mu\mu}) = C(\rho_{4\times 4}^{\mu e}) = 0.$$
 (6.24)

We see that concurrence is zero for all the states as expected because they are separable

states and we know that there should not be any quantum correlations exist between any two sub systems $(\rho_{2\times 2}^e)$ and $\rho_{2\times 2}^\mu$ of a given separable state. However, if a given state is not separable $|\nu_{e\mu}(\theta,\phi)\rangle \neq |\nu_e(\theta,\phi)\rangle \otimes |\nu_{\mu}(\theta,\phi)\rangle$ then it is an entangled state.

Now, we map the neutrino mass eigenstates $|\nu_1\rangle$ and $|\nu_2\rangle$ directly to the bi-partite qubit states as $|\nu_1\rangle = |1\rangle_1 \otimes |0\rangle_2$, $|\nu_2\rangle = |0\rangle_1 \otimes |1\rangle_2$. In that case, using Eq.(1.26), the time evolved electron flavour neutrino state $|\nu_e(t)\rangle$ in superposition of two qubit mass eigenstates (see Eq.(1.29)), parametrized by θ and ϕ , can be written as

$$|\nu_e(\theta,\phi)\rangle = \cos\theta |10\rangle - \sin\theta e^{-i\phi} |01\rangle,$$
 (6.25)

and its two-qubit density matrix is

$$\rho_{4\times4}^{e} = \begin{pmatrix} 0 & 0 & 0 & 0\\ 0 & \cos^{2}\theta & -\cos\theta\sin\theta e^{i\phi} & 0\\ 0 & -\sin\theta\cos\theta e^{-i\phi} & \sin^{2}\theta & 0\\ 0 & 0 & 0 & 0 \end{pmatrix}.$$
 (6.26)

Using Eq.(6.26) in Eq.(6.16) and in Eq.(6.17), the Bloch matrix **M** (see Eq.(6.18)) for $\rho_{4\times4}^e$ is obtained as

$$\mathbf{M}_{e} = \begin{bmatrix} 1 & 0 & 0 & -\cos^{2}\theta + \sin^{2}\theta \\ 0 & -2\sin\theta\cos\theta\cos\phi & -2\cos\theta\sin\theta\sin\phi & 0 \\ 0 & 2\cos\theta\sin\theta\sin\phi & -2\cos\theta\sin\theta\cos\phi & 0 \\ \cos^{2}\theta - \sin^{2}\theta & 0 & 0 & -\cos^{2}\theta - \sin^{2}\theta \end{bmatrix}.$$
(6.27)

We notice from Eq.(6.27) that some components of the local Bloch vector for the individual system is zero, and thus we cannot decompose the Bloch matrix \mathbf{M}_e in terms of Bloch-vectors components of two subsystems. Therefore, the two-qubit density matrix $\rho_{4\times4}^e$ of the state $|\nu_e(\theta,\phi)\rangle$ is an entangled state. At $\theta = \frac{\pi}{4}$ and $\phi = 0$, the Bloch matrix \mathbf{M}_e of $\rho_{2\times2}^e$ become

$$\mathbf{M}_{\psi^{-}} = \begin{bmatrix} 1 & 0 & 0 & 0 \\ 0 & -1 & 0 & 0 \\ 0 & 0 & -1 & 0 \\ 0 & 0 & 0 & -1 \end{bmatrix}, \tag{6.28}$$

which is identified as the Bloch matrix of two qubit Bell's state $|\psi^{-}\rangle = \frac{1}{\sqrt{2}}(|01\rangle - |10\rangle)$.

Similarly, for the state $|\nu_{\mu}(\theta,\phi)\rangle = \sin\theta |10\rangle + \cos\theta e^{-i\phi} |01\rangle$, we have

$$\rho_{4\times4}^{\mu} = \begin{pmatrix} 0 & 0 & 0 & 0\\ 0 & \sin^2\theta & \cos\theta\sin\theta e^{i\phi} & 0\\ 0 & \sin\theta\cos\theta e^{-i\phi} & \cos^2\theta & 0\\ 0 & 0 & 0 & 0 \end{pmatrix}, \tag{6.29}$$

and the corresponding Bloch Matrix is

$$\mathbf{M}_{\mu} = \begin{bmatrix} \frac{1}{0} & 0 & 0 & -\cos^{2}\theta + \sin^{2}\theta \\ 0 & 2\sin\theta\cos\theta\cos\phi & 2\cos\theta\sin\theta\sin\phi & 0 \\ 0 & -2\cos\theta\sin\theta\sin\phi & 2\cos\theta\sin\theta\cos\phi & 0 \\ \cos^{2}\theta - \sin^{2}\theta & 0 & 0 & -\cos^{2}\theta - \sin^{2}\theta \end{bmatrix}. \tag{6.30}$$

At $\theta = \frac{\pi}{4}$ and $\phi = 0$, the Bloch-matrix \mathbf{M}_{μ} become

$$\mathbf{M}_{\psi^{+}} = \begin{bmatrix} \frac{1 & 0 & 0 & 0 \\ 0 & 1 & 0 & 0 \\ 0 & 0 & 1 & 0 \\ 0 & 0 & 0 & -1 \end{bmatrix}, \tag{6.31}$$

which is identified as the Bloch matrix of two qubit Bell's state $|\psi^{+}\rangle = \frac{1}{\sqrt{2}}(|01\rangle + |10\rangle)$. Furthermore, concurrence for $\rho_{4\times 4}^{e}$ and $\rho_{4\times 4}^{\mu}$ we get as $C(\rho_{4\times 4}^{e}) = C(\rho_{4\times 4}^{\mu}) = \sin 2\theta$, which tends to 1 at $\theta = \frac{\pi}{4}$. The non-zero value of concurrence shows that $\rho_{4\times 4}^{e}$ and $\rho_{4\times 4}^{\mu}$ is a bipartite entangled state when time evolved neutrino flavour state are linear superposition of mass eigestates basis.

However, in general, neutrinos change its flavour while traveling in space with time. Therefore, it is useful to quantify concurrence when time evolved neutrino flavour states are linear superposition of flavour basis. In that case, using Eq.(1.27), Eq.(1.28) in Eq.(1.29) and in Eq.(1.30), the time evolved electron and muon flavour neutrino state ($|\nu_e(t)\rangle$ and $|\nu_{\mu}(t)\rangle$) in linear superposition of flavour basis, parametrized by θ , ϕ , can be simply written as

$$|\nu_{e}(\theta,\phi)\rangle_{f} = (\cos^{2}\theta + \sin^{2}\theta e^{-i\phi}) |\nu_{e}\rangle + \sin\theta \cos\theta (1 - e^{-i\phi}) |\nu_{\mu}\rangle,$$

$$|\nu_{\mu}(\theta,\phi)\rangle_{f} = \sin\theta \cos\theta (1 - e^{-i\phi}) |\nu_{e}\rangle + (\sin^{2}\theta + \cos^{2}\theta e^{-i\phi}) |\nu_{\mu}\rangle,$$
(6.32)

respectively, where suffix f represent that the flavour neutrino state should be written in flavour basis but not in mass basis.

If we map flavour states at time t=0 to bi-partite state in the two qubit system as $|\nu_e\rangle$ =

 $|1\rangle_e \otimes |0\rangle_\mu$ and $|\nu_\mu\rangle = |0\rangle_e \otimes |1\rangle_\mu$, therefore Eq.(6.32) become

$$|\nu_{e}(\theta,\phi)\rangle_{f} = (\cos^{2}\theta + \sin^{2}\theta e^{-i\phi}) |10\rangle + \sin\theta \cos\theta (1 - e^{-i\phi}) |01\rangle,$$

$$|\nu_{\mu}(\theta,\phi)\rangle_{f} = \sin\theta \cos\theta (1 - e^{-i\phi}) |10\rangle + (\sin^{2}\theta + \cos^{2}\theta e^{-i\phi}) |01\rangle.$$
(6.33)

These states are equivalent to Eq.(5.5) and Eq.(5.6) and for such states we have already quantified concurrence in terms of neutrino transitions probabilities which is given in Eq.(5.9). The result shows that these states are bi-partite qubit entangled state.

6.3 SU(3) Poincaré sphere for three-flavour neutrinos

In this section, we use the Gell-Mann matrices, instead of Pauli's matrices, to map the three flavour neutrino states onto the SU(3) Poincaré sphere. In the same way as the mass eigenstates of a two flavour neutrino system were mapped to qubits in the two-dimensional Hilbert space \mathcal{H}^2 , we now consider the three-dimension Hilbert space \mathcal{H}^3 . A qutrit is realized by three mutually orthogonal states [47]: $|1\rangle$, $|2\rangle$, $|3\rangle$.

A quantum state in the Hilbert space \mathcal{H}^3 spanned by the three orthogonal qtrit states $|1\rangle =$

$$\begin{pmatrix} 1 \\ 0 \\ 0 \end{pmatrix}; |2\rangle = \begin{pmatrix} 0 \\ 1 \\ 0 \end{pmatrix}; \text{ and } |3\rangle = \begin{pmatrix} 0 \\ 0 \\ 1 \end{pmatrix} \text{ is } |\psi\rangle = \alpha |1\rangle + \beta |2\rangle + \gamma |3\rangle \text{ where } |\alpha|^2 + |\beta|^2 + |\gamma|^2 = 1$$

. Using the polar representation a quantum state $|\psi\rangle$ does not change if multiplied by an overall phase, the equivalent quantum state is

$$|\psi\rangle = e^{\xi_1} \sin(\theta) \cos(\phi) |1\rangle + e^{i\xi_2} \sin(\theta) \sin(\phi) |2\rangle + \cos(\theta) |3\rangle. \tag{6.34}$$

The corresponding density matrix for the state $|\psi\rangle$ is

$$\rho_{3\times3}(\psi) = |\psi\rangle\langle\psi| = \begin{pmatrix} \sin^2\theta\cos^2\phi & \frac{e^{i(\xi_1 - \xi_2)}}{2}\sin^2\theta\sin(2\phi) & \frac{e^{i\xi_1}}{2}\sin(2\theta)\cos\phi\\ \frac{e^{i(\xi_2 - \xi_1)}}{2}\sin^2\theta\sin(2\phi) & \sin^2\theta\sin^2\phi & \frac{e^{i\xi_2}}{2}\sin(2\theta)\sin\phi\\ \frac{e^{-i\xi_1}}{2}\sin(2\theta)\cos\phi & \frac{e^{-i\xi_2}}{2}\sin(2\theta)\sin\phi & \cos^2\theta \end{pmatrix}.$$

$$(6.35)$$

The pure state $|\psi\rangle$ in Eq.(6.34) is dependent on 4 parameters θ , ϕ , ξ_1 , ξ_2 . However, the five parameters are needed to characterize the neutrino state, and the sum of the squares of the state's coefficients should be 1.

Now we will define the density operator of a qutrit system using SU(3) in general and

then map it to the neutrino system. The density matrix $\rho_{3\times3}=|\psi\rangle\langle\psi|$ is a 3×3 unitary matrix such that $(\rho_{3\times3})^\dagger=\rho_{3\times3}$; and $Tr(\rho_{3\times3})=1$. The qutrit representation of the density matrix takes the eight (Hermitian, traceless) generators of SU(3) as an operator basis called the Gell-Mann matrices [47]. By supplementing the eight Gellmann matrices $\lambda_i, i=1...8$ with the unit operator $\lambda_0 \equiv \sqrt{\frac{2}{3}}1$, the qutrit density matrix operator is a vector in the space spanned by $\lambda_\alpha, \alpha=0,...,8$ and therefore can be written as

$$\rho_{3\times3} = |\psi\rangle\langle\psi| = \frac{1}{3}c_{\alpha}\lambda_{\alpha} = (\alpha|1\rangle + \beta|2\rangle + \gamma|3\rangle)(\alpha^*\langle1| + \beta^*\langle2| + \gamma^*\langle3|), \tag{6.36}$$

$$= \sqrt{\frac{3}{2}}\lambda_{0} + \frac{1}{2}(\alpha\beta^{*} + \beta\alpha^{*})\lambda_{1} + \frac{i}{2}(\alpha\beta^{*} - \beta\alpha^{*})\lambda_{2}$$

$$+ \frac{1}{2}(|\alpha|^{2} - |\beta|^{2})\lambda_{3} + \frac{1}{2}(\alpha\gamma^{*} + \gamma\alpha^{*})\lambda_{4} + \frac{i}{2}(\alpha\gamma^{*} - \gamma\alpha^{*})\lambda_{5}$$

$$+ \frac{1}{2}(\beta\gamma^{*} + \gamma\beta^{*})\lambda_{6} + \frac{i}{2}(\beta\gamma^{*} - \gamma\beta^{*})\lambda_{7} + \frac{1}{2\sqrt{3}}(|\beta|^{2} - 2|\gamma|^{2})\lambda_{8},$$
(6.37)

the (real) expansion coefficients are

$$c_{\alpha} = \frac{3}{2} tr(\rho_{3\times 3} \lambda_{\alpha}). \tag{6.38}$$

Normalization implies that $c_0 = \sqrt{\frac{3}{2}}$, so $\rho_{3\times 3}$ can be simplified to the SU(3) equivalent of Eq.(6.5), which we shall show is the Poincaré sphere representation of the qutrit states

$$\rho_{3\times 3} = \frac{1}{3}(1 + c_j\lambda_j) = \frac{1}{3}(1 + \vec{c}.\vec{\lambda}), \tag{6.39}$$

where, $\vec{c} = c_j \hat{e_j}$ and $\vec{\lambda} = \lambda_j \hat{e_j}$.

To find the coefficients c_i we note that

$$\rho_{3\times 3}^2 = \frac{1}{9}(1 + \frac{2}{3}\vec{c}.\vec{c})1 + \frac{1}{3}\vec{\lambda}.(\frac{2}{3}\vec{c} + \frac{1}{3\sqrt{3}}\vec{c} \star \vec{c}), \tag{6.40}$$

where the "star" product is defined as

$$\vec{c} \star \vec{d} \equiv \hat{e}_i d_{ikl} c_k d_l. \tag{6.41}$$

The characterization of the Gell-Mann matrices and d_{jkl} value can be found in [210] or any group theory textbook. The star product condition is well explained in ref. [47]. For a pure state $|\psi\rangle$, $\rho_{3\times3}^2 = \rho_{3\times3}$, $\vec{c}.\vec{c} = 3$ and $\vec{c} \star \vec{c} = \sqrt{3}\vec{c}$. Taking $\hat{n} = \vec{c}/\sqrt{3}$ which is eight dimensional unit vector, qutrit pure state density matrix is

$$\rho_{3\times3} = |\psi\rangle\langle\psi| = \frac{1}{3}(I + \sqrt{3}\hat{n}.\vec{\lambda}),\tag{6.42}$$

where \hat{n} satisfies

$$\hat{n}.\hat{n} = 1 \text{ and } \hat{n} \star \hat{n} = \hat{n}. \tag{6.43}$$

Eq.(6.42) is the equation for the 7-dimensional unit sphere $\hat{n} \in S^7$ embedded in Euclidean eight dimensional space \mathcal{R}^8 spanned by the Gell-Mann matrices, that represents coset space SU(3)/U(2) [205], with components of unit vector \hat{n} given by

$$n_{j} = \frac{\sqrt{3}}{2} tr(\rho_{3\times3}\lambda_{j}) = \frac{\sqrt{3}}{2} \langle \psi | \lambda_{j} | \psi \rangle.$$
 (6.44)

Thus, we have outlined the Poincaré sphere representation of the density matrix in \mathcal{H}^3 .

Three-flavour neutrino oscillations involve a Hilbert space \mathcal{H}^3 and the mixing matrix is given by the SU(3) matrix. Let the mass eigenstates of the three flavour neutrino system be $|\nu_1\rangle$, $|\nu_2\rangle$ and $|\nu_3\rangle$ then the relation between the mass eigenstates and the flavour states is (see Eq.(1.1))

$$\begin{pmatrix} |\nu_e\rangle \\ |\nu_\mu\rangle \\ |\nu_\tau\rangle \end{pmatrix} = U^*(\theta, \phi, \eta, \delta_{CP}) \begin{pmatrix} |\nu_1\rangle \\ |\nu_2\rangle \\ |\nu_3\rangle \end{pmatrix}, \tag{6.45}$$

where $U(\theta, \phi, \eta, \delta_{CP})$ is the Unitary PMNS neutrino mixing matrix

$$U(\theta, \phi, \eta, \delta_{CP}) = \begin{pmatrix} C_{\theta}C_{\phi} & S_{\theta}C_{\phi} & S_{\phi}e^{-i\delta_{CP}} \\ -S_{\theta}C_{\eta} - C_{\theta}S_{\phi}S_{\eta}e^{i\delta_{CP}} & C_{\theta}C_{\eta} - S_{\theta}S_{\phi}S_{\eta}e^{i\delta_{CP}} & C_{\phi}S_{\eta} \\ S_{\theta}S_{\eta} - C_{\theta}S_{\phi}C_{\eta}e^{i\delta_{CP}} & -C_{\theta}S_{\eta} - S_{\theta}S_{\phi}C_{\eta}e^{i\delta_{CP}} & C_{\phi}C_{\eta} \end{pmatrix} \in SU(3),$$

$$(6.46)$$

where $(S_{\theta}, S_{\phi}, S_{\eta}) \equiv (Sin\theta_{12}, Sin\theta_{13}, Sin\theta_{23});$ $(C_{\theta}, C_{\phi}, C_{\eta}) \equiv (Cos\theta_{12}, Cos\theta_{13}, Cos\theta_{23}),$ the θ_{ij} 's are the neutrino mixing angles between the states i and j (i, j = 1, 2, 3) [52, 209]. Here, Eq.(6.46) is similar to Eq.(1.2).

The three flavour states of a neutrino system can be written in the qutrit basis by identifying the mass eigenstates with the qutrit basis states of the three dimension Hilbert space

 \mathcal{H}^3 as

$$|1\rangle = |\nu_1\rangle \ ; |2\rangle = |\nu_2\rangle \ ; |3\rangle = |\nu_3\rangle .$$
 (6.47)

Without loss of generality, we take $\delta_{CP} = 0$ and write the time evolved electron flavour neutrino state as

$$|\nu_{e}(t)\rangle = e^{-iE_{1}t/\hbar}C_{\theta}C_{\phi}|1\rangle + e^{-iE_{2}t/\hbar}(-S_{\theta}C_{\eta} - C_{\theta}S_{\phi}S_{\eta})|2\rangle + e^{-iE_{3}t/\hbar}(S_{\theta}S_{\eta} - C_{\theta}S_{\phi}C_{\eta})|3\rangle. (6.48)$$

Similarly, the time evolved $|\nu_{\mu}(t)\rangle$ and $|\nu_{\tau}(t)\rangle$ neutrino flavour states can be written as

$$|\nu_{\mu}(t)\rangle = e^{-iE_{1}t/\hbar}S_{\theta}C_{\phi}|1\rangle + e^{-iE_{2}t/\hbar}(C_{\theta}C_{\eta} - S_{\theta}S_{\phi}S_{\eta})|2\rangle + e^{-iE_{3}t/\hbar}(-C_{\theta}S_{\eta} - S_{\theta}S_{\phi}C_{\eta})|3\rangle, (6.49)$$

$$and \quad |\nu_{\tau}(t)\rangle = e^{-iE_{1}t/\hbar}S_{\phi}|1\rangle + e^{-iE_{2}t/\hbar}C_{\phi}S_{\eta}|2\rangle + e^{-iE_{3}t/\hbar}C_{\phi}C_{\eta})|3\rangle, \tag{6.50}$$

respectively. Taking the ultra-relativistic limit $L \approx t$ ($c = 1, \hbar = 1$) and defining $\xi_1 = (E_3 - E_1)t/\hbar \approx \Delta m_{31}^2 L/2E$, and $\xi_2 = (E_2 - E_1)t/\hbar \approx \Delta m_{21}^2 L/2E$, the normalized time evolved electron neutrino flavour state $|\nu_e(t)\rangle$ in qutrit basis, parametrized by three different mixing angle θ , ϕ , η and with two arbitrary phases ξ_1 and ξ_2 ($0 \le \theta$, ϕ , $\eta \le \frac{\pi}{2}$; $0 \le \xi_1, \xi_2 < 2\pi$) is

$$|\nu_e(\theta, \phi, \eta, \xi_1, \xi_2)\rangle = e^{i\xi_1} C_{\theta} C_{\phi} |1\rangle + e^{i\xi_2} (-S_{\theta} C_{\eta} - C_{\theta} S_{\phi} S_{\eta}) |2\rangle + (S_{\theta} S_{\eta} - C_{\theta} S_{\phi} C_{\eta}) |3\rangle.$$
 (6.51)

The 3 × 3 density matrix of the state $|\nu_e(\theta, \phi, \eta, \xi_1, \xi_2)\rangle$ is

$$\rho_{3\times3}^e = |\nu_e(\theta, \phi, \eta, \xi_1, \xi_2)\rangle \langle \nu_e(\theta, \phi, \eta, \xi_1, \xi_2)|, \qquad (6.52)$$

which, in matrix form, is

$$=\begin{pmatrix} C_\theta^2 C_\phi^2 & -e^{-i(\xi_2-\xi_1)} C_\theta C_\phi (S_\theta C_\eta + C_\theta S_\phi S_\eta) & e^{i\xi_1} C_\theta C_\phi (S_\theta S_\eta - C_\theta C_\phi C_\eta) \\ -e^{i(\xi_2-\xi_1)} C_\theta C_\phi (S_\theta C_\eta + C_\theta S_\phi S_\eta) & (S_\theta C_\eta + C_\theta S_\phi S_\eta)^2 & -e^{i\xi_2} (S_\theta C_\eta + C_\theta S_\phi S_\eta) (S_\theta S_\eta - C_\theta C_\phi C_\eta) \\ e^{-i\xi_1} C_\theta C_\phi (S_\theta S_\eta - C_\theta C_\phi C_\eta) & -e^{-i\xi_2} (S_\theta C_\eta + C_\theta S_\phi S_\eta) (S_\theta S_\eta - C_\theta C_\phi C_\eta) & (S_\theta S_\eta - C_\theta C_\phi C_\eta)^2 \end{pmatrix}.$$

The density matrix $\rho_{3\times3}^e$ satisfies the relation $(\rho_{3\times3}^e)^{\dagger} = (\rho_{3\times3}^e)^2 = \rho_{3\times3}^e$; and $Tr(\rho_{3\times3}^e) = 1$. The density matrix for the time evolved electron flavour neutrino state $|\nu_e(\theta, \phi, \eta, \xi_1, \xi_2)\rangle$ can now be cast into the form

$$\rho_{3\times 3}^{e} = |\nu_{e}(\theta, \phi, \eta, \xi_{1}, \xi_{2})\rangle \langle \nu_{e}(\theta, \phi, \eta, \xi_{1}, \xi_{2})| = \frac{1}{3}(I + \sqrt{3}\hat{n}.\vec{\lambda}).$$
 (6.53)

The unit vector $(\hat{n}.\hat{n}=1)$, in the Euclidean eight dimensional space \mathcal{R}^8 is

$$\hat{n}(\theta, \phi, \eta, \xi_1, \xi_2) = n_1 \hat{e}_1 + n_2 \hat{e}_2 + n_3 \hat{e}_3 + n_4 \hat{e}_4 + n_5 \hat{e}_5 + n_6 \hat{e}_6 + n_7 \hat{e}_7 + n_8 \hat{e}_8. \tag{6.54}$$

Using the density matrix form $(\rho_{3\times 3}^e)$ of Eq.(6.52) in Eq.(6.44), the components of the unit vector $\hat{n}(\theta, \phi, \eta, \xi_1, \xi_2)$ can be obtained as:

$$n_{1} = -\sqrt{3}C_{\theta}C_{\phi}(S_{\theta}C_{\eta} + C_{\theta}S_{\phi}S_{\eta})Cos(\xi_{2} - \xi_{1});$$

$$n_{2} = -\sqrt{3}C_{\theta}C_{\phi}(S_{\theta}C_{\eta} + C_{\theta}S_{\phi}S_{\eta})Sin(\xi_{2} - \xi_{1});$$

$$n_{3} = \frac{\sqrt{3}}{2}[C_{\theta}^{2}C_{\phi}^{2} - (S_{\theta}C_{\eta} + C_{\theta}S_{\phi}S_{\eta})^{2}];$$

$$n_{4} = \sqrt{3}C_{\theta}C_{\phi}(S_{\theta}S_{\eta} - C_{\theta}C_{\phi}C_{\eta})Cos\xi_{1};$$

$$n_{5} = -\sqrt{3}C_{\theta}C_{\phi}(S_{\theta}S_{\eta} - C_{\theta}C_{\phi}C_{\eta})Sin\xi_{1};$$

$$n_{6} = -\sqrt{3}(S_{\theta}C_{\eta} + C_{\theta}S_{\phi}S_{\eta})(S_{\theta}S_{\eta} - C_{\theta}C_{\phi}C_{\eta})Cos\xi_{2};$$

$$n_{7} = \sqrt{3}(S_{\theta}C_{\eta} + C_{\theta}S_{\phi}S_{\eta})(S_{\theta}S_{\eta} - C_{\theta}C_{\phi}C_{\eta})Sin\xi_{2};$$

$$n_{8} = \frac{1}{2}[C_{\theta}^{2}C_{\phi}^{2} + (S_{\theta}C_{\eta} + C_{\theta}S_{\phi}S_{\eta})^{2} - 2(S_{\theta}S_{\eta} - C_{\theta}C_{\phi}C_{\eta})^{2}].$$
(6.55)

The result shows that the time evolved electron flavour neutrino state lies on the S^7 sphere in the eight dimensional real vector spaces. Not all the operators on the unit-sphere are pure state, so the star product condition $\hat{n} \star \hat{n} = \hat{n}$ (see Eq.(6.43)) imposes three constraints on the unit vector $\hat{n}(\theta, \phi, \eta, \xi_1, \xi_2)$ (see Eq.(6.54)) and therefore reduces the number of arbitrary parameters for the neutrino states. The three constraints give us three orthonormal components of $\hat{n}(\theta, \phi, \eta, \xi_1, \xi_2)$. In the following Table.(6.1), we list the three constraints and their corresponding orthonormal unit vectors.

	Constraints	Corresponding \hat{n}
1.	$\theta = \phi = 0, \ \eta = \frac{\pi}{2}, \ \xi_1 \ \text{and} \ \xi_2$ are arbitrary	$\hat{n}_1 = \frac{\sqrt{3}}{2}\hat{e}_3 + \frac{1}{2}\hat{e}_8$
	are arbitrary	
2.	$\theta = \pi/2, \phi = \eta = 0, \xi_1 \text{ and }$	$\hat{n}_2 = -\frac{\sqrt{3}}{2}\hat{e}_3 + \frac{1}{2}\hat{e}_8$
	ξ_2 are arbitrary	
3.	$\theta = \phi = \eta = \pi/2, \xi_1 \text{ and } \xi_2$	$\hat{n}_3 = -\hat{e}_8$
	are arbitrary	

Table 6.1: The three constraints coming from star product condition $\hat{n} \star \hat{n} = \hat{n}$ (see Eq.(6.43)) and their corresponding orthonormal unit vectors.

These orthonormal states also satisfies the condition [205]

$$|\langle \psi | \psi' \rangle|^2 = tr(\rho \rho') = \frac{1}{3} (1 + 2\hat{n}.\hat{n}'),$$

 $0 \le tr(\rho \rho') \le 1 \iff 0 \le Cos^{-1}(\hat{n}.\hat{n}') \le \frac{2\pi}{3}.$ (6.56)

We find that the angle formed between any two unit vectors $(\hat{n}_1, \hat{n}_2, \hat{n}_3)$ is $\frac{2\pi}{3}$, since $Cos^{-1}(\hat{n}_1.\hat{n}_2) = Cos^{-1}(\hat{n}_1.\hat{n}_3) = Cos^{-1}(\hat{n}_2.\hat{n}_3) = Cos^{-1}(\frac{-1}{2}) = \frac{2\pi}{3}$. Identifying the three orthonormal basis of qutrit as the mass eigenstates of neutrinos (see Eq.(6.47)), the Eq.(6.56) shows that the pure state $|\nu_e(\theta, \phi, \eta, \xi_1, \xi_2)|$ in an orthonormal basis $(|\nu_1\rangle, |\nu_2\rangle, |\nu_3\rangle)$ has unit vectors $(\hat{n}_1, \hat{n}_2, \hat{n}_3)$ that lie in a plane at the vertices of an equilateral triangle which we term as a "qutrit triangle". If one takes the three canonical basis vectors of \mathcal{H}^3 as usual, the three vertices of an equilateral triangle are

$$(n_3, n_8)_A = (\frac{\sqrt{3}}{2}, \frac{1}{2}) \longrightarrow (1, 0, 0)^T = |1\rangle = |\nu_1\rangle;$$
 (6.57)

$$(n_3, n_8)_B = (-\frac{\sqrt{3}}{2}, \frac{1}{2}) \longrightarrow (0, 1, 0)^T = |2\rangle = |\nu_2\rangle;$$
 (6.58)

$$(n_3, n_8)_c = (0, -1) \longrightarrow (0, 0, 1)^T = |3\rangle = |\nu_3\rangle;$$
 (6.59)

which are identified with the generalized W-states of neutrinos that we have discussed in Chapter 3. Thus, we generalize the concept of tri-partite mode entanglement by considering neutrinos as quirits.

The diagonal density matrix in the orthonormal basis is the triangle operator, or interior [47,208]. We map the neutrino state density matrix $\rho_{3\times3}^e$ of SU(3) space directly to the λ_3 and λ_8 basis (two diagonal Gell-Mann matrices) to construct a mixed state density matrix $\rho_{d(3\times3)}^e$. Thus, the density matrix $\rho_{3\times3}^e$ of Eq.(6.53) is now reduced to a mixed state as

$$\rho_{d(3\times3)}^{e} = \frac{1}{3}(I + \sqrt{3}(n_3\lambda_3 + n_8\lambda_8)) = \frac{1}{3} \begin{pmatrix} 1 + \sqrt{3}n_3 + n_8 & 0 & 0\\ 0 & 1 - \sqrt{3}n_3 + n_8 & 0\\ 0 & 0 & 1 - 2n_8 \end{pmatrix}, (6.60)$$

where $x_1 = \frac{1}{3}(1+\sqrt{3}n_3+n_8)$, $x_2 = \frac{1}{3}(1-\sqrt{3}n_3+n_8)$, and $x_3 = \frac{1}{3}(1-2n_8)$ are three eigenvalues of $\rho_{d(3\times3)}^e$ in terms of n_3 and n_8 . The value of n_3 and n_8 are given in Eq.(6.55). We calculate

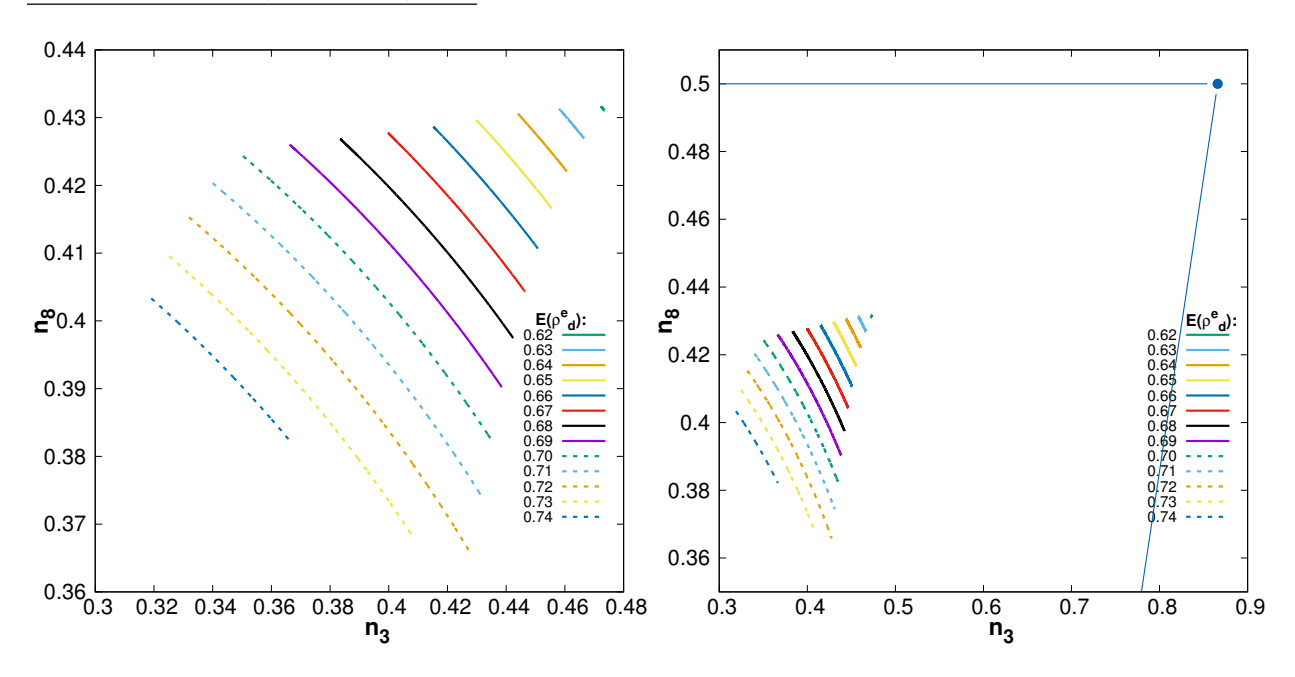


Figure 6.1: In Fig.(a) the equi-mixing curves of $E(\rho_d^e)$ in the n_3 and n_8 plane is shown using the current experimental bounds of the 3σ range of neutrino parameters [197]. Fig.(b) shows the equi-mixing curves of $E(\rho_d^e)$ in the n_3 and n_8 plane inside the qutrit triangle.

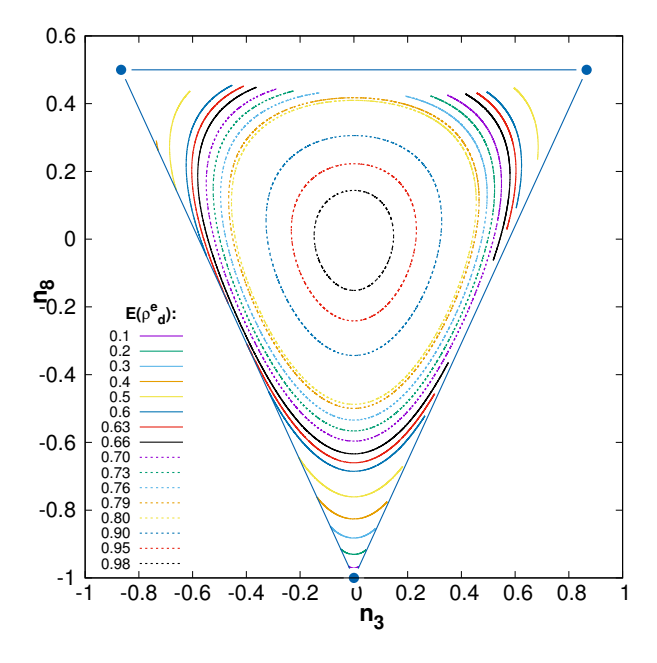


Figure 6.2: The equi-mixing curves of $E(\rho_d^e)$ is shown in the n_3 and n_8 plane when θ and η are vary from 0 to $\pi/2$.

the entropy of mixing of the mixed state $\rho_{d(3\times3)}^e$ by using the formula [208]:

$$E(\rho_{d(3\times3)}^e) = -x_1 \log_3(x_1) - x_2 \log_3(x_2) - x_3 \log_3(x_3).$$
(6.61)

In Fig.(6.1) (Fig.(a) and Fig.(b)), we plot the equi-mixing curves of $E(\rho_d^e)$ in the n_3 and n_8 plane. We vary $\theta \equiv \theta_{12}$ and $\eta \equiv \theta_{23}$ over 3σ range of current experimental bounds [197], we find that neutrinos are inside qutrit triangle for the range of entropy of mixing $E(\rho_d^e)$ approximately between 0.62 to 0.74. In Fig.(6.2) we vary θ and η from 0 to $\pi/2$, and we see that this put the constraints on θ_{12} and θ_{23} to be greater than 23 degrees for physical result.

Furthermore, the SU(2) Poincaré sphere representation for two-flavour neutrino oscillations can be deduced from the three-flavour Poincaré sphere in SU(3) by imposing the conditions

$$tan\theta_{23} \ tan\theta_{12} = sin\theta_{13}. \tag{6.62}$$

In the limit when the mixing between 2 and 3 (49 degrees), and 1 and 2 (33.44 degrees) is greater than the mixing between 1 and 3, $\theta_{13} \approx 0$ (8.57 degrees, $Sin\theta_{13} \approx 0.15$). We set $\theta_{13} \approx 0$, so that the Eq.(6.51) $|\nu_e(\theta, \phi, \eta, \xi_1, \xi_2)\rangle$ can be reduced to

$$|\nu_e(\theta, \xi_1, \xi_2)\rangle = \begin{pmatrix} e^{i\xi_1} cos\theta \\ -e^{i\xi_2} sin\theta \\ 0 \end{pmatrix} \quad (0 \le \theta \le \frac{\pi}{2}, \ 0 \le \xi_1, \xi_2 < 2\pi).$$
 (6.63)

We calculate the density matrix $\rho_{3\times3}^e = |\nu_e(\theta, \xi_1, \xi_2)\rangle \langle \nu_e(\theta, \xi_1, \xi_2)|$ of the above reduced state and use it in Eq.(6.44). We find that the unit vector \hat{n} in eight-dimensional real vector space has now reduces to only four non-vanishing components

$$n_1 = -\frac{\sqrt{3}}{2}sin2\theta cos(\xi_2 - \xi_1);$$
 $n_2 = \frac{\sqrt{3}}{2}sin2\theta sin(\xi_2 - \xi_1);$ $n_3 = \frac{\sqrt{3}}{2}cos2\theta;$ $n_8 = \frac{1}{2}$,(6.64)

else all are zero i.e, $n_4 = n_5 = n_6 = n_7 = 0$. Hence, when there is a hierarchy of mixing between the three states 1, 2 and 3 with the third state almost decoupled (small mixing angle), we retrieve the SU(2) Poincaré sphere from the SU(3) Poincaré sphere.

So far, we have considered the Poincare' sphere representation of a time evolved electronneutrino flavour state. For completeness, we give the Poincare' sphere representation of a time evolved muon-neutrino flavour state. The state $|\nu_{\mu}(t)\rangle$ (see Eq.(6.49)) parametrized by $\theta, \phi, \eta, \xi_1, \xi_2$ in the qutrit basis is

$$|\nu_{\mu}(\theta, \phi, \eta, \xi_{1}, \xi_{2})\rangle = e^{i\xi_{1}} S_{\theta} C_{\phi} |1\rangle + e^{i\xi_{2}} (C_{\theta} C_{\eta} - S_{\theta} S_{\phi} S_{\eta}) |2\rangle + (-C_{\theta} S_{\eta} - S_{\theta} S_{\phi} C_{\eta}) |3\rangle), (6.65)$$

and its corresponding density matrix $\rho_{3\times 3}^{\mu} = |\nu_{\mu}(\theta, \phi, \eta, \xi_1, \xi_2)\rangle \langle \nu_{\mu}(\theta, \phi, \eta, \xi_1, \xi_2)|$ is

$$\rho_{3\times3}^{\mu} = \begin{pmatrix} \mathbf{S}_{\theta}^{2} \mathbf{C}_{\phi}^{2} & \mathbf{e}^{-\mathbf{i}(\xi_{2} - \xi_{1})} \mathbf{S}_{\theta} \mathbf{C}_{\phi} (\mathbf{C}_{\theta} \mathbf{S}_{\eta} - \mathbf{S}_{\theta} \mathbf{S}_{\phi} \mathbf{S}_{\eta}) & \mathbf{e}^{\mathbf{i}\xi_{1}} \mathbf{S}_{\theta} \mathbf{C}_{\phi} (-\mathbf{C}_{\theta} \mathbf{S}_{\eta} - \mathbf{S}_{\theta} \mathbf{S}_{\phi} \mathbf{S}_{\eta}) \\ \mathbf{e}^{\mathbf{i}(\xi_{2} - \xi_{1})} \mathbf{S}_{\theta} \mathbf{C}_{\phi} (\mathbf{C}_{\theta} \mathbf{S}_{\eta} - \mathbf{S}_{\theta} \mathbf{S}_{\phi} \mathbf{S}_{\eta}) & (\mathbf{C}_{\theta} \mathbf{S}_{\eta} - \mathbf{S}_{\theta} \mathbf{S}_{\phi} \mathbf{S}_{\eta})^{2} & \mathbf{e}^{\mathbf{i}\xi_{2}} (\mathbf{C}_{\theta} \mathbf{S}_{\eta} - \mathbf{S}_{\theta} \mathbf{S}_{\phi} \mathbf{S}_{\eta}) (-\mathbf{C}_{\theta} \mathbf{S}_{\eta} - \mathbf{S}_{\theta} \mathbf{S}_{\phi} \mathbf{S}_{\eta}) \\ \mathbf{e}^{-\mathbf{i}\xi_{1}} \mathbf{S}_{\theta} \mathbf{C}_{\phi} (-\mathbf{C}_{\theta} \mathbf{S}_{\eta} - \mathbf{S}_{\theta} \mathbf{S}_{\phi} \mathbf{S}_{\eta}) & \mathbf{e}^{-\mathbf{i}\xi_{2}} (-\mathbf{C}_{\theta} \mathbf{S}_{\eta} - \mathbf{S}_{\theta} \mathbf{S}_{\phi} \mathbf{S}_{\eta}) (\mathbf{C}_{\theta} \mathbf{S}_{\eta} - \mathbf{S}_{\theta} \mathbf{S}_{\phi} \mathbf{S}_{\eta}) & (-\mathbf{C}_{\theta} \mathbf{S}_{\eta} - \mathbf{S}_{\theta} \mathbf{S}_{\phi} \mathbf{S}_{\eta})^{2} \end{pmatrix}. (6.66)$$

The density matrix $\rho_{3\times 3}^{\mu}$ can be expanded in the Gell-mann basis as

$$\rho_{3\times 3}^{\mu} = \frac{1}{3}(I + \sqrt{3}\hat{n'}.\vec{\lambda}),\tag{6.67}$$

and by using the Eq.(6.66) in Eq.(6.44), we get the components of the unit vector $\hat{n}'(\theta, \phi, \eta, \xi_1, \xi_2)$ as

$$n'_{1} = \sqrt{3}S_{\theta}C_{\phi}(C_{\theta}S_{\eta} - S_{\theta}S_{\phi}S_{\eta})Cos(\xi_{2} - \xi_{1});$$

$$n'_{2} = \sqrt{3}S_{\theta}C_{\phi}(C_{\theta}S_{\eta} - S_{\theta}S_{\phi}S_{\eta})Sin(\xi_{2} - \xi_{1});$$

$$n'_{3} = \frac{\sqrt{3}}{2}[S_{\theta}^{2}C_{\phi}^{2} - (C_{\theta}S_{\eta} - S_{\theta}S_{\phi}S_{\eta})^{2}];$$

$$n'_{4} = \sqrt{3}S_{\theta}C_{\phi}(-C_{\theta}S_{\eta} - S_{\theta}S_{\phi}S_{\eta})Cos\xi_{1};$$

$$n'_{5} = -\sqrt{3}S_{\theta}C_{\phi}(-C_{\theta}S_{\eta} - S_{\theta}S_{\phi}S_{\eta})Sin\xi_{1};$$

$$n'_{6} = \sqrt{3}(C_{\theta}S_{\eta} - S_{\theta}S_{\phi}S_{\eta})(-C_{\theta}S_{\eta} - S_{\theta}S_{\phi}S_{\eta})Cos\xi_{2};$$

$$n'_{7} = -\sqrt{3}(C_{\theta}S_{\eta} - S_{\theta}S_{\phi}S_{\eta})(-C_{\theta}S_{\eta} - S_{\theta}S_{\phi}S_{\eta})Sin\xi_{2};$$

$$n'_{8} = \frac{1}{2}[S_{\theta}^{2}C_{\phi}^{2} + (C_{\theta}S_{\eta} - S_{\theta}S_{\phi}S_{\eta})^{2} - 2(C_{\theta}S_{\eta} - S_{\theta}S_{\phi}S_{\eta})^{2}].$$
(6.68)

6.4 Two qutrits flavour neutrino states and generalized concurrence

In general, any two qutrits state is defined as the tensor product of two three dimensional Hilbert spaces, i.e., $\mathcal{H}^3 \otimes \mathcal{H}^3$. This section represents a two-qutrit density matrix of the neutrino system based on Gell-Mann matrix tensor products, with the coefficients constituting a generalized matrix analogous to a two-qubit Bloch matrix of neutrinos.

According to Eq.(6.45), Eq.(6.46) and Eq.(6.47), in the three neutrino system, in general the time evolved neutrino flavour states in qutrit basis ($|1\rangle$, $|2\rangle$, $|3\rangle$) for the two different sub-system A and B can be represented as $(A, B = e, \mu, \tau)$:

$$|\nu_A(\theta, \phi, \eta, \xi_1, \xi_2)\rangle = \alpha_1 |1\rangle + \alpha_2 |2\rangle + \alpha_3 |3\rangle$$

$$|\nu_B(\theta, \phi, \eta, \xi_1, \xi_2)\rangle = \alpha_1' |1\rangle + \alpha_2' |2\rangle + \alpha_3' |3\rangle$$
(6.69)

where, $|\nu_A(\theta, \phi, \eta, \xi_1, \xi_2)\rangle \in \mathcal{H}_A^3$ and $|\nu_B(\theta, \phi, \eta, \xi_1, \xi_2)\rangle \in \mathcal{H}_B^3$, and $|\alpha_1|^2 + |\alpha_2|^2 + |\alpha_3|^2 = 1$ and $|\alpha_1'|^2 + |\alpha_2'|^2 + |\alpha_3'|^2 = 1$.

We express the two qutrits time evolved flavour neutrino state as $|\nu_{AB}(\theta, \phi, \eta, \xi_1, \xi_2)\rangle = |\nu_A(\theta, \phi, \eta, \xi_1, \xi_2)\rangle \otimes |\nu_B(\theta, \phi, \eta, \xi_1, \xi_2)\rangle$, and find its the density matrix in the two qutrit standard basis $\{|11\rangle, |12\rangle, |13\rangle, |21\rangle, |22\rangle, |23\rangle, |31\rangle, |32\rangle, |33\rangle\} \in \mathcal{H}_A^3 \otimes \mathcal{H}_B^3$ as

$$\rho_{9\times9}^{AB} = \rho_{3\times3}^{A} \otimes \rho_{3\times3}^{B} = |\nu_{A,B}(\theta, \phi, \eta, \xi_{1}, \xi_{2})\rangle \langle \nu_{A,B}(\theta, \phi, \eta, \xi_{1}, \xi_{2})|
= \begin{pmatrix} |\alpha_{1}|^{2} & \alpha_{1}\alpha_{2}^{*} & \alpha_{1}\alpha_{3}^{*} \\ \alpha_{2}\alpha_{1}^{*} & |\alpha_{2}|^{2} & \alpha_{2}\alpha_{3}^{*} \\ \alpha_{3}\alpha_{1}^{*} & \alpha_{3}\alpha_{2}^{*} & |\alpha_{3}|^{2} \end{pmatrix} \otimes \begin{pmatrix} |\alpha'_{1}|^{2} & \alpha'_{1}{\alpha'_{2}^{*}} & \alpha'_{1}{\alpha'_{3}^{*}} \\ \alpha'_{2}{\alpha'_{1}^{*}} & |\alpha'_{2}|^{2} & \alpha'_{2}{\alpha'_{3}^{*}} \\ \alpha'_{3}{\alpha'_{1}^{*}} & \alpha'_{3}{\alpha'_{2}^{*}} & |\alpha'_{3}|^{2} \end{pmatrix} = (...)_{9X9}$$
(6.70)

where, $\rho_{3\times3}^A = |\nu_A(\theta, \phi, \eta, \xi_1, \xi_2)\rangle \langle \nu_A(\theta, \phi, \eta, \xi_1, \xi_2)|$ and $\rho_{3\times3}^B = |\nu_B(\theta, \phi, \eta, \xi_1, \xi_2)\rangle \langle \nu_B(\theta, \phi, \eta, \xi_1, \xi_2)|$ are density matrix of two sub-systems A and B, respectively. Also, $\alpha_1^*, \alpha_2^*, \alpha_3^*$ and $\alpha_1'^*, \alpha_2'^*, \alpha_3'^*$ are complex cojugate of $\alpha_1, \alpha_2, \alpha_3$ and $\alpha_1', \alpha_2', \alpha_3'$, respectively.

Alternatively, the density matrix in Eq.(6.70) is uniquely expanded as

$$\rho_{9\times9}^{AB} = \left(\frac{1}{3}(I + \sqrt{3}\hat{n}.\vec{\lambda}^A) \otimes \left(\frac{1}{3}(I + \sqrt{3}\hat{n}'.\vec{\lambda}^B)\right)$$

$$= \frac{1}{9}(I \otimes I + \sqrt{3}\vec{\lambda}^A.\hat{n} \otimes I + \sqrt{3}I \otimes \vec{\lambda}^B.\hat{n}' + \frac{3}{2}\sum_{i,j=1}^8 c_{ij}\lambda_i^A \otimes \lambda_j^B). \tag{6.71}$$

The (real) expansion coefficients in Eq.(6.71) are given by

$$n_{i} = \frac{\sqrt{3}}{2} tr(\rho^{AB} \lambda_{i} \otimes I)$$

$$n'_{j} = \frac{\sqrt{3}}{2} tr(\rho^{AB} I \otimes \lambda_{j})$$

$$c_{ij} = \frac{3}{2} tr(\rho^{AB} \lambda_{i} \otimes \lambda_{j}).$$
(6.72)

where n_i and n_j are components of unit vector \hat{n} and \hat{n}' of the two subsystems: $\rho_{3\times 3}^A$ and $\rho_{3\times 3}^B$

and i, j = 1, ..., 8. The coefficients c_{ij} form a 8×8 correlation matrix R.

The two qutrit density matrix shown in Eq.(6.71) can be also cast into the form as

$$\rho_{9\times9}^{AB} = \rho_{3\times3}^{A} \otimes \rho_{3\times3}^{B} = (\frac{1}{3}c_{\alpha}\lambda_{\alpha}) \otimes (\frac{1}{3}c_{\beta}\lambda_{\beta}) = \frac{1}{9}c_{\alpha\beta}\lambda_{\alpha} \otimes \lambda_{\beta}, \tag{6.73}$$

where the expansion coefficients are given by

$$c_{\alpha\beta} = \frac{9}{4} tr(\rho_{9\times9}^{AB} \lambda_{\alpha} \otimes \lambda_{\beta}). \tag{6.74}$$

 $\alpha, \beta = 0, ..., 8$ and normalization requires that $c_{00} = \frac{3}{2}$. Thus, Eq.(6.74) form a generalized matrix **GM** which is split into four components: a scalar of $\frac{3}{2}$, two eight-dimensional vectors, and a 8×8 correlation matrix R such that

$$\mathbf{GM} = \begin{bmatrix} \frac{3}{2} & c_{01} & \dots & c_{08} \\ \hline c_{10} & c_{11} & \dots & c_{18} \\ \vdots & \vdots & \dots & \vdots \\ \vdots & \vdots & \dots & \vdots \\ c_{80} & c_{81} & \dots & c_{88} \end{bmatrix}, \tag{6.75}$$

where $n_i = c_{i0}$ and $n_j = c_{0j}$ (i, j = 1, ..., 8) are the components of local unit Bloch vectors \hat{n} and \hat{n}' , respectively of the two single qutrit sub-systems $(\rho_{3\times3}^A \text{ and } \rho_{3\times3}^B)$, c_{ij} (i, j = 1, ..., 8) are the matrix elements of correlation matrix R. Therefore, according to the above Eq.(6.75), all possible combination of neutrinos two qutrits density matrix like $\rho_{9\times9}^{ee} = \rho_{3\times3}^e \otimes \rho_{3\times3}^e$, $\rho_{9\times9}^{e\mu} = \rho_{3\times3}^e \otimes \rho_{3\times3}^\mu$, $\rho_{9\times9}^{\mu\mu} = \rho_{3\times3}^\mu \otimes \rho_{3\times3}^\mu$, $\rho_{9\times9}^{\mu\mu} = \rho_{3\times3}^\mu \otimes \rho_{3\times3}^\mu$, etc., resembles a product or separable state.

In general, the entanglement measure generalized concurrence for the two qutrits mixed state density matrix $\rho_{9\times9}$ is defined as [201]

$$C_3(\rho_{9\times 9}) = \max\{0, 2\mu_1 - \sum_{i=1}^9 \mu_i\},$$
 (6.76)

where the μ_i (with i=1,2,...,9) are the square roots of the eigenvalues of the non-Hermitian matrix $\rho_{9\times9}\tilde{\rho}_{9\times9}$ in decreasing order. $\tilde{\rho}_{9\times9}$ is the spin-flip density matrix

$$\tilde{\rho}_{9\times 9} = (O_3 \otimes O_3) \rho^*_{9\times 9} (O_3 \otimes O_3), \tag{6.77}$$

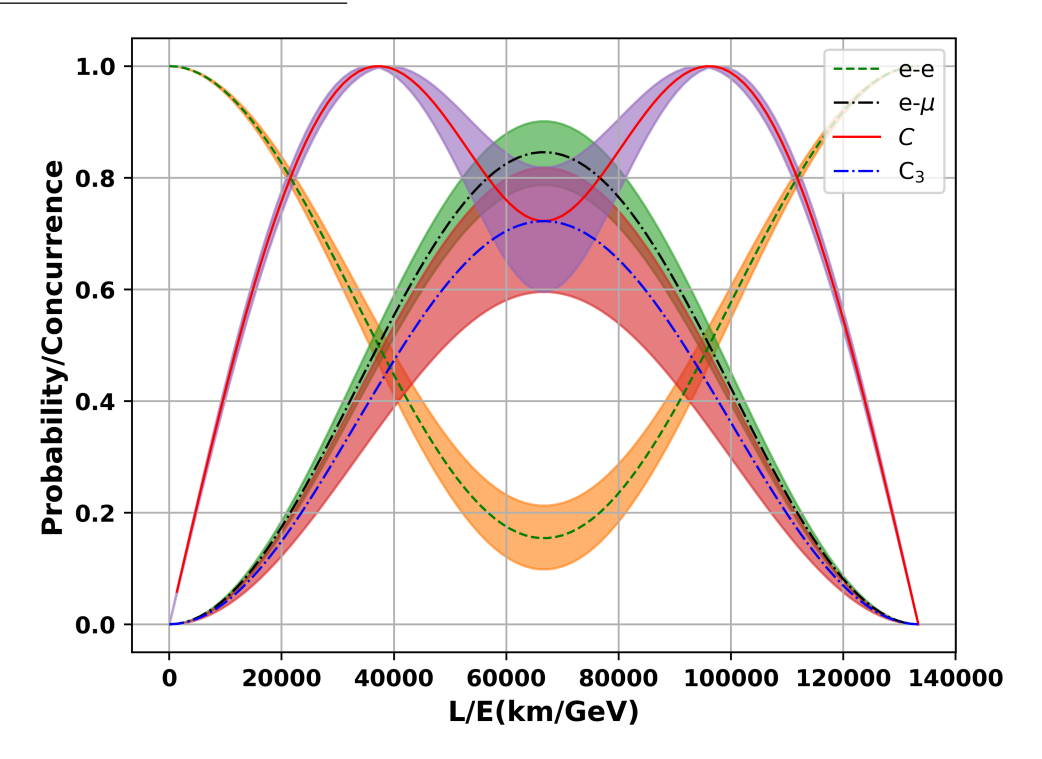


Figure 6.3: The violet band shows the ν_e concurrence $C(\rho^e(t))$ (Red, solid line) in the bipartite qubit system and the pink band shows the generalized concurrence $C_3(\rho_{f_{9\times 9}}^e)$ (Blue, dash dotted line) in the bi-partite qutrit system. Both entanglement measures are compared with the green band which shows the ν_e probability $P_{e\to e}$ (Black, dash dotted line) and with the orange band which shows the $P_{e\to\mu}$ probability (Green, dashed line), using the current experimental bounds of the 3σ range of neutrino parameters [197].

with $\rho^*_{9\times9}$ being the complex conjugate of $\rho_{9\times9}$ and O_3 is the transformation matrix for qutrits

$$O_3 = \begin{pmatrix} 0 & -i & i \\ i & 0 & -i \\ -i & i & 0 \end{pmatrix}. \tag{6.78}$$

Here, $O_3 \otimes O_3$ is analogous to the $\sigma_y \otimes \sigma_y$ in the two qubit system (see Eq.(2.34)). We find that the generalized concurrence for possible combination of two qutrits product state density matrix is zero i.e., $C_3(\rho_{9\times 9}^{ee}) = C_3(\rho_{9\times 9}^{e\mu}) = C_3(\rho_{9\times 9}^{\mu\mu}) = C_3(\rho_{9\times 9}^{\mu\nu}) = \dots = 0$.

Furthermore, to investigate two qutrits entanglement in neutrino oscillations, we study two flavour neutrino oscillations in the bi-partite qutrit system and quantify the generalized concurrence. We map the neutrino flavour state at t=0 to bi-partite qutrit states as $|\nu_e\rangle = |1\rangle \otimes |2\rangle$ and $|\nu_{\mu}\rangle = |2\rangle \otimes |1\rangle$. Then using Eq.(6.32), the normalized time evolved electron

flavour neutrino state in linear superposition of bi-partite qutrit neutrino flavour basis is

$$|\nu_e(\theta,\phi)\rangle_f = (\cos^2\theta + \sin^2\theta e^{-i\phi})|12\rangle + \sin\theta \cos\theta (1 - e^{-i\phi})|21\rangle, \qquad (6.79)$$

and its density matrix in the two qutrit standard basis $\{|11\rangle, |12\rangle, |13\rangle, |21\rangle, |22\rangle, |23\rangle, |31\rangle, |32\rangle, |33\rangle\}$ is

where, $a_1 = (\cos^2\theta + \sin^2\theta e^{-i\phi})$, and $b_1 = \sin\theta\cos\theta(1 - e^{-i\phi})$ are the coefficients of bi-partite qutrit flavor basis $|\nu_e\rangle$ and $|\nu_\mu\rangle$, respectively, and a_1^* , b_2^* are complex conjugate of a_1 and b_1 , respectively.

Using Eq.(6.80) in Eq.(6.77), we construct the spin-flip density matrix $\tilde{\rho}_{f_{9\times9}}^e = (O_3 \otimes O_3)\rho_{f_{9\times9}}^{*e}(O_3 \otimes O_3)$. We find that one of the square root of eigenvalues of the matrix $\rho_{f_{9\times9}}^e\tilde{\rho}_{f_{9\times9}}^e$ is non-zero, i.e., $\mu_1 = 4\cos\theta\sin\theta(\cos^2\theta - \sin^2\theta)\sin^2\frac{\phi}{2}$. Thus using Eq.(6.76), the generalized concurrence of the time evolved electron flavour neutrino state $|\nu_e(\theta,\phi)\rangle_f$ in the bi-partite qutrit system is quantified as

$$C_3(\rho_{f_{9\times 9}}^e) = 4\cos\theta\sin\theta(\cos^2\theta - \sin^2\theta)\sin^2\frac{\phi}{2}.$$
 (6.81)

In Fig.(6.3), the generalized concurrence $C_3(\rho_{f_{9\times 9}}^e)$ (see Eq.(6.81)) of the time evolved electron flavour neutrino state in the bi-partite qutrit system is compared with the concurrence $C(\rho^e(t))$ (see Eq.(5.9)) in the bi-partite qubit system. Thus, the nonzero value of the generalized concurrence $(C_3(\rho_{f_{9\times 9}}^e) \neq 0)$ shows that in the two neutrino systems, the time evolved neutrino flavour state is a bi-partite qutrit entangled state. Therefore, the plot results warrant a study of two qutrits entanglement in the three-flavour neutrino oscillation.

Chapter 7

Conclusion and Future work

7.1 Experimental consideration

The study presented in this thesis naturally prompts the question: What is a measurable characteristic experimental signal for genuine tri-partite entanglement in Neutrino interactions? Recently, the Daya-Bay experiment has analyzed the wave-packet model of neutrino oscillations to study quantum entanglement in neutrino systems. The coherent evolution of the electron neutrino state and subsequent decoherence has been the subject of a recent experimental paper [29]. Quantum coherence in experimentally observed neutrino oscillations, using the tools of quantum resource theory, has produced results for the longest distance over which quantumness has been experimentally determined for quantum particles other than photon [190]. Different neutrino oscillation experiments, including Daya-Bay, KamLAND, Minos, and T2K, have assessed Quantum coherence over large length scales. Coherence is related to the concurrence: bi-partite entanglement and tri-partite entanglement. In Fig. (7.1) and Fig. (7.2), we show the bi-partite entanglement measure- concurrence (see Eq. (5.9)) vary with ratio L/E changing for the short-range $\nu_e \to \nu_e$ and long-range $\nu_\mu \to \nu_\mu$ survival probabilities using the Daya Bay and Minos experimental data, respectively [211, 212]. Both experiments exhibited good agreement with the theoretical prediction. We compare the results of bi-partite entanglement with the experiment. We extend our calculation further to study both tri-partite entanglement and wave-packet approach in experimentally observed neutrino oscillations. Thus, it is of interest for future experiments to justify three-way entanglement in neutrino oscillations and see how to explore it further. Since quantum optical systems, unlike neutrino oscillations experiments, our work is interested in further exploring

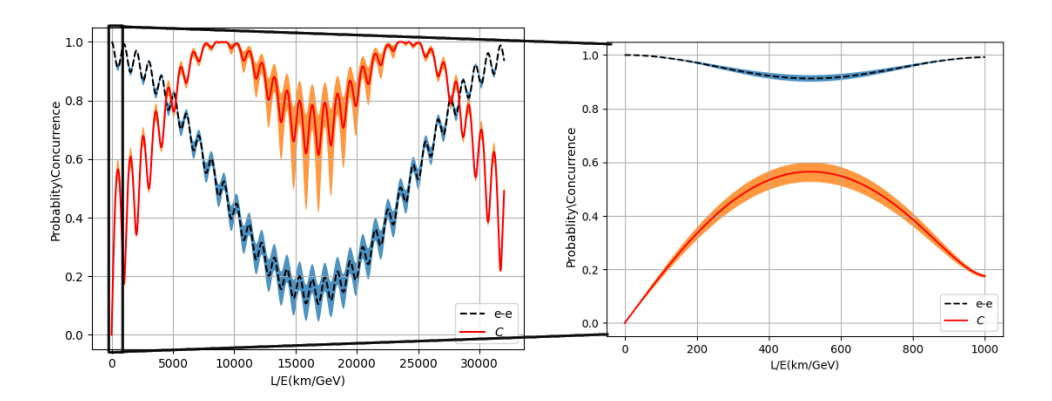


Figure 7.1: The blue band shows the short range ν_e disappearance probability (Black, dashed line) and the orange band shows concurrence (Red, solid line) in two flavour neutrino oscillations, using the Daya Bay experimental data [197,211].

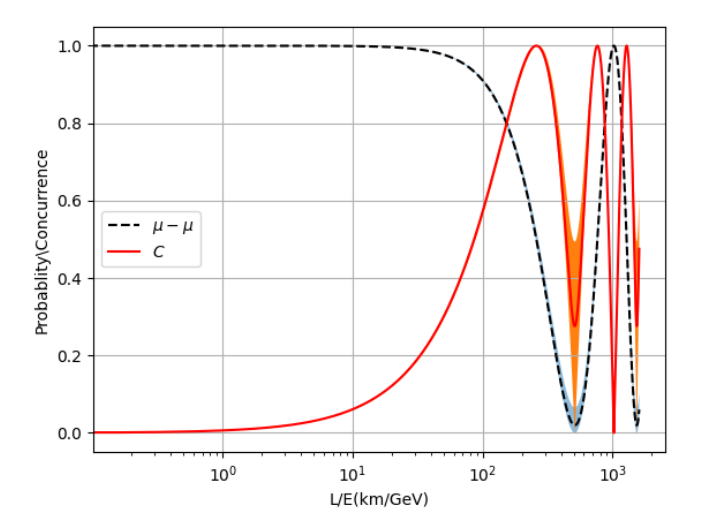


Figure 7.2: The blue band represents the long-range survival probability $\nu_{\mu} \rightarrow \nu_{\mu}$ (Black, dashed line) and it compared with orange band which gives concurrence (Red, solid line) in two flavour neutrino oscillations, using the Minos experimental data [197,212].

the characteristics of neutrino oscillation quantum entanglement.

7.2 Conclusion

In the introductory Chapter 1, we briefly reviewed the phenomenon of neutrino oscillations and discussed the derivation of neutrino flavour transition probabilities using the plane wave and wave packet picture. In Chapter 2, we have studied different types of entangled quantum systems, such as the two-qubit Bell's state and the three-qubit GHZ and W states, which are valuable resources for quantum information processing. We have also outlined various entanglement measures of bi-partite and tri-partite quantum systems.

In Chapter 3, we explored various bi-partite and tri-partite entanglement measures for neutrino flavour oscillations and compared our results with the two-qubit and three-qubit states used in quantum information theory. In the bi-partite quantum system, all quantum correlations like tangle, concurrence, and negativity are quantified in terms of neutrino survival and disappearance probabilities and coincide with the linear entropy (a lower approximation to the von Neumann entropy). The entanglement measures show that the $|\nu_e(t)\rangle$ is a bi-partite entangled pure state. We find that more substantial mixing leads to more entanglement. For the bi-partite two ν system, we see a laboratory analogue of a beam splitter placed at an angle representing the two neutrino systems. Neutrino mixing is akin to entanglement swapping in quantum optics systems. Moreover, we quantify tri-partite entanglement in the three neutrino systems in two ways: (a) in terms of measures of bi-partite entanglement and (b) genuine tri-partite entanglement. Both are related to neutrino transition probabilities. The three flavour neutrino oscillation satisfies the CKW inequality criterion and exhibits the property of the class of W-states, which are one of two different genuinely entangled tri-partite states. We can mimic the three neutrino systems by using a collection of beam splitters. This analogy helps study neutrino entanglement and understand new phenomena in quantum information theory.

In Chapter 4, we described quantum computing techniques to simulate the Bell's state, the GHZ-state and the W-state on an IBM quantum cloud computer. We have proposed quantum circuit concurrence for the two-qubit Bell's state and shown its simulation on IBMQ processors.

In Chapter 5, we find that in the bi-partite two neutrino system, the l_1 - norm of coherence and concurrence coincide. We use this information to study quantum coherence in the neutrino system based on the IBMQ platform. We have constructed a Bell-like superposition

quantum computer circuit for the time evolved electron and muon flavour neutrino state using the Universal quantum gate U(3), S-gate, Controlled-NOT and Pauli (X) gate. Using the spin-flipped $\sigma_y \otimes \sigma_y$ gate and Hadamard gate, we outline the simulation of concurrence in the two neutrino systems for the time evolved electron flavour neutrino state on a quantum simulator and quantum hardware of IBM. We discuss the implications of implementing bipartite entanglement in the two neutrino systems in a vacuum and the uniform matter background for the time evolved muon flavour neutrino state on IBMQ processors. The simulation results strongly suggested that the matter effects do not decohere the neutrinos much. In subsequent studies, we shall simulate the coherence of neutrinos propagating in a multi-layer medium with uniform or varying matter background on the IBMQ platform [213]. In future, the quantum algorithm presented in this chapter could also be helpful to study the matter effect with non-standard interaction (NSI) [214]. Moreover, the study of coherence distribution in the neutrino system using the quantum circuit of entanglement, which measures concurrence, would be of great interest to explore further on the IBMQ platform [215]. We hope that using quantum computing as a tool for future work in this could be helpful to learn more about this topic.

In general, the class of W state violates Mermin's inequality [187] and this result is simulated on the IBMQ processor in ref. [216,217]. In future, we shall construct the quantum circuit for the W state of neutrinos and show violation of Mermin's inequalities for three particle neutrino states on the IBMQ platform. Along these lines, we predict that we can execute a circuit to simulate tri-partite entanglement in neutrino oscillations on a quantum computer.

In chapter 6, we use the Pauli matrices to characterize the two-flavour neutrino oscillations on the Poincaré sphere $S^2 = SU(2)/U(1)$. The Poincaré vector of the time evolved flavour neutrino state lies on the unit sphere in the three-dimensional real vector space. This result helps us to characterize the two neutrino systems as qubits.

In the two-qubit systems, we have shown the Poincaré sphere representation of two neutrino system. We constructed a two-qubit density matrix of neutrinos based on the Dirac matrices. The coefficients of the Dirac matrices form the Bloch matrix, which shows that the two-qubit neutrino state is separable. We map the mass eigenstates of neutrinos directly to the bipartite qubit system. The resultant Bloch matrix construction shows that the bi-partite qubit neutrino state is entangled.

We use the Gell-Mann matrices to construct the Poincaré sphere $S^7 = SU(3)/U(2)$ in the three-flavour neutrino oscillation. The SU(3) result allows us to identify the three neutrino

system as qutrits which generalize the concept of entangled tri-partite states of neutrinos. We calculate the entropy of mixing $E(\rho_d^e)$ of the time evolved flavour neutrino mixed state in a single qutrit system using the current experimental bound on the neutrino oscillation parameters, and we find that the equi-mixing curves of $E(\rho_d^e)$ lie inside the qutrit triangle.

In the two-qutrit system, constructing a generalized Poincaré sphere using the Gell-Mann matrix tensor products led to the generalized Bloch matrix in the Bloch vector space of the three neutrino system. The quantification of the generalized concurrence in the two neutrino system implies that the two flavour neutrino oscillations are bi-partite qutrit entangled states. We have compared the generalized concurrence of the bi-partite qutrit neutrinos that of the bi-partite qubit neutrino. Both measures provide a qualitatively non zero amount of information in the two neutrino system. In a subsequent study, we shall examine two qutrit entanglement in the three neutrino system [218].

A quantum computer has done the quantum simulation of bi-partite qubit entanglement of two flavour neutrino oscillations. New studies claim that qutrits offer a promising path towards extending the frontier of quantum computers [219,220]. Our results lead us to a new direction of ternary computing using qutrits. We hope the results of this work will be helpful to explore neutrino oscillations on a qutrit quantum computer. Thus, in brief, neutrinos can be considered potential candidates for quantum information and quantum computing task.

7.3 Future work

Neutrino oscillations are a very subtle quantum phenomenon [221]. In the introductory Chapter 1 two assumptions were made when deriving the oscillation probability formula. The first was the plane wave approximation for neutrino wave functions; the second was that all the mass eigenstates have equal momentum and energy. Although they allow reaching the final result quickly and straightforwardly, there is no reason for these to hold in general. For pion decay, these requirements are not satisfied. Conceptual problems associated with such conditions are problematic. A plane wave describes the same momentum of neutrinos with a flat distribution probability found in any point of the space, which disagrees with the need for well-defined production and detection regions for the oscillations to occur. To handle such problems, a wave packet approach is mandatory, and a careful study of the coherence properties of the wave packet.

In Sec.(1.3), we have discussed about the coherence condition and coherence length (L^{Coh}) when the propagating neutrinos considered as a superposition of three Gaussian wave pack-

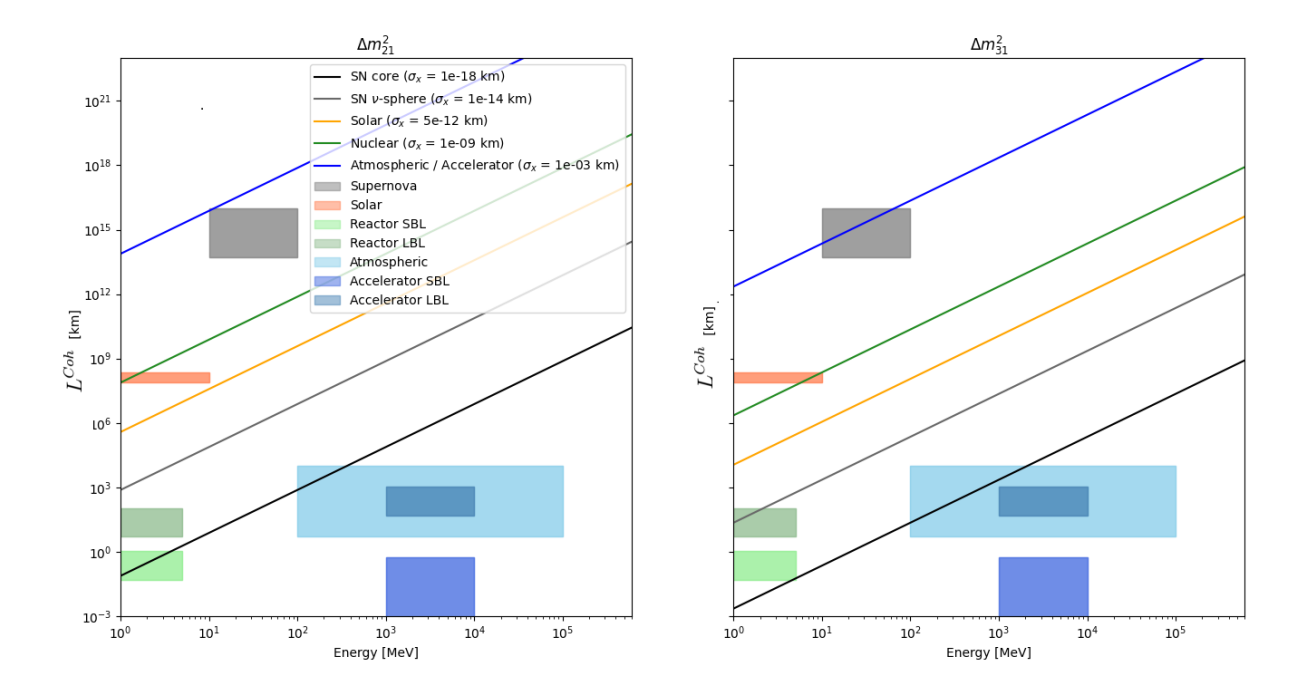


Figure 7.3: The Coherence length L^{Coh} (Km) vs Energy (MeV) graph is shown using the wave packet sizes σ_x from ref [197, 222].

ets, one for each mass eigenstate and where each mass eignstate have different momentum. The expression of neutrino flavour transition probabilities using the wave packet picture is given in Eq.(1.75) which can be re-written as

$$P_{\nu_{\alpha} \to \nu_{\beta}} \propto \sum_{jk} exp(-(L/L_{jk}^{Coh})^2) \times Osc. \text{ terms},$$

$$\text{where, } L_{jk}^{Coh} = \frac{4\sqrt{2}E^2}{\Delta m_{jk}^2} \sigma_x. \tag{7.1}$$

In Fig.(7.3), we estimate the propagation distance L^{Coh} at which the wave packets becomes separated. We use the wave packet sizes σ_x from ref. [222]. We observed from Fig.(7.3) that solar neutrino and supernova neutrino (SN) sources is decoherence relevant. In general, supernova neutrinos arrives at earth as an incoherent superposition of mass eigenstates [213]. Using the PMNS matrix Eq.(1.2) in the two neutrino system as $U(\theta) \equiv \begin{pmatrix} U_{e1} & U_{e2} \\ U_{\mu 1} & U_{\mu 2} \end{pmatrix} = \begin{pmatrix} \cos\theta & \sin\theta \\ -\sin\theta & \cos\theta \end{pmatrix}$, and putting it in Eq.(1.9), we find an expression for the probability for observing a ν_2 as ν_e , by assuming neutrinos do not travel through significant amounts of

Earth matter prior to detection as

$$P_{\nu_2 \to \nu_e} = |\langle \nu_e | \nu_2 \rangle|^2 = |\sum_{\alpha} \langle \nu_e | U_{\alpha 2} | \nu_\alpha \rangle|^2 = |U_{e2}|^2.$$
 (7.2)

Moreover, this probability expression can be modify if neutrinos travel the Earth before being detected. The flavour-to-flavour transition matrix for the evolution of neutrinos through layer with effective θ_m and Δm_m^2 is

$$\mathcal{U} = U_m \operatorname{diag}[\exp(i\frac{\Delta m_m^2 L_m}{2E}), 1] U_m^{\dagger}, \ U_m = \begin{pmatrix} \cos\theta_m & \sin\theta_m \\ -\sin\theta_m & \cos\theta_m \end{pmatrix}.$$
 (7.3)

We construct simple Earth with inner core as

$$\mathcal{U}^{Earth} = \mathcal{U}^m \mathcal{U}^c \mathcal{U}^m. \tag{7.4}$$

Therefore, the probability for observing a ν_2 as ν_e become

$$P_{\nu_2 \to \nu_e} = |\langle \nu_e | \nu_2 \rangle|^2 = |\sum_{\alpha} \sum_{\beta} \langle \nu_e | \mathcal{U}_{\alpha\beta}^{Earth} U_{\beta 2} | \nu_{\alpha} \rangle|^2 = |U_{e2} \mathcal{U}_{ee}^{Earth} + U_{\mu 2} \mathcal{U}_{e\mu}^{Earth}|^2, (7.5)$$

where in the above expression ν_2 need to rotate to flavour basis before plugging into \mathcal{U}^{Earth} . This probability expression is useful for studying neutrinos crossing the shock waves in supernova and for neutrinos propagating inside the earth in a multi-layer medium. Quantum studies of neutrino oscillations has been done on quantum computer in chapter 6. Recently, the complete protocol for quantum simulation of oscillations between 2^n arbitrarily mixed neutrinos with arbitrary masses, including CP-violation, has been examined on an n-qubit quantum computer [223]. Thus, it would be interesting to explore coherence/decoherence properties of supernova neutrinos using quantum computers in future.

Bibliography

- [1] W. Pauli, "Dear radioactive ladies and gentlemen," Phys. Today **31N9** (1978), 27, http://cdsweb.cern.ch/record/83282/files/meitner_0393. pdf https://doi.org/10.1063/1.2995181
- [2] Becquerel, H, "Sur les radiations invisibles mises par les corps phosphorescents," Comptes rendus de l'Acadmie des Sciences Paris 122 (1896) 501. http://cds.cern.ch/record/261888
- [3] Becquerel, H, "Sur quelques proprits nouvelles des radiations invisibles mises par divers corps phosphorescents," Comptes rendus de l'Acadmie des Sciences Paris 122 (1896) 559. https://www.academie-sciences.fr/pdf/dossiers/Becquerel_pdf/CR1896_p559.pdf
- [4] Becquerel, H, "Sur les radiations invisibles mises par les sels duranium," Comptes rendus de l Acadmie des Sciences Paris 122 (1896) 689.https://www.academie-sciences.fr/pdf/dossiers/Becquerel/Becquerel_pdf/CR1896_p689.pdf
- [5] Curie, M, "Rayons mis par les composes de luranium et du thorium," Comptes rendus de l Acadmie des Sciences Paris 126 (1898) 1101-1103. https://www.academie-sciences.fr/archivage_site/activite/archive/dossiers/Curie/Curie_pdf/CR1898_p1101.pdf

[6] J. Chadwick, "Possible Existence of a Neutron," Nature 129 (1932) 312. https://doi.org/10.1038/129312a0

- [7] C. D. Ellis, W. A. Wooster, "The average energy of disintegration of radium E," Proceedings of the Royal Society of London A: Mathematical, Physical and Engineering Sciences 117 (1927) no. 776, 109-123, https://doi.org/10.1098/rspa.1927.0168.
- [8] W. Pauli, "On the Earlier and more recent history of the neutrino," Cambridge Monogr. Part. Phys. Nucl. Phys. Cosmol. 14 (2000) 1-22. https://doi.org/ 10.1007/978-3-662-02994-7_22
- [9] E. Fermi, "An attempt of a theory of beta radiation," Z. Phys. 88 (1934) 161-177. https://doi.org/10.1007/BF01351864
- [10] F. Reines, C. L. Cowan, F. B. Harrison, A. D. McGuire, and H. W. Kruse, "Detection of the Free Antineutrino," Phys. Rev. 117 (1960) 159-173. https://doi.org/10.1103/PhysRev.117.159
- [11] B. Pontecorvo, "Mesonium and anti-mesonium," Sov. Phys. JETP 6 (1957), 429. https://www.osti.gov/biblio/4344536
- [12] B. Pontecorvo, "Inverse beta processes and nonconservation of lepton charge," Zh. Eksp. Teor. Fiz. **34** (1957), 247. https://www.osti.gov/biblio/4349231
- [13] M. Gell-Mann and A. Pais, "Behavior of neutral particles under charge conjugation," Phys. Rev. 97 (1955), 1387-1389. https://doi.org/10.1103/PhysRev. 97.1387
- [14] B. Pontecorvo, "Electron and Muon Neutrinos," Zh. Eksp. Teor. Fiz. **37** (1959), 1751-1757. https://inspirehep.net/authors/1020083
- [15] G. Danby, J. M. Gaillard, K. A. Goulianos, L. M. Lederman, N. B. Mistry, M. Schwartz and J. Steinberger, "Observation of High-Energy Neutrino Reactions and the Existence of Two Kinds of Neutrinos," Phys. Rev. Lett. 9 (1962), 36-44. https://doi.org/10.1103/PhysRevLett.9.36
- [16] Z. Maki, M. Nakagawa and S. Sakata, "Remarks on the unified model of elementary particles," Prog. Theor. Phys. 28 (1962), 870-880. https://doi.org/10.1143/PTP.28.870

[17] B. T. Cleveland, T. Daily, R. Davis, Jr., J. R. Distel, K. Lande, C. K. Lee, P. S. Wildenhain and J. Ullman, "Measurement of the solar electron neutrino flux with the Homestake chlorine detector," Astrophys. J. 496 (1998), 505-526. https://doi.org/10.1086/305343

- [18] B. Pontecorvo, "Neutrino Experiments and the Problem of Conservation of Leptonic Charge," Zh. Eksp. Teor. Fiz. 53 (1967), 1717-1725. http://www. jetp.ras.ru/cgi-bin/dn/e_026_05_0984.pdf
- [19] V. N. Gribov and B. Pontecorvo, "Neutrino astronomy and lepton charge," Phys. Lett. B 28 (1969), 493. https://doi.org/10.1016/0370-2693(69) 90525-5
- [20] K. Kodama et al. [DONUT], "Observation of tau neutrino interactions," Phys. Lett. B 504 (2001), 218-224. https://doi.org/10.1016/S0370-2693(01) 00307-0
- [21] Kamiokande, K.S. Hirata et al., "Observation of ⁸B solar neutrinos in the Kamiokande-II detector," Phys. Rev. Lett. 63 (1989) 16. https://doi.org/ 10.1103/PhysRevLett.63.16
- [22] Kamiokande, Y. Fukuda et al., "Solar Neutrino Data Covering Solar Cycle 22," Phys. Rev. Lett. 77 (1996) 1683. https://doi.org/10.1103/PhysRevLett. 77.1683
- [23] S. Fukuda *et al.* [Super-Kamiokande], "Determination of solar neutrino oscillation parameters using 1496 days of Super-Kamiokande I data," Phys. Lett. B **539** (2002), 179-187. https://doi.org/10.1016/S0370-2693(02)02090-7
- [24] KamLAND, T. Araki et al., "Measurement of Neutrino Oscillation with Kam-LAND: Evidence of Spectral Distortion," Phys. Rev. Lett. 94 (2005) 081801. https://doi.org/10.1103/PhysRevLett.94.081801
- [25] Q. R. Ahmad *et al.* [SNO], "Measurement of the rate of $\nu_e + d \rightarrow p + p + e^-$ interactions produced by ⁸B solar neutrinos at the Sudbury Neutrino Observatory," Phys. Rev. Lett. **87** (2001), 071301. https://doi.org/10.1103/PhysRevLett. 87.071301
- [26] Q. R. Ahmad *et al.* [SNO], "Direct evidence for neutrino flavor transformation from neutral current interactions in the Sudbury Neutrino Observatory," Phys.

- Rev. Lett. **89** (2002), 011301. https://doi.org/10.1103/PhysRevLett.89. 011301
- [27] E. K. Akhmedov and A. Y. Smirnov, "Paradoxes of neutrino oscillations," Phys. Atom. Nucl. 72 (2009), 1363-1381. https://doi.org/10.1134/S1063778809080122
- [28] Boris Kayser, "On the quantum mechanics of neutrino oscillation," Phys. Rev. D 24, 110 (1981). https://doi.org/10.1103/PhysRevD.24.110
- [29] F. P. An *et al.* [Daya Bay Collaboration], "Study of the wave packet treatment of neutrino oscillation at Daya Bay," Eur. Phys. J. C **77** (2017) no.9, 606. https://doi.org/10.1140/epjc/s10052-017-4970-y
- [30] Y. L. Chan, M. C. Chu, K. M. Tsui, C. F. Wong and J. Xu, "Wave-packet treatment of reactor neutrino oscillation experiments and its implications on determining the neutrino mass hierarchy," Eur. Phys. J. C 76 (2016) no.6, 310. https://doi.org/10.1140/epjc/s10052-016-4143-4
- [31] W. Grimus and P. Stockinger, "Real oscillations of virtual neutrinos," Phys. Rev. D 54 (1996), 3414-3419. https://doi.org/10.1103/PhysRevD.54.3414
- [32] W. Grimus, P. Stockinger and S. Mohanty, "The Field theoretical approach to coherence in neutrino oscillations," Phys. Rev. D 59 (1999), 013011. https://doi.org/10.1103/PhysRevD.59.013011
- [33] M. Beuthe, "Oscillations of neutrinos and mesons in quantum field theory," Phys. Rept. 375 (2003), 105-218. https://doi.org/10.1016/S0370-1573% 2802%2900538-0
- [34] E. K. Akhmedov and J. Kopp, "Neutrino Oscillations: Quantum Mechanics vs. Quantum Field Theory," JHEP 04 (2010), 008 [erratum: JHEP 10 (2013), 052]. https://doi.org/10.1007/JHEP04%282010%29008
- [35] Yong. Cheng. Ou and Heng. Fan, "Monogamy inequality in terms of negativity for three-qubit states," Phys. Rev. A 75, no.6, 062308 (2007). https://doi. org/10.1103/PhysRevA.75.062308
- [36] Xing-Ri Jin, Xin Ji, Ying-Qiao Zhang, Shou Zhang, Suc-Kyoung Hong, Kyu-Hwang Yeon, Chung-In Um, "Three-party quantum secure direct communication based on GHZ states," Phys. Lett. A 354, 67 (2006). https://doi.org/10.1016/j.physleta.2006.01.035

[37] B. K. Behera, A. Banerjee, P.K. Panigrahi, "Experimental realization of quantum cheque using a five-qubit quantum computer," Quantum Inf Process 16, 312 (2017). https://doi.org/10.1007/s11128-017-1762-0

- [38] Jiu-Cang Hao, Chuan-Feng Li, and Guang-Can Guo, "Controlled dense coding using the Greenberger-Horne-Zeilinger state," Phys. Rev. A 63, 054301 (2001). https://doi.org/10.1103/PhysRevA.63.054301
- [39] Jaewoo Joo1, Young-Jai Park, Sangchul Oh and Jaewan Kim, "Quantum teleportation via a W state," New J. Phys. 5 136 (2003). https://doi.org/10. 1088/1367-2630/5/1/136
- [40] Wang Jian1, Zhang Quan1 and Tang Chao-Jing1, "Quantum Secure Communication Scheme with W State," Commun. Theor. Phys. 48 637 (2007). https://doi.org/10.1088/0253-6102/48/4/013
- [41] Dagmar Bruß, David P. DiVincenzo, Artur Ekert, Christopher A. Fuchs, Chiara Macchiavello, and John A. Smolin, "Optimal universal and state-dependent quantum cloning," Phys. Rev. A 57, 2368 (1998). https://doi.org/10.1103/ PhysRevA.57.2368
- [42] M. Blasone, F. Dell'Anno, S. De Siena and F. Illuminati, "Entanglement in neutrino oscillations," EPL 85, 50002 (2009). https://doi.org/10.1209/ 0295-5075/85/50002
- [43] A. K. Alok, S. Banerjee and S. U. Sankar, "Quantum correlations in terms of neutrino oscillation probabilities," Nucl. Phys. B **909**, 65 (2016). https://doi.org/10.1016/j.nuclphysb.2016.05.001
- [44] IBM Quantum Experience. http://www.research.ibm.com/ibm-q/
- [45] Nielsen, M., and Chuang, I.L., "Quantum Computation and Quantum Information," 10th Anniversary Edition. Cambridge: Cambridge University Press (2010). https://doi.org/10.1017/CB09780511976667
- [46] C. A. Argüelles and B. J. P. Jones, "Neutrino Oscillations in a Quantum Processor," Phys. Rev. Research. 1 (2019), 033176. https://doi.org/10.1103/PhysRevResearch.1.033176
- [47] Carlton M. Caves and Gerard J. Milburn, "Qutrit entanglement," Optics Communications, Volume 179, Issue 1-6, p.439-446 (2000).https://doi.org/10.1016/S0030-4018(99)00693-8

[48] S. Eliezer and A. R. Swift, "Experimental Consequences of electron Neutrino-Muon-neutrino Mixing in Neutrino Beams," Nucl. Phys. B 105 (1976), 45-51. https://doi.org/10.1016/0550-3213(76)90059-6

- [49] H. Fritsch, P. Minkowski, "Vectorlike weak currents, massive neutrinos, and neutrino beam oscillations," Physics Letters B, Volume 62, Issue 1, 1976, Pages 72-76, ISSN 0370-2693, https://doi.org/10.1016/0370-2693(76)90051-4.
- [50] S. M. Bilenky and B. Pontecorvo, "Lepton Mixing and Neutrino Oscillations," Phys. Rept. 41 (1978), 225-261. https://doi.org/10.1016/0370-1573(78) 90095-9
- [51] S. M. Bilenky, "The History of neutrino oscillations," Phys. Scripta T 121, 17 (2005). https://doi.org/10.1088/0031-8949/2005/T121/001
- [52] C. Giganti, S. Lavignac and M. Zito, "Neutrino oscillations: the rise of the PMNS paradigm," Prog. Part. Nucl. Phys. 98, 1 (2018). https://doi.org/ 10.1016/j.ppnp.2017.10.001
- [53] M. C. Gonzalez-Garcia, M. Maltoni and T. Schwetz, "Updated fit to three neutrino mixing: status of leptonic CP violation," JHEP 1411 (2014) 052. https://doi.org/10.1007/JHEP11(2014)052
- [54] I. Esteban, M. C. Gonzalez-Garcia, A. Hernandez-Cabezudo, M. Maltoni and T. Schwetz, "Global analysis of three-flavour neutrino oscillations: synergies and tensions in the determination of θ_{23} , δ_{CP} , and the mass ordering," JHEP 1901, 106 (2019). https://doi.org/10.1007/JHEP01(2019)106
- [55] L. Wolfenstein, "Neutrino Oscillations in Matter," Phys. Rev. D 17 (1978), 2369-2374. https://doi.org/10.1103/PhysRevD.17.2369
- [56] V. Barger, K. Whisnant, S. Pakvasa, and R. J. N. Phillips, "Matter effects on three-neutrino oscillations," Phys. Rev. D 22, 2718(1980). https://doi.org/ 10.1103/PhysRevD.22.2718
- [57] M. Blennow and A. Y. Smirnov, "Neutrino propagation in matter," Adv. High Energy Phys. **2013** (2013), 972485. https://doi.org/10.1155/2013/972485
- [58] S. P. Mikheyev and A. Y. Smirnov, "Resonance Amplification of Oscillations in Matter and Spectroscopy of Solar Neutrinos," Sov. J. Nucl. Phys. 42 (1985), 913-917. https://inspirehep.net/literature/1620788

[59] Mikheyev, S.P., Smirnov, A.Y. "Resonant amplification of ν_e oscillations in matter and solar-neutrino spectroscopy," Il Nuovo Cimento C **9**, 17–26 (1986). https://doi.org/10.1007/BF02508049

- [60] H. A. Bethe, "A Possible Explanation of the Solar Neutrino Puzzle," Phys. Rev. Lett. 56 (1986), 1305. https://doi.org/10.1103/PhysRevLett.56.1305
- [61] A. Y. Smirnov, "The Mikheyev-Smirnov-Wolfenstein (MSW) Effect," https://doi.org/10.48550/arXiv.1901.11473
- [62] R.G. Winter, "Neutrino oscillation kinematics," Lett. Nuovo Cimento 30, 101–104 (1981), https://doi.org/10.1007/BF02817319
- [63] C. Giunti and C. W. Kim, Fundamentals of neutrino physics and astrophysics. Oxford; New York: Oxford University Press, 2007. http://dx.doi.org/10. 1093/acprof:oso/9780198508717.001.0001
- [64] S. Nussinov, "Solar Neutrinos and Neutrino Mixing," Phys. Lett. B 63 (1976),201-203. https://doi.org/10.1016/0370-2693(76)90648-1
- [65] K. Kiers, S. Nussinov and N. Weiss, "Coherence effects in neutrino oscillations," Phys. Rev. D 53 (1996), 537-547. https://doi.org/10.1103/PhysRevD.53. 537
- [66] C. Giunti and C. W. Kim, "Coherence of neutrino oscillations in the wave packet approach," Phys. Rev. D 58 (1998), 017301. https://doi.org/10. 1103/PhysRevD.58.017301
- [67] C. Giunti, "Coherence and wave packets in neutrino oscillations," Found. Phys. Lett. 17 (2004), 103-124. https://doi.org/10.1023/B:FOPL.0000019651. 53280.31
- [68] A. Peres, "Separability criterion for density matrices," Phys. Rev. Lett. 77 (1996), 1413-1415. https://doi.org/10.1103/PhysRevLett.77.1413
- [69] M. Horodecki, P. Horodecki and R. Horodecki, "On the necessary and sufficient conditions for separability of mixed quantum states," Phys. Lett. A 223 (1996), 1. https://doi.org/10.1016/S0375-9601(96)00706-2
- [70] W. K. Wootters, "Entanglement of formation of an arbitrary state of two qubits," Phys. Rev. Lett. 80, 2245 (1998). https://doi.org/10.1103/ PhysRevLett.80.2245

[71] M. B. Plenio and S. Virmani, "An Introduction to entanglement measures," Quant. Inf. Comput. 7 (2007), 1-51. https://doi.org/10.48550/arXiv.quant-ph/0504163

- [72] V. Coffman, J. Kundu and W. K. Wootters, "Distributed entanglement," Phys. Rev. A 61, 052306 (2000). https://doi.org/10.1103/PhysRevA.61.052306
- [73] T. Baumgratz, M. Cramer, M. B. Plenio, "Quantifying Coherence," Phys. Rev. Lett. 113, 140401 (2014), doi:10.1103/PhysRevLett.113.140401. https://doi. org/10.1103/PhysRevLett.113.140401
- [74] A. Einstein, B. Podolsky, and N. Rosen, "Can Quantum-Mechanical Description of Physical Reality Be Considered Complete?," Phys. Rev. 47, 777 (1935). https://doi.org/10.1103/PhysRev.47.777
- [75] E.Schrodinger, "Probability relations between separated systems," Mathematical Proceedings of the Cambridge Philosophical Society, 32(3), 446-452 (1936). https://doi.org/10.1017/S0305004100019137
- [76] J. S. Bell, "On the Einstein Podolsky Rosen paradox," Physics Physique Fizika 1, 195 (1964). https://doi.org/10.1103/PhysicsPhysiqueFizika.1.195
- [77] Alain Aspect, Philippe Grangier, and Gerard Roger, "Experimental Tests of Realistic Local Theories via Bell's Theorem," Phys. Rev. Lett. 47, 460 (1981). https://doi.org/10.1103/PhysRevLett.47.460
- [78] F.F. Fanchini, D. de Oliveira Soares Pinto, G. Adesso, "Lectures on General Quantum Correlations and Their Applications," (Springer, Berlin, 2017). http://dx.doi.org/10.1007/978-3-319-53412-1
- [79] R. Horodecki, P. Horodecki, M. Horodecki and K. Horodecki, "Quantum entanglement," Rev. Mod. Phys. 81 (2009), 865-942. https://doi.org/10.1103/RevModPhys.81.865
- [80] Otfried Gühne, Geza Toth, "Entanglement detection," Physics Reports 474, 1 (2009), doi:10.1016/j.physrep.2009.02.004. https://doi.org/10.1016/j. physrep.2009.02.004
- [81] C. H. Bennett, D. P. DiVincenzo, J. A. Smolin and W. K. Wootters, "Mixed state entanglement and quantum error correction," Phys. Rev. A

- **54** (1996), 3824-3851 doi:10.1103/PhysRevA.54.3824. https://doi.org/10.1103/PhysRevA.54.3824
- [82] S. Hill and W. K. Wootters, "Entanglement of a pair of quantum bits," Phys. Rev. Lett. 78 (1997), 5022-5025. https://doi.org/10.1103/PhysRevLett. 78.5022
- [83] G. Vidal and R. F. Werner, "Computable measure of entanglement," Phys. Rev. A 65 (2002) 032314. https://doi.org/10.1103/PhysRevA.65.032314
- [84] Nicholas A. Peters, Tzu-Chieh Wei, Paul G. Kwiat, "Mixed state sensitivity of several quantum information benchmarks," Phys. Rev. A 70 052309, (2005). https://doi.org/10.1103/PhysRevA.70.052309
- [85] L. Amico, R. Fazio, A. Osterloh and V. Vedral, "Entanglement in many-body systems," Rev. Mod. Phys. 80 (2008), 517-576. https://doi.org/10.1103/ /RevModPhys.80.517
- [86] R.Raussendorf and H.J. Briegel, "A One-Way Quantum Computer," Phys.Rev.Lett. 86, 5188 (2001). https://doi.org/10.1103/PhysRevLett. 86.5188
- [87] V. Vedral, M. B. Plenio, M. A. Rippin and P. L. Knight, "Quantifying entanglement," Phys. Rev. Lett. 78 (1997), 2275-2279. https://doi.org/10.1103/PhysRevLett.78.2275
- [88] G. Weihs, T. Jennewein, C. Simon, H. Weinfurter and A. Zeilinger, "Violation of Bell's inequality under strict Einstein locality conditions," Phys. Rev. Lett. 81 (1998), 5039-5043. https://doi.org/10.1103/PhysRevLett.81.5039
- [89] DARIUSZ KURZYK, "Introduction to Quantum entanglement," Theoretic and Applied Informatics **24**, IISN 1896-5334, Vol.**24**(2020),no.2,pp.135-150. http://dx.doi.org/10.2478/v10179-012-0010-7
- [90] K. Zyczkowski, P. Horodecki, A. Sanpera and M. Lewenstein, "On the volume of the set of mixed entangled states," Phys. Rev. A 58 (1998) 883. https: //doi.org/10.1103/PhysRevA.58.883
- [91] M. Horodecki, P. Horodecki and R. Horodecki, "Mixed state entanglement and distillation: Is there a 'bound' entanglement in nature?," Phys. Rev. Lett. 80 (1998) 5239. https://doi.org/10.1103/PhysRevLett.80.5239

[92] W. Dur, G. Vidal and J. I. Cirac, "Three qubits can be entangled in two inequivalent ways," Phys. Rev. A 62 (2000) 062314. https://doi.org/10. 1103/PhysRevA.62.062314

- [93] George Svetlichny, "Distinguishing three-body from two-body non separability by a Bell-type inequality," Phys. Rev. D 35, 3066 (1987). https://doi.org/ 10.1103/PhysRevD.35.3066
- [94] Greenberger, D.M., Horne, M.A., Zeilinger, A. (1989). Going Beyond Bell's Theorem. In: Kafatos, M. (eds) Bell's Theorem, Quantum Theory and Conceptions of the Universe. Fundamental Theories of Physics, vol 37. Springer, Dordrecht. https://doi.org/10.1007/978-94-017-0849-4_10
- [95] A. Acin, D. Bruss, M. Lewenstein, A. Sanpera, "Classification of mixed three-qubit states," Phys. Rev. Lett. 87, 040401 (2001). https://doi.org/10.1103/PhysRevLett.87.040401
- [96] W. Dur, J. I. Cirac and R. Tarrach, "Separability and distillability of multiparticle quantum systems," Phys. Rev. Lett. 83 (1999), 3562-3565. https://doi.org/10.1103/PhysRevLett.83.3562
- [97] Tobias J. Osborne and Frank Verstraete, "General Monogamy Inequality for Bipartite Qubit Entanglement," Phys. Rev. Lett. 96, 220503 (2006). https://doi.org/10.1103/PhysRevLett.96.220503
- [98] Kai Chen, Sergio Albeverio, and Shao-Ming Fei, Phys. Rev. Lett. 95, 040504, "Concurrence of Arbitrary Dimensional Bipartite Quantum States," https://doi.org/10.1103/PhysRevLett.95.040504
- [99] B. Kayser, "Neutrino Oscillation Physics,". https://doi.org/10.48550/ arXiv.1206.4325
- [100] F. P. An et al. [Daya Bay Collaboration], "Observation of electron-antineutrino disappearance at Daya Bay," Phys. Rev. Lett. 108, 171803 (2012). https://doi.org/10.1103/PhysRevLett.108.171803
- [101] P. Adamson *et al.* [MINOS Collaboration], "Improved search for muon-neutrino to electron-neutrino oscillations in MINOS," Phys. Rev. Lett. **107**, 181802 (2011). https://doi.org/10.1103/PhysRevLett.107.181802

[102] K. Abe et al. [T2K Collaboration], "Indication of Electron Neutrino Appearance from an Accelerator-produced Off-axis Muon Neutrino Beam," Phys. Rev. Lett. 107, 041801 (2011). https://doi.org/10.1103/PhysRevLett.107.041801

- [103] P. Adamson et al. (NOvA Collaboration), "First measurement of muon-neutrino disappearance in NOvA," Phys. Rev. D 93, 051104(R) (2016). https://doi. org/10.1103/PhysRevD.93.051104
- [104] Qiao, et al. "Entanglement activation from quantum coherence and superposition" Phys. Rev. Lett. 98, 052351 (2018). https://doi.org/10.1103/ PhysRevA.98.052351
- [105] A. Streltsov, G. Adesso and M. B. Plenio, "Quantum Coherence as a Resource," Rev. Mod. Phys. 89, no. 4, 041003 (2017). https://doi.org/10.1103/RevModPhys.89.041003
- [106] M. Blasone, F. Dell'Anno, S. De Siena, M. Di Mauro and F. Illuminati, "Multipartite entangled states in particle mixing," Phys. Rev. D 77, 096002 (2008). https://doi.org/10.1103/PhysRevD.77.096002
- [107] M. Blasone, F. Dell'Anno, S. De Siena and F. Illuminati, "On entanglement in neutrino mixing and oscillations," J. Phys. Conf. Ser. 237, 012007 (2010). https://doi.org/10.1088/1742-6596/237/1/012007
- [108] M. Blasone, F. Dell'Anno, S. De Siena and F. Illuminati, "A field-theoretical approach to entanglement in neutrino mixing and oscillations," EPL **106**, no. 3, 30002 (2014) doi:10.1209/0295-5075/106/30002 [arXiv:1401.7793 [quant-ph]].
- [109] M. Blasone, F. Dell'Anno, S. De Siena and F. Illuminati, "Flavor entanglement in neutrino oscillations in the wave packet description," EPL 112 (2015) no.2, 2007. https://doi.org/10.1209/0295-5075/106/30002
- [110] E. Lisi, A. Marrone and D. Montanino, "Probing possible decoherence effects in atmospheric neutrino oscillations," Phys. Rev. Lett. 85 (2000), 1166-1169. https://doi.org/10.1103/PhysRevLett.85.1166
- [111] G. L. Fogli, E. Lisi, A. Marrone and D. Montanino, "Status of atmospheric nu(mu) —> nu(tau) oscillations and decoherence after the first K2K spectral data," Phys. Rev. D 67 (2003), 093006. https://doi.org/10.1103/PhysRevD.67.093006

[112] G. Di Molfetta and A. Pérez, "Quantum walks as simulators of neutrino oscillations in a vacuum and matter," New J. Phys. 18 (2016) no.10, 103038. https://doi.org/10.1088/1367-2630/18/10/103038

- [113] S. Banerjee, A. K. Alok, R. Srikanth and B. C. Hiesmayr, "A quantum information theoretic analysis of three flavor neutrino oscillations," Eur. Phys. J. C 75, no. 10, 487 (2015). https://doi.org/10.1140/epjc/s10052-015-3717-x
- [114] N. F. Bell, A. A. Rawlinson and R. F. Sawyer, "Speedup through entanglement: Many body effects in neutrino processes," Phys. Lett. B **573** (2003), 86-93. https://doi.org/10.1016/j.physletb.2003.08.035
- [115] A. Friedland and C. Lunardini, "Neutrino flavor conversion in a neutrino background: Single particle versus multiparticle description," Phys. Rev. D 68 (2003), 013007. https://doi.org/10.1103/PhysRevD.68.013007
- [116] A. Friedland and C. Lunardini, "Do many particle neutrino interactions cause a novel coherent effect?," JHEP 10 (2003), 043. https://doi.org/10.1088/ 1126-6708/2003/10/043
- [117] S. Birol, Y. Pehlivan, A. B. Balantekin and T. Kajino, "Neutrino Spectral Split in the Exact Many Body Formalism," Phys. Rev. D 98 (2018) no.8, 083002. https://doi.org/10.1103/PhysRevD.98.083002
- [118] A. V. Patwardhan, M. J. Cervia and A. Baha Balantekin, "Eigenvalues and eigenstates of the many-body collective neutrino oscillation problem," Phys. Rev. D 99 (2019) no.12, 123013. https://doi.org/10.1103/PhysRevD.99. 123013
- [119] E. Rrapaj, "Exact solution of multiangle quantum many-body collective neutrino-flavor oscillations," Phys. Rev. C **101** (2020) no.6, 065805. https://doi.org/10.1103/PhysRevC.101.065805
- [120] M. J. Cervia, A. V. Patwardhan, A. B. Balantekin, ‡. S. N. Coppersmith and C. W. Johnson, "Entanglement and collective flavor oscillations in a dense neutrino gas," Phys. Rev. D 100 (2019) no.8, 083001. https://doi.org/10. 1103/PhysRevD.100.083001
- [121] F. Ming, X.-K. Song, J. Ling, L. Ye, D. Wang, "Quantification of quantumness in neutrino oscillations," Eur. Phys. J. C 80, 275 (2020). https://doi.org/ 10.1140/epjc/s10052-020-7840-y

[122] M. Blasone, S.De Siena, and C.Matrella, "Wave packet approach to quantum correlations in neutrino oscillations," Eur. Phys. J. C 81, 660 (2021). https://doi.org/10.1140/epjc/s10052-021-09471-4

- [123] Li-Juan Li, Fei Ming, Xue-Ke Song, Liu Ye, Dong Wang, "Characterizing entanglement and measurement's uncertainty in neutrino oscillations," Eur. Phys. J. C 81, 728 (2021). https://doi.org/10.1140/epjc/s10052-021-09503-z
- [124] A. J. Leggett and A. Garg, "Quantum Mechanics versus Macroscopic Realism: Is the Flux There When Nobody Looks?," Phys. Rev. Lett. **54**, 857 (1985). https://doi.org/10.1103/PhysRevLett.54.857
- [125] J. A. Formaggio, D. I. Kaiser, M. M. Murskyj and T. E. Weiss, "Violation of the Leggett-Garg Inequality in Neutrino Oscillations," Phys. Rev. Lett. 117 (2016) no.5, 050402. https://doi.org/10.1103/PhysRevLett.117.050402
- [126] J.Naikoo, et al. "A quantum information theoretic quantity sensitive to the neutrino mass-hierarchy," Nucl. Phys. B **951**, 114872 (2020). https://doi.org/10.1016/j.nuclphysb.2019.114872
- [127] J. Naikoo, A. Kumar Alok, S. Banerjee and S. Uma Sankar, "Leggett-Garg inequality in the context of three flavour neutrino oscillation," Phys. Rev. D 99 (2019) no.9, 095001. https://doi.org/10.1103/PhysRevD.99.095001
- [128] S. Shafaq and P. Mehta, "Enhanced violation of Leggett-Garg inequality in three flavour neutrino oscillations via non-standard interactions," J. Phys. G 48 (2021) no.8, 085002. https://doi.org/10.1088/1361-6471/abff0d
- [129] M. S Kim., W. Son., V. Bužek, P. L. Knight "Entanglement by a beam splitter: Nonclassicality as a prerequisite for entanglement," Phys. Rev. A 65 (2002) 032323, https://doi.org/10.1103/PhysRevA.65.032323
- [130] G. S. Agarwal and J. Banerji, "Entanglement by linear SU(2) transformations: generation and evolution of quantum vortex states," Journal of Physics A Mathematical general Vol.(39), 2006, https://doi.org/10.1088/0305-4470/39/37/011
- [131] Manfred. Eibl, Nikolai. Kiesel, Mohamed. Bourennane, Christian. Kurtisefer, Harald. Weinfurter, "Experimental Realization of a Three-Qubit Entangled W State," Phy. Rev. Lett. 92, 077901, (2004). https://doi.org/10.1103/ PhysRevLett.92.077901

[132] Pan. J. W., Bouwmeester, D., Daniell, M., Weinfurter, H., and Zeilinger, A. (2000). "Experimental test of quantum nonlocality in three-photon Greenberger-Horne-Zeilinger entanglement," Nature, **403** (6769), 515-519. https://doi.org/10.1038/35000514

- [133] K. Abe et al. [T2K Collaboration], "Combined Analysis of Neutrino and Antineutrino Oscillations at T2K," Phys. Rev. Lett. 118 (2017) no.15, 151801. https://doi.org/10.1103/PhysRevLett.118.151801
- [134] A. A. Klyachko, B. Öztop, and A. S. Shumovsky, "Measurable entanglement," Appl. Phys. Lett.88, 124102, (2006). https://doi.org/10.1063/1.2187398
- [135] Michael Walter, David Gross, and Jens Eisert, "Multi-partite entanglement in Quantum Information: From Foundation to quantum technology operations," Wiley Online Library, Chapter 14, (2016). https://doi.org/10.48550/arXiv.1612.02437
- [136] M. Cunha, M.; Fonseca, A.; O. Silva, E. "Tripartite Entanglement: Foundations and Applications". Universe 2019, 5, 209. https://doi.org/10.3390/universe5100209.
- [137] P.Benioff, "The computer as a physical system: A microscopic quantum mechanical Hamiltonian model of computers as represented by Turing machines," J Stat Phys 22, 563–591 (1980). https://doi.org/10.1007/BF01011339
- [138] R.P.Feynman, "Simulating physics with computers," Int J Theor Phys 21, 467–488 (1982). https://doi.org/10.1007/BF02650179
- [139] R.P.Feynman, "Quantum mechanical computers," Found Phys **16**, 507–531 (1986). https://doi.org/10.1007/BF01886518
- [140] David Deutsch, "Quantum theory, the Church-Turing principle and the universal quantum computer," Proc. R. Soc. Lond. A **400**: 97–117, 1985. https://doi.org/10.1098/rspa.1985.0070
- [141] David Deutsch, "Quantum Computational Networks," Proceedings of the Royal Society of London. Series A, Mathematical and Physical Sciences, vol. **425**, no. 1868, The Royal Society, 1989, pp. 73–90. https://doi.org/10.1098/rspa. 1989.0099

[142] David Deutsch and Richard Jozsa, "Rapid solution of problems by quantum computation," Proc. R. Soc. Lond. A 439 553-558, 1992. https://doi.org/ 10.1098/rspa.1992.0167

- [143] Ethan Bernstein and Umesh Vazirani, "Quantum Complexity Theory," SIAM J. Comput., 26 (5), 1411–1473. (63 pages). https://doi.org/10.1137/ S009753979630092
- [144] D. R. Simon, "On the power of quantum computation," Proceedings 35th Annual Symposium on Foundations of Computer Science, 1994, pp. 116-123. https://doi.org/10.1109/SFCS.1994.365701
- [145] P. W. Shor, "Polynomial time algorithms for prime factorization and discrete logarithms on a quantum computer," SIAM J. Sci. Statist. Comput. **26** (1997), 1484. https://doi.org/10.1137/S0097539795293172
- [146] L. K. Grover, "A Fast quantum mechanical algorithm for database search," https://doi.org/10.48550/arXiv.quant-ph/9605043
- [147] Peng, X. H., Zhang, J. F., Du, J. F. and Suter, D. "Quantum simulation of a system with competing two- and three-body interactions," Phys. Rev. Lett. 103, 140501 (2009). https://doi.org/10.1103/PhysRevLett.103.140501
- [148] Feng, G. R., Xu, G. F. and Long, G. L. "Experimental realization of nonadiabatic holonomic quantum computation," Phys. Rev. Lett. **110**, 190501 (2013). Experimental realization of nonadiabatic holonomic quantum computation
- [149] Zhang, J. F., Wei, T. C. and Laflamme, R. "Experimental quantum simulation of entanglement in many-body systems," Phys. Rev. Lett. **107**, 010501 (2011). https://doi.org/10.1103/PhysRevLett.107.010501
- [150] Edwards, E. E. et al. "Quantum simulation and phase diagram of the transverse-field Ising model with three atomic spins," Phys. Rev. B 82, 060412 (2010). https://doi.org/10.1103/PhysRevB.82.060412
- [151] Lanyon, B. P. et al. "Towards quantum chemistry on a quantum computer," Nat. Chem. 2, 106 (2010). https://doi.org/10.1038/nchem.483
- [152] Du, J. F. et al. "NMR implementation of a molecular hydrogen quantum simulation with adiabatic state preparation," Phys. Rev. Lett. **104**, 030502 (2010). https://doi.org/10.1103/PhysRevLett.104.030502

[153] Kassal, I., Whitfield, J. D., Perdomo-Ortiz, A., Yung, M. H. and Aspuru-Guzik, A. "Simulating Chemistry using Quantum Computers.," Annu. Rev. Phys. Chem. 62, 185-207 (2011). https://doi.org/10.1146/ annurev-physchem-032210-103512

- [154] Zohar, E. and Reznik, B. "Confinement and lattice quantum-electrodynamic electric flux tubes simulated with ultracold atoms," Phys. Rev. Lett. **107**, 275301 (2011). https://doi.org/10.1103/PhysRevLett.107.275301
- [155] Cirac, J. I. et al. "Cold atom simulation of interacting relativistic quantum field theories," Phys. Rev. Lett. 105, 190403 (2010). https://doi.org/10.1103/ PhysRevLett.105.190403
- [156] Casanova, J. et al. "Quantum simulation of quantum field theories in trapped ions," Phys. Rev. Lett. 107, 260501 (2011). https://doi.org/10.1103/ PhysRevLett.107.260501
- [157] Jordan, S. P. et al. "Quantum algorithms for quantum field theories," Science 336, 1130-1133 (2012). https://doi.org/10.1126/science.1217069
- [158] A. Warshel, Z. Chu, "Nature of the surface crossing process in bacteriorhodopsin: computer simulations of the quantum dynamics of the primary photochemical event," The Journal of Physical Chemistry B **105** (40) (2001) 9857–9871. http://doi.org/10.1021/Jp010704A
- [159] M. Schuld, I. Sinayskiy, F. Petruccione, "Simulating a perceptron on a quantum computer," Physics Letters A 379 (7) (2015) 660-663. https://doi.org/10.1016/j.physleta.2014.11.061
- [160] V. K. Mulligan, H. Melo, H. I. Merritt, S. Slocum, B. D. Weitzner, A. M. Watkins, P. D. Renfrew, C. Pelissier, P. S. Arora, R. Bonneau, "Designing peptides on a quantum computer," bioRxiv (2020) 752485. https://doi.org/10.1101/752485
- [161] J. Mielczarek, "Spin foam vertex amplitudes on quantum computer—preliminary results," Universe 5 (8)(2019)179.https: //doi.org/10.3390/universe5080179
- [162] R. Schack, "Using a quantum computer to investigate quantum chaos," Physical Review A 57 (3) (1998) 1634. https://doi.org/10.1103/PhysRevA.57.1634

[163] Atas, Y.Y., Zhang, J., Lewis, R. et al. "SU(2) hadrons on a quantum computer via a variational approach". Nat Commun 12, 6499 (2021). https://doi.org/10.1038/s41467-021-26825-4

- [164] Tseng, C. H. et al. "Quantum simulation of a three-body-interaction Hamiltonian on an NMR quantum computer," Phys. Rev. A **61**, 012302 (1999). https://doi.org/10.1103/PhysRevA.61.012302
- [165] Negrevergne, C. et al. "Liquid-state NMR simulations of quantum many-body problems," Phys.Rev. A 71, 032344 (2005). https://doi.org/10.1103/PhysRevA.71.032344
- [166] Somaroo, S. et al. "Quantum simulations on a quantum computer," Phys. Rev. Lett. 82, 5381-5384 (1999). https://doi.org/10.1103/PhysRevLett. 82.5381
- [167] Gerritsma, R., Kirchmair, G., Zähringer, F. et al. "Quantum simulation of the Dirac equation," Nature 463, 68-71 (2010). https://doi.org/10.1038/nature08688
- [168] Gerritsma, R. et al. "Quantum simulation of the Klein paradox with trapped ions," Phys. Rev. Lett. 106, 060503 (2011). https://doi.org/10.1103/ PhysRevLett.106.060503
- [169] Kinoshita T, Wenger T, Weiss DS. "Observation of a one-dimensional Tonks-Girardeau gas," Science. 2004 Aug 20;305(5687):1125-8. https://doi.org/10.1126/science.1100700
- [170] Ma, X. S. et al. "Quantum simulation of the wave function to probe frustrated Heisenberg spin systems," Nat. Phys. 7, 399-405 (2011). https://doi.org/ 10.1038/nphys1919
- [171] Preskill, J. "Quantum Computing in the NISQ era and beyond," Quantum 2, 79 (2018). https://doi.org/10.22331/q-2018-08-06-79
- [172] Nguyen, T. L. et al. "Towards Quantum Simulation with Circular Rydberg Atoms," Phys. Rev. X 8, 011032 (2018). https://doi.org/10.1103/PhysRevX.8.011032
- [173] Kivlichan, I. D. et al. "Quantum Simulation of Electronic Structure with Linear Depth and Connectivity," Phys. Rev. Lett. **120**, 110501 (2018). https://doi.org/10.1103/PhysRevLett.120.110501

[174] Hempel, C. et al. "Quantum Chemistry Calculations on a Trapped-Ion Quantum Simulator," Phys. Rev. X 8, 031022 (2018). https://doi.org/10.1103/PhysRevX.8.031022

- [175] Noh, C. and Angelakis, D. G. "Quantum simulations and many-body physics with light," Rep. Prog. Phys. 80, 016401 (2016). https://doi.org/10.1088/ 0034-4885/80/1/016401
- [176] Georgescu, I. M. et al. "Quantum simulation," Rev. Mod. Phys. 86, 153 (2014). https://doi.org/10.1103/RevModPhys.86.153
- [177] Cirac, J. I. and Zoller, P. "Goals and opportunities in quantum simulation," Nat. Phys. 8, 264–266 (2012). https://doi.org/10.1038/nphys2275
- [178] Daniel Alsina and José Ignacio Latorre, "Experimental test of Mermin inequalities on a five-qubit quantum computer," Phys. Rev. A **94**, 012314 (2016). https://doi.org/10.1103/PhysRevA.94.012314
- [179] Diego García-Martín, Germán Sierra, "Five Experimental Tests on the 5-Qubit IBM Quantum Computer," Journal of Applied Mathematics and Physics Vol.6 No.7, 1460-1475, (2018). https://doi.org/10.4236/jamp.2018.67123
- [180] Swain, M., Rai, A., Behera, B.K. et al. "Experimental demonstration of the violations of Mermin's and Svetlichny's inequalities for W and GHZ states," Quantum Inf Process 18, 218 (2019). https://doi.org/10.1007/ s11128-019-2331-5
- [181] Bikash K. Behera, Anindita Banerjee, Prasanta K. Panigrahi, "Experimental realization of quantum cheque using a five-qubit quantum computer," Quantum Inf. Process. 16, 312 (2017). https://doi.org/10.1007/s11128-017-1762-0
- [182] James R Wootton, "Demonstrating non-Abelian braiding of surface code defects in a five qubit experiment," Quantum Sci. Technol. 2 015006 (2017). https://doi.org/10.1088/2058-9565/aa5c73
- [183] Sayan Gangopadhyay, Manabputra, Bikash K. Behera, Prasanta K. Panigrahi, "Generalization and Demonstration of an Entanglement Based Deutsch-Jozsa Like Algorithm Using a 5-Qubit Quantum Computer," Quantum Inf. Process. 17, 160 (2018). https://doi.org/10.1007/s11128-018-1932-8

[184] I. Yalçınkaya, Z. Gedik, "Optimization and experimental realization of the quantum permutation algorithm," Phys. Rev. A **96**, 062339 (2017). https://doi.org/10.1103/PhysRevA.96.062339

- [185] Debjit Ghosh, Pratik Agarwal, Pratyush Pandey, Bikash K. Behera, Prasanta K. Panigrahi, "Automated Error Correction in IBM Quantum Computer and Explicit Generalization," Quantum Inf. Process. 17, 153 (2018). https://doi.org/10.1007/s11128-018-1920-z
- [186] Alba Cervera-Lierta, "Exact Ising model simulation on a quantum computer," Quantum 2, 114 (2018). https://doi.org/10.22331/q-2018-12-21-114
- [187] Jose L. Cereceda, "Three-particle entanglement versus three-particle nonlocality," Phys. Rev. A 66 (2002) 024102. https://doi.org/10.1103/PhysRevA. 66.024102
- [188] G. Romero, C. E. López, F. Lastra, E. Solano, and J. C. Retamal, "Direct measurement of concurrence for atomic two-qubit pure states," Phys. Rev. A 75, 032303 (2007). https://doi.org/10.1103/PhysRevA.75.032303.
- [189] Wang Hong-Fu and Zhang Shou "Application of quantum algorithms to direct measurement of concurrence of a two-qubit pure state," Chin. Phys. B, 2009, Vol. 18(7): 02642. https://doi.org/10.1088/1674-1056/18/7/004
- [190] X. K. Song, Y. Huang, J. Ling and M. H. Yung, "Quantifying Quantum Coherence in Experimentally-Observed Neutrino Oscillations," Phys. Rev. A 98 (2018) no.5, 050302. https://doi.org/10.1103/PhysRevA.98.050302
- [191] M. M. Ettefaghi, Z. S. Tabatabaei Lotfi and R. Ramezani Arani, "Quantum correlations in neutrino oscillation: Coherence and entanglement," EPL 132 (2020) no.3, 31002. https://doi.org/10.1209/0295-5075/132/31002
- [192] Y. Chen, Y. Ma and S. Zhou, "Quantum Simulations of the Non-Unitary Time Evolution and Applications to Neutral-Kaon Oscillations,". https://doi.org/ 10.48550/arXiv.2105.04765
- [193] A. Mallick, S. Mandal, and C.M Chandrashekar, "Neutrino oscillations in discrete-time quantum walk framework," Eur. Phys. J. C 77, 85 (2017). https://doi.org/10.1140/epjc/s10052-017-4636-9

[194] B. Hall, A. Roggero, A. Baroni and J. Carlson, "Simulation of collective neutrino oscillations on a quantum computer," Phys. Rev. D **104** (2021) no.6, 063009. https://doi.org/10.1103/PhysRevD.104.063009

- [195] Yeter-Aydeniz, K., Bangar, S., Siopsis, G. et al. "Collective neutrino oscillations on a quantum computer," Quantum Inf Process 21, 84 (2022). https://doi.org/10.1007/s11128-021-03348-x
- [196] A. Roggero, "Dynamical phase transitions in models of collective neutrino oscillations," Phys. Rev. D 104, no.12, 123023 (2021). https://doi.org/10.1103/PhysRevD.104.123023
- [197] I. Esteban, M. C. Gonzalez-Garcia, M. Maltoni, T. Schwetz and A. Zhou, "The fate of hints: updated global analysis of three-flavor neutrino oscillations," JHEP **09** (2020), 178. https://doi.org/10.1007/JHEP09(2020)178
- [198] P. Horodecki, "Separability criterion and inseparable mixed states with positive partial transposition," Phys. Lett. A 232 (1997), 333. https://doi.org/10.1016/S0375-9601(97)00416-7
- [199] A. B. Klimov, R. Guzmán, J. C. Retamal, and C. Saavedra, "Qutrit quantum computer with trapped ions", Phys. Rev. A 67, 062313 (2003). https://doi.org/10.1103/PhysRevA.67.062313
- [200] Bruno Juliá-Díaz, Joseph M. Burdis and Frank Tabakin, "QDENSITY A Mathematica Quantum Computer simulation," Comp. Phys. Comm., 174 (2006) 914-934. https://doi.org/10.1016/j.cpc.2005.12.021. Also see: Comp. Phys. Comm., 180, (2009) 474. https://doi.org/10.1016/j.cpc.2008.10.006

 Frank Tabakin, Bruno Juliá-Díaz, "QCWAVE A Mathematica quantum computer simulation update," Computer Physics Communications Vol 182, Issue 8, pp 1693-1707 (2011), https://doi.org/10.1016/j.cpc.2011.04.010-Frank Tabakin, "QDENSITY/QCWAVE: A Mathematica quantum computer simulation update," Computer Physics Communications, Vol 201, pp 171-172, (2017) https://doi.org/10.1016/j.cpc.2015.12.015,
- [201] César Herreño-Fierro, J. R. Luthra, "Generalized concurrence and limits of separability for two qutrits," arXiv:quant-ph/0507223v1. https://doi.org/10.48550/arXiv.quant-ph/0507223

[202] Omar Gamel, "Entangled Bloch spheres: Bloch matrix and two-qubit state space," Phys. Rev. A 93, 062320 (2016). https://doi.org/10.1103/PhysRevA.93.062320

- [203] P. Mehta, "Topological phase in two flavor neutrino oscillations," Phys. Rev. D 79 (2009), 096013. https://doi.org/10.1103/PhysRevD.79.096013
- [204] M. Blasone, P. A. Henning and G. Vitiello, "Berry phase for oscillating neutrinos," Phys. Lett. B 466 (1999), 262-266. https://doi.org/10.1016/ S0370-2693(99)01137-5
- [205] Arvind, K. S. Mallesh and N. Mukunda, "A Generalized Pancharatnam geometric phase formula for three level quantum systems," J. Phys. A 30 (1997), 2417-2431. https://doi.org/10.1088/0305-4470/30/7/021
- [206] K.S. Mallesh, N. Mukunda "The algebra and geometry of SU(3) matrices," Pramana J Phys 49, 371–383 (1997). https://doi.org/10.1007/BF02847424
- [207] G. Khanna, S. Mukhopadhyay, R. Simon, and N. Mukunda, "Geometric phases for SU(3) representations and three level quantum systems," Ann. Phys. (N.Y.) 253, 55–82 (1997). https://doi.org/10.1006/aphy.1997.5601
- [208] A. T. Bölükbasi and T. Dereli, "On the SU(3) Parametrization of Qutrits," Journal of Physics: Conference Series, Volume **36**, Issue 1, pp. 28-32 (2006). https://doi.org/10.1088/1742-6596/36/1/006
- [209] A. Upadhyay and M. Batra, "Phenomenology of Neutrino Mixing in Vacuum and Matter," ISRN High Energy Phys. 2013 (2013), 206516. https://doi. org/10.1155/2013/206516
- [210] D. B. Lichtenberg, Unitary Symmetry and Elementary Particles (Second Edition Book), Chapter 6 Multiplets, Academic Press, 1978, Pages 72-101, ISBN 9780124484603, https://doi.org/10.1016/B978-0-12-448460-3.50011-7.
- [211] F. P. An *et al.* [Daya Bay], "New Measurement of Antineutrino Oscillation with the Full Detector Configuration at Daya Bay," Phys. Rev. Lett. **115** (2015) no.11, 111802. https://doi.org/10.1103/PhysRevLett.115.111802
- [212] A. B. Sousa [MINOS and MINOS+], "First MINOS+ Data and New Results from MINOS," AIP Conf. Proc. 1666 (2015) no.1, 110004. https://doi.org/ 10.1063/1.4915576

[213] J. Kersten and A. Y. Smirnov, "Decoherence and oscillations of supernova neutrinos," Eur. Phys. J. C **76** (2016) no.6, 339. https://doi.org/10.1140/epjc/s10052-016-4187-5

- [214] T. Ohlsson, "Status of non-standard neutrino interactions," Rept. Prog. Phys. **76** (2013), 044201. https://doi.org/10.1088/0034-4885/76/4/044201
- [215] Xianfei Qi, Ting Gao, Fengli Yan, "Measuring Coherence with Entanglement Concurrence," J. Phys. A: Math. Theor. 50 (2017) 285301. https://doi.org/ 10.1088/1751-8121/aa7638
- [216] Manoranjan Swain, Amit Rai, Bikash K. Behera, Prasanta K. Panigrahi, " Experimental demonstration of the violations of Mermin's and Svetlichny's inequalities for W and GHZ states," Quantum Information Processing, Volume 18, Issue 7, article id. 218, 11 pp. https://doi.org/10.1007/ s11128-019-2331-5
- [217] Cruz, D., et al., "Efficient Quantum Algorithms for GHZ and W States, and Implementation on the IBM Quantum Computer," Adv. Quantum Technol., 2: 1900015, (2019). https://doi.org/10.1002/qute.201900015
- [218] Jafarizadeh, M. A.; Akbari, Y.; Behzadi, N. "Two-qutrit entanglement witnesses and Gell-Mann matrices," The European Physical Journal D, Volume 47, Issue 2, 2008, pp.283-293. https://doi.org/10.1140/epjd/e2008-00041-3
- [219] P. Gokhale, J. M. Baker, C. Duckering, F. T. Chong, N. C. Brown and K. R. Brown, "Extending the Frontier of Quantum Computers With Qutrits," in IEEE Micro, vol. 40, no. 3, pp. 64-72, (2020). https://doi.org/10.1109/MM. 2020.2985976
- [220] Bin Li, Zu-Huan Yu, Shao-Ming Fei, "Geometry of Quantum Computation with Qutrits," Scientific Reports, Volume 3, id. 2594 (2013). https://doi.org/10. 1038/srep02594
- [221] E. Akhmedov, "Quantum mechanics aspects and subtleties of neutrino oscillations," [arXiv:1901.05232 [hep-ph]]. https://doi.org/10.48550/arXiv. 1901.05232
- [222] C. W. Kim, "Neutrino physics: Fundamentals of neutrino oscillations," J. Korean Phys. Soc. **29** (1996), 157 [arXiv:hep-ph/9607391 [hep-ph]]. https://doi.org/10.48550/arXiv.hep-ph/9607391

[223] M. J. Molewski and B. J. P. Jones, "Scalable qubit representations of neutrino mixing matrices," Phys. Rev. D 105 (2022) no.5, 056024. https://doi.org/ 10.1103/PhysRevD.105.056024

Quantum Aspects of Oscillatory Neutrinos

by Abhishek Kumar Jha

Submission date: 13-Apr-2022 03:06PM (UTC+0530)

Submission ID: 1809597881

File name: Abhishek_Kumar_Jha.pdf (6.55M)

Word count: 34212 Character count: 159604

Quantum Aspects of Oscillatory Neutrinos

ORIGINALITY REPORT

29% SIMILARITY INDEX

22%

INTERNET SOURCES

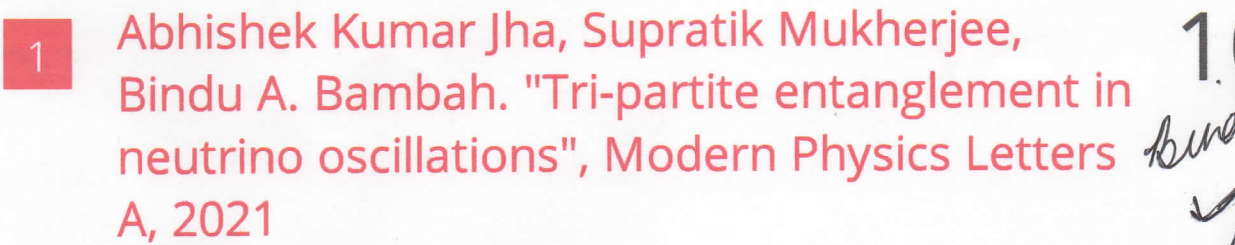
26%

PUBLICATIONS

1%

STUDENT PAPERS

PRIMARY SOURCES



Publication

Abhishek Kumar Jha, Akshay Chatla.
"Quantum studies of neutrinos on IBMQ
processors", The European Physical Journal
Special Topics, 2021

Publication

link.springer.com

4 export.arxiv.org

5 arxiv.org

6 indico.fnal.gov

Birdung 3 %

Burdu 2% Burlow

Prof: Bindu A Bambah This is to certify that out of School of Physics
University of Hyderabad Hyderabad STUDENTS OWN PUBLICATIONS

Leaving 51 Similarity

Leaving 51 Similarity

8	Yong-Cheng Ou, Heng Fan. "Monogamy inequality in terms of negativity for three-qubit states", Physical Review A, 2007 Publication	<1%
9	Omar Gamel. "Entangled Bloch spheres: Bloch matrix and two-qubit state space", Physical Review A, 2016 Publication	<1%
10	eprints.library.iisc.ernet.in Internet Source	<1%
11	eprints.nottingham.ac.uk Internet Source	<1%
12	Ciaran Hughes, Joshua Isaacson, Anastasia Perry, Ranbel F. Sun, Jessica Turner. "Quantum Computing for the Quantum Curious", Springer Science and Business Media LLC, 2021 Publication	<1%
13	Submitted to University of Durham Student Paper	<1%
14	Massimo Blasone, Silvio De Siena, Cristina Matrella. "Wave packet approach to quantum correlations in neutrino oscillations", The European Physical Journal C, 2021 Publication	<1%
15	hdl.handle.net Internet Source	<1%

16	JIN-MING LIU, YU-ZHU WANG. "THREE-MODE ENTANGLED STATE OF AN ATOMIC BOSE– EINSTEIN CONDENSATE IN A THREE-WELL POTENTIAL", International Journal of Modern Physics B, 2012 Publication	<1%
17	Submitted to Nazarbayev University Student Paper	<1%
18	"Quantum Information", Wiley, 2016 Publication	<1%
19	M. J. Molewski, B. J. P. Jones. "Scalable qubit representations of neutrino mixing matrices", Physical Review D, 2022 Publication	<1%
20	Massimo Blasone. "On entanglement in neutrino mixing and oscillations", Journal of Physics Conference Series, 06/01/2010 Publication	<1%
21	Submitted to Queen's University of Belfast Student Paper	<1%
22	pendientedemigracion.ucm.es Internet Source	<1%
23	C. A. Argüelles, B. J. P. Jones. "Neutrino oscillations in a quantum processor", Physical Review Research, 2019 Publication	<1%

24	www.niser.ac.in Internet Source	<1%
25	Yat-Long Chan, MC. Chu, Ka Ming Tsui, Chan Fai Wong, Jianyi Xu. "Wave-packet treatment of reactor neutrino oscillation experiments and its implications on determining the neutrino mass hierarchy", The European Physical Journal C, 2016 Publication	<1%
26	Dokshitzer, Yu L, P Lévai, and J Nyíri. "NEUTRINO OSCILLATIONS IN QUANTUM MECHANICS AND QUANTUM FIELD THEORY", Gribov-80 Memorial Volume, 2011. Publication	<1%
27	repository.dl.itc.u-tokyo.ac.jp Internet Source	<1%
28	Submitted to Marquette University Student Paper	<1%
29	Pranav Gokhale, Jonathan M. Baker, Casey Duckering, Natalie C. Brown, Kenneth R. Brown, Fred Chong. "Extending the Frontier of Quantum Computers with Qutrits", IEEE Micro, 2020 Publication	<1%
30	Xue-Ke Song, Yanqi Huang, Jiajie Ling, Man- Hong Yung. "Quantifying quantum coherence	<1%

in experimentally observed neutrino oscillations", Physical Review A, 2018

Publication

31	polen.itu.edu.tr Internet Source	<1%
32	www.win.tue.nl Internet Source	<1%
33	Jürgen Audretsch. "Entangled Systems", Wiley, 2007 Publication	<1%
34	Kurzyk, Dariusz. "Introduction to Quantum Entanglement", Theoretical and Applied Informatics, 2012. Publication	<1%
35	Nakahara, . "Qubits and Quantum Key Distribution", Quantum Computing From Linear Algebra to Physical Realizations, 2008.	<1%
36	Xuezhong Guan, Ligang Sun, Fangfei Yu, Xin Li. "Sunspot number time series prediction using neural networks with quantum gate nodes", Proceeding of the 11th World Congress on Intelligent Control and Automation, 2014 Publication	<1%
37	core.ac.uk Internet Source	<1%

38	Internet Source	<1%
39	Jörn Kersten, Alexei Yu. Smirnov. "Decoherence and oscillations of supernova neutrinos", The European Physical Journal C, 2016 Publication	<1%
40	eldorado.uni-dortmund.de:8080 Internet Source	<1%
41	tesi.cab.unipd.it Internet Source	<1%
42	Submitted to University College London Student Paper	<1%
43	Submitted to University of Nottingham Student Paper	<1%
44	coek.info Internet Source	<1%
45	Blasone, M, F Dell'Anno, S De Siena, and F Illuminati. "Entanglement in Quantum Field Theory: particle mixing and oscillations", Journal of Physics Conference Series, 2013. Publication	<1%
46	Boris Kayser. "Neutrino physics, superbeams and the neutrino factory", Journal of Physics G Nuclear and Particle Physics, 08/01/2003	<1%

47	vdoc.pub Internet Source	<1%
48	www-reynal.ensea.fr Internet Source	<1%
49	Lecture Notes in Computer Science, 2011. Publication	<1%
50	Ming Li, Shao-Ming Fei, Xianqing Li-Jost. "Quantum Entanglement: Separability, Measure, Fidelity of Teleportation, and Distillation", Advances in Mathematical Physics, 2010 Publication	<1%
51	qiskit.org Internet Source	<1%
52	"Open Quantum Systems", 'Springer Science and Business Media LLC', 2018 Internet Source	<1%
53	Leonid Zaichik, Vladimir M. Alipchenkov, Emmanuil G. Sinaiski. "Particles in Turbulent Flows", Wiley, 2008	<1%
54	Submitted to Orissa University of Agriculture & Technology Student Paper	<1%
55	Submitted to University of Sussex Student Paper	<1%

56	d-nb.info Internet Source	<1%
57	stars.library.ucf.edu Internet Source	<1%
58	"Quantum Information Theory and Quantum Statistics", Springer Science and Business Media LLC, 2008 Publication	<1%
59	Soumya Das, Goutam Paul. "A New Error- Modeling of Hardy's Paradox for Superconducting Qubits and Its Experimental Verification", ACM Transactions on Quantum Computing, 2020 Publication	<1%
60	edoc.ub.uni-muenchen.de Internet Source	<1%
61	www.theory.caltech.edu Internet Source	<1%
62	Submitted to Università di Parma Student Paper	<1%
63	Y Yang, J P Kneller. "Neutrino flavour evolution through fluctuating matter", Journal of Physics G: Nuclear and Particle Physics, 2018 Publication	<1%

Exclude quotes

Exclude bibliography

Exclude matches

< 14 words

Contifued 29/ that out of 29/ Similarly the Similarly 5/ Students only 5/ Simlarly Simlarly Sindu A. Bunkah

Prof. Bindu A Bambah School of Physics University of Ave tre minu versity of Try 06 (T.S.) | WOIA